TWO-DIMENSIONAL ANALYSIS OF FOUR TYPES OF WATER-FILLED GEOMEMBRANE TUBES AS TEMPORARY FLOOD-FIGHTING DEVICES

By

Meeok Kim

Dissertation submitted to the faculty of the Virginia Polytechnic Institute and State University in partial fulfillment of the requirements for the degree of

Doctor of Philosophy

in

Civil Engineering

Raymond H. Plaut, Co-Chair

George M. Filz, Co-Chair

Marte S. Gutierrez

Kamal B. Rojiani

Carin L. Roberts-Wollmann

February, 2003

Blacksburg, Virginia

Keyword: Soil-Structure Interaction, Flexible Structure, Geomembrane, FLAC, Inflatable Tube Dam, Flood Protection

TWO-DIMENSIONAL ANALYSIS OF FOUR TYPES OF WATER-FILLED GEOMEMBRANE TUBES AS TEMPORARY FLOOD-FIGHTING DEVICES

By
Meeok Kim

Dr. Raymond. H. Plaut, Chair
Dr. George M. Filz, Chair

Charles E. Via, Jr. Department of Civil and Environmental Engineering

(ABSTRACT)

Two-dimensional analysis of four types of water-filled tube dams is carried out: an apron-tube dam, a single baffle tube dam, a sleeved tube dam, and a stacked tube dam. Since the analysis of the water-filled tube dam involves highly nonlinear geometric deformations and interactions with soil, fluid, and structure, it is solved numerically with the explicit finite difference program FLAC.

The tube is numerically modeled with beam elements. The predicted contact regions are modeled with interface elements. The Mohr-Coulomb constitutive model is used for the soil. Water inside and outside of the tube is modeled as hydrostatic pressure and the pressures are continuously updated as the configuration of the tube is changed. The change of the internal water pressure head (IWPH) for maintaining a constant tube area during the deformation is simulated. The simulation is achieved by two iterative procedures, the secant method and the factored secant method.

The numerical analysis results show good agreement with the experimental results overall: the deformation of the tube(s), the IWPH changes, and the critical external water heights. From the numerical simulation of the experiments and the parametric studies, the behavior of each type of water-filled tube dam is clarified. Also, the failure modes of the tube dams are examined. The failure mode of a tube dam depends on the configuration and IWPH of the tube dam and the characteristics of the soil surface.

To my son, Jinhyung

Acknowledgements

I would like to express my sincere gratitude to my advisor, Dr. Raymond H. Plaut for providing me with the opportunity to work with him and his never-ending guidance. I also would like to thank Dr. George M. Filz for his invaluable suggestions and guidance. I have greatly benefited from their wealth of knowledge and insight and I could not ask for better advisors.

I wish to thank Dr. Marte S. Gutierrez for his help and useful advice regarding FLAC modeling. I also wish to express appreciation to Dr. Kamal B. Rojiani and Dr. Carin L. Roberts-Wollmann for their suggestions regarding theoretical and practical aspects.

I wish to thank Dr. Peter Cundall from Itasca Consulting Group for his responses and suggestions whenever I encountered a problem in FLAC. My special thanks go to Dr. Hyunyoung Cho and Dr. Duhoi Chung for their care and encouragement.

I greatly appreciate the financial support provided by National Science Foundation Grant No. CMS-9807335.

I would like to thank my friends including Redzuan Abdullah, Miguel Pando, Sandra Dika, Songwut Hengprathanee, Dr. Youngjin Woo, Hyun Shin, Eunyoung Kim, and Chul Park for their encouragement and friendship. Thanks also go to Yuko Mizutani and Yujin Park for their warmhearted friendship and support.

My deepest appreciation goes to my best friend, colleague, and husband, Youngjin Park for his unbiased understanding and endless encouragement of the pursuit of my Ph.D. He has supported me with his love and sincerity since we met. Also, I feel grateful and am deeply indebted to my son, Jinhyung, for growing up far away from me. I could not have done this work without support and love from my parents and parents-in-law and I cannot thank them enough.

Contents

List of Figures

List of Tables

Chapter 1. Introduction

1.1. Problem statement

Much damage has been caused and many lives have been lost by floods. Floods have been with us since the beginning of civilization and so has the history of flood control. However, there is still tremendous destruction due to flooding.

A water-filled dam is a geosynthetic tube (or several tubes), which has been developed for the purpose of fluid confinement or as a fluid barrier. It has evolved into various configurations, such as a tube with a wedge, a tube with an apron, a tube with a baffle, two tubes in a sleeve, and stacked tubes, to expand its efficiency and stability toward external water.

Among the various use of a water-filled tube dam, the most profitable, worthwhile, and significant usage is flood fighting. A water-filled tube dam can be an alternative to labor-intensive, time-consuming, and environmentally-unfriendly sandbags, which have been used for temporary flood protection in most flooding areas. In contrast to a sandbag, a water-filled tube dam can be installed in a very short time and by a small number of people, and the tube dam also can be withdrawn easily without unpleasant aftermath. In addition, the filling material, water, is very accessible, especially in an area where flooding is expected, and the tubes can be used repeatedly.

Labor and time for installation of temporary flood-fighting devices are the most important factors when a flood is imminent. As one of the nonstructural flood defense procedures, prospective flooding areas may be warned to prepare for the evacuation of people and the construction of temporary flood barriers. Because of the amount of time and the number of people needed for preparation, the forecasting of flooding should be done as early as possible, even though it is accompanied by uncertainties. Using a water-filled tube dam for temporary protection requires a shorter preparation time with fewer people than sandbags. As a result, a more effective flood defense can be established.

In spite of all the benefits and advantages of a water-filled dam, the use of sandbags has not really been supplanted. One of the reasons is that the cost of a water-filled dam is higher than sandbags, but most of all are the unknown reliability of different types of water-filled dams and the lack of confidence of users toward the capability of a water-filled tube dam.

Several tube manufacturers have altered or adjusted the basic design to improve the efficiency and stability, from a simple oval cylindrical shape of the tube to different types, such as a baffled tube, apron-attached tube, two tubes in a sleeve, and stacked tubes. The companies claim that their tubes are safe up to a certain external water level, and the tubes have been used successfully in a number of cases. There are some articles about these cases or case studies with a tube dam, but there are also some cases which did not succeed. Little research has been done so far to investigate this thoroughly in theoretical terms, and to ensure the dam's safety and reliability.

Therefore, the main purpose of this research is to examine the reliability, the effectiveness, and the extensive behavior of types of water-filled tube dams through numerical analysis. To ensure the accuracy of the results of the analysis, outcomes will be compared with experimental work done by other graduate students. The results from this study, combined with the previous tests, will give a better understanding of the behavior and effectiveness, guidelines for design and installation of water-filled tube dams, and insights for the development and the improvement of tube dams.

The analysis of a water-filled tube dam is a combined problem involving fluid, soil, and structure, and the exact behavior cannot be found neglecting one of these factors. However, other investigators examined the relationship between the tube and soil, and concluded that the maximum tension of the tube is influenced slightly by the stiffness of the soil except for very soft soil (Plaut and Suherman, 1998; Huong, 2001).

This study will focus on examining the critical external water level, the maximum tension, overall deformations, and the efficiency and types of failure of different kinds of tube dams resting on soil.

1.2. Scope of Research

Several kinds of inflated tubes have been developed to provide more stability against floods or external water forces. One of them is a tube with a wedge, which was investigated by Huong (2001). Other types are a tube with an apron, two tubes in a sleeve, a single or double baffled tube, and stacked tubes. For this research, an apron tube, a single baffle tube, two tubes in a sleeve, and three stacked tubes are investigated.

- Apron-tube: It consists of one tube with a certain length of apron which is attached to the top of the tube and spreads to the headwater side. When the floodwater rises, friction is developed between the ground and the apron, and this friction increases the stability of the apron-tube system. The tube can successfully resist the floodwater up to the tube height with a proper length of apron.
- Single baffle tube: A diaphragm is attached inside tube, running along the length of a tube. The manufacturer claims that the perforated baffle restrains a tube from rolling when a tube is exposed to the external loading.
- Two tubes in a sleeve: Two tubes are inflated and surrounded by a membrane sleeve; the sleeve makes the two inflated tubes intact. The friction between the two tubes prevents rolling failure, and gives more stability than two tubes alone.
- Three stacked tubes: Several inflated tubes can be stacked to make one large inflated tube dam. A two-one formation, two tubes at the bottom and one tube on top, is investigated. It is believed that the weight of the stacked tubes, and the friction between tubes and the ground, provide stability to the system and withstand the flood up to about two-thirds of the height of the structure.

Since water-filled tubes have a larger dimension in the longitudinal direction compared to the perpendicular direction, the external forces acting on the tubes do not vary much along the length of the tubes, so the tube dams are considered here as two-dimensional problems. The dynamic loading from the flood will not be treated in the present work. The change of the internal water pressure head (IWPH) during the deformation of the tube is considered.

The examination will focus on the system parameters which can give a guide to the design, the installation of the existing types of tubes, and the development of new types of tube dams. For example, the maximum tension in the tube is an important factor for selecting proper tube material, since the manufacturers specify the ultimate strength as a characteristic of such material. Overall behavior is also a necessary factor because if the displacement of a tube dam is sensitive to the external water level, the tube dam may be less safe than other types. The ratio of the critical external water height to the height of the tube is a critical factor too; if the ratio is close to the upper limit, 1.0, the tube is more effective. Last, knowing the type of failure of a tube dam at its critical external water level is also important, because improvements for preventing such a failure can be invented to make more efficient and safer tube dams. In addition, the results will be compared with the previous tests as much as possible to verify the numerical analysis.

1.3. Outline of Dissertation

In Chapter 2, a summary of the information presented in the previous literature is briefly presented. The introduced literature is associated with floods and flood mitigation, the application and the development of geosynthetic tubes and their case stories, and previous research work on fluid-filled tube dams.

In Chapter 3, the development of a numerical model for the water-filled tube dam is explained. The main assumptions in modeling and the characteristics and the properties of the numerical models are discussed. The iteration methods developed for the change of the IWPH are explained.

Some basic, yet essential studies are summarized in Chapter 4. Some of the works are related to some of the assumptions made in the numerical modeling. Some analytical solutions from the literature are presented, with a comparison with the numerical results.

The analyses of four types of dams, an apron-tube dam, a single baffle tube dam, a sleeved tube dam, and a stacked tube dam, are presented from Chapter 5 through Chapter 8 accordingly. In the beginning of the chapters, the modeling procedure for each water-filled tube dam is described because of the unique configuration of each type. The numerical

results are compared with the experimental results and are analyzed to understand the behavior of the water-filled tube dam.

Last, in Chapter 9, the summary of the present dissertation is provided. The failure modes of each water-filled tube dam are discussed, along with the efficiency of the dam. In addition, a few suggestions for future studies and developments are presented.

Chapter 2. Literature Review

2.1. Floods and Flood Control

Floods caused about a third of the natural disasters which were recorded between 1986 and 1995 and claimed the deaths of 200,000 people in the world in the same period. In Bangladesh alone, 140,000 lives were lost by a flood, which was caused by a storm surge in April, 1991. Also, economic losses by floods were 31 % of total losses by natural disasters and were estimated at about 251 billion dollars from 1987 to 1996 in the world (UNDHA,1997).

However, in North America, the number of deaths caused by flooding is low compared to other regions such as Asia, but the financial and economic losses are higher because of high standard of living and high values at risk. For example, the flood damage in the United States was approximately 3 billion dollars in 1985 (Parker, 2000). The Great Flood of ’93 caused about 4.5 billion dollars of property damage and 6.5 billion dollars of agricultural loss alone (Associated Press, 1993).

The mitigation of flood hazards can be classified into structural protection and nonstructural flood management. Structural flood defense systems are based on flood abatement or protection of human settlement, whereas nonstructural methods involve the adjustment of human activity to accommodate the flood hazard (like land-use planning, or loss-sharing such as disaster funds and insurance). Since the 1970s, flood control methods have shifted from mainly structural flood protection to nonstructural and structural flood management, because of threats to the ecosystem of rivers by artificial levees, basins, and dams, and questions as to its effectiveness (Gruntfest, 2000).

Different kinds of structures have been developed and constructed to deal with floods. They include dikes, levees, and stop-banks to keep rivers off flood plains, artificial reservoirs to store floodwaters and to release them slowly, and river channel improvement to evacuate floodwaters quickly. These structures have been somewhat effective and popular for a long time, but the structures are designed to protect up to a certain flood level, which is called the design flood and usually is based on 100 years for levees. For that reason, when a flood which exceeds the design flood occurs, people will be more vulnerable to floods. Also, the cost of construction of these structures can be very expensive, because they have to be built and maintained largely to cope with a certain design flood level, and these structures can cause environmental problems (UNDHA, 1997).

Sandbags are mostly used as a flood-fighting device when flooding is predicted or a levee has failed. The Federal Emergency Management Agency reported that 26.5 million bags were used in the Great Flood of ‘93. The sandbags are very cheap and efficient up to five feet high, but after flooding, the sandbags are not easy to disassemble and can cause environmental damage (Associated Press, 1993).

Other methods have been developed for flood fighting to replace sandbags. For example, inflatable tubular geomembranes, such as water or air-filled tubes, are very easy to install in a short time with a small number of people. The geomembrane tubes are very efficient as temporary structures up to floodwater levels of 1.5 m. Cellular structures can give protection under harsh conditions, especially as a stream confinement or diversion in fast-flowing stream with sharp and dangerous debris in extreme weather; they can resist water up to 3 m high. Another structure is the Jersey highway barrier. If flooding occurs where these barriers are accessible, like in an urban area, the barriers may be a satisfactory choice for a flood-fighting device (Biggar and Masala, 1998).

2.2. Applications of Geotextile/Geomembrane Tubes

Tube dams can be used in various ways, such as retaining water, protecting shore lines or banks, retaining back-filled soil, diverting water, and fighting against flooding. The tubes can be filled with air, slurry, sand, water, or concrete.

Anchored rubber dams have been constructed in Japan for the intake of water from rivers at more than 800 stations. Most of the dams are filled with air and the other dams are inflated with water. The advantage of the rubber dam is that it can be easily deflated or inflated depending on the situation. The inflation and deflation of these water-filled, anchored tube dams can be operated fully automatically without additional power (Ogihara, 1983).

Anchored rubber dams have been an excellent choice for flood mitigation and environmental protection in Hong Kong due to the characteristics of the inflation and deflation. The major disadvantage of the rubber dam is the vulnerability against sharp objects. The rubber dam material has been improved using ceramic chips as coating and stainless steel meshes against punctures, but the cost of the construction of the rubber dam is much higher because of that (Tam and Zhang, 1999).

Sand-filled flexible tubes have been used for costal protection on the German North Sea coast; tubes up to a diameter of 1.8 m were installed in the area parallel to the coast. It is reported that sand-filled tubes can be used as long-term beach erosion protectors as long as they are protected from sunlight; the tubes can be utilized up to one decade without sunlight protection (Erchinger, 1993).

The largest anchored rubber dam, 13 ft high and 291 ft long, was constructed in Fremont, California. It was designed to hold runoff and imported water for groundwater recharging purposes. The dam is coated with ceramic chips to prevent puncture or cut-off and it was inflated with air. The life expectancy of the dam was 30-50 years (Anonymous, 1998).

At Sea Isle City, New Jersey, three 300-ft tubes filled and covered with sand have been installed along the ocean as a 900-ft dune for protecting homes threatened by beach erosion. An interesting feature of these geomembrane tubes is that they have an apron on the ocean side to prevent waves from eroding the sand under the tubes (Anonymous, 1998).

After about 2.5 million dollars of damage and losses from 1997 Northern California floods, residents of the Woodside condominium, in northeastern Sacramento, prepared for another flood in 1998 by establishing 1,700 ft of length, 1-ft to 3-ft-high unanchored water dams temporarily. The Skylark Shores Motel Resort in Northern California's Lake County was also protected from the 1998 flood, because 3-ft and 4-ft-high geotextile tubes filled with water were installed for approximately 1,000 ft around the property of the resort (Landis, 2000).

The Pennsylvania Department of Transportation used a permeable woven nylon tube for repairing the scour under one pier of a 28-span girder bridge which crosses the Susquehanna River. This tube was pressure-filled with fine aggregate concrete and placed under the pier, and some voids between the tubes and piers were filled with the same concrete (Koerner and Welsh, 1980).

Aqua-Barriers™, one of the water-inflated tubes that is manufactured, employs one or two restraint baffles inside the tube for providing resistance to rolling. The single-baffled tube can withstand rising water as much as its height, but it is not recommended for use in water that is moving, and the double-baffled tube can be installed in moving water but the tube can resist only two-thirds of its height. The company also claims that baffled tubes have been installed successfully and used for protecting areas from rising floodwaters and keeping water out from construction sites (Aqua-Barriers, 2000).

Aqua dam is another type of water-filled tube dam; it consists of two inner tubes and one outer tube or a master tube. The manufacturer states that the outer tube restrains the inner tubes and the counter friction of the two inner tubes makes the tube dam system

stabilize. The dam has been used for various purposes, such as at the sites of repair or of construction for diverting the water. Also, the dam has been utilized for the protection of wetlands (Aqua dam, 2002)

NOAQ, a company in Sweden, has developed an air-filled tube, which is interconnected with a protective layer called an apron or skirt. The company claims that the layer is pressed down by the weight of the water on it and that provides the stability to the system during the flooding, similar to the principle of a bookend. The NOAQ flood fighting system has drainage under the apron and the tube which helps reduce the pore pressure beneath the system (NOAQ, 2002).

Superior Dam has aprons for better stability and it can be inflated with air or water. The dam is constructed with two tubes side by side and the two tubes are connected to each other at the ends to allow water to flow from one tube to another. In addition, the tube dam has aprons at both sides, the headwater side and the tailwater side. The company claims that the apron on the tailwater side prevents the foundation from overflow erosion (Superior Dam LLC, 2002).

2.3. Previous Studies

Kazimierowicz (1994) investigated the deformation of “sand-sausages” filled with material of known unit weight by assuming the tube as a shell structure. He did not consider the friction between the structure and a rigid foundation. A conclusion of the research was that the shape of the cross section depends on the height of the shell, the pressure at the highest point, the self-weight, and the circumference of the cross section. Kazimierowicz established several formulas for defining the length of the contact segment between the foundation and the structure, and the contact length was related to the pressure value of the highest point.

Seay investigated the three-dimensional behavior of a tube resting on an elastic foundation (1998). Two different initial shapes of the tube were used, and elastic foundations with two different spring stiffness were examined. The tube was modeled with shell elements in ABAQUS and the internal hydrostatic pressures were applied to the structure. The hydrostatic pressure head was constant during the analysis, but the pressures were added in increments by increasing the density of the assumed fluid.

Plaut and Suherman (1998) examined geosynthetic tubes filled with dredged material or mortar in a two-dimensional analysis of the cross section. The tube was considered as a weightless membrane and inextensible. Some approximate analytical solutions were derived to avoid the complicated closed form solutions. For the case of a tube on a rigid foundation, the results depend on the internal pressure head, the density of the internal liquid, and the circumference of the tube. For another case, a partially or fully submerged tube, the results also depend on the external pressure head and the density of the external liquid. The hydrostatic pressure of the external water tends to decrease the tension in the tube. For the case of a tube on a tensionless Winkler foundation, the solutions depend on the foundation stiffness coefficient.

Plaut and Klusman (1999) investigated stacked tubes, filled with slurry, on a deformable foundation. The foundation was assumed to induce a normal upward pressure proportional to the downward deflection. The friction between the soil and structure was not considered, The bending stiffness and the extensibility of the tubes were neglected. Two types of stacked shape were examined; one type was the 1-1 formation, one tube on the bottom and the other tube on top, and the other was a stacked 2-1 formation with two tubes on the bottom and one tube on top, like a triangular shape. For both cases, an increase in the internal pressure head leads to increased tension and height of each tube. An increase in the foundation stiffness causes an increase in the total height of the stacked tube.

A computer program, GeoCops (Version 1.0), was developed to guide the selection of geosynthetic tube products as a dredged material containment system by Leshchinsky et al. (1996). The selection is based on partial safety factors for the seam strength, potential

installation damage, and possible degradation of the material. The program was verified with numerical and experimental results obtained by other investigators.

Different types of water-filled tubes, such as a tube with a wedge, two tubes in a sleeve, and a tube with an apron, were fabricated at Virginia Tech to examine the deformation and stability of tubes under increasing external water level (FitzPatrick et al., 2001). Interface tests also were conducted to determine the friction angle and the shear stiffness between two materials. The tests found that a tube with a wedge is the simplest configuration to set up, but the horizontal displacement of the tube begins to develop with low external water level and the displacement becomes large when the external water level reaches a critical level. Another discovery was that a tube with an apron is the most effective configuration of the three types of systems tested; the apron-tube dam can withstand an external water height as much as its height with a small length of apron. Tests on two tubes in a sleeve showed that a longer circumference of the sleeve can resist a higher external water level.

Analyses of water-filled tubes were carried out and presented in Huong (2001) and Huong et al. (2002) using FLAC (Version 3.4), a finite difference program. The material of the tube was considered as elastic with Young's modulus 1.0 GPa, the thickness of the tube was 0.0508 mm, and the weight of the tube was neglected. Different types of soil were tested as ground conditions numerically. Water was modeled as a hydrostatic pressure inside and outside of the tube. Also, a geomembrane filter and wedges were modeled to compare with the pilot tests done by FitzPatrick et al. (2001).

The water-filled tube was assumed to be unsealed; therefore the internal water pressure head remained constant during the analysis, in contrast to the field condition. The tests of tubes showed a change of internal water pressure head when the external water head increased.

It was found that the maximum tension decreases as the shear strength of the soil increases. However, the trend of the relationship between the soil and the maximum tension of the tube is not linear. For instance, the relationship between the tension of the tube and stiffness of the soil is somewhat linear when the soil is very soft, but other than

that, the maximum tension of the tube is reduced very slightly when the soil gets much stiffer. Also, stresses in the tube are most critical when the tube is resting on soil with a certain level of water inside the tube and without external water, just before the flood arrives, and the stresses are higher in the case of the tube lying on clay rather than on sand.

With a filter layer under the tube to prevent piping problems for sandy soil, and a proper block for keeping the tube from sliding, the tube usually fails in rolling at a critical external water height, about 70~85% of the tube's height depending on the size of the wedge and the internal water pressure head. Also, it was discovered that pore pressure in the soil has almost no effect on the rolling failure of the tube, because the weight of the water-filled tube is much greater than the uplifting force by pore pressure. But the pore pressure can surely affect sliding failure.

Moler et al. (2001) conducted tests of the stacked tube dam as a continuation of the previous tests by FitzPatrick et al. (2001). They examined the stability of the stacked tube dam with various strapping systems, and with different locations of the drain system. Also, more accurate measurement techniques were used to observe the relative deformations of the tubes. Thirteen tests of the stacked tube dams were carried out.

Also, tests were conducted to find accurate Young's modulus of the tube material and the strap material. Interface tests for defining the friction angle between the two tube materials and the tube and between the straps were carried out.

Chapter 3. Model Development

A finite difference program, FLAC version 4.0 (Itasca, 1999), is employed to analyze various types of water-filled tube dams numerically. Since a tube dam is made of a flexible geomembrane, deformations of the structure occur to a great extent when the dam is inflated with water inside and the inflated dam is then partially subjected to external water. Because of the nonlinear geometric characteristics of the deformations, the tube dam is analyzed using double-precision and a large-strain mode in FLAC.

The water-filled tube dam is modeled in two dimensions. Water-filled tubes have a larger dimension in the longitudinal direction compared to the transversal direction, and the external forces acting on the tube dam, and its deformations, do not vary much along the length.

By considering the water-filled tube dam as a plane strain problem in the numerical analysis, it is assumed that the end conditions in the longitudinal direction do not influence the outcome. It is noted that the ends of the tube dam in the longitudinal direction in the previous experiments were placed at the end of the sand box using grease, bentonite paste, and polyethylene sheets to reduce friction as much as possible.

The numerical modeling of a water-filled tube dam, which rests on the ground, requires the modeling of structures, soil, and fluid, and their interactions. Structural components, like the tube, apron, and straps, are modeled with beam elements. The soil and the drain are defined by grids (the drain is made of a geotextile material). The contact regions or expected contact regions between the tubes and between the tube and the foundation are equipped with interface elements. Water inside and outside of the tube or acting on the apron is modeled as a hydrostatic pressure. Groundwater flow is also induced by the difference of the head between the headwater side and the tailwater side, and this produces the pore pressures in the soil grid.

One of the results of the interactions of structure, soil, and fluid is the change of the internal water pressure head of the tube by external forces, mostly by the external water pressure. This state is artificially imitated by two iteration methods.

3.1. FLAC (Fast Lagrangian Analysis of Continua)

FLAC is an explicit finite difference program. It conducts a Lagrangian analysis for two-dimensional problems and it was originally developed for geotechnical and mining engineering (Itasca, 1999).

In the finite difference method, derivatives in the governing equations are converted to algebraic expressions in terms of variables at discrete points in space, whereas in the finite element method, the field quantities vary within each element in a certain fashion, such as shape functions or interpolation functions which involve parameters. Also, FLAC is well suited for modeling a physically unstable problem. When the physical system becomes unstable, the strain energy in the system is transmitted into kinetic energy. Since the dynamic equations of motion are incorporated in the formulations of FLAC, this process will be modeled directly without causing problems numerically. In addition, the explicit solution technique allows solution of the problems with accumulation of the timesteps. Each timestep is modified to be small enough to have a linear stress-strain relationship for the step, even for a nonlinear large-strain problem (Itasca, 1999).

FLAC allows users to easily investigate the parameters related to the soil. FLAC has interface elements to simulate distinct planes along which slip or separation can occur and the interface elements can be assigned between the grids, between beam elements, and between the grid and beam elements.

One of the other reasons for using FLAC in this study is FISH (FlacISH), the built-in programming language in FLAC. This feature allows the user to create new variables, functions, and sequence of procedures to achieve a better solution or to make difficult tasks easier.

3.2. Characteristics and Modeling of Materials and Interfaces

The structures involved, such as a tube, a strap, and an attached apron, are modeled with beam elements. The soil and the drain are defined by grids. The flow of the groundwater also is considered in variables in grids. Interface elements are employed here to represent constantly-changing contact regions between the tube dam and ground.

3.2.1. Geomembrane (Tube and Apron)

All water-filled tube dams were fabricated in the previous experiments with the same material, reinforced PVC (polyvinyl chloride). It is an 18-ounce coated vinyl with polyester reinforcement from the manufacturer, Detroit Tarp of Romulus, Michigan (FitzPatrick et al., 2001; Moler et al., 2001). A recent material property test of the tube was carried out by M. Moler, a graduate student in Civil and Environmental Engineering at Virginia Tech. The test was conducted utilizing a constant-strain-rate extensometer device, and the data were acquired by a laser extensometer. Various lengths of the material, from 42.3 mm to 165.1 mm, were tested.

The results show that the reinforced PVC has orthogonal properties; the Young's modulus in the circumferential direction of the tube and in the longitudinal direction are different. For the longitudinal direction of the tube, the stress versus strain relation is not linear because of the reinforcing fibers. The Young's modulus in that direction is 1.1 GPa when the stress is under 10 MPa. The secant modulus is 0.34 GPa when the stress is from 10 MPa to 18 MPa. However, in the circumferential direction of the tube, the material has almost a linear stress-strain relation with a lower Young's modulus, approximately E=0.12 GPa.

Therefore, the Young's modulus E=0.12 GPa for the circumferential direction is used in the analysis and a linear stress-strain relationship is assumed.

The thickness and the moment of inertia of the tube material for unit length, 1.0 m, are 0.508×10^{-3} m and 1.09×10^{-11} m^4, respectively.

3.2.2. Strapping Material

Straps were utilized in the stacked tube dam tests. The strap material used in the experiments was a woven nylon and had a width of 25.4 mm and a thickness of 1.6 mm. By the identical test as used with the tube materials, it was found that the tangent modulus is approximately 0.33 GPa when the stress level is 4 MPa, and the secant modulus is 0.20 GPa (Moler et al., 2001). Thus, 0.33 GPa is used here as Young's modulus and the stress-strain relationship is assumed to be linear.

3.2.3. Soil and Groundwater

The soil is defined as a grid and the total dimension of the grid is 3.25 m × 0.508 m. The grid consists of multifarious sizes of meshes as shown in Figure 3.1. The finest mesh is allocated at the top-middle part of soil, most of which is in contact with the water-filled tube dam. The size of the finest mesh is 1.25 cm × 1.25 cm.

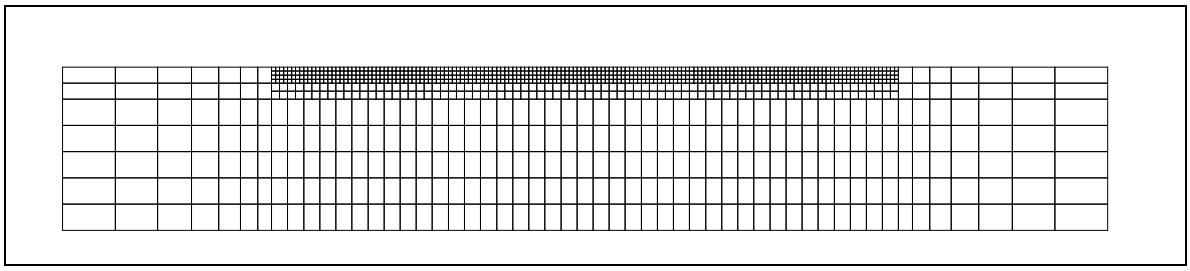

Figure 3.1. Example of grid

The mechanical boundary conditions are assigned at the left, bottom, and right edges of the grid. Pore pressures are initialized in every zone, assuming that the soil is fully saturated during the inflation of the tube. As the external water level rises, new pore pressure values are assigned at the surface of the grid on the headwater side, and at the left edge of the grid. The Mohr-Coulomb model is adopted to represent the silty sand foundation. The properties of soil used in the analysis are: dry density, 1600 kg/m^3; internal friction angle, 36 degrees; dilation angle, 7 degrees; Poisson's ratio, 0.292; bulk modulus, 16 MPa; shear modulus, 7.7 MPa; porosity, 0.4; and permeability, 0.02 mm/sec.

The bulk modulus of water in soil is taken as 100 Pa for the purpose of obtaining faster convergence in FLAC, instead of 2×10^9 Pa. The formulation of the adjusting water bulk modulus range for the numerical modeling is presented in the FLAC manual (Itasca, 1999). The range of water bulk modulus that can be used in this water-filled tube dam study was discussed by Houng (2001).

3.2.4. Interfaces

One of the unique characteristics of the analysis of water-filled tube dams on the ground is that there is no ordinary or typical boundary condition, such as a specified restraint on a degree of freedom. The tube dam can deform wherever the equilibrium of the structure leads it. Also, when the system becomes unstable, the structure may slide or roll on the ground.

In addition, the contact region between two components (e.g., tube and soil) changes constantly. It may be impossible to simulate these behaviors of the system without proper interface elements. The interface element in FLAC is represented by Coulomb sliding and/or separation, and can have the properties of friction, cohesion, dilation, normal and shear stiffnesses, and tensile strength to simulate accurately.

The interfaces of the water-filled tube dam models are defined by shear and normal stiffness and friction angle in this study. It is assumed that the cohesion between geomembrane and soil or between two geomembrane materials is negligible. Thus, the frictional resistance is directly related to the friction angle.

The interface properties between the geomembrane and foundation materials utilized in the experiments were evaluated by FitzPatrick et al. (2001) using the shear box test. The geomembrane (tube material) on the silty sand gives a peak friction angle of 34 degrees and a residual friction angle of 32 degrees. The geomembrane contact with geotextile material (drain) gives 17 degrees for both peak and residual friction angles. Therefore, the residual friction angles are used in the modeling of the interfaces. The evaluated shear stiffnesses between the geomembrane and the silty sand, and between the geomembrane and the geotextile, are 50 MPa and 70 MPa, respectively.

The friction angle between the geomembrane and the strapping materials, and between two geomembranes used in the experiments, were investigated by Moler et al.

(2001) using the shear box test. The friction angles between the geoemembrane and the strapping materials were evaluated as 25 degrees and 18 degrees for the peak and residual values, respectively. Again, the residual friction angle is employed as the friction angle in the numerical model.

The interface test between the two geomembranes showed a very scattered distribution in terms of the peak friction angles and large differences between the peak and the residual friction angles with strain softening after the peak. It was suspected that the scatter was caused by the initial alignment of the materials at the time of the test. Also, it was assumed that the woven surfaces cause interlock between two geomembrane materials and produce high peak friction angle values. The values are 54 degrees and 14 degrees for the peak and the residual friction angle, accordingly. The residual friction value of 14 degrees is chosen as the friction angle in this study for conservative calculations.

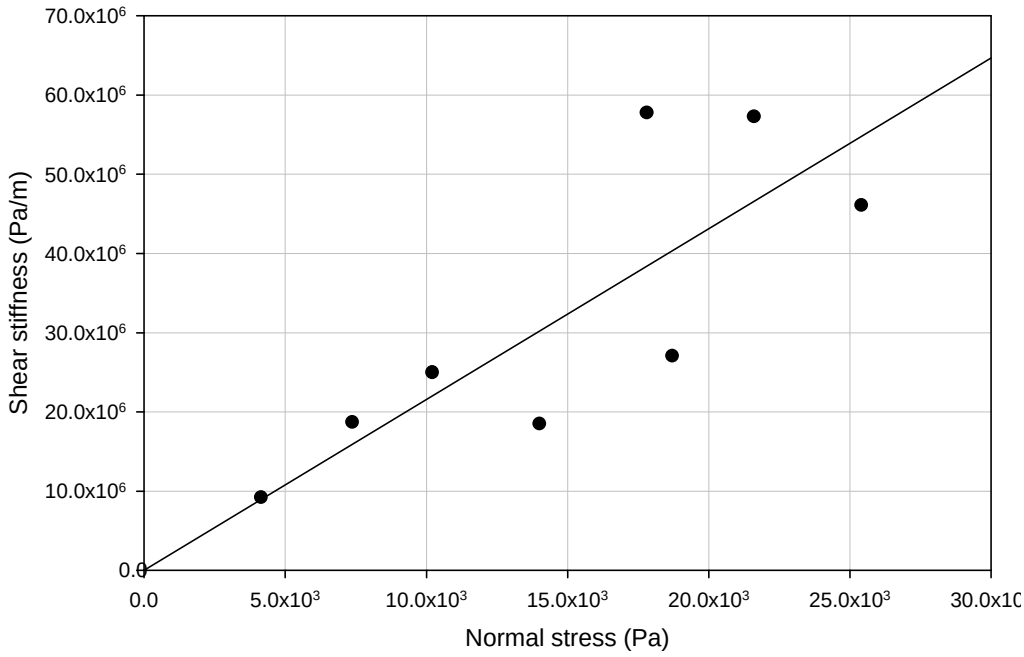

Figure 3.2. Shear stiffness distribution of the interface between two geomembrane materials

The shear stiffness estimations from the test also display scatter as shown in Figure 3.2. Considering the range of the normal stress of the water-filled tube dams studied in this research, the shear stiffness is assumed to be 10 MPa.

3.3. Hydrostatic Pressure

Since water has no shear resistance and can be considered as incompressible, the internal water and the external water are modeled as hydrostatic pressures. The pressures, which are applied to the elements in the normal direction, are converted to point loads with x, y components at each node of the beam elements as shown in Figure 3.3. The components of the point load can be defined as in Equations (3.1) and (3.2). As the beam elements deform during the inflation and flooding, the magnitudes of the point load's components are continuously altered.

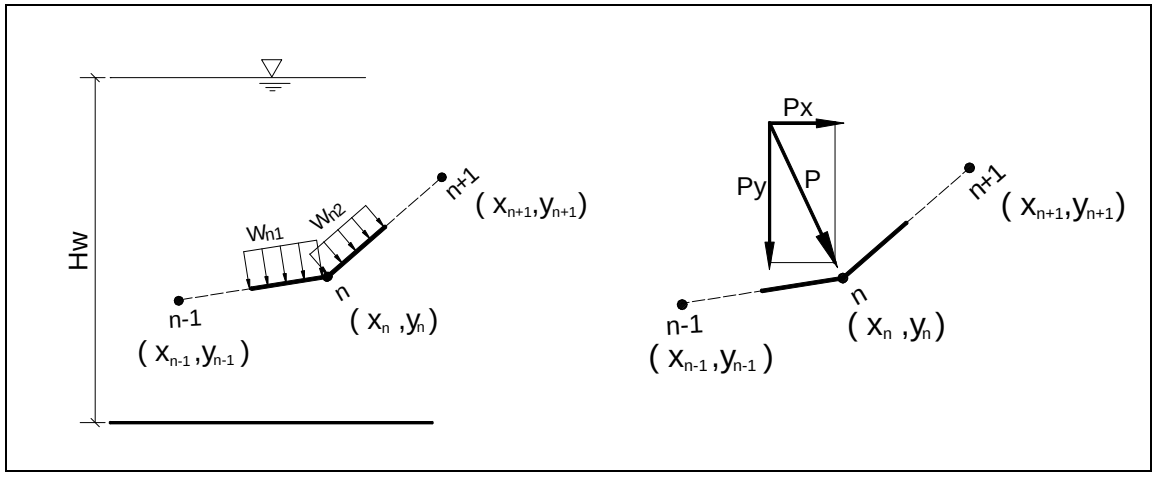

Figure 3.3. Transformation from pressures to a point load

$$P_x = w_{n2}\left(\frac{y_{n+1} - y_n}{2}\right) + w_{n1}\left(\frac{y_n - y_{n-1}}{2}\right)$$

Equation 3.1

$$P_y = w_{n2}\left(\frac{x_{n+1} - x_n}{2}\right) + w_{n1}\left(\frac{x_n - x_{n-1}}{2}\right)$$

Equation 3.2

where, $w_{n1} = \left\{H_w - \left(y_n - \frac{y_n - y_{n-1}}{4}\right)\right\} g_w$, $w_{n2} = \left\{H_w - \left(y_n + \frac{y_{n+1} - y_n}{4}\right)\right\} g_w$

g_w : Specific weight of water

H_w: Water pressure head

In addition, moments are generated by the pressures. At node n, two moments are produced by the pressures which act on the adjacent two beam elements. Since the two moments have opposite signs, the sum of the two moments at node n is not considerable. Therefore it is assumed that the moments can be neglected as loads in the numerical calculation. Further discussions are presented in Chapter 4.

3.4. Change of Internal Water Pressure Head

The previous experiments on water-filled tube dams conducted by FitzPatrick et al. (2001) and Moler et al. (2001) showed that the internal water pressure head of the tube changes when the external water level increases. The tube is sealed after the inflation and the total volume of water is not changed during deformation because of incompressibility. Thus, the internal pressure head changes as soon as the deformation occurs in the cross section of the tube, when the tube is subjected to external water. It is noted that very little deformation was observed in the longitudinal direction of the tube in the experiments.

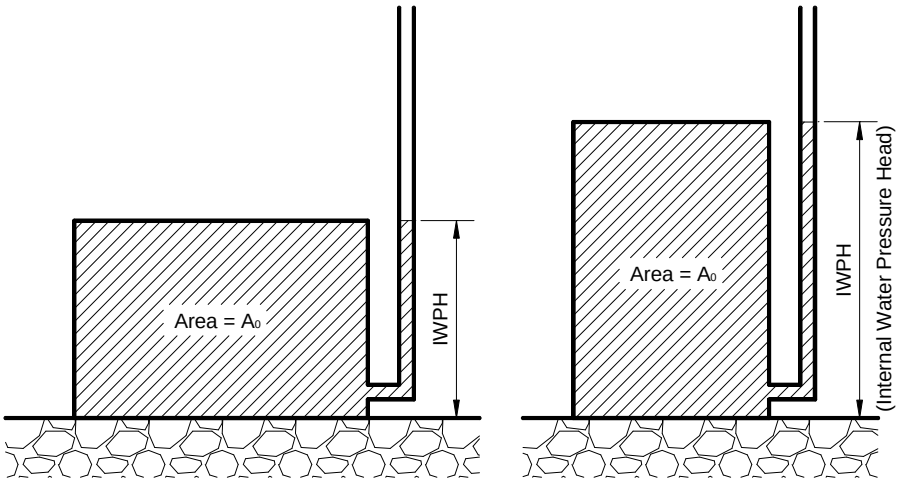

(a) Initial shape (b) Deformed shape

Figure 3.4. Change of internal water pressure head

This phenomenon can be explained easily by considering a very flexible rectangular section in two dimensions. Here, the volume of a tube is represented as the area of the section. First, assume that somehow the section of the water-filled tube is rectangular (Figure 3.4(a)) with the internal water pressure head the same as the height of the section, for simplicity. If the tube is subjected to uniform pressure at the left side, the tube may deform as in Figure 3.4(b), since the area of the tube cannot be changed because the tube is sealed. Therefore the vertical deformation of the tube causes a change of internal water pressure head of the tube.

The previous analysis done by Huong (2001) disregarded the effect of internal water pressure head change of the water-filled tube. It assumed that the tube is not sealed and so the area of the tube cross section can be changed and the internal water pressure head remains constant when the tube is subjected to external force[1]. But it was observed that the internal water pressure head of water-filled tubes varied up to 10~15 % according to the tests. Also, it was reported that the pressure head increased more than 50% for the test of a stacked tube dam (Moler et al., 2001).

Therefore, for more accurate numerical simulation of water-filled tubes, it is assumed that the cross-sectional area of the tube remains constant in this research. Two iteration methods are developed using FISH to satisfy the constant tube area assumption.

3.4.1. Secant Method

To simulate the change of the internal water pressure head to keep the tube area constant, the secant method is employed. The procedure is described from step 1 to step 5 in the next paragraph with an example of the rise of internal water pressure head during the flooding. The sequence of iterations was programmed initially as shown in Figure 3.5 from point 0 to point 1, then point 2, and so on. Since the secant method requires another initial estimate for the next IWPH, at STEP 3 the $IWPH_2$ is just evaluated as a factor of $IWPH_1$. From the estimation of $IWPH_3$, the secant method is used.

---

[1] However, Huong did make use of pressure results from the experiments in some of his numerical calculations.

- **STEP 1:**

The tube is inflated with an initial internal water pressure head ($IWPH_0$) and the initial tube area ($TAREA_0$) is measured when there is no external water.

- **STEP 2:**

After external water is applied to the headwater side of the tube, the area of the deformed tube ($TAREA_1$) is measured. At this step, the $IWPH_1$ is the same as $IWPH_0$.

- **STEP 3:**

If the difference of tube areas ($TAREA_1$ - $TAREA_0$) is positive, a new trial internal water pressure head ($IWPH_2$) is assigned as the initial internal water pressure head ($IWPH_0$) with a reduction; if it is negative, the initial internal water pressure head with an increment is assigned as the new internal water pressure head. The magnitude of the reduction or the increment is adjusted based on the situation.

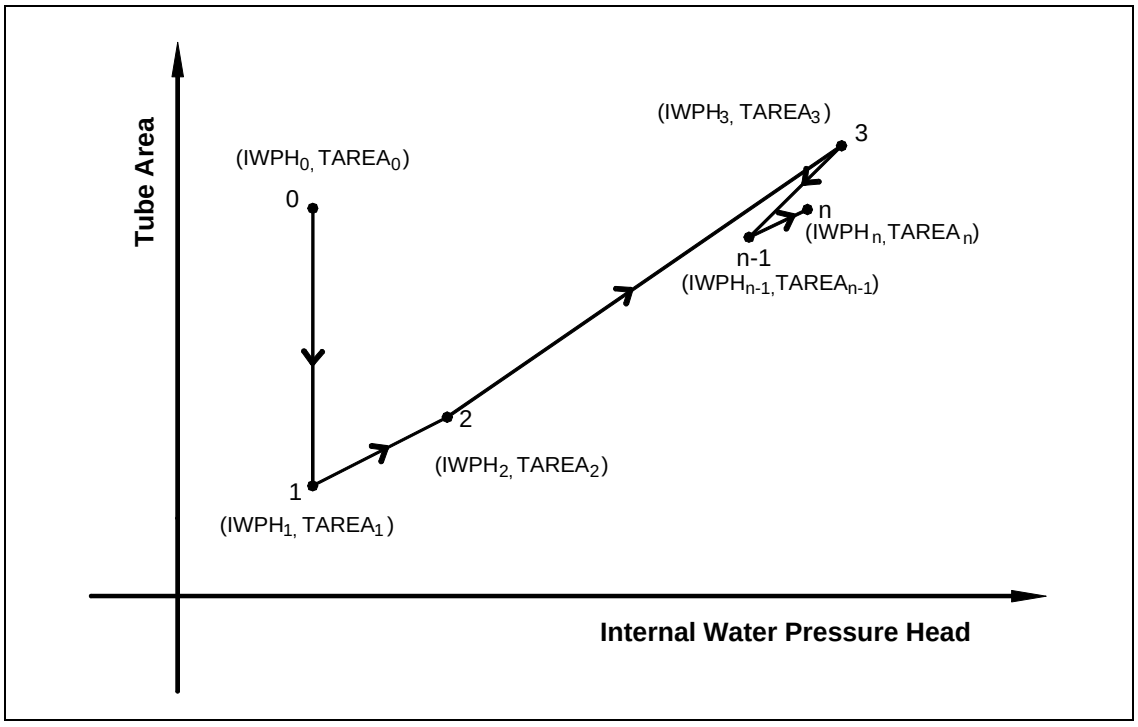

Figure 3.5. Iterative procedure using secant method

- **STEP 4:**

Recalculate the tube area ($TAREA_2$) based on the new internal water pressure head ($IWPH_2$) from step 3. Then, a linear equation can be found from two sets of internal water pressure heads and tube areas as follows

$$IWPH_3 = \frac{IWPH_2 - IWPH_1}{TAREA_2 - TAREA_1}\left(TAREA_0 - TAREA_1\right) + IWPH_1$$

Equation 3.3

- **STEP 5:**

Calculate the tube area ($TAREA_3$) again with the new internal water pressure head ($IWPH_3$) from the equation of step 4; if the new area is not the same as the initial area of the tube, then STEP 4 and STEP 5 are repeated until the difference of tube areas ($TAREA_i$ - $TAREA_0$) is negligible. The Equation (3.3) can be generalized as follows to calculate $IWPH_{i.}$ for $TAREA_0$:

$$IWPH_i = \frac{IWPH_{i-1} - IWPH_{i-2}}{TAREA_{i-1} - TAREA_{i-2}}\left(TAREA_0 - TAREA_{i-2}\right) + IWPH_{i-2}$$

where $i \geq 3$

Equation 3.4

The procedure of the iteration was modified to cope with the characteristic of the path dependency of soil and flow problems (Figure 3.6). The solution of structural problems with static loads and elastic properties does not depend on the stress-strain path, but soil and flow problems do, because soil is modeled here using a Mohr-Coulomb model (plastic) and flow in the ground is time-dependent. For example, the numerical analysis continues from point *2* to point 3 and so on until it finds the final IWPH of the tube. The soil underneath the tube can be overloaded at one point and underloaded at the next point throughout the iteration process. To avoid these undesirable situations, the sequence of the procedure is revised from point 0 to point 1, from point 0 to point 2, and so on. However, the new $IWPH_i$ is still predicted by extrapolating a tangent of the TAREAs to the IWPHs. When the new iteration is proceeded with $IWPH_i$, the pressure head is increased from the

initial water pressure head ($IWPH_0$) to the current pressure head in the revised secant methods.

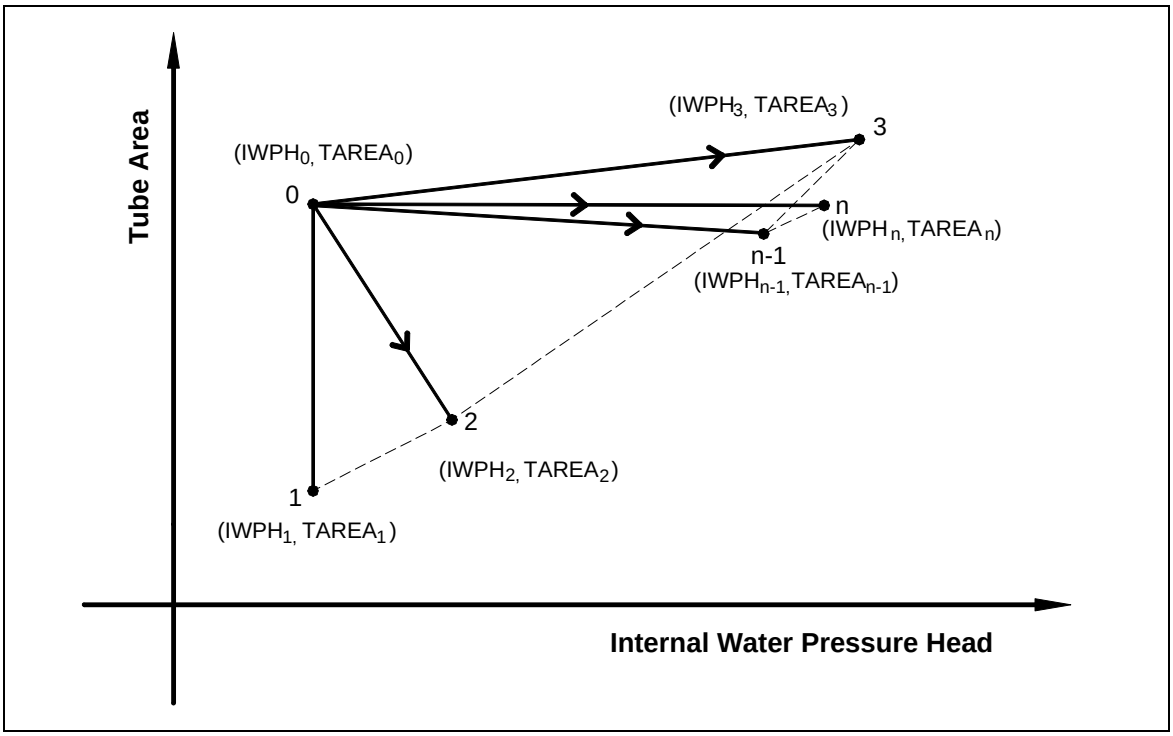

Figure 3.6 Revised iterative procedure using secant method

3.4.2. Factored Secant Method

The procedure presented in the previous section basically finds the unknown IWPH using the secant method. During the numerical studies of the water-filled tube dam, it was found that the internal water pressure head of the tube influences the stability of the dam. So it may be critical to simulate the change of water pressure head of the tube realistically for the investigation of the critical external water height.

For example, the internal water pressure head of a single tube dam decreases when the external water height increases, and the water pressure head in the tube is changed from the initial water pressure head to the new pressure head directly in the physical world. However, in the numerical analysis, the new IWPH can be computed to be less than the final IWPH with the current secant method during the iterations. As a result, the water-

filled tube dam can fail by this incorrect estimation of the IWPH. Thus it is vital to develop a new iteration technique to determine the new IWPH within the range from the initial IWPH to the unknown final IWPH.

The new iteration method is developed by modifying the previous secant method. It is based on the assumption that $IWPH_i$ gets close to the final IWPH as the number of iterations increases. Thus, the later calculated IWPH gets more credibility while the early calculated IWPH gets less credibility during the iterations. For example, $IWPH_9$ will have a closer value to the unknown final IWPH than, say, $IWPH_4$ or $IWPH_7$, when iterations continue, therefore $IWPH_9$ is reevaluated with a higher value of the factor, while $IWPH_4$ or $IWPH_7$ is adjusted with a lower value.

The factored secant method can be expressed with Equation 3.5 and Equation 3.6. The new IWPHs from equation (3.4) are adjusted to $IWPH^f$ using a factor a_i in the new method as follows:

$$IWPH_i^f = a_i IWPH_i$$

Equation 3.5

$$a_i = (A + Bi) \leq 1.0$$

Equation 3.6

where $i \geq 3$

A and B: Positive real numbers and less than 1.0

The factor, a_i, grows to 1.0 during the iterations. For example, when A and B are both 0.1, a_3 becomes 0.4, a_6 is 0.7, and $a_9 = a_{10} = a_{11}$ are all 1.0. A and B are determined based on the deformation characteristics of a tube dam. If the IWPH is predicted to change rapidly as a tube deforms, A will be assigned a greater value. If the area of the tube changes sensitively depending on the IWPH, B will be assigned to a much lower value. The new iteration method is called here the “factored secant method”.

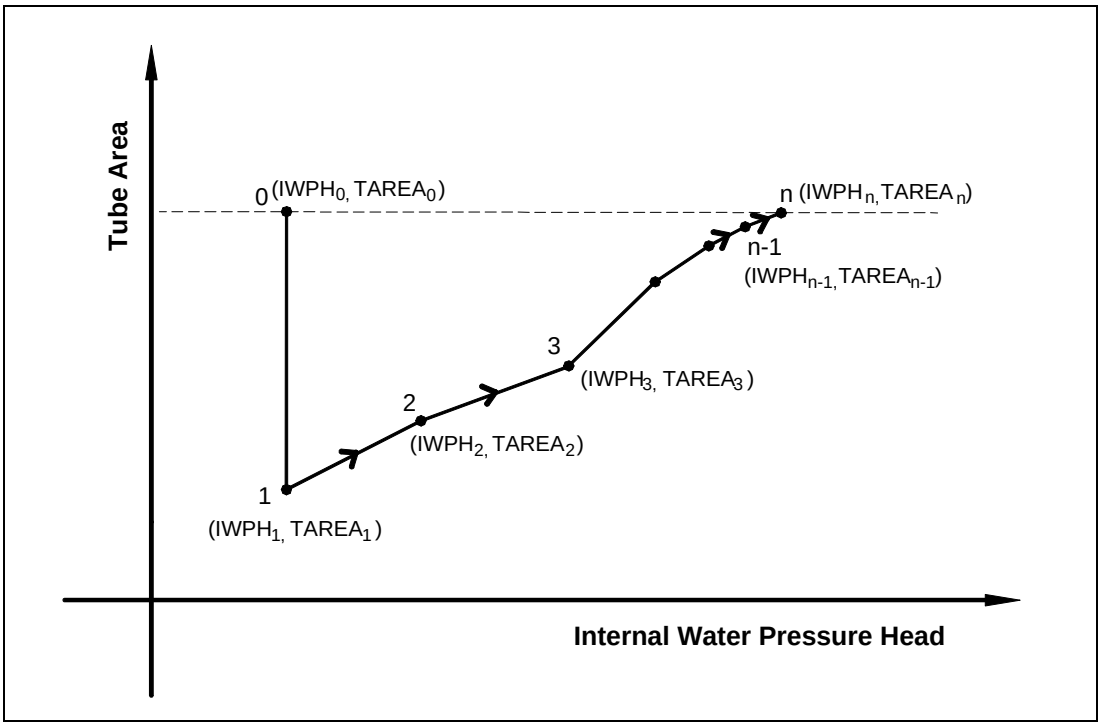

Figure 3.7. Factored secant method

Figure 3.7 illustrates the factored secant method with a case of increase of the internal water pressure head at flooding. Similar to the previous method, the third IWPH is evaluated from a linear interpolation of points 1 and 2. Then the increment of IWPH from point 2 to point 3 is reduced by a factor since the new IWPH should not be larger than the unknown final IWPH. If the factor, a_i, is always 1.0, the current method is identical with the secant method. The factor in the early stage of iterations is less than 1.0 and grows gradually to 1.0 as the iteration continues and TAREA converges to the initial tube area.

Since IWPH always increases from one iteration to the next, for example, point 2 to point3 in Figure 3.7, there is no need to restart from point *0* to point *i* as in the previous method. However, even though the number of required iterations for the factored secant method is generally more than for the first method, the time consumed for convergence to the initial tube area is not longer than for the first procedure.

Chapter 4. Preliminary Study

4.1. Effect of Young's Modulus

The Young's modulus of the reinforced PVC membrane was measured by M. Moler et al. (2001). As results, the Young's moduli for the longitudinal and the circumferential direction are 1.1 GPa and 0.12 Gpa, respectively.

The measurement of Young's modulus varies depending on the size of the specimen and the testing method[1]. Also, a geomembrane can be made of different materials such as HDPE (high density polyethylene), EPDM (ethylene propylene diene terpolymer), ECB (ethylenecopolymer bitumen), and PVC (polyvinylchloride), and Young's moduli of the geomembranes differ along with the materials (Van Santvoort, 1994). Since Young's modulus is an essential property in the numerical modeling, the effect of Young's modulus of a water-filled tube is investigated in this section as a preliminary study.

The tube is modeled with 102 beam elements to form the initial shape, which is a long capsule shape, "$\subset\supset$". The thickness of the tube is 0.508 mm and the moment of inertia is 1.09×10^{-11} m^4 for unit length 1.0 m. Four different values of Young's modulus are used in this investigation, 1.0 GPa, 0.5 GPa, 0.2 GPa, and 0.12 GPa. A linear stress-strain relationship is assumed.

The tube is assumed to lie on the rigid ground with its circumference 1.4859 m, and is inflated by internal water pressure head 0.4458 m which is 0.3 as normalized pressure head[2]. The deformed shapes, tensile forces, and moments, when the tube is not subjected to external water, are examined.

---

[1] The specimens were tested using laser extensometer and machine extension measurement

[2] Normalized Pressure Head (N.P.H.) = water pressure head divided by the circumference of the tube.

The numerical results show that the Young's modulus of the tube membrane does not affect the deformation of the cross-section of the tube significantly. The differences of the height of the tube or the contact length among the four materials are not noticeable (Figure 4.1). The tube with Young's modulus E = 1.0 GPa has the lowest tube height, and the tube with E=0.12 GPa has the highest height, which is reasonable.

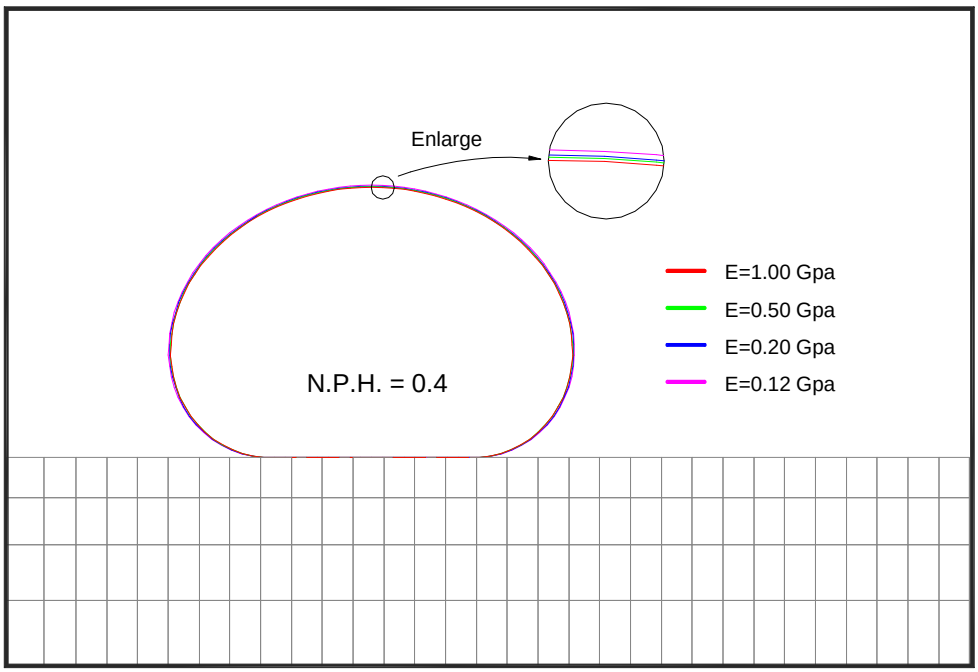

Figure 4.1. Comparison of deformed shapes (water-filled tube); N.P.H.=0.4

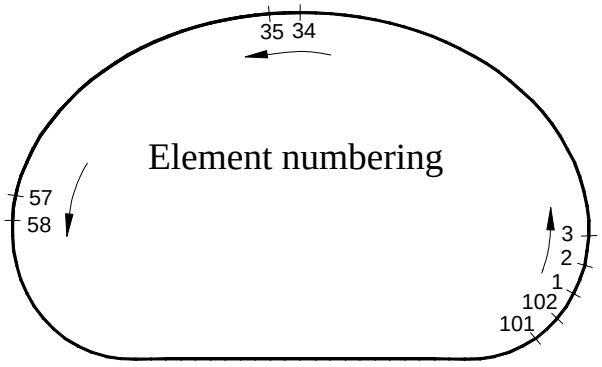

Figure 4.2. Element numbering of the tube

The element numbers of the tube are presented in Figure 4.2. The element number starts from the lower right and increases in the counter-clockwise direction. The graph of the tensile force is shown in Figure 4.3, and the tensile force is given as a negative number by FLAC. The maximum tensile value occurs in the non-contact region, between element numbers 1 and 72 or 73, and from 95 or 96 to 102, and the values for four different cases are almost the same, about 453 ~455 N. It can be concluded that Young's modulus does not influence the maximum tensile magnitude very much. But a change in Young's modulus causes some difference in the tensile force in the contact region (Figure 4.3).

In contrast to the graph of tensile forces, the moments in the tube show more variation with the Young's modulus of the tube (Figure 4.4). But the range of moment values is small. Because the thickness of the tube is small, the moment of inertia is almost zero and the tube is very flexible.

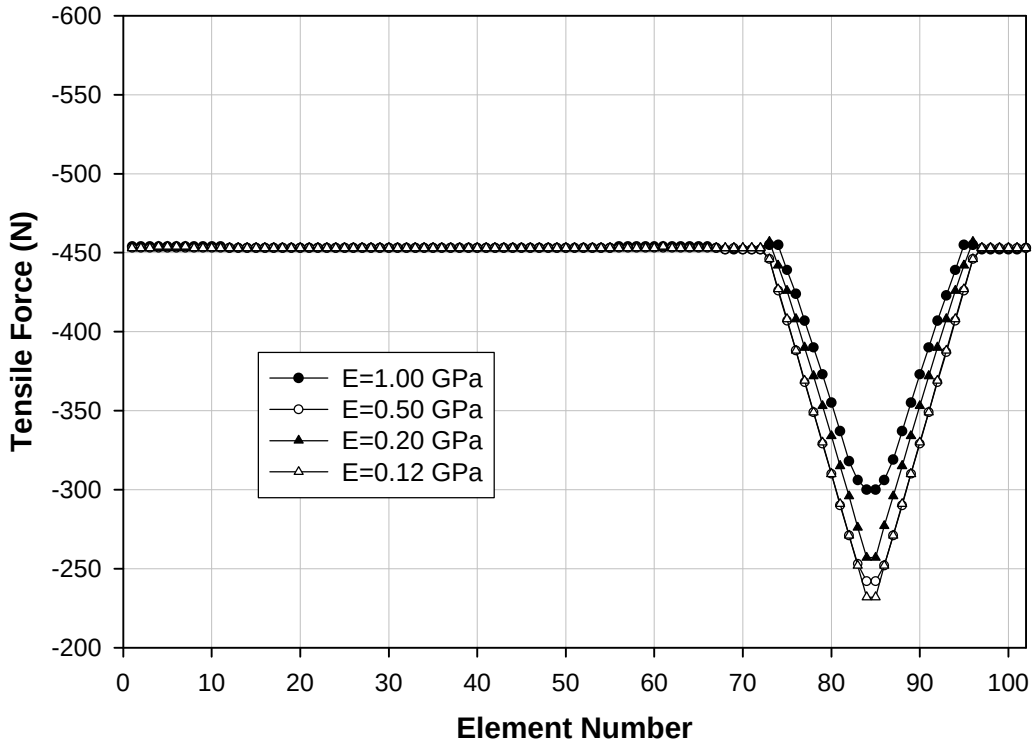

Figure 4.3. Comparison of tensile forces (N.P.H. = 0.3)

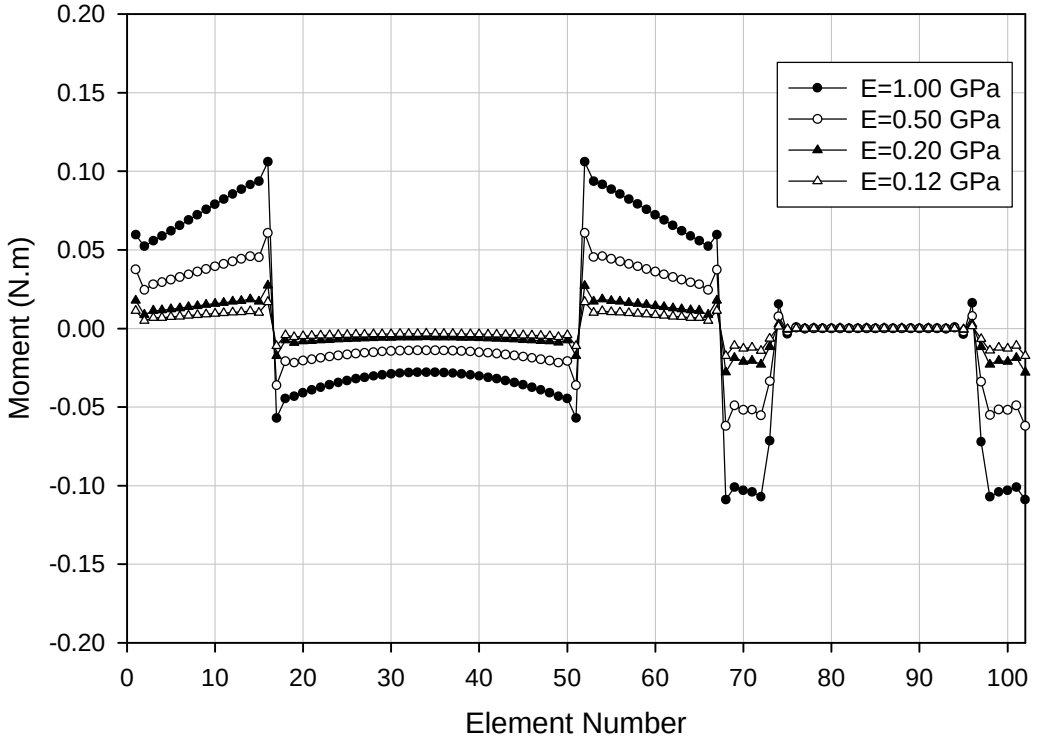

Figure 4.4. Comparison of moments (N.P.H. = 0.3)

4.2. Effect of Internal Water Pressure Head

The water-filled tube is modeled similarly to that of section 4.1, a tube on a rigid foundation with Young's modulus 0.12 GPa. The tube is inflated by different water pressure heads. The value of the water pressure is normalized by the circumference of the tube and noted here as N.P.H (Normalized Pressure Head). The other properties are the same as for the tubes of section 4.1.

The deformed shapes of the tubes are presented in Figure 4.5 for N.P.H. = 0.3, 0.4, and 0.5. The height of the tube increases and the contact length of the tube decreases as the internal pressure head increases.

It was discovered that the tensile force is mainly dependent on the internal water pressure head (Huong, 2000). The tensile force graph (Figure 4.6) shows that maximum tensile forces are approximately 450, 750, and 1050 N when normalized pressure heads are

0.3, 0.4, and 0.5, respectively, except in the contact region. The absolute values of the tensile forces in the contact region are lower than the tensile forces in other areas.

The moments in the tube are very low and the differences between the cases are very small.

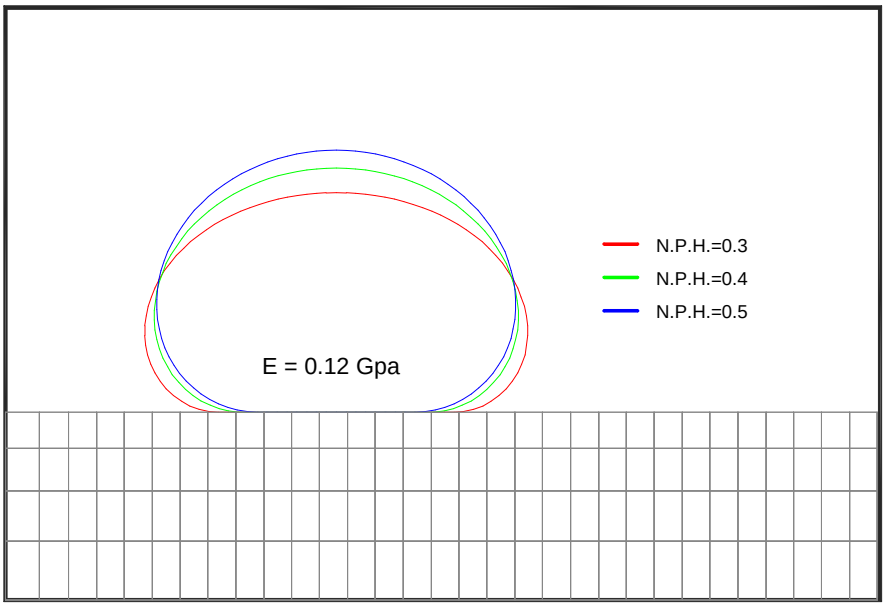

Figure 4.5. Deformed shapes of tubes for different pressure heads

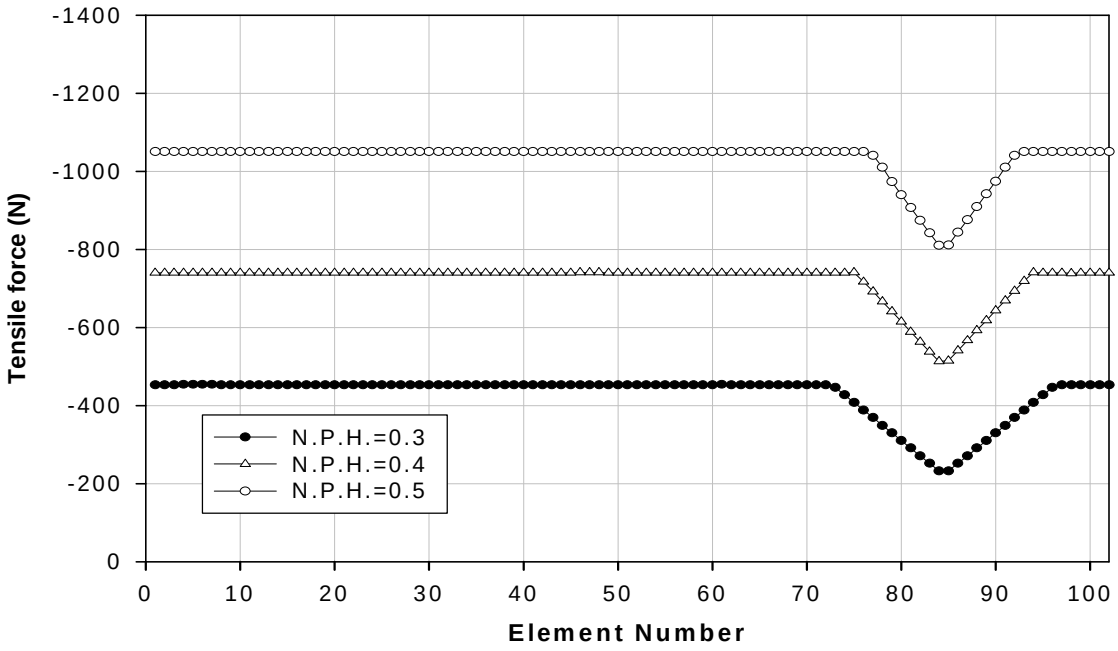

Figure 4.6. Comparison of tensile forces (E=0.12 GPa)

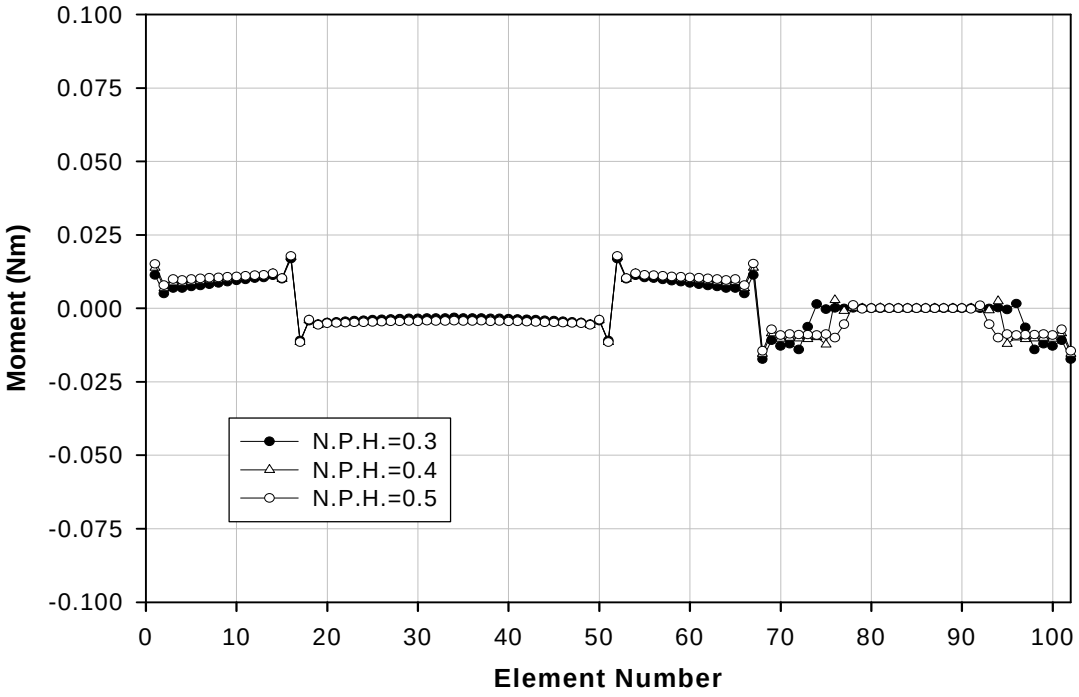

Figure 4.7. Comparison of moments (E=0.12 GPa)

4.3. Effect of Inclusion of Moments

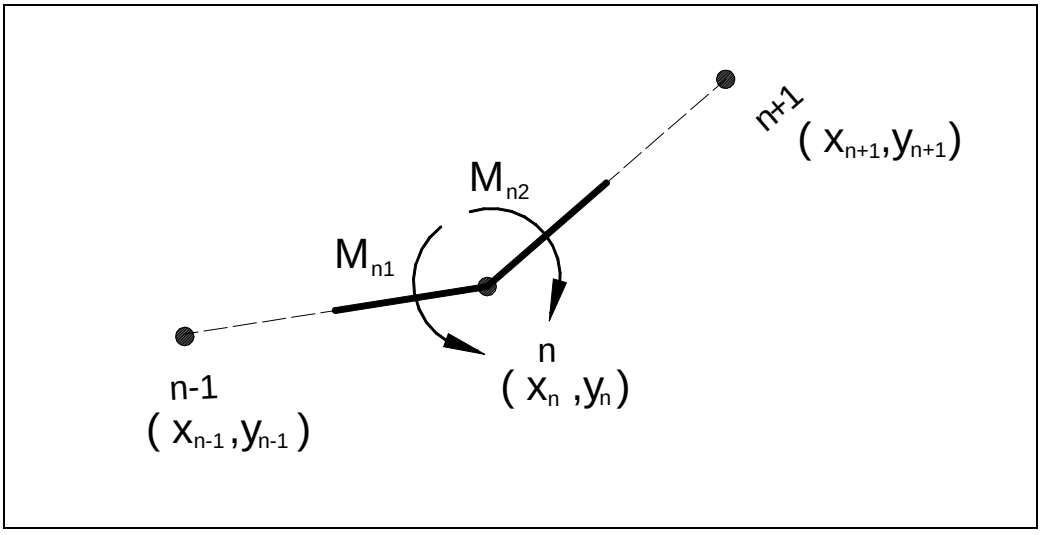

Figure 4.8. Moments at a node

It is assumed that the moments, which are induced by the pressures, are negligible since the moment at the node n, M_n, is the sum of the two moments, M_{n1} and M_{n2} (see Figure 3.3 and Figure 4.8). The moments, M_{n1} and M_{n2}, are given in Equation 4.1 and Equation 4.2. If the distances between adjacent pairs of two nodes (n-1 and n, and n and n+1) are the same and the pressures w_{n1} and w_{n2} are identical, the moment at the middle node (n) becomes zero. In our water-filled tube model, the distances between two adjacent nodes are the same since the length of a beam element is determined by dividing the circumference by the total number of beam elements. However, the pressures are not equal; the pressure varies linearly along the beam elements.

$$M_{n1} = \frac{w_{n1}}{8}\left(\left(x_n - x_{n-1}\right)^2 + \left(y_n - y_{n-1}\right)^2\right)$$

Equation 4.1

$$M_{n2} = -\frac{w_{n2}}{8}\left(\left(x_{n+1} - x_n\right)^2 + \left(y_{n+1} - y_n\right)^2\right)$$

Equation 4.2

Therefore, a tube dam model with moments numerically analyzed and the results are compared with the numerical results from the current tube dam model, which does not involve the moment in the formulation. The same circumference and number of beam elements as in the previous study are used. The applied pressures for the inflation are 0.3 and 0.5 in normalized terms. The material properties are the same and Young's modulus of 0.12 GPa is employed.

Figure 4.9 and Figure 4.10 depict the numerical results of moments. The solid dots and the hollow dots present results when the moments from the pressure are included in the loads and when only the point loads from the pressure are included, respectively. The difference between the two models is not considerable, as shown in both figures. The moments are exactly the same between the two models at the bottom of the tube since the pressures are the same between the neighboring elements of that region and the lengths of the beam elements are equal. Therefore, neglecting the moment loads is acceptable.

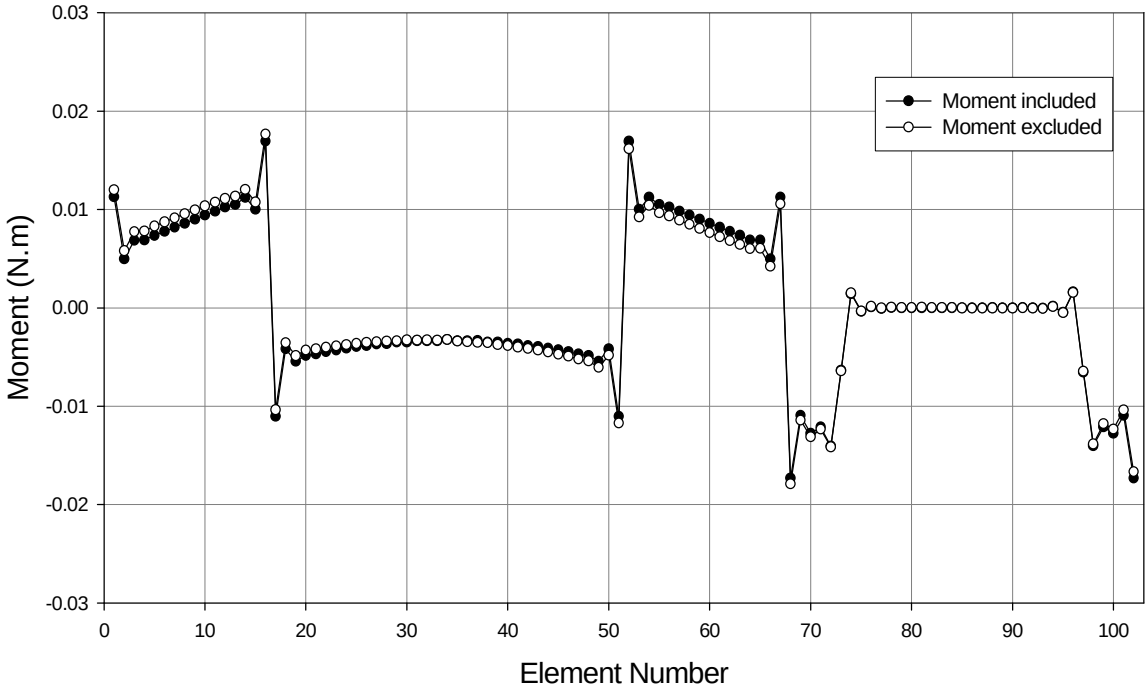

Figure 4.9. Comparison of moments (N.P.H=0.3)

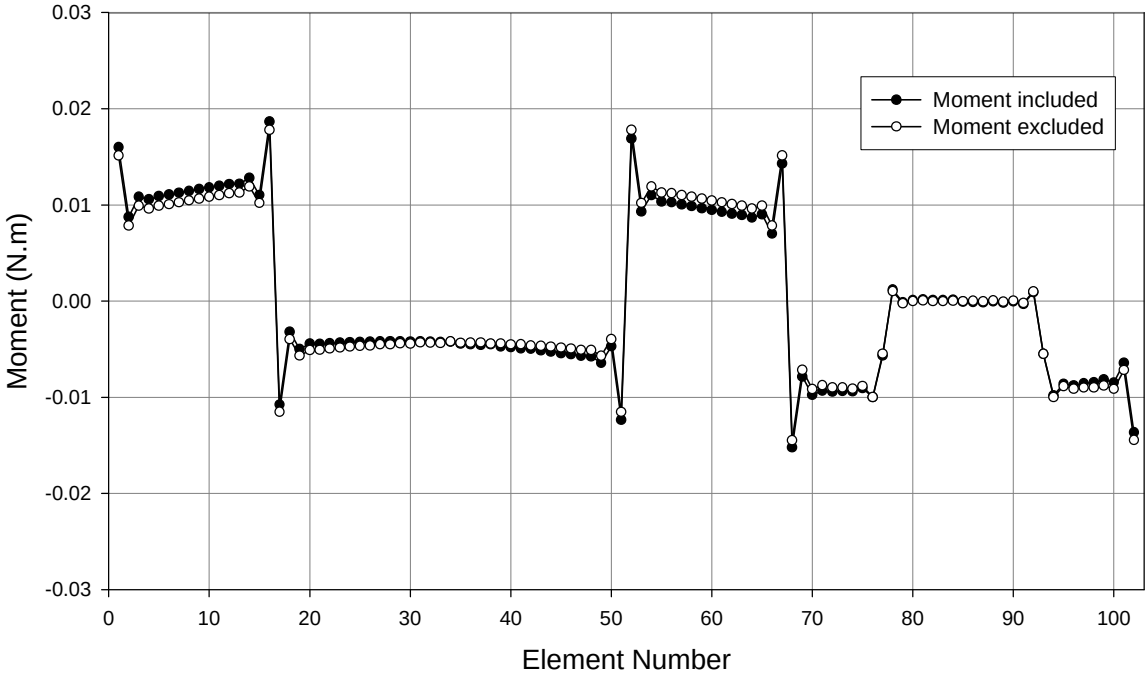

Figure 4.10. Comparison of moments (N.P.H=0.5)

4.4. Investigation of Analytical Solution

Analytical solutions for the cross-sectional shape and circumferential tension have been developed and presented previously in the literature (Namias, 1985; Plaut and Suherman, 1997). Since the closed form analytical solution involves elliptic integrals, approximate solutions were offered using expansion forms of the elliptic integral (Plaut and Suherman, 1997). Here, these approximate formulas are evaluated and compared with the exact formulas.

First, the exact and the approximate formulations of the tube for the parameter k, the contact length, and the width of the tube are briefly introduced.

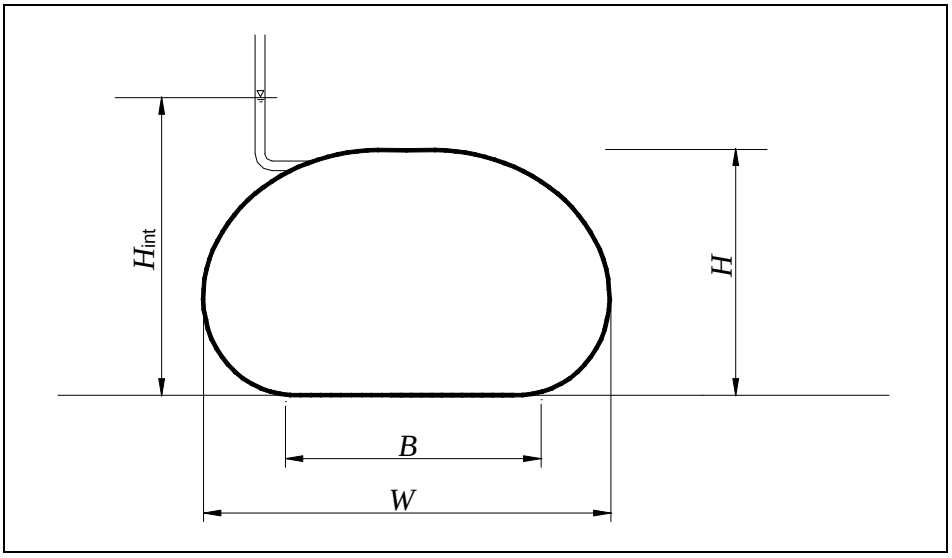

Figure 4.11. Notations of tube cross section

The analytical solutions are formulated considering a tube on a rigid and horizontal foundation. The tube is assumed to be inextensible, weightless, and filled with incompressible fluid with unit weight g_{int}. The pressure head of the fluid inside the tube is H_{int}, and the width and the contact length of the tube are denoted here as W and B as shown in Figure 4.11.

The formulations are derived in terms of nondimensional quantities as in Equation 4.3 for convenience. P_{bot} is the pressure at the bottom of the tube and L is the circumference of the tube. The circumferential tension of the tube is notated here as T.

$$b = \frac{B}{L}, \qquad w = \frac{W}{L}$$
$$h = \frac{H}{L}, \qquad h_{\text{int}} = \frac{H_{\text{int}}}{L}, \qquad p_{bot} = \frac{P_{bot}}{g_{\text{int}} L} = h_{\text{int}}, \qquad t = \frac{T}{g_{\text{int}} L^2}$$

Equation 4.3

The analytical solutions of the shape and the tension in the tube were derived in terms of a parameter k. The definition of the parameter k is the following, and the derivation and the limitation can be found in the literature (Namias, 1985; Plaut and Suherman,1997):

$$k = \frac{2\sqrt{t}}{p_{bot}}$$

Equation 4.4

The k can be calculated from the following Equation 4.5 as a condition, where $K(k)$ and $E(k)$ are the complete elliptic integrals of the first and the second kind, respectively.

$$2\left[K(k) - E(k)\right] p_{bot} = 1$$

Equation 4.5

The contact length and the width of the tube can be assessed using k and t from the above equations:

$$b = 1 - 2k\sqrt{t}K(k)$$

Equation 4.6

$$w = b + 2\left[E\left(\frac{p}{4}, k\right) - \left(1 - \frac{k^2}{2}\right)F\left(\frac{p}{4}, k\right)\right] p_{bot}$$

Equation 4.7

where F and E are elliptic integrals of the first and the second kind, respectively. Since the determination of the contact length and the width together with k requires solving the complicated equations, approximate solutions were developed (Plaut and Suherman, 1997). The alternative approximate equations are:

$$k^2 \cong \frac{2}{p\, p_{bot}} - \frac{3}{2p^2 p_{bot}^2} + \frac{3}{8p^3 p_{bot}^3}$$

Equation 4.8

$$k^2 \cong 1 - 16\exp\left[-\frac{1}{p_{bot}} - 2\right]$$

Equation 4.9

If the normalized pressure, p_{bot}, is less than 0.35, which gives k close to 1.0, Equation 4.9 should be used. For other cases, Equation 4.8 can give k parameters properly. Equations for contact length, b, and width, w, which do not involve elliptic integrals, are:

$$b \cong 1 - p\, k\sqrt{t}\left(1 + \frac{1}{4}k^2 + \frac{9}{64}k^4 + \frac{225}{2304}k^6\right)$$

Equation 4.10

$$w \cong \frac{1}{2}\, p_{bot} k^2 \left(2 + \frac{k^2}{16}(12 - p) + \frac{3k^4}{64}(12 - p)\right)$$

Equation 4.11

First, the assessment of the parameter, k, is discussed since the analytical solutions of the cross-sectional shape and the tensile force of the tube are derived in terms of this parameter.

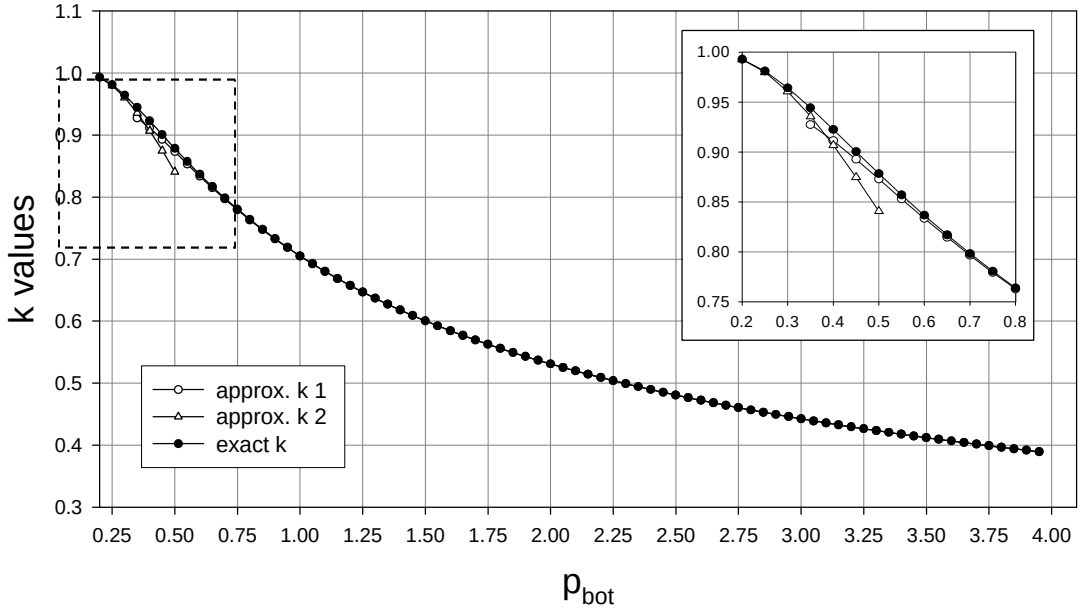

Figure 4.12. Comparison of k

Figure 4.12 displays the k parameters from two approximate formulas, Equation 4.8 and Equation 4.9, and the exact solution, Equation 4.5. When the normalized pressure head of the tube is very low, less than 0.35, Equation 4.9 gives a very good estimation for the exact k. As the normalized pressure head increases, the approximate k from Equation 4.8 produces excellent agreement with the exact k.

It is noted that the exact k values are employed in the following comparisons for a fair assessment of the approximate equations.

Figure 4.13 illustrates the tube contact length b. The contact lengths from the exact formulation, Equation 4.6, and the approximate formulation, Equation 4.10, are represented here as black dots and hollow dots, respectively. The difference between the two formulas is much higher at low pressure heads. For example, the exact contact length, b, is 0.23 and the approximate contact length is 0.37 when the normalized pressure head is 0.30. The difference is about 60 percent. But the approximate formulation shows better agreement with the exact solution as the normalized pressure head increases. Especially if the normalized pressure head is greater than 1.0, there is no distinguishable difference between the two formulas.

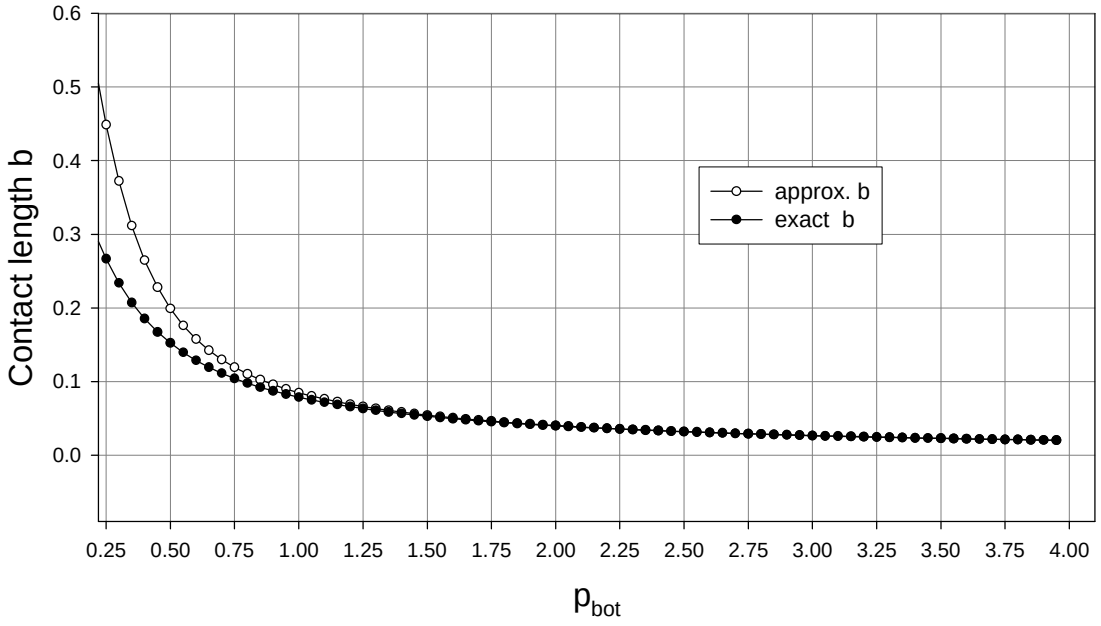

Figure 4.13. Comparison of contact length b

During this study, it was found that the approximate formula for the tube width, Equation 4.11, was not derived correctly. The approximate solution of the tube width should be given by the following equation, and it contains the tube contact length, b. It is noted that the exact solution for the width also involves the contact length, b.

$$w \cong \frac{1}{2} p_{bot} k^2 \left\{ 1 + \frac{k^2 p}{32} - \frac{k^4 (3p - 10)}{64} \right\} + b$$

Equation 4.12

Figure 4.14 displays the results from this formula for the tube width. The new approximate formulation is evaluated with the exact b and the approximate b, and these are plotted in Figure 4.14 with the hollow triangular and the hollow squares, correspondingly. The exact values from Equation 4.7 are displayed as black dots. The new approximate solution gives a fair assessment if the exact contact length b is used, even if the normalized pressure head is not high.

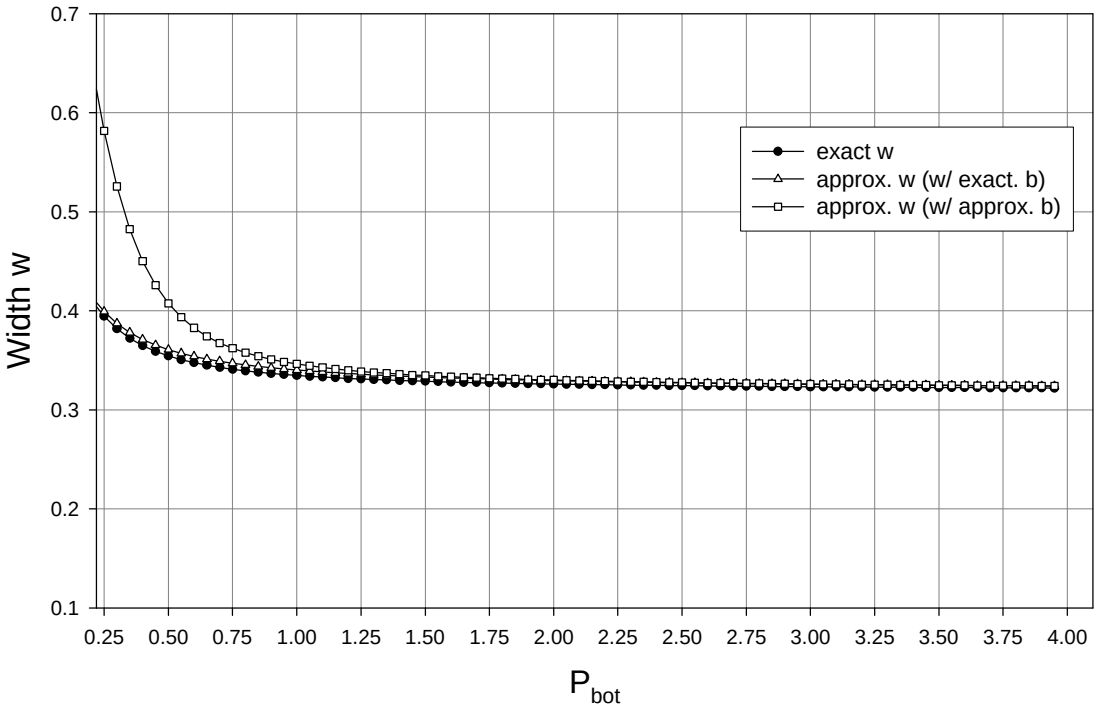

Figure 4.14. Comparison of width w

The following conclusions are drawn from the comparisons of the exact and the approximate formulations.

The parameter *k* can be assessed fairly accurately by the approximate equations. However, the proper equation should be chosen between two approximate formulas depending on the normalized pressure head. The contact length from the approximate formulation is a crude estimation when the normalized pressure head is less than 1.0. As a result, the approximate formulation for the width also gives an unsatisfactory result since the formulation constitutes the contact length term. But if the contact length from the exact solution is used in the approximate equation for the width, the result is very competitive with the exact width. Overall, when the normalized pressure head is greater, the results from the approximate formulations are more accurate.

4.5. Comparison of Numerical and Analytical Result of Tube

The numerical results and analytical calculations for tube height and tube area are discussed here, when there is no external water. The tube is assumed to be extensible and to lie on the deformable foundation in the numerical simulation in FLAC, while the analytical calculations are based on an inextensible tube and an extensible tube set on a rigid foundation.

The formulas for tube height and tube area of an inextensible tube were developed using elliptic integrals by Namias (1985), and approximate formulas are also available in expansion forms of the elliptic integrals. It is found that the approximate formulas cannot provide suitable results if the range of normalized internal water pressure head is less than 1.0, even with a few higher expansion terms, especially in the range of normalized pressure head in this study. Therefore, the analytical results of the tube height and tube area of the inextensible tube here are obtained by elliptic integrals using the Microsoft IMSL MATH/LIBRARY by FORTRAN programming.

The analytical solutions for the cross-section of an extensible tube on rigid foundation are briefly introduced here and they were derived by R. Plaut (see Figure 4.15):

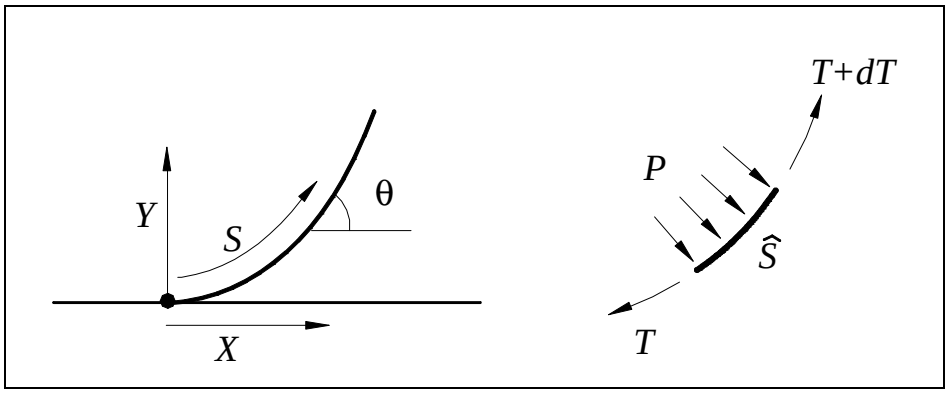

Figure 4.15. Notations of extensible tube

$$\frac{dT}{d\hat{S}} = 0, \qquad Tdq = Pd\hat{S}, \qquad d\hat{S} = (1+e)dS$$

Equation 4.13

where $e = \frac{s}{E} = \frac{T}{E \cdot h_t}$ and h_t is the thickness of the tube and E is Young's modulus of the tube material.

The above formulations are very similar to those in the inextensible tube case (Namias, 1985, Plaut and Suherman, 1997) except for the new variable $\hat{S}$. The formulations of the cross-section of the tube have the following relationships, similar to the inextensible tube case with additional terms involving $e = T/Eh_t$;

$$\frac{dX}{dS} = (1+e)\cos q = (1+\frac{T}{E \cdot h_t})\cos q$$

Equation 4.14

$$\frac{dY}{dS} = (1+e)\sin q = (1+\frac{T}{E \cdot h_t})\sin q$$

Equation 4.15

$$\frac{dq}{dS} = \left(\frac{1}{T} + \frac{1}{E \cdot h_t}\right)(P_{bot} - g_{\text{int}} Y)$$

Equation 4.16

The above equations can be normalized with the following relationships, L is the original circumference of the tube and g_{int} is the specific weight of the internal fluid:

$$x = \frac{X}{L}, \qquad y = \frac{Y}{L}, \qquad s = \frac{S}{L}$$

$$t = \frac{T}{g_{\text{int}} L^2}, \qquad e_t = \frac{E h_t}{g_{\text{int}} L^2}$$

Equation 4.17

Therefore, the normalized cross-section of the tube can be found from the next three equations.

$$\frac{dx}{ds} = (1 + \frac{t}{e_t})\cos q$$

Equation 4.18

$$\frac{dy}{ds} = (1 + \frac{t}{e_t})\sin q$$

Equation 4.19

$$\frac{dq}{ds} = (\frac{1}{t} + \frac{1}{e_t})(p_{bot} - y)$$

Equation 4.20

Since e_t is a constant, the above equations can be solved using a shooting method in Mathematica with the boundary conditions $x = y = q = 0$ at $s = 0$. The height of the tube is the maximum value of y, Equation 4.19, and the area of the tube is evaluated by integration of the shape.

The maximum height of the inextensible tube in Figure 4.16, which is presented as a dashed line, is the diameter of a circle which has the circumference of the tube. If the foundation is rigid, the tube shape will approach a circle as the internal pressure of the tube increases to a very high value. The maximum area of the inextensible tube also can be found in a similar way.

Because the tube is assumed to be extensible in the numerical calculations, the tube height and tube area by numerical simulation are greater than by the analytical solution for an inextensible tube. Overall, differences between these two results in the range of IWPH of this study are not great.

Even though the analytical formulas of the extensible tube were developed based on the assumption of a tube on a rigid foundation, the comparisons between the numerical values and analytical results for an extensible tube in Figure 4.16 and Figure 4.17 exhibit no distinguishable differences. They agree very well with each other, because the simulated foundation in the numerical analysis is not very soft and does not have a significant deformation under the tube weight (Huong, 2001). If the pressure head is increased to a

much higher value, the difference between the analytical solution of the extensible tube on the rigid foundation and the numerical result of the extensible tube on the deformable foundation will be noticeable. However, the pressure heads used in the inflation of the water-filled tube dam are usually less than 1.0 in terms of normalized pressure head.

Therefore it can be concluded that both analytical formulations of the inextensible and extensible tube have very competitive results with the numerical results in the range of IWPH (internal water pressure head) from 0.35 m to 0.75 m, which are from 0.25 to 0.50 in normalized pressure head.

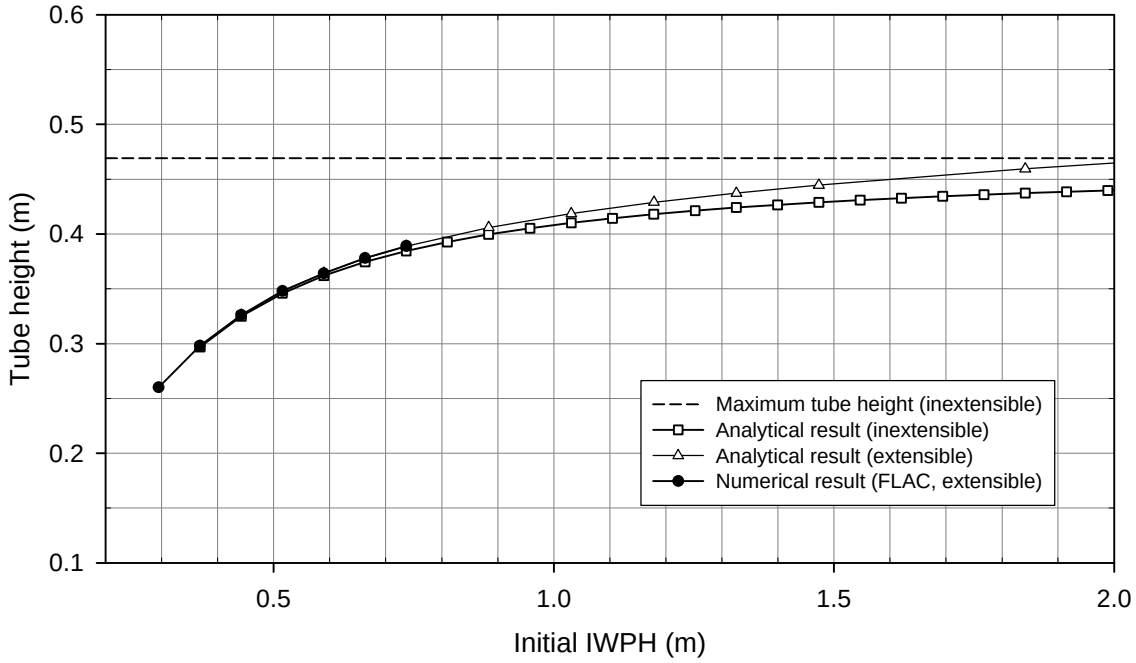

Figure 4.16. Comparison of tube heights in numerical and analytical results (initial circumference of the tube = 1.4732 m)

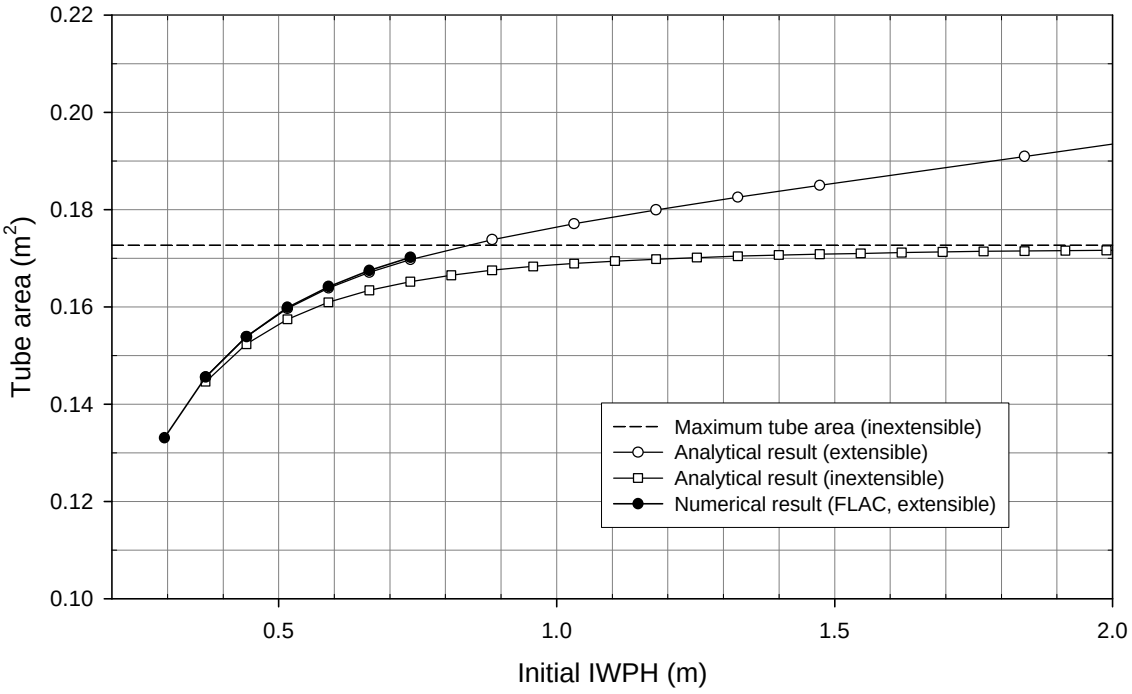

Figure 4.17. Comparison of tube areas in numerical and analytical results (initial circumference of the tube = 1.4732 m)

Chapter 5. Apron-tube Dam

5.1. Introduction

An apron-tube geomembrane dam consists of one tube and a layer of apron on one side. The apron is made of one sheet of geomembrane, which is attached to the top of the tube, and overlaps about half of the top surface of the tube as shown in Figure 5.1. The apron-tube dam is set up on the ground to resist floodwaters on the headwater side. Part of the apron-tube dam may be placed on a drain.

The apron provides more stability than a tube dam without an apron, because additional friction between the apron and the ground makes it possible for an apron-tube dam to resist more external force. Another reason is that the apron forms a thin barrier between the external water and the tube, especially close to the ground; because of this barrier, the external water pressure hardly acts near the bottom of the tube to lift it, which could increase instability of the apron-tube dam if there were no apron.

Experiments of apron-tube dams were conducted at Virginia Tech by FitzPatrick and Nevius (FitzPatrick et al., 2001). Several lengths of apron were tested to study the deformation and stability. The circumference of the tube was 1.4732 m (58.0 in.) for all tests and the lengths of the aprons were 0.25 m (10 in.), 0.30 m (12 in.), 0.41 m (16 in.), 0.56 m (22 in.), 0.76 m (30 in.), and 1.07 m (42 in.). The apron and tube both were constructed of the same reinforced PVC material and the apron was connected to the tube using glue.

Because the tube was sealed after inflation and the volume of the tube dam could not be changed when the tube dam was deformed by external water pressure, a change of the internal water pressure head was observed during the increase of the external water in the tests. The simulation of the change of internal water pressure head is achieved numerically by adopting the secant iterative procedure in the analysis.

Apron lengths of 0.25 m, 0.30 m, 0.41 m, and 0.56 m are modeled, and the tube is inflated with the same initial internal water pressure head (IWPH) as in the tests numerically to compare the deformations and the critical external water level of each case, and to verify the numerical modeling. In addition, tensions in the apron and the tube and friction between the ground and the apron, and the ground and the tube, are investigated to understand the behavior of the apron-tube dam more comprehensively.

Furthermore, the effects of different initial shapes of the apron, and the critical external water levels based on the internal water pressure head of the tube, are studied. Also, the relationship of the friction angle between two materials and the critical external water level will be studied, since the friction angle can vary for different types and conditions of soil, geomembrane, and geotextile.

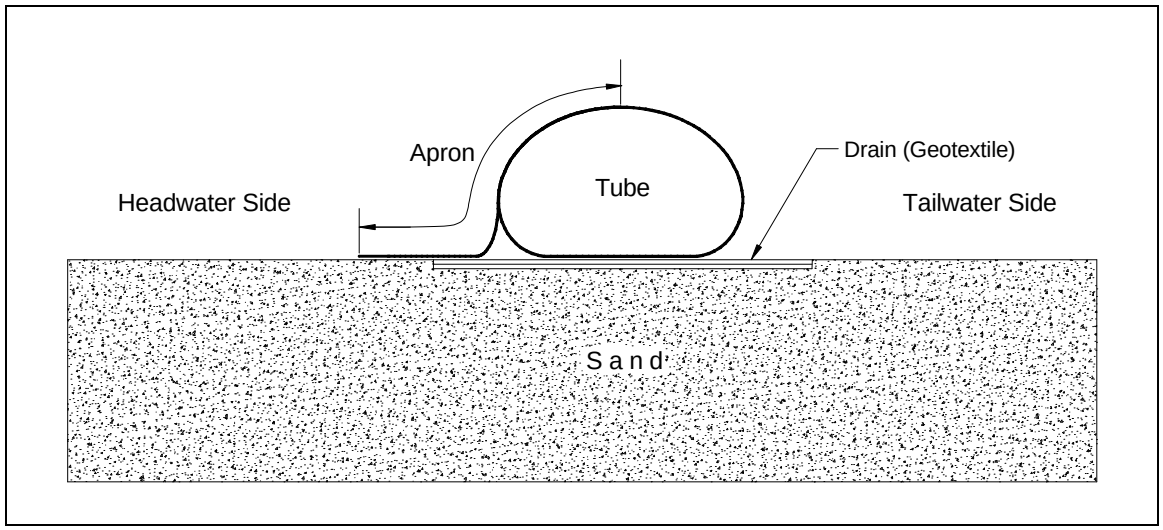

Figure 5.1. Apron-tube dam

5.2. Numerical Modeling

5.2.1. Outline of Modeling

The apron and tube are modeled using beam elements. The beam elements in FLAC are two-dimensional elements with three degrees of freedom at each end node: x-translation, y-translation, and rotation.

The tube is formulated with 102 beam elements from 102 nodes and the initial shape is a long capsule shape, "⊂⊃", since the tube is empty in the beginning (Huong, 2001). An apron is attached at the top of the tube after inflating the tube with initial internal water pressure. The apron consists of 61 elements with 62 nodes for the 0.25 m apron, and the numbers of nodes and elements of the apron increase as the length of the apron increases.

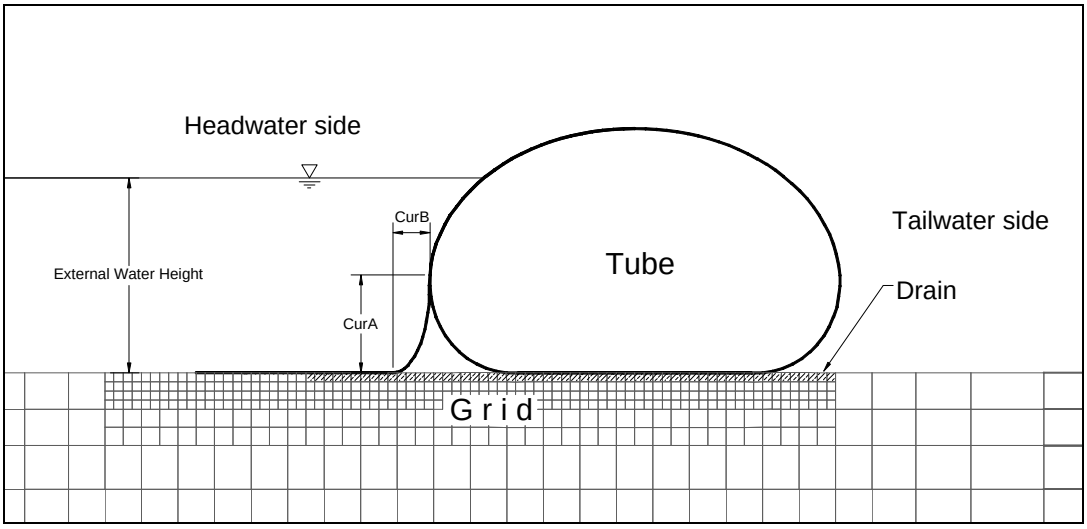

Figure 5.2. Modeling of the apron-tube dam

The initial shape of the apron is divided into three parts: apron on the tube, apron curve, and apron on the ground. The beam elements of the apron on the tube lie along the inflated tube. The apron curve forms one-quarter of an ellipse with radii of CurA and CurB; CurA is the distance from the ground and the leftmost point of the tube, and CurB varies depending on how the apron tube is installed (see Figure 5.2). CurA is predetermined by the shape of the tube, and for CurB, 5.08 cm (2.0 in.) is used for comparison with the tests.

The properties of the tube and the apron are the same since they are constructed with identical material. Young's modulus E=0.12 GPa is used for the analysis and a linear stress-strain relationship is assumed. Other properties of the tube and the apron are introduced in Section 3.2.1.

The soil is defined as a grid mesh. Two types of constitutive models are used in the study. The Mohr-Coulomb model, which represents sand well, is mainly used in this numerical study, and the elastic isotropic model is employed during the development of

programs for the numerical analysis. The properties of soil which are used in the analysis are listed in Section 3.2.3.

The interface elements are assigned in the expected contact regions, between the headwater side of the tube and the apron, between the apron and the soil, between the apron and the drain, and between the tube and the drain. The properties of the interfaces are discussed in Section 3.2.4.

5.2.2. Numerical Analysis Procedure

It is clear that the numerical analysis of an apron-tube dam requires many user-defined functions and needs the main programs to control these functions in FLAC, because of the complexity of the problem. Since the apron-tube dam is made of very flexible material and deformation of the system is large, the applied loads on the elements, which are transformed from the hydrostatic pressures, are not constant during the procedure, even if the water pressure head is constant. Also, the apron-tube dam goes through a change of internal water pressure when the external water pressure is applied. Several programs are developed to account for these effects in the analysis.

The program may be divided into several program units. The first program unit is developed to install and inflate the tube on the ground with initial internal water pressure head and to attach the apron on the tube. The second program unit involves application of the external water pressure on the apron and development of flows in the soil based on the level of external water. The last program unit is the main control program; it raises the external water level with given values and the most important thing is that it controls the internal water pressure head of the tube. The following sections will describe these steps in detail.

The analysis of the apron-tube dam is divided into several processes listed below. The processes from 1 through 3 and 4 are controlled by the first and second program unit, respectively. The processes 5, 6, and 7 are run by the third program unit.

It is noted that parts of the processes from 1 through 4 were developed by Huong (2001). Some modifications are made to the processes to obtain more accurate solutions and

faster running times, since the solution requires several iterations in the processes from 5 to 7.

1) The soil mesh grid is formed and a tube having the shape of a long capsule is formed with beam elements.
2) The tube is inflated with initial internal water pressure gradually to simulate the real situation and to stabilize the deformation of the tube; since the tube goes through large deformation, it is proper to not apply all the water pressure in one step.
3) An apron is attached. The part of the apron on the tube is predetermined by the shape of the tube. For the free part, an apron curve is defined by a quarter of an ellipse with two radii, CurA and CurB (see Figure 5.2). The rest of the apron is placed on the ground in a straight line.
4) With given external water height, the external water pressure is applied to the apron and the headwater-side surface of the soil. The pore pressure boundary conditions are reassigned at the left edge of the soil grid and the headwater-side surface of the soil and the flow is activated in the soil meshes.
5) After the apron-tube and soil system reaches equilibrium, the area of the deformed tube is measured and the IWPH is adjusted using the secant method or the factored secant method.
6) The process 5 is repeated until the area of the tube has converged to the initial area of the tube within a specified tolerance, from 0.05 % to 0.1 %.
7) With new given external water height, the processes 4, 5, and 6 are repeated.

5.3. Numerical Simulation of Test

Since the modeling of the apron-tube dam resisting the external water involves fluid, soil, and flexible structures and their intricate interaction, the verification of the numerical simulation can be accomplished by a comparison with the tests. Also, a more comprehensive understanding of the behavior of the apron-tube dam may be achieved by this investigation.

The “apron length” is defined here as the horizontal distance between the end of the apron and the leftmost point of the tube. The apron may be divided into two parts; one is the part of the apron on the sand and the other is the apron on the drain. The “apron on drain” part does not contact entirely with the drain; part of it is free from contact (see Figure 5.3).

A tube dam with different lengths of apron is simulated to compare with the tests; 0.25 m (10 in.), 0.30 m (12 in.), 0.41 m (16 in.), and 0.56 m (22 in.) apron lengths are modeled. The same initial internal water pressures from the tests are applied to inflate the tube, and the same location and length of the drain are used. Table 5.1 shows the initial parameters that are used in the numerical analysis. The circumference of the tube is 1.4732 m for all cases.

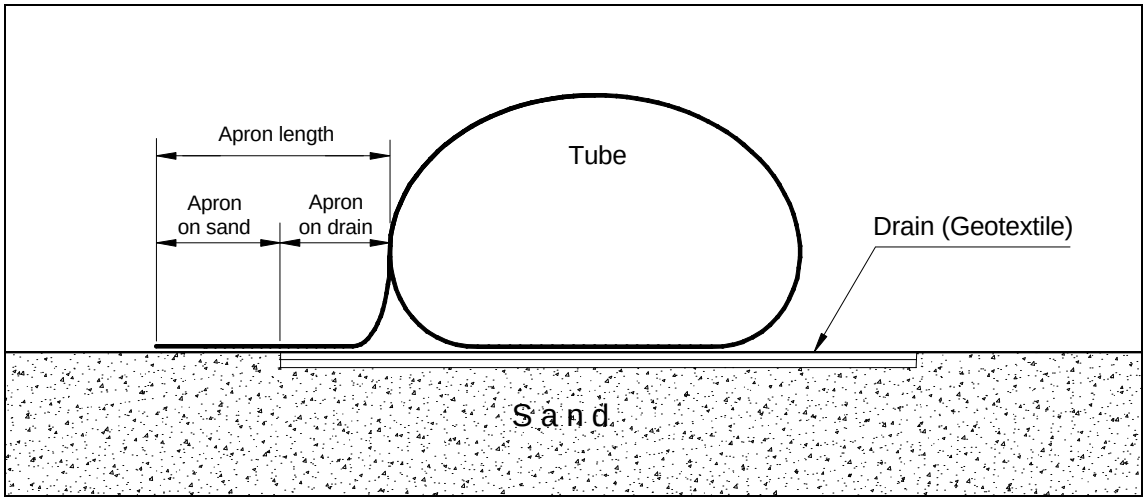

Figure 5.3. Designation of Apron

Table 5.1. Initial conditions of apron-tube dam

Apron Length		Apron on Drain (filter)		Apron on Sand		Initial IWPH
in.	m	in.	m	in.	m	m
22	0.56	8	0.20	14	0.36	0.475
16	0.41	8	0.20	8	0.20	0.492
12	0.30	5	0.13	7	0.18	0.470
10	0.25	6	0.15	4	0.10	0.475

5.3.1. Critical External Water Height

The critical external water height is the height of the floodwater level from the ground that makes the apron-tube dam fail. The critical external water level is a very important factor for this kind of tube dam system; if it is impossible to predict the critical external water level, users cannot utilize the tube dam system with confidence. Table 5.2 shows the comparison of the critical external water level from the numerical analysis and the tests for the apron-tube dams.

For apron lengths 0.25 m and 0.30 m, the apron-tube dams fail at 0.25 m and 0.32 m of external water level, respectively, in the numerical analysis, but at 0.26 m and 0.28 m in the experiments. Both 0.41 m and 0.56 m apron lengths can withstand the external water level as high as the height of the apron-tube dam in both numerical and experimental investigations.

Therefore it is clear that the apron provides resistance to the movement of the dam, and the length of the apron is the main factor for the stability of the apron-tube dam system. But the proper length of the apron cannot be easily determined. It may be different from one situation to another; it could be affected by the type of soil, conditions of the ground, and the material of the apron-tube dam. However, the most certain fact is that a longer length of apron provides more stability.

Table 5.2. Critical external water height of apron-tube dam

Apron Length	Critical External Water Height	
	Numerical Result	Experimental Result
0.25 m (10 in.)	0.254 m	0.260 m
0.30 m (12 in.)	0.317 m	0.280 m
0.41 m (16 in.)	At top of tube	At top of tube
0.56 m (22 in.)	At top of tube	At top of tube

5.3.2. Change of Internal Water Pressure Head (IWPH)

Each numerical model of the apron-tube dam is inflated with the same internal water pressure head as in the experiments. When external water pressure is applied to the surface of the headwater side of the apron, it produces deformation of the tube. Since the area of the cross section of the tube cannot be changed, the internal water pressure head is increased or decreased to keep the area constant.

Figure 5.4 shows the change of internal water pressure head for each tube-apron case: 0.25 m, 0.30 m, 0.41m, and 0.56 m of apron. The initial internal water pressure heads, which are used to inflate the tube, range approximately from 0.470 m to 0.495 m in the test.

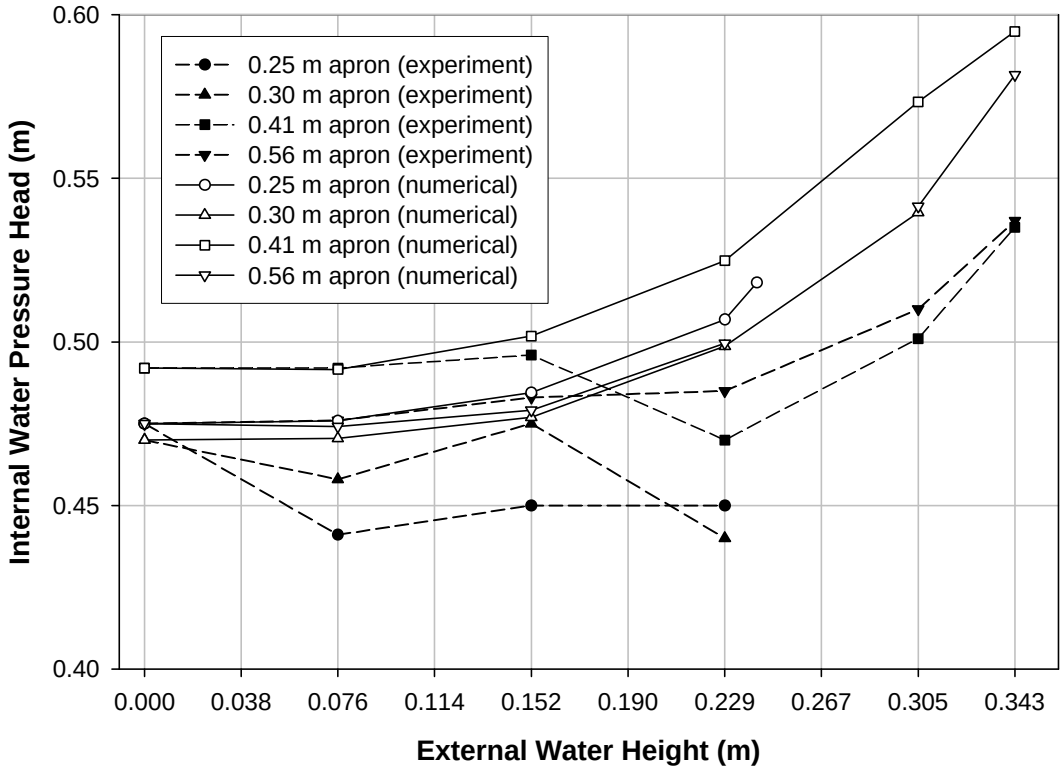

Figure 5.4. Change of internal water pressure head

The results of the numerical analysis show that the internal water pressure head (IWPH) increases as the external water level increases. But the experiments display an increase in some cases and decrease at some external water levels. For example, when the

external water level is 0.076 m (3.0 in.), the 0.25 m and 0.30 m apron cases show a decrease in IWPH, but the 0.41 m and 0.56 m apron cases display an increase, and at external water level 0.229 m (9 in.), the IWPHs of 0.30 m and 0.41 m decrease. But, when the external water level is 0.152 m (6 in.) and higher than 0.305 m (12 in.), the IWPHs of all apron cases increase as the external water level increases.

The differences of the internal water pressure heads in the numerical analysis and experiments may come from several factors. The first is that some leaks were noticed during the tests and these may contribute to some decrease in internal water pressure head. The second is that the end condition in the longitudinal direction of the tube dam in the experiments may contribute those differences.

5.3.3. Deformation of Apron-tube Dam

Figure 5.5 and Figure 5.6 show the deformed shape of the apron-tube dam at different external water levels. Dots in the figures represent measured deformed shapes of the tube in the test and solid lines correspond to the numerical analysis. There were three series of measurements for the deformed tube shape at each external water height along the length of the tube dam in the test. Series 1 and series 3 were measured 1.12 m from each end of the tube in the longitudinal direction, and the length of the tube dam in the experiments was 4.47 m. Series 2 was measured at the middle of the tube dam, and these data are used in this comparison.

When the applied external water level is 0.076 m (6 in.), the tube deforms to the headwater side first, which is opposite to the direction of the external water pressure. This deformation occurs because the external water mostly applies pressure on the curved apron portion, which is between the apron on the ground and the apron over the tube. After the external water level is increased to 0.152 m, 0.229 m, and so on, the tube deforms in the tailwater direction.

The measurements from the test and the results from the numerical analysis agree well with each other for all apron-tube cases. Some differences in the deformed shapes between numerical analysis and experiments may come from observational errors in the tests or they may result from the difference in end conditions of the apron-tube dam in the numerical analysis. The difference may be resulted by the incorrect assessment of the

circumference of the tube between the tests and the numerical model. Also, there was a small loss of internal water pressure head of the tube in some cases during the tests because of leaking.

Figure 5.5 shows the 0.25 m apron length case when subjected to external water heights of 0.076 m, 0.152 m, and 0.229 m. The apron-tube dam fails after 0.254 m (10 in.) of external water height in the numerical analysis. A dot over the apron and the foundation in Figure 5.5 (a) is presumed to represent an uneven apron surface at the time of the measurement and the dot moves down, just above the apron and the foundation, when the external water height increases, as shown in Figure 5.5 (b) through Figure 5.5(d).

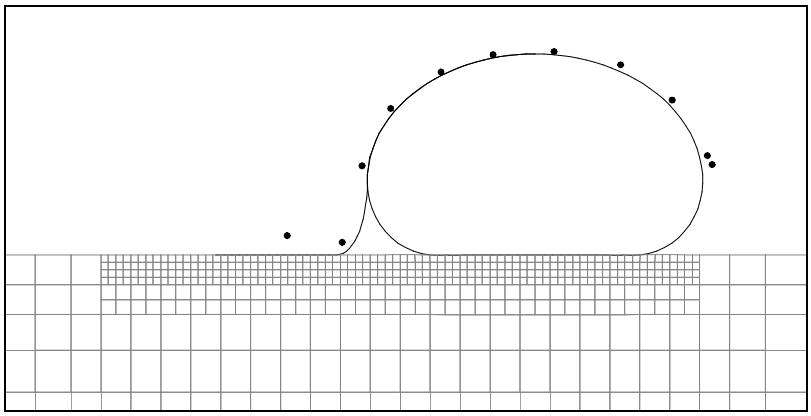

a) External water level 0.0 m

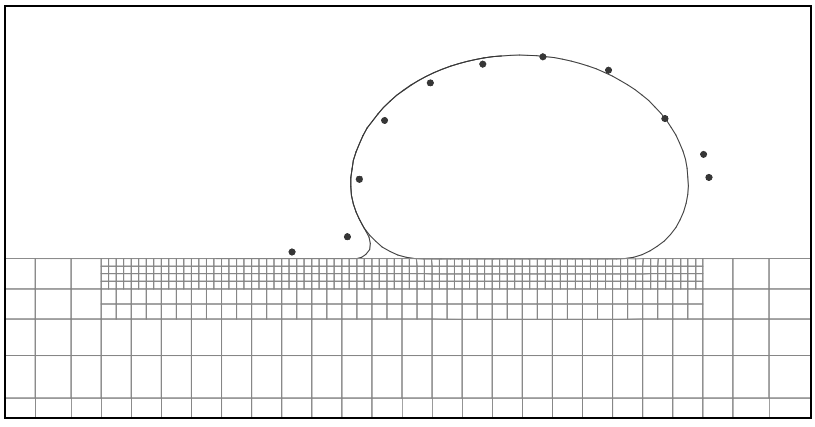

b) External water level 0.076 m (3 in.)

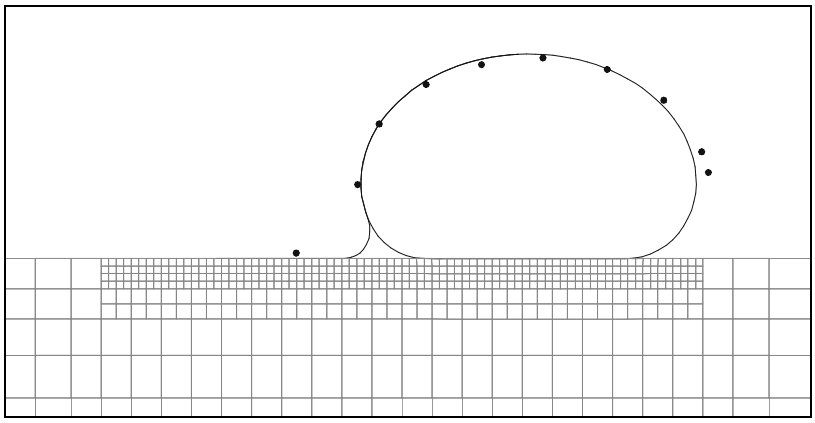

c) External water level 0.152 m (6 in.)

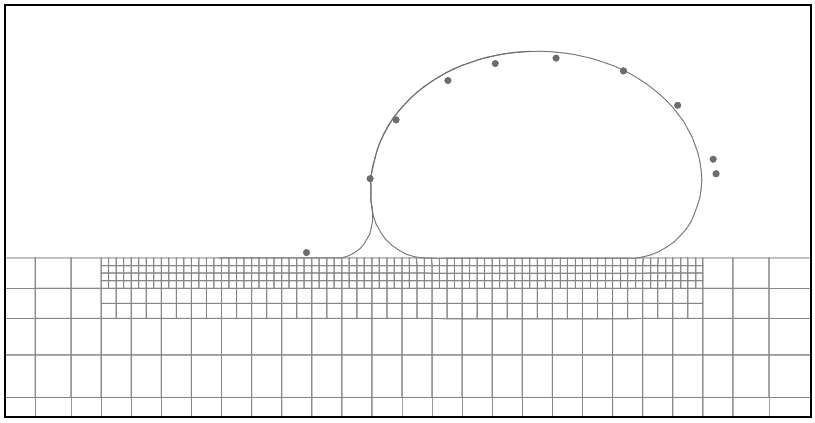

d) External water level 0.229 m (9 in.)

Figure 5.5. Deformation with 0.25 m apron length

Figure 5.6 shows the deformed cross-section of 0.56 m apron length case. The numerical result show fair agreements with the experimental result. The apron-tube dam withstands the external water height as high as the height of the tube.

Note that the numerical results of the cross-section are slightly smaller than the experimental measurements when the external water height is low, such as 0.0 m or 0.0762 m (see Figure 5.6(a) or Figure 5.6(b)). But as the external water height increases, the difference between two results vanishes (see Figure 5.6(e) or Figure 5.6(f)).

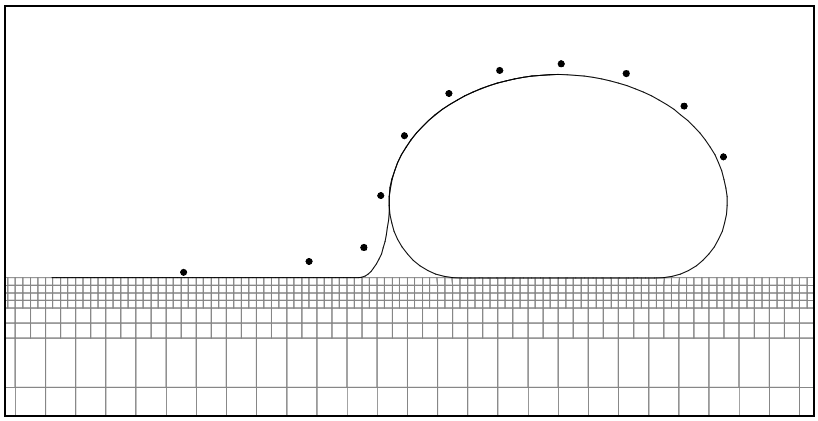

a) External water level 0.0 m

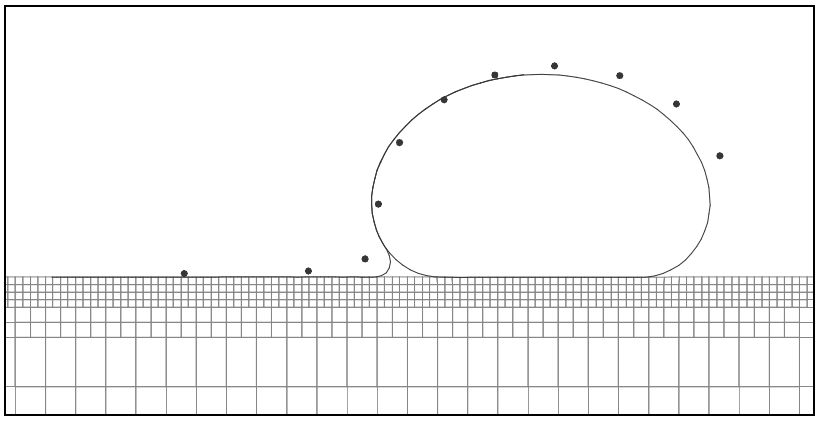

b) External water level 0.076 m (3 in.)

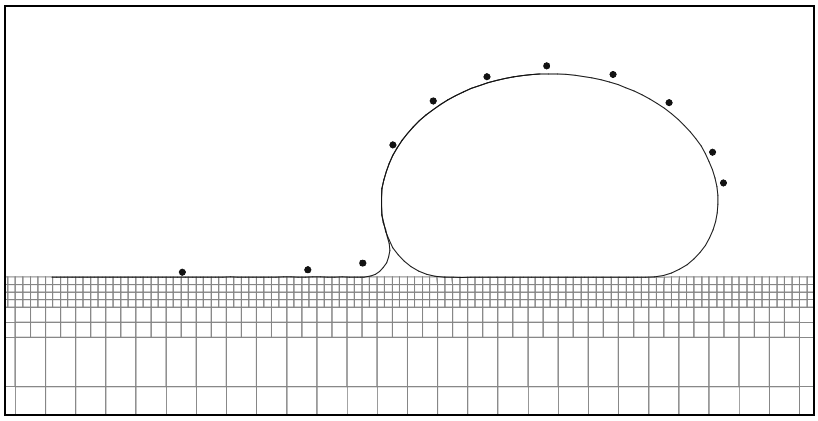

c) External water level 0.152 m (6 in.)

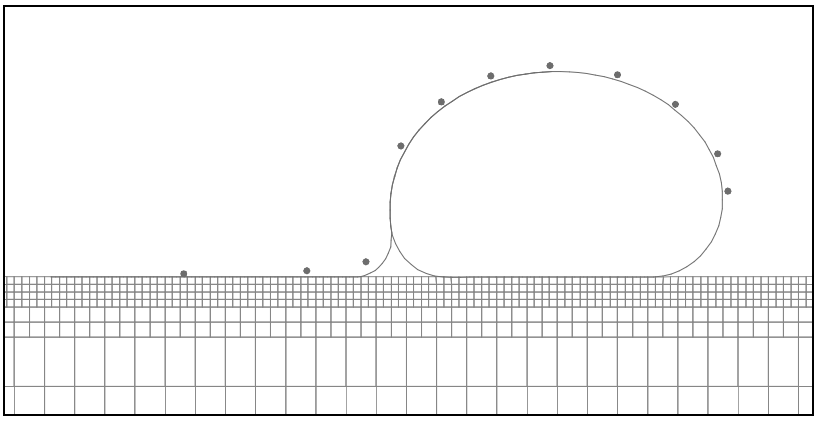

d) External water level 0.229 m (9 in.)

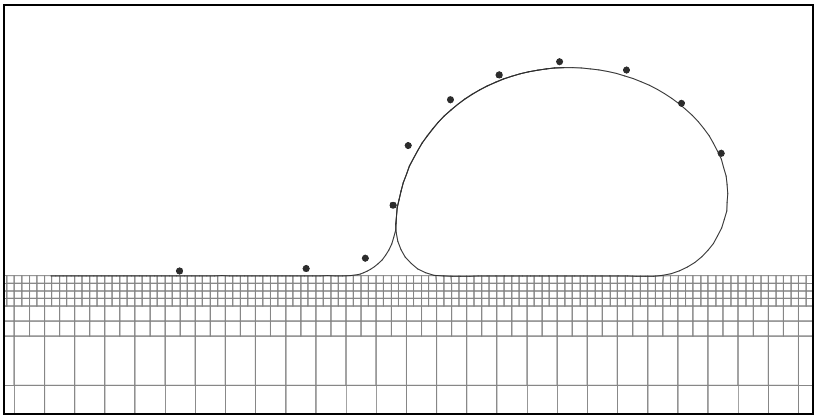

e) External water level 0.305 m (12 in.)

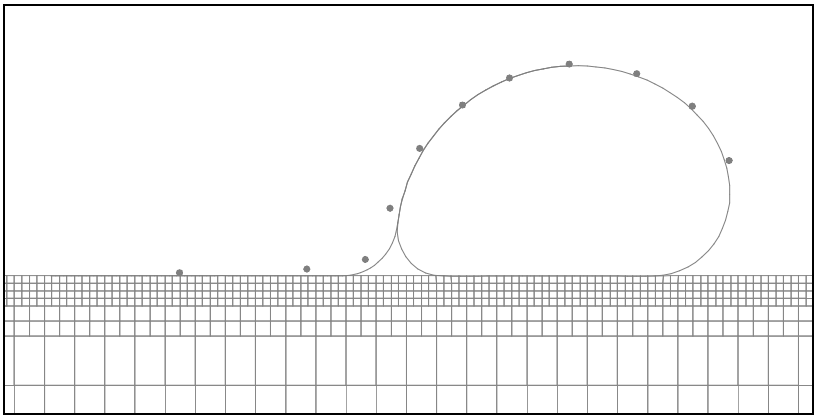

f) External water level 0.343 m (13.5 in.)

Figure 5.6. Deformation with 0.56 m apron length

5.3.4. Contact Length of Apron

Figure 5.7 represents the change of contact length of the apron as the external water height varies. The results of apron lengths of 0.41 m and 0.30 m are presented. The graph displays the decrease in the contact length of the apron as the external water level rises. The contact length of the apron is reduced approximately from 0.38 m to 0.33 m and 0.28 m to 0.23 m for 0.41 m and 0.30 m apron lengths, respectively.

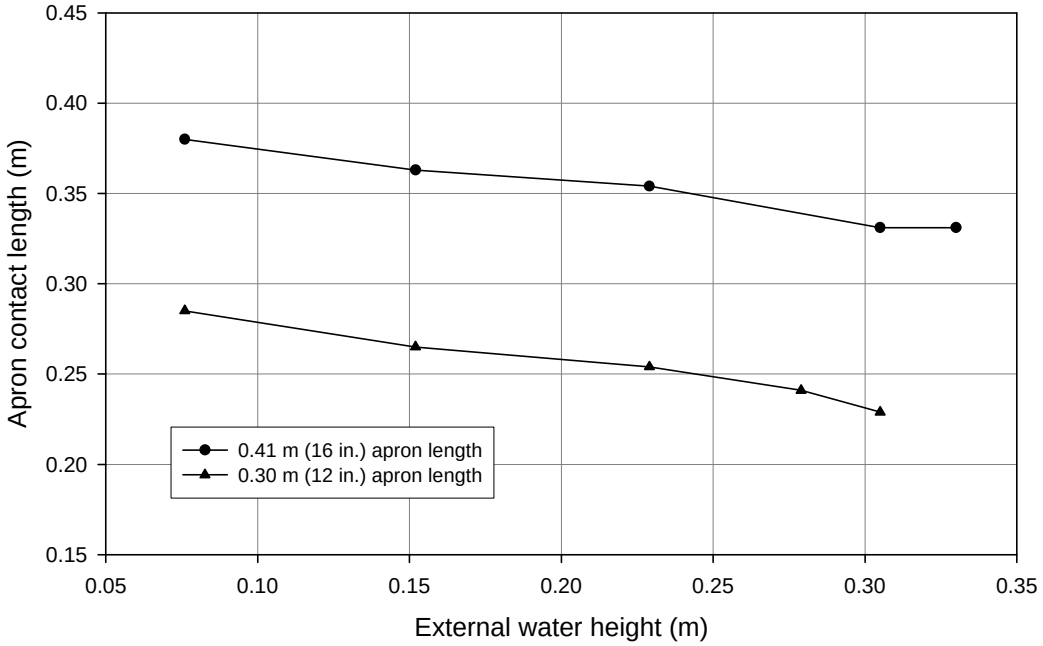

Figure 5.7. Change of apron contact length of different apron tube dams

5.3.5. Pore Pressure

The pore pressure of the soil is plotted in Figure 5.8 for the 0.41 m (16 in.) apron length case when the external water level is as high as the height of the tube, which is approximately 0.34 m. The colored contours represent the pore pressures in the soil; the pore pressure of red color ranges from 0 Pa to 1000 Pa and the blue color is from 7000 Pa to 8000 Pa. The pore pressures at the headwater side surface and the left edge of the soil grid are given as the boundary conditions when the external water height increases. The groundwater flow produces the change of the pore pressures inside of the grid.

The comparison of pore pressures at 10 cm below the ground is presented in Figure 5.9. Dots represent the experimental results and a curved solid line indicates the result from

the numerical analysis. The experimental measurements and the numerical results agree well. Since half of the apron is placed on the sand and the other half on the drain, pore pressures from the numerical analysis and the experiment decrease close to the beginning of the drain. This tendency of pore pressure is more evident just below the ground, which is 0.625 cm below the surface of the soil grid in the numerical model, and the pore pressure decreases almost linearly (Figure 5.10).

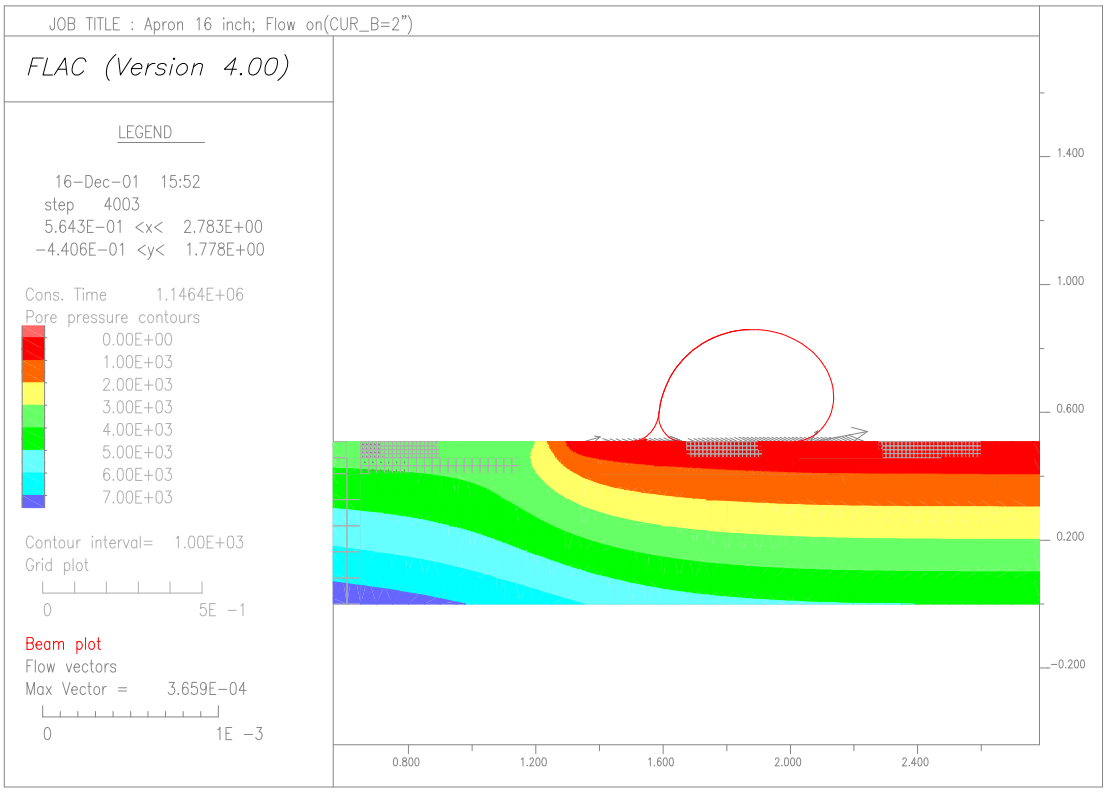

Figure 5.8. Pore pressure contour in ground
(0.41 m apron length with external water level = 0.34 m)

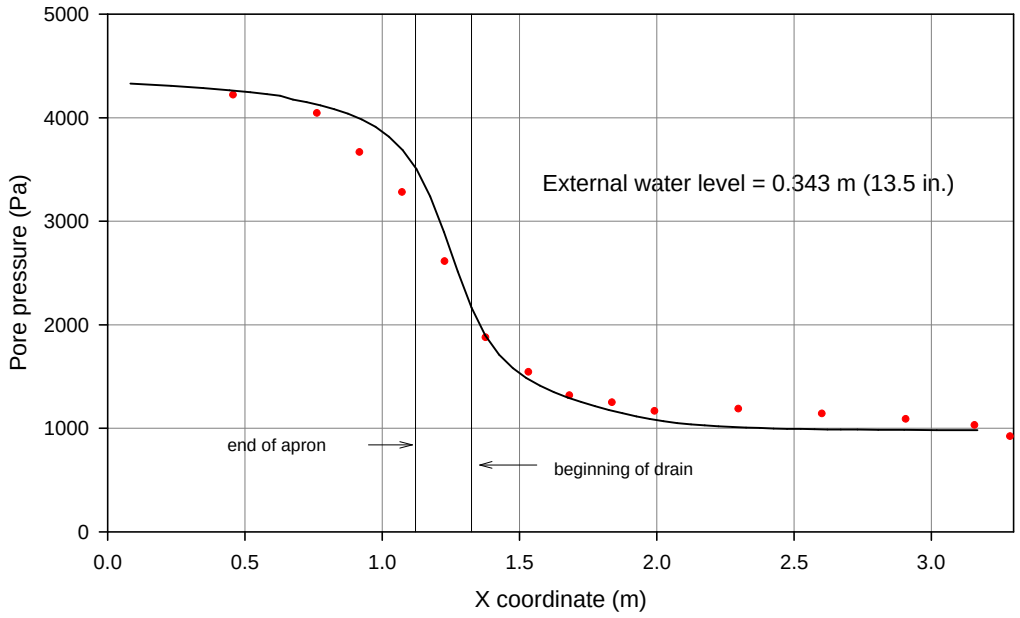

Figure 5.9. Comparison of pore pressure at 10 cm below ground
(dots: experimental results; solid line: numerical analysis)

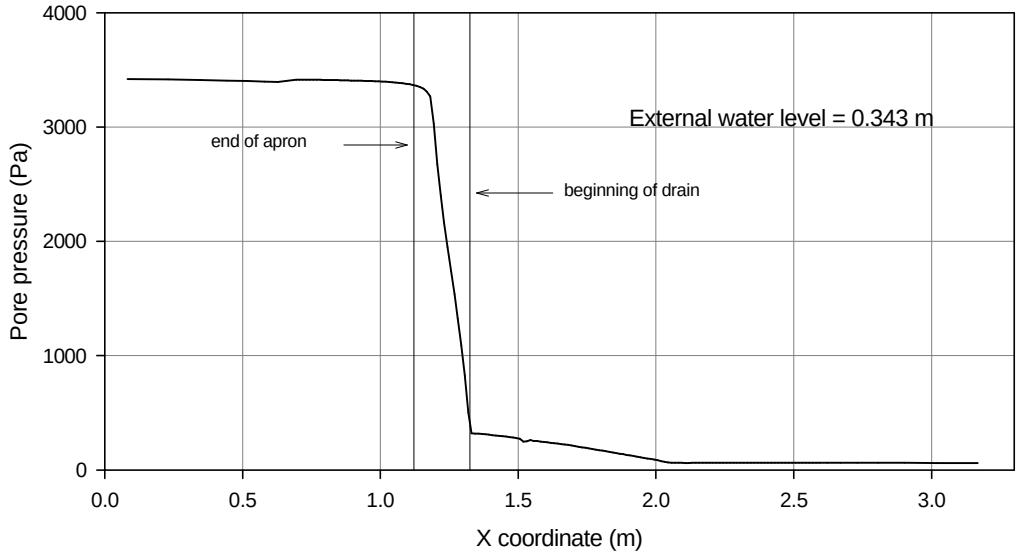

Figure 5.10. Pore pressure just below ground

5.3.6. Tension in Apron-tube Dam

Figure 5.11 illustrates the locations of the node numbers. The tube contains node 1 through node 102 and the apron starts from node 103 for all apron-tube cases. The beam elements 1 and 2 are from node 1 to node 2 and node 2 to node 3, respectively, and the element 102 starts from node 102 and ends at node 1. The beam element numbering of the apron begins with 103, which consists of node 103 and node 104, and ends with n-1, which consists of node n-1 and node n.

The contacted portions between tube and soil and between apron and soil are approximately from nodes 74 to 94, and from nodes 145 to 163, respectively, for the 0.25 m (10 in.) apron length. The node numbers of the contact region change slightly based on the internal water pressure head of each apron case and the external water level.

Tensions in the apron-tube dam subjected to different external water levels are plotted according to the element numbers from Figure 5.12 to Figure 5.14. All plots show that the maximum tensions in the apron and tube increase as the external water level rises. The increment of maximum tension in the apron is caused directly by applied hydrostatic pressure from the external water, but the increase of maximum tension in the tube is generated by the rise of internal water pressure head. It is noted that the internal pressure of the flexible tube does not always increase as the external pressure increases; the internal water pressure decreases as the external pressure increases in some other types of tube dams (FitzPatrick et al., 2001).

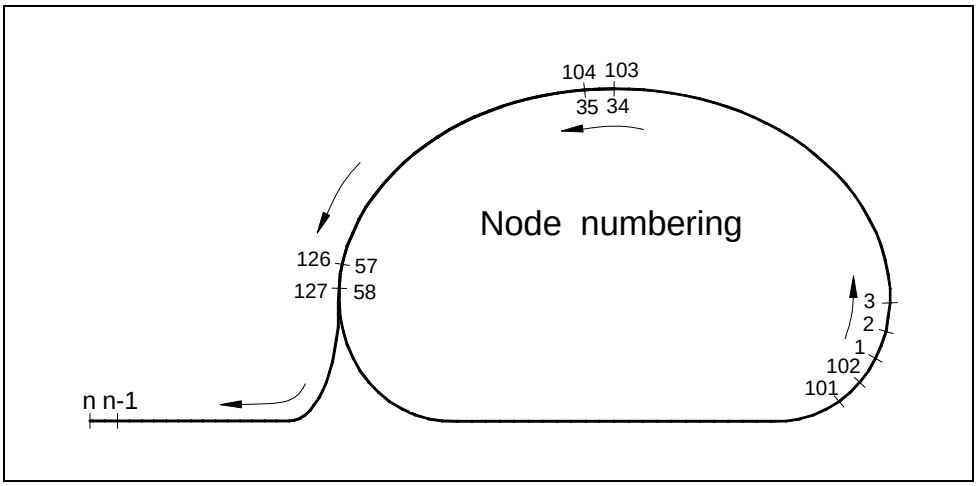

Figure 5.11. Node numbering in apron-tube dam

The tensions in the contacted portions, which are between soil and tube, apron and tube, and apron and soil, vary with a constant slope. The difference in tension between two nodes is the friction force in the contact plane for that element.

Since the friction force is represented as shear between two materials, such as apron and soil, and tube and soil, the friction is proportional to the normal force acting on the element; the shear and normal force are proportional. Therefore the friction force is constant (or the plot of tension is linear) in the tube and soil contact plane, for example, from node 74 to node 94 in Figure 5.12, because the normal force acting on the region is constant (since the internal water pressure acting on the region is constant).

In contrast to the contact region of tube and soil, the tension in the portion of the apron on the sand varies nonlinearly as shown in Figure 5.12 from node 152 to the end of the apron. The reason is that the pore pressure in the sand acts in the opposite direction to the external water pressure, which acts as a normal force. The pore pressure decreases to almost zero close to the drain; therefore the net normal force acting on this part is not constant, and it varies almost linearly from zero at the end of apron. It produces a varying friction, from zero at the end of the apron to a certain value at the beginning of the drain.

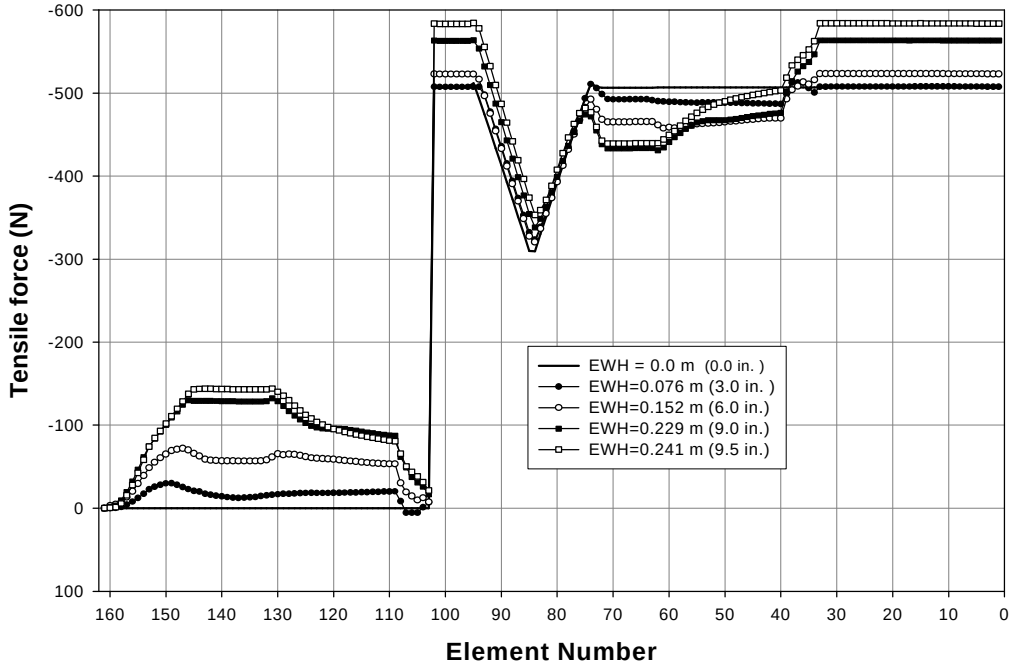

Figure 5.12. Tension in 0.25 m (10 in.) apron-tube dam (EWH: the height of external water)

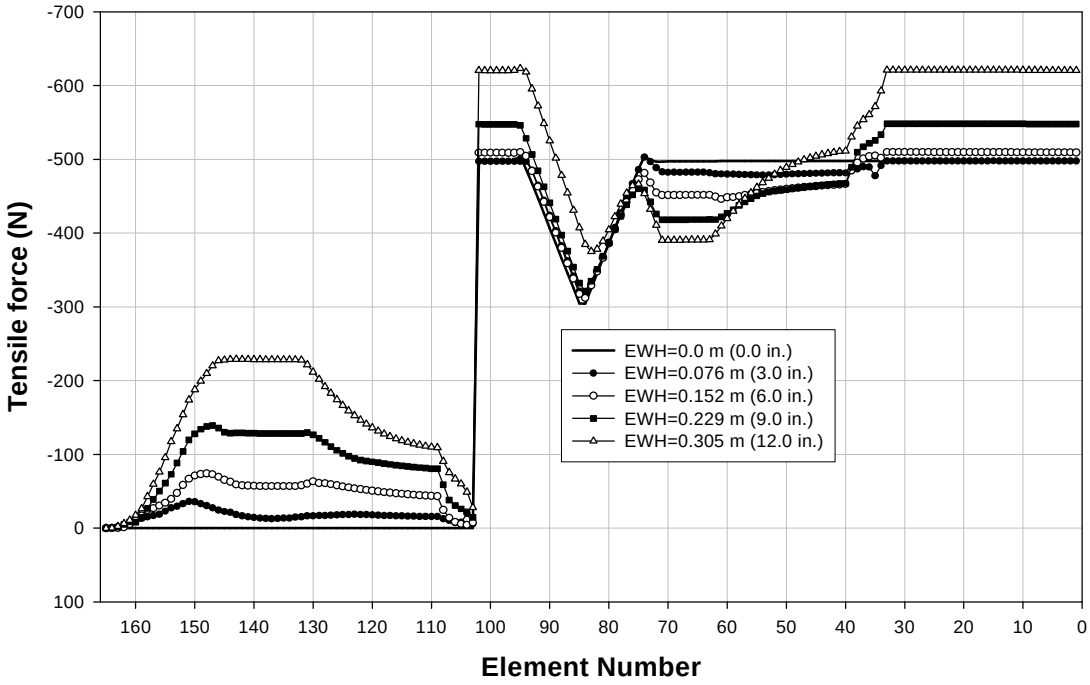

Figure 5.13. Tension in 0.30 m (12 in.) apron-tube dam (EWH: height of external water)

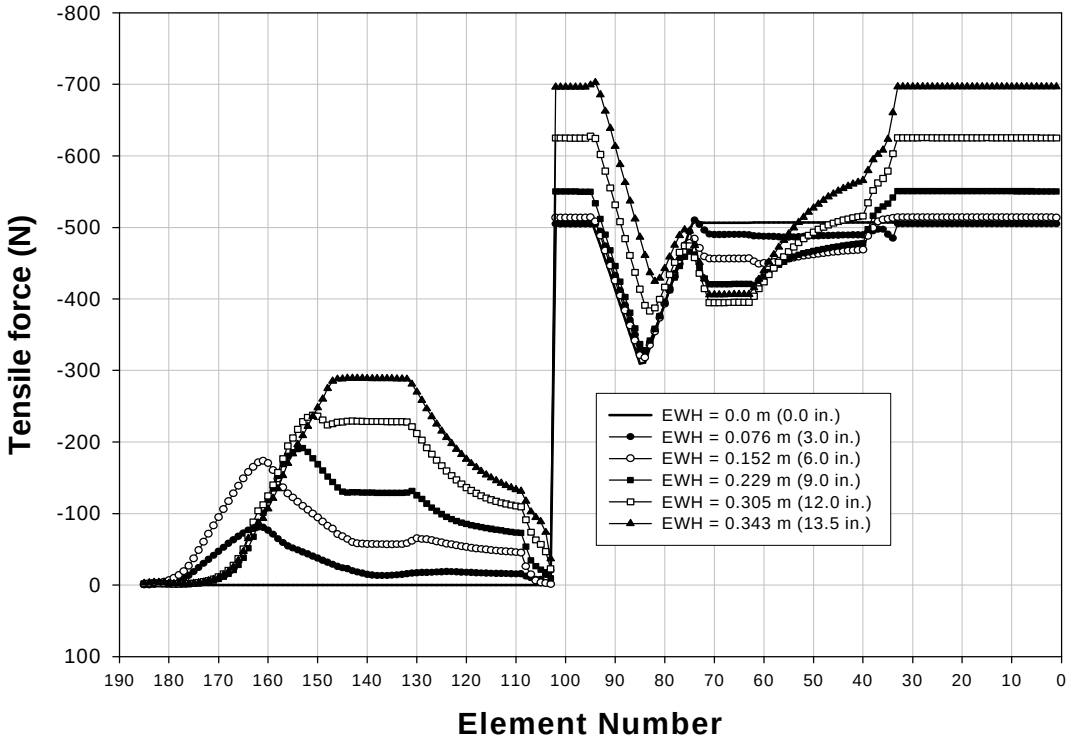

Figure 5.14. Tension in 0.51 m (22 in.) apron-tube dam (EWH: height of external water)

5.3.7. Friction between Apron-tube Dam and Foundation

An apron-tube dam resists the applied force due to the external water by friction between the apron and ground, and tube and ground. As mentioned in the previous section, the difference between tensions in contacting elements is caused by a friction force. Table 5.3 presents the applied force caused by the external water and the calculated friction in contact planes from the numerical analysis for the 0.25 m apron length.

Table 5.3. Friction (0.25 m apron-tube dam)

External Water Level (m)	Applied Force (N)	Friction under Apron		Sum	Friction under Tube		Sum	Total Friction (N)
0.076	**28.47**	T1	29.18	14.13	T3	18.20	14.9	**29.0**
		T2	-15.05		T4	-187.40		
					T5	184.10		
		Percentage(%)		48.67	Percentage(%)		51.33	
0.152	**113.89**	T1	72.00	59.06	T3	24.40	54.5	**113.6**
		T2	-12.94		T4	-172.00		
					T5	202.10		
		Percentage(%)		52.01	Percentage(%)		47.99	
0.229	**256.25**	T1	129.00	129	T3	35.80	125.0	**254.0**
		T2	0.00		T4	-136.10		
					T5	225.30		
		Percentage(%)		50.79	Percentage(%)		49.21	
0.241	**285.51**	T1	143.10	143.1	T3	39.50	142.0	**285.1**
		T2	0.00		T4	-128.70		
					T5	231.20		
		Percentage(%)		50.19	Percentage(%)		49.81	

The results in Table 5.3 show that the friction between the apron and the ground has two components, T1 and T2, and the friction between the tube and the ground has three components, T3, T4 and T5. Figure 5.15 shows the notation for friction forces and their directions. It is found that the friction between the apron and the ground is almost the same as the friction between the tube and the ground; the total friction resisting the applied force is almost equally shared in the two contact planes. Also, the direction of some of the

friction components (T2 and T4) is not against the applied force. The friction component T2 becomes zero when the external water level reaches the critical level.

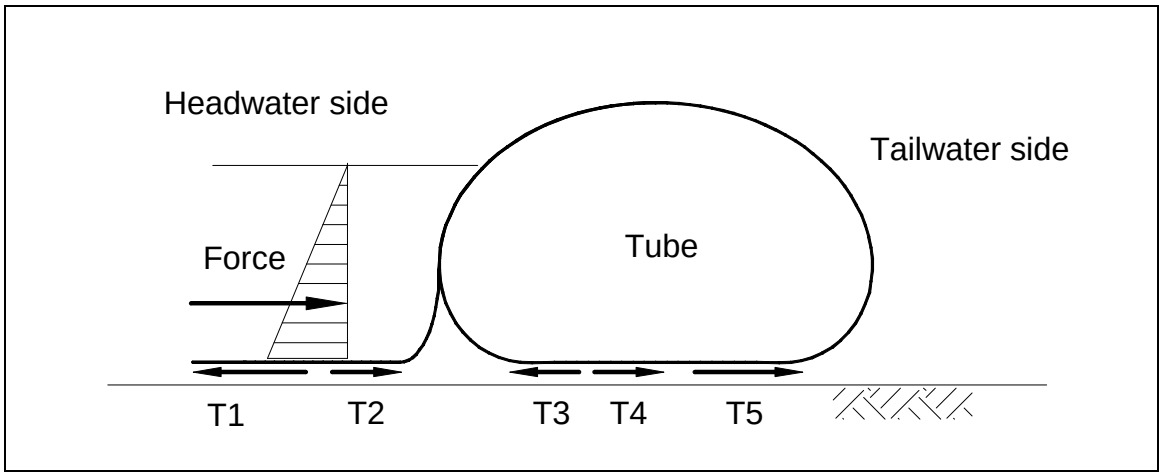

Figure 5.15. Notation of friction forces

5.4. Parametric Study

5.4.1. Effect of Initial Shape of Apron

When an apron-tube dam is installed on the ground, the initial shape of the apron may be different in each case. As shown in Figure 5.16, the apron curve may be defined with a quarter of an ellipse, which has radii of CurA and CurB. CurA is predetermined after the tube is inflated, because it is the distance from the ground to the leftmost point on the tube. CurB varies by the way the apron is installed. In fact, CurB changes from 2 cm to 15 cm in the tests. Therefore, different shapes of the initial apron curve are examined in this study.

It is assumed that CurA is fixed if the initial internal water pressure is the same for all cases, and CurB is changed. Values for radii CurB of 5.08 cm (2 in.), 7.62 cm (3 in.), and 12.7 cm (5 in.) are used to investigate the effect of the initial shape of the curve. The length of the apron is 0.41 m for this analysis.

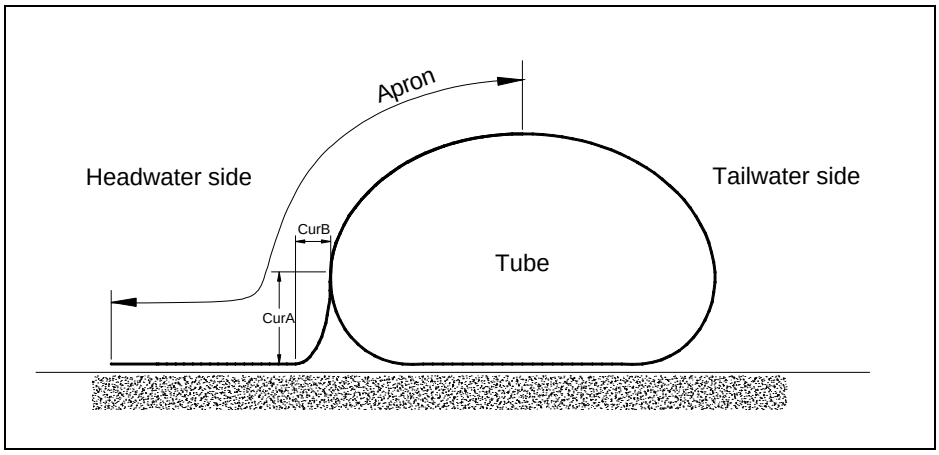

Figure 5.16. Initial shape of apron

It is noted that Young's modulus used in this section is 1.0 GPa instead of 0.12 GPa because of a technical problem in FLAC. When the Young's modulus is very low and the structure deforms extensively, FLAC sometimes produces odd strain results. This problem did not happen with FLAC 4.0 except in this case.

The use of higher Young's modulus within a range[1] was justified in the preliminary study. It was found that if the system is very flexible, the contribution of Young's modulus is much less than other factors such as the length of an element and the applied force. Because of that, the change of Young's modulus does not affect the outcome much.

The deformations of the apron-tube dam with different values of CurB are presented in Figure 5.17. The black dots represent the observations of the experiment; black, blue, and red lines denote radii 5.08 cm (2 in.), 7.62 cm (3 in.), and 12.7 cm (5 in.), respectively. The initial shapes of the apron are different as shown in Figure 5.17(a). The apron-tube dam with radius 12.7 cm deforms to the headwater side more than the apron-tube dam with radii 5.08 cm and 7.62 cm, when the external water height is 0.152 m (Figure 5.17(b)), and the apron-tube dam with radius 5.08 cm deforms more than the other cases to the tailwater side at the external water level 0.343 m (Figure 5.17(c)). However the differences of the deformations are not large. Also, it is noted that the contact length of the apron does not change much as the external water height increases.

[1] In the preliminary study, Young's modulus values of 0.12 GPa, 0.20 GPa, 0.5 GPa, and 1.0 GPa were used.

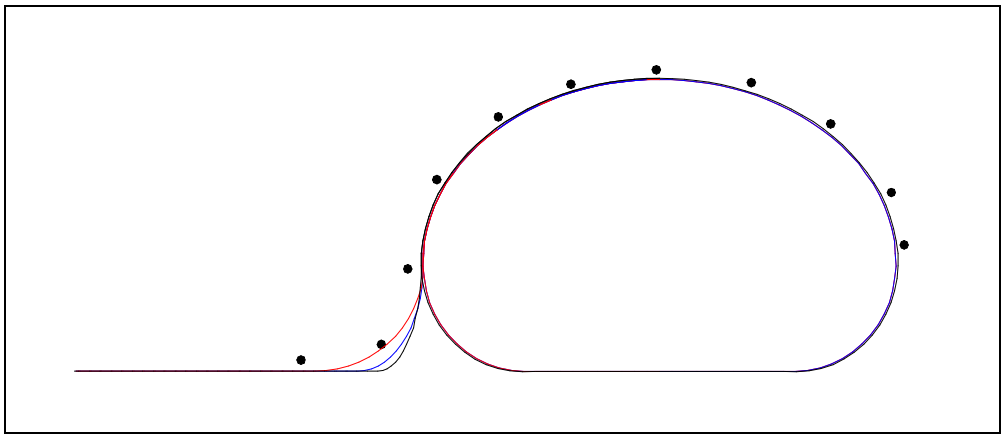

External water level 0.0 m (0.0 in.)

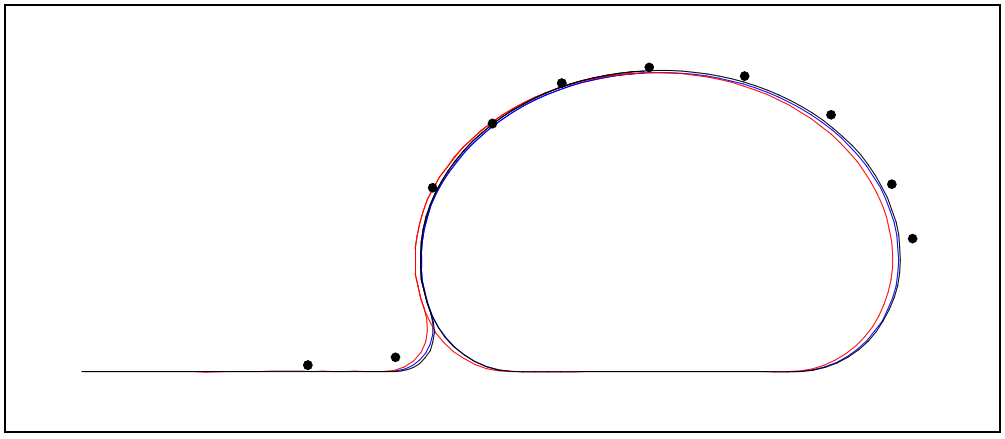

External water level 0.152 m (6.0 in.)

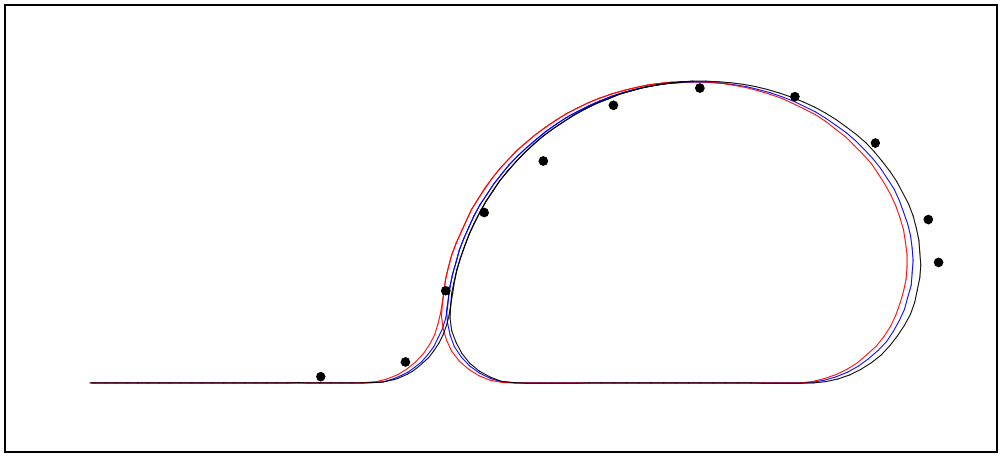

External water level 0.343 m (13.5 in.)

Figure 5.17. Deformation of 0.41 m apron length based on the initial shape of apron

Figure 5.18 shows the change of apron contact length with the variation of external water height for three values of CurB. It seems that the apron contact length is slightly longer if CurB is smaller. Also, the apron contact length becomes shorter as the external water height becomes higher. However, the variation due to the change of the values of CurB is not much. The difference of the apron contact length by CurB is 1 cm to 2.5 cm; thus, the apron contact length is not affected significantly by the CurB value.

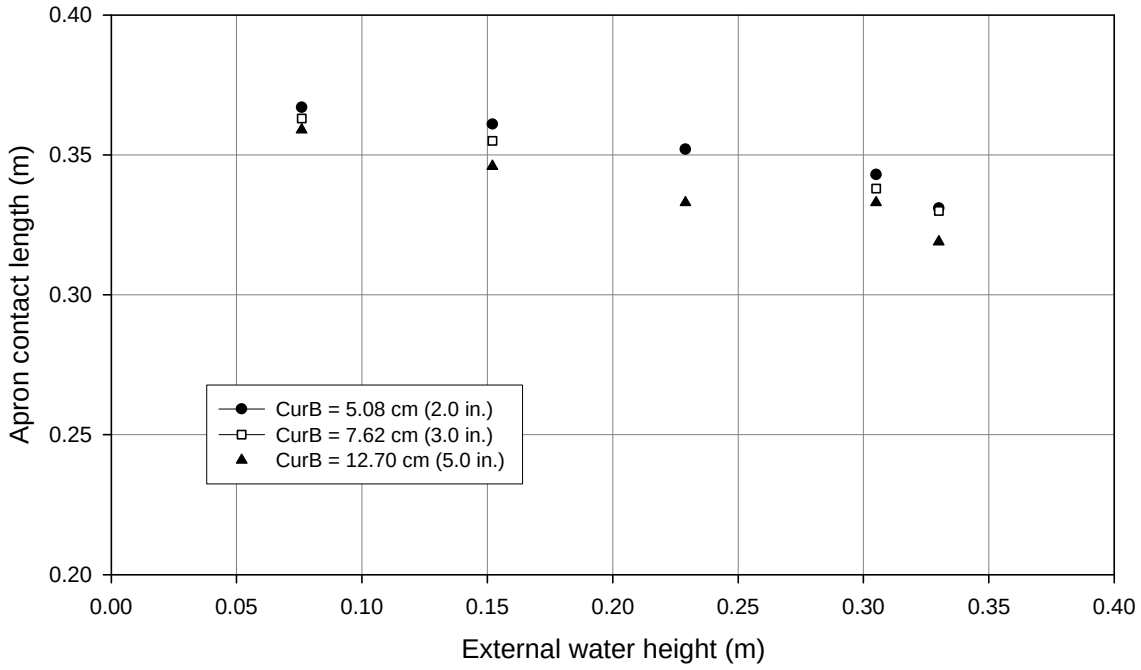

Figure 5.18. Apron contact length change in terms of CurB

Figure 5.19 shows tensions for a 0.41 m (16 in.) apron length with different initial apron curves when the external water level reaches the top of the tube, which is approximately 0.34 m high. Tensions in the contact regions, such as between the apron and the ground (node 172 ~ node 146), the apron and the tube (node 130 ~ node 103 and node 62~ node 34), and the tube and the ground (node 93 ~ node 72), are a little bit different. But there is no difference in maximum tension in the apron and the tube with different initial apron curves. The maximum tension in the apron is almost 300 N and the maximum tension in the tube is about 730 N. The locations of the maximum tension are on the apron curve (node 132~ node 144) and on the tailwater side of the tube (node 72 ~ node 62).

Therefore it can be concluded that the initial shape of the apron curve does not influence the deformation and the maximum tension of the apron-tube dam much overall. The contact lengths of the apron are slightly influenced by the CurB but the difference is not significant. However, it is recommended that the apron should be installed to have minimum CurB.

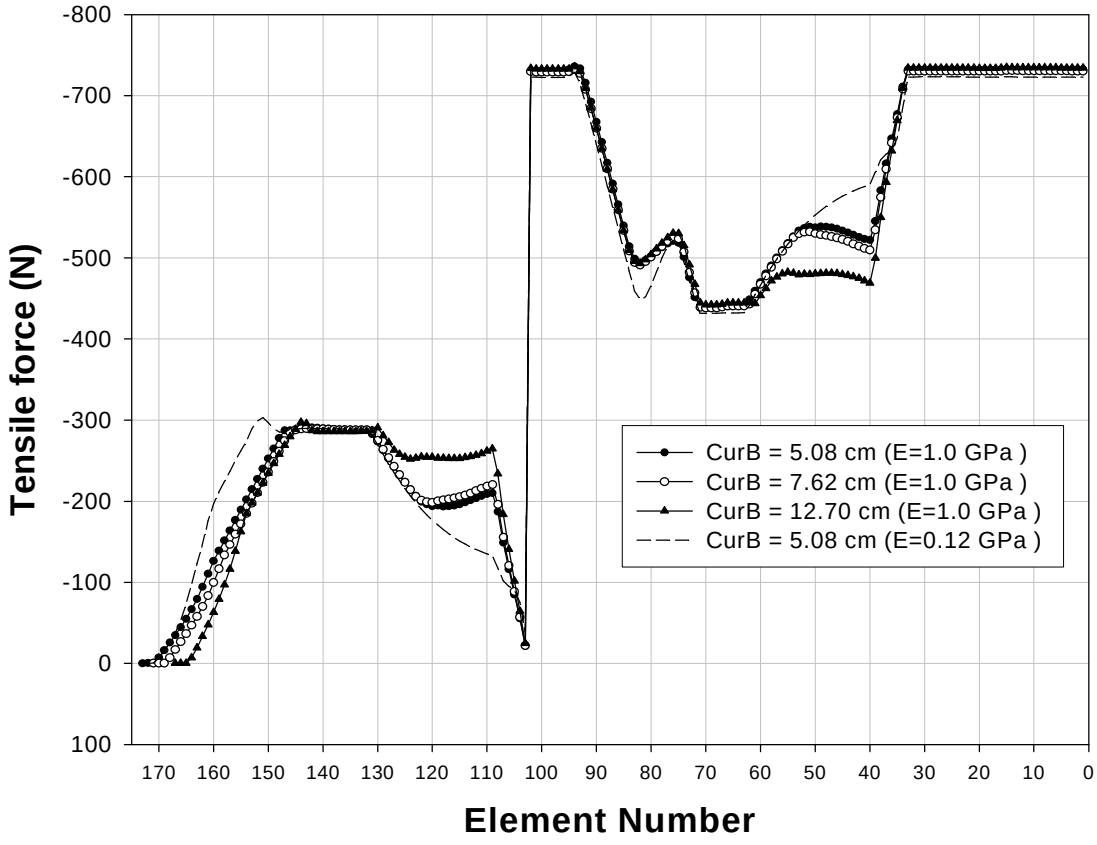

Figure 5.19. Tension on apron-tube dam based on initial shapes of apron

5.4.2. Effect of Internal Water Pressure Head on Critical Eternal Water Height (with Secant Method)

It is found that friction between the apron and the ground, and the tube and the ground, provides the stability of the apron-tube dam. The friction between the tube and the ground resists half of the applied force by the external water. The maximum capacity of the

friction is related to the normal pressure on the contact plane, which is the external water pressure or the internal water pressure. Also, in some cases, such as the wedged geomembrane tube dam (Huong et al., 2002), the critical external water height increases as the internal water pressure head of the tube increases. Therefore, the relationship between the critical external water level and the internal water pressure head of the tube is investigated. A higher internal water pressure provides a higher tube height generally, but it may not provide a higher critical external water level for a tube dam.

The 0.25 m and 0.30 m apron length tube dams are analyzed for this purpose. The material and geometric properties used are the same as in the previous study except for the proportion of the apron on the sand and on the drain; both apron-tube dams are assumed to have half of the apron on the sand and the remaining half on the drain (see Figure 5.3). Two cases are investigated, first assuming constant internal water pressure head and second considering the change of the internal water pressure head.

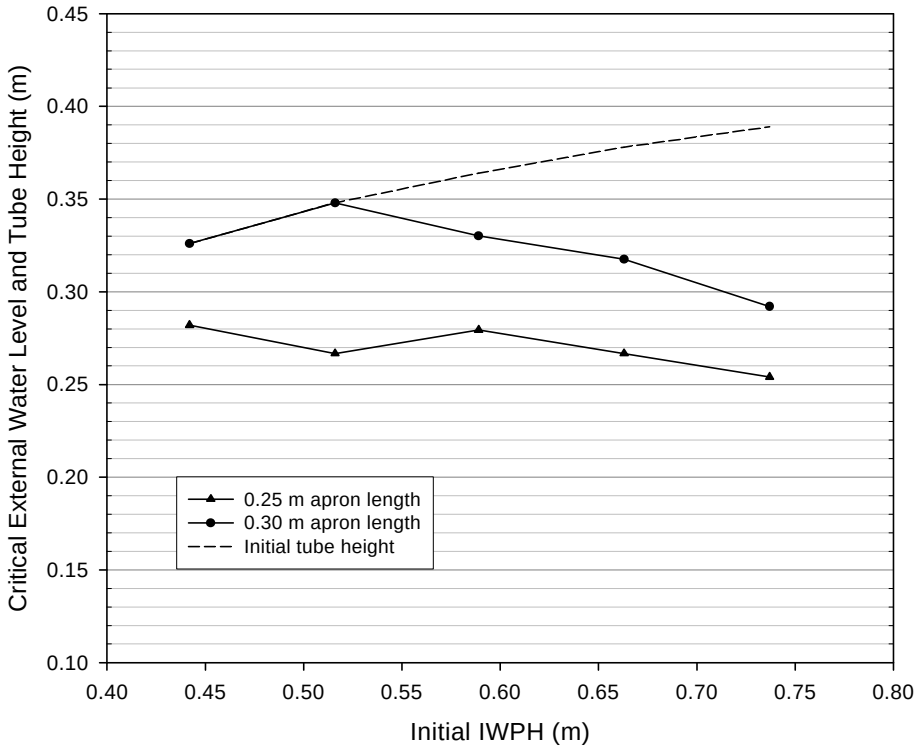

Figure 5.20. Critical external water levels versus initial internal water head (Assumes constant internal water pressure head)

Figure 5.20 displays the results for the apron-tube dams that are assumed to have a constant internal water pressure when the external water pressure is applied to the apron. The constant internal water pressure is not a realistic assumption except when the external water level is low, but the assumption is made for the simplicity of the analysis.

The dashed line represents the initial height of the tube based on the internal water pressure head, both apron length cases have the almost identical tube height initially; the height of the tube changes as the tube deforms. The solid lines with marks represent the critical external water level. For most of each curve, the critical external water level does not increase when the internal water pressure head increases and the height of the tube increases.

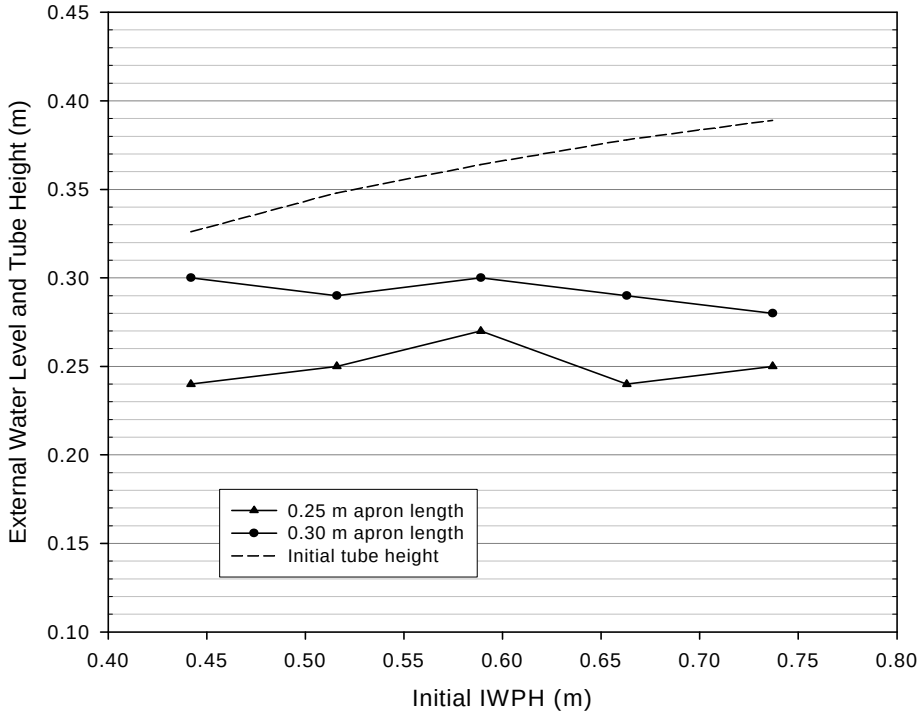

Figure 5.21. Critical external water levels versus initial internal water head (assumes constant tube area)

Figure 5.21 presents the critical external water height when the change of the internal water pressure head is considered. The dashed line indicates the relation of the initial internal water pressure head and the initial tube height; when the external water is applied to the apron, the internal water pressure head and the tube height are altered. The

solid lines with marks denote the critical external water versus the initial water pressure head. As the initial water pressure head increases, the critical external water height sometimes increases and sometimes decreases.

It is noted that the changed internal water pressure for this case is always higher than the initial internal water pressure head. Table 5.4 presents the final internal water pressure head, the critical external water height, and the final tube height in detail for both cases.

Table 5.4. Critical EWH[2] and tube height based on IWPH of the tube

(a) 0.25 m apron length case

Initial IWPH		Final IWPH	Critical EWH	Height of tube (m)	
Normalized[3]	(m)	(m)	(m)	Initial	Final
0.30	0.442	0.477	0.24	0.326	0.333
0.35	0.516	0.558	0.25	0.348	0.354
0.40	0.589	0.647	0.27	0.364	0.371
0.45	0.663	0.693	0.24	0.378	0.380
0.50	0.737	0.764	0.25	0.389	0.390

(b) 0.30 m apron length case

Initial IWPH		Final IWPH	Critical EWH	Height of tube (m)	
Normalized	(m)	(m)	(m)	Initial	Final
0.30	0.442	0.512	0.30	0.326	0.336
0.35	0.516	0.575	0.29	0.348	0.355
0.40	0.589	0.662	0.30	0.364	0.371
0.45	0.663	0.721	0.29	0.378	0.382
0.50	0.737	0.912	0.28	0.389	0.402

[2] EWH: External Water Height

[3] Normalized: initial IWPH is normalized by the circumference of the tube (1.4732 m)

To investigate the critical EWH in more detail, the shear stresses from the numerical analysis are compared with the shear strength. Detailed shear stress and shear strength in the contact regions for the 0.30 m apron length case, when the IWPH is 0.589 m and EWH is 0.330 m, and the IWPH is 0.737 m and EWH is 0.292 m in Figure 5.20, are presented in Figure 5.22 and Figure 5.23, respectively.

The solid lines without marks represent the shear strength in the contact region, which is proportional to the normal pressure and the friction angle on the region and can be evaluated with the following Coulomb shear strength formulation (see Equation 5.1): the shear stress can not be greater than the shear strength. If the value of shear stress on the plane exceeds the shear strength, the contact plane slips. Again, adhesion is neglected in this study. Since the apron is on two kinds of material, soil and drain, the shear strength of the apron contact region has two portions. The shear strength between the soil and the apron linearly increases as the pore pressure decreases linearly when it approaches the drain. The shear strength between the drain and the apron is constant since the pore pressure is assumed to be zero.

$$t_f = c + s \tan f$$

Equation 5.1

where t_f : shear strength

c : cohesion (assumed as 0)

s : normal stress

f : friction angle

The dashed lines with marks represent the absolute value of shear stress from the numerical result, which is the difference of tensions at the ends in the element, divided by the length of the element. The sum of the shear stress over the contact length is the friction force and the sum of the shear strength is the maximum friction (or friction capacity).

Figure 5.22 and Figure 5.23 show that most of the shear stresses in the apron are as great as the shear strength at the critical external water height, while most of the shear stresses in the tube do not reach the shear strength. Therefore, the failure of the apron-tube dam is produced by slip between the apron and the ground. Note that the shear stresses

between the soil and the drain (in the dashed circle) from the numerical results have very high values; they should not be greater than the shear strength of the drain.

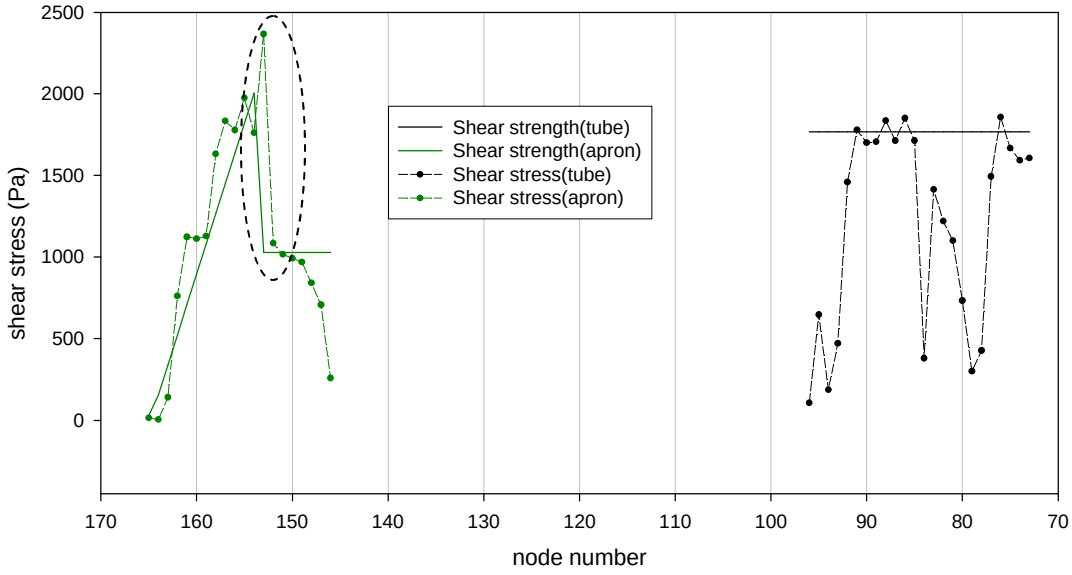

Figure 5.22. Shear stress and shear strength in contact region
(0.30 m apron length case with IWPH 0.589 m and EWH 0.330 m)

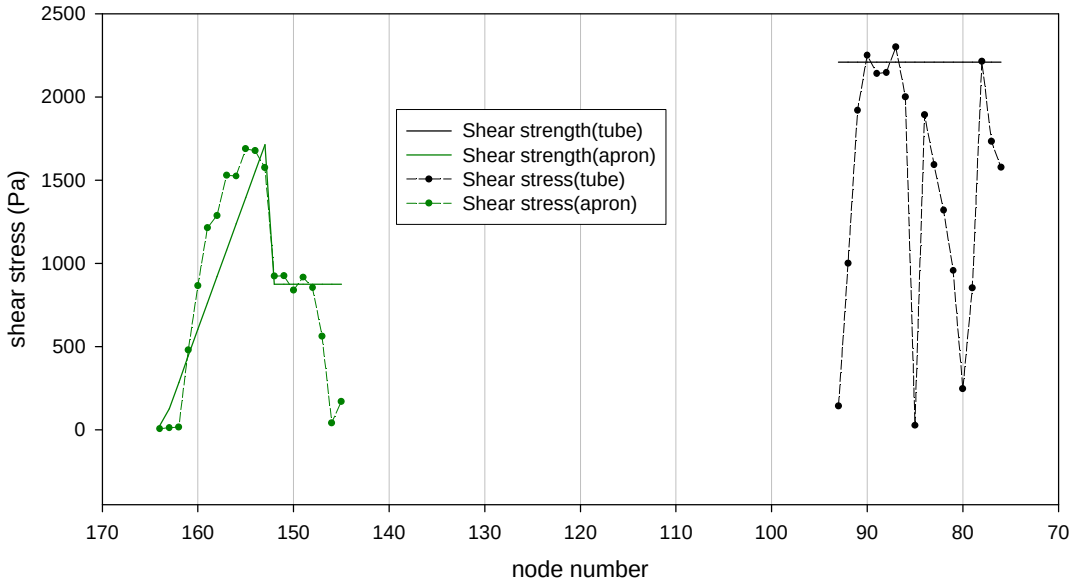

Figure 5.23. Shear stress and shear strength in contact region
(0.30 m apron length case with IWPH 0.737 m and EWH 0.292 m)

Therefore it is concluded that a higher IWPH of the tube should not increase the stability of the apron-tube dam. In other words, the IWPH of the tube should not affect the critical EWH. The main reason is that the friction between the tube and the ground is always less than the total shear strength over the contact region. Failure of the apron-tube dam starts by slip between the apron and the ground, and the tube begins to roll over to the tailwater side together with slip of the apron. Therefore, the friction between the apron and the ground is the main factor for failure of the apron-tube dam system, and this friction force depends on the external water pressure head. This conclusion is limited so far for 0.25 m and 0.30 m apron length cases with the normalized IWPH range from 0.30 to 0.50.

However, at this point, it is not clear why the critical EWH changes as the initial IWPH changes as shown in Figure 5.21. It should be almost constant based on the apron length. One of the suspected reasons is that the failures of the apron-tube dam are induced by slip between the apron and the ground. As slip continues, the tube rolls to the tailwater side in Figure 5.24 (but it is evident that there is no roll before the apron slips). If the instability of the apron-tube dam is influenced partly by the rolling, a rounder tube, which is inflated with higher pressure, rolls more easily than a flatter tube.

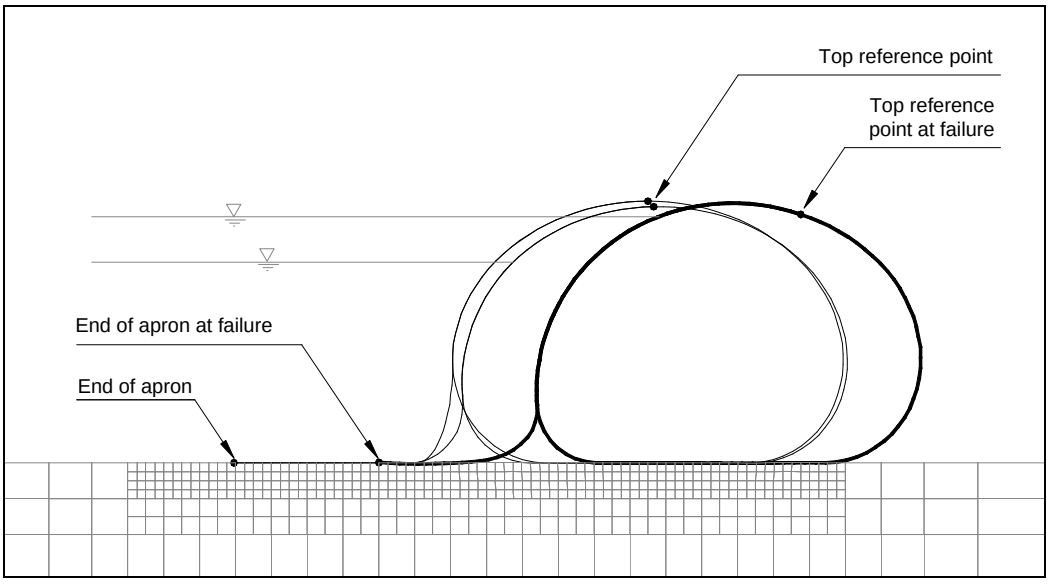

Figure 5.24. Example of failure of apron-tube dam

5.4.3. Effect of Internal Water Pressure Head on Critical External Water Height (with Factored Secant Method)

The numerical results of the previous parametric study show inconclusive results. The suspected reasons are:

- There are large differences in the two interface properties (especially friction angles between apron and drain, 17 degrees, and apron and sand, 32 degrees). This may not be simulated perfectly in FLAC when the apron on the sand begins to slip on the drain side because of the sudden difference in shear strengths (see encircled portion in Figure 5.22).
- For each IWPH of the tube, the locations of the drain are not exactly the same for all cases. It was attempted to have the proportion of the apron on the sand be one-half of the total length of the apron, but the proportions are not the same for all different IWPH cases in numerical modeling although the proportions are close to 0.5. This is because the initial setup locations of the tube before inflation for different IWPH cases are fixed in terms of the location of the tube's center (see Figure 5.25(a)). In addition, the apron, soil, and drain are modeled with a certain number of beam elements or a certain size of the mesh.

To get a better understanding of the critical external water level dependence on the internal water pressure head of the tube, with the current interface element in FLAC, some modifications are attempted. First, the friction angles and the shear stiffness between the apron and sand and the apron and drain are assumed to be the same, so the shear strengths of the two different contact regions are the same. It is expected that this will help to ensure a smooth transition when the apron on the soil slips on the drain.

Next, the location of the tube is determined by fixing the far leftmost point of the tube to a certain coordinate so the locations of the apron and the drain are identical for all different IWPH cases (see Figure 5.25(b)). This setup provides a fixed location of the drain

and the precise length of the apron on the sand for all IWPH cases. Also, the FLAC program is updated from version 4.00.252 to 4.00.297[4].

The properties of the apron-tube dam model used in this study are unchanged from the other parametric study except for the length of the apron and the friction angles. The length of the apron is exactly 0.30 m, and the friction angles between the geomembrane (apron or tube) and the sand and between the geomembrane and the geotextile (drain) are 15 degrees.

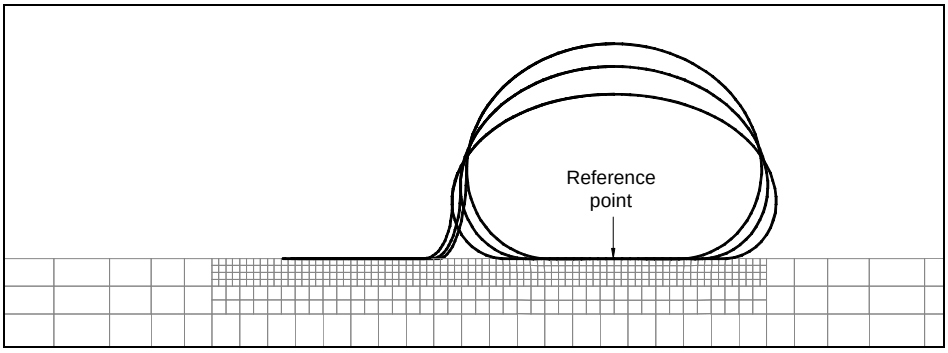

(a) Previous installation of apron-tube dam models

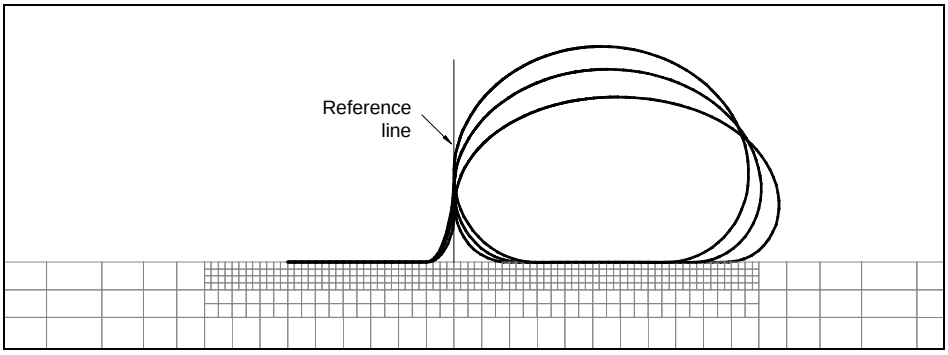

(b) Revised installation of apron-tube dam models

Figure 5.25. Setup of apron-tube dams for different IWPHs

The seven different initial internal water pressure heads, 0.295 m, 0.368 m, 0.442 m, 0.516 m, 0.589 m, 0.663 m, and 0.736 m (0.20, 0.25, 0.30, 0.35, 0.40, 0.45, and 0.50 in

[4] Between the FLAC version 4.00.252 and 4.00.297, there are a few modifications and improvements of the interface element.

terms of normalized IWPH[5]), are examined numerically. The external water level is increased in 0.01 m increments from 0.18 m until the apron-tube dam fails. As in the real situation, the internal water pressure head is changed to keep the area of the tube constant when the external water level increases. Also, it is noted that the factored secant method is employed to increase the water pressure head of the tube from the known initial IWPH incrementally to the unknown final IWPH without exceeding the final value. For the investigation of the effect of the IWPH on the critical external water height, it is critical to control the IWPH carefully during the iteration procedure. This is because the IWPH of the tube increases rapidly near the critical external water height (see Figure 5.4) and the overestimation or the underestimation of the IWPH beyond the range may result in the failure of the apron-tube dam during the iteration procedure.

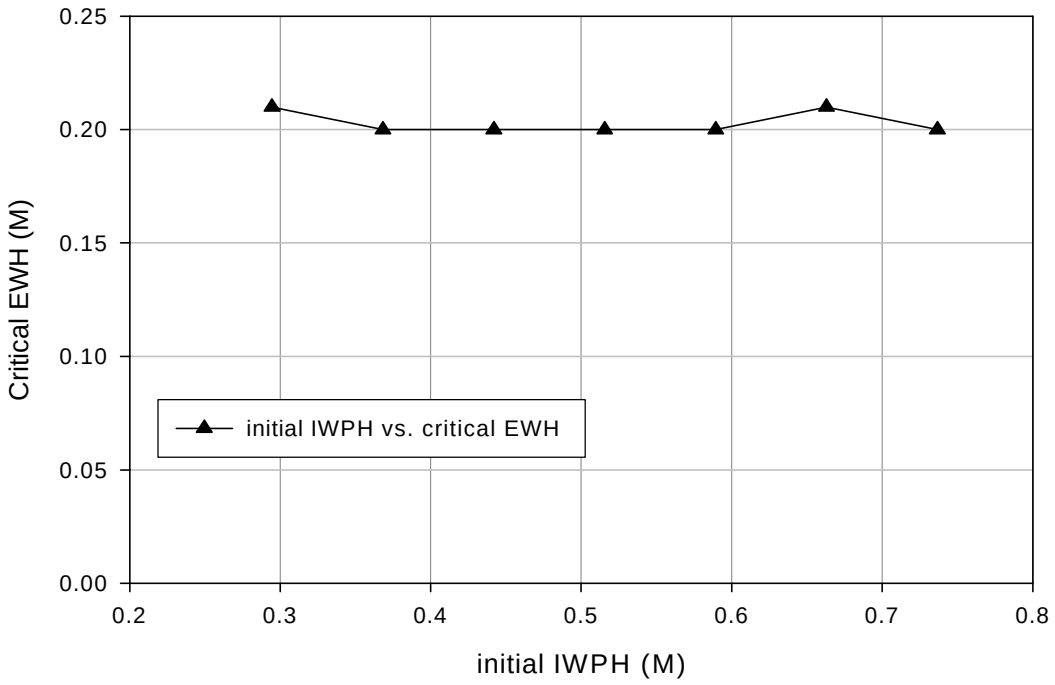

Figure 5.26. Critical external water height versus initial internal water pressure head (friction angle=15 degrees; apron length=0.30 m)

Figure 5.26 shows the relation between the critical external water height and the initial internal water pressure head of the tube. The critical external water height is 0.21 m

[5] Normalized IWPH is internal water pressure head divided by the circumference of the tube.

when the initial IWPH of the tube is 0.295 m and 0.663 m, and it is 0.20 m for the other IWPH cases.

It is concluded from these results that the critical external water height does not depend much on the initial internal water pressure head of the tube when the friction angles between the apron and sand and the apron and drain are 15 degrees for the range of IWPH shown, and the length of the apron is 0.30 m. The reason for this is that the apron-tube dam fails for all IWPH cases by slip between the apron and the ground (sand and drain) rather than slip between the tube and ground, because the maximum friction capacity of the apron, which is the sum of the shear strength over the apron length, is less than the maximum friction capacity of the tube. Therefore, the IWPH of the tube does not produce much effect on the critical external water height of the apron tube dam. More detailed explanations will be presented in the next section.

5.5. Mechanics of Apron-tube Dam

It is found that the apron-tube dam becomes unstable by slip failure between the apron and the foundation for the specific examples in the previous parametric study numerically. The failure of the apron-tube dam is discussed here in general regarding how an apron-tube dam fails and what circumstance causes the failure.

In addition, the slip failure of the tube on the foundation is discussed with the help of analytical solutions of a free-standing tube from previous research. Also, the slip failure of the apron on the foundation is examined with theoretical solutions and the numerical results.

During the research on the apron-tube dam at Virginia Tech, it was found that the external force induced by the external water is resisted by the friction between the apron and the ground and between the tube and ground equally; therefore the friction forces under the apron and the tube are identical. If the friction force between two materials reaches the maximum friction capacity, it causes a slip and it leads to the failure of the apron-tube dam.

Figure 5.27 shows the notation which is employed in the equations of the apron-tube dam in this section. The maximum friction capacity of the apron and ground (drain and

sand) and the tube and ground can be written as Equation 5.2 and Equation 5.3, respectively, since the cohesion factor is neglected in this study:

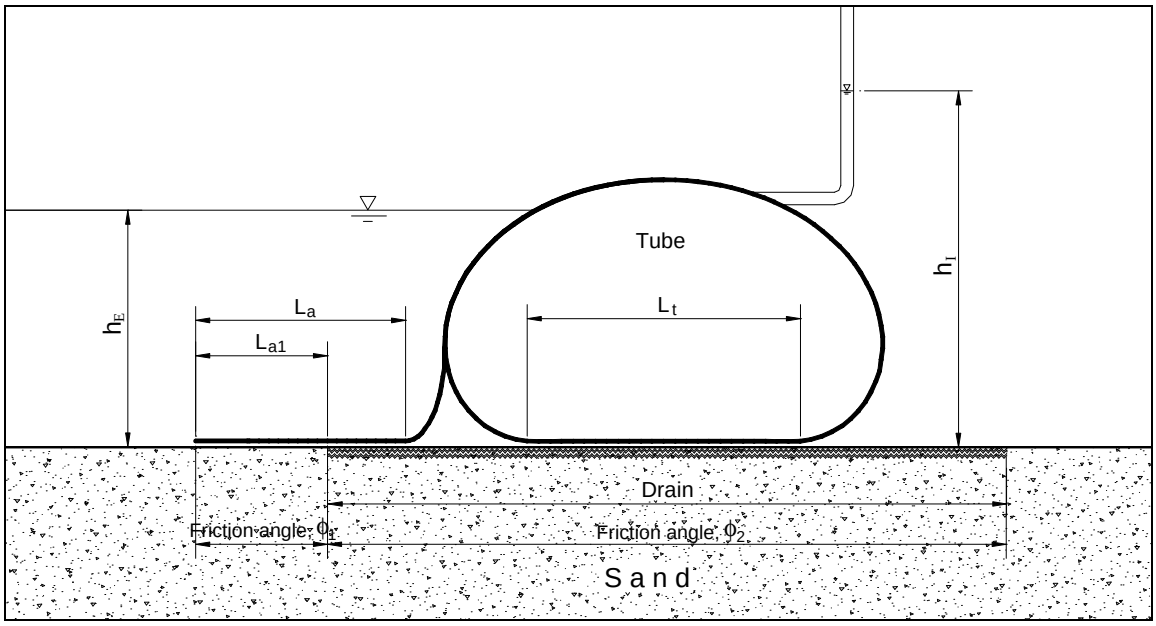

Figure 5.27. Notations of apron-tube dam

$$F_{\max\_a} = \tfrac{1}{2} g_w h_E L_{a1} \tan f_1 + g_w h_E (L_a - L_{a1}) \tan f_2$$

Equation 5.2

$$F_{\max\_t} = g_w h_I L_t \tan f_2$$

Equation 5.3

where

g_w = Unit weight of the water

h_I = Internal water pressure head of the tube

h_E = External water level from the ground

$F_{\max\_a}$ = Maximum friction force of apron and ground (drain and sand)

$F_{\max\_t}$ = Maximum friction force of tube and ground

f_1 = Friction angle between the geomembrane (apron and tube) and sand

f_2 = Friction angle between the geomembrane (apron and tube) and geotextile (drain)

L_{a1} = Apron length on sand

L_a = Apron length on sand and drain

L_t = Tube contact length

The total horizontal external force acting on the headwater side of the apron-tube dam by external water is

$$F = \tfrac{1}{2} g_w h_E^2$$

Equation 5.4

The apron-tube dam can fail by slip of the apron or of the tube. If one of the maximum friction force capacities, Equation 5.2 and Equation 5.3, is equal to half of the external water force, Equation 5.4, the apron-tube dam will slip.

The maximum friction force capacity of the apron is mainly a function of the friction angles between the two materials and the length of the apron. Therefore, the maximum friction force of the apron can be as large as half of the external water force at a given external water level, even with a very low value of the friction angle if the apron is long enough. The designing of the proper apron length will be discussed later. First, failure of the apron-tube dam induced by slip of the tube on the foundation is examined.

5.5.1. Slip Failure by Tube

If the apron-tube dam fails by slip between the tube and the ground rather than slip by the apron, i.e., the friction capacity under the tube is equal to the friction induced by the external force, the slip condition of the tube can be written from Equation 5.3 and Equation 5.4 as

$$F_{\max\_t} = F_t$$

$$g_w h_I L_t \tan f_2 = \tfrac{1}{4} g_w h_E^2$$

The contact length times the internal water pressure head of the tube is the same as the weight of the water in the tube per unit length of tube. If the unit weight of the water is eliminated from both sides, the previous equation can be written as follows:

$$A_t \tan f_2 = \tfrac{1}{4} h_E^2$$

Equation 5.5

where A_t = Area of tube

The external water height, h_E, can increase as high as the height of the tube as long as the apron-tube dam does not fail and it can be related to the height of the tube. Therefore, if we replace h_E by the product of a factor and the height of the tube, ah_t, we get Equation 5.6, which is written in terms of the friction angle in Equation 5.7

$$A_t \tan f_2 = \tfrac{1}{4} a^2 h_t^2$$

Equation 5.6

$$f_2 = \tan^{-1}\left(\frac{a^2 h_t^2}{4A_t} \right)$$

Equation 5.7

The factor, α, is greater than zero but cannot be greater than 1.0. If the apron-tube dam can withstand external water height as high as the height of the tube, the factor α is 1.0. It is noted that the height of the tube is slightly altered as the external water produces the deformation of the tube, however the change of the height is not substantial.

Analytical solutions for tube area and tube height of an inextensible tube with no bending resistance on a rigid foundation were developed by Namias (1985), and also the equations of tube area and tube height for an extensible tube on a rigid foundation were obtained by Plaut. Although the tube is considered extensible in this study, the formulas by Namias (1985) can be used to compute the friction angle f_2, since the internal water pressure heads of the tube are from 0.20 to 0.50 in normalized pressure head (or 0.295 m to 0.737 m in terms of the IWPH of the tube) and do not cause much extension in the tube (see Section 4.4). The analytical formulations for an extensible tube on a rigid foundation also are used to estimate the friction angle f_2. In addition, the Mohr-Coulomb model is employed in the numerical model to imitate the sand foundation, but the deformation of the foundation is

not sufficiently large for the apron-tube dam cases to influence the height or the area of the tube.

Figure 5.28 shows the friction angle f_2 according to Equation 5.7, when the apron-tube dam fails by slip between the tube and the ground. The solid line and the black dots represent the boundary of the friction angle between the inextensible tube and the drain and the extensible tube and the drain, respectively, when the critical external water level is as high as the height of the tube; the line and the dots will converge to 17.66 degrees as the initial IWPH increases.

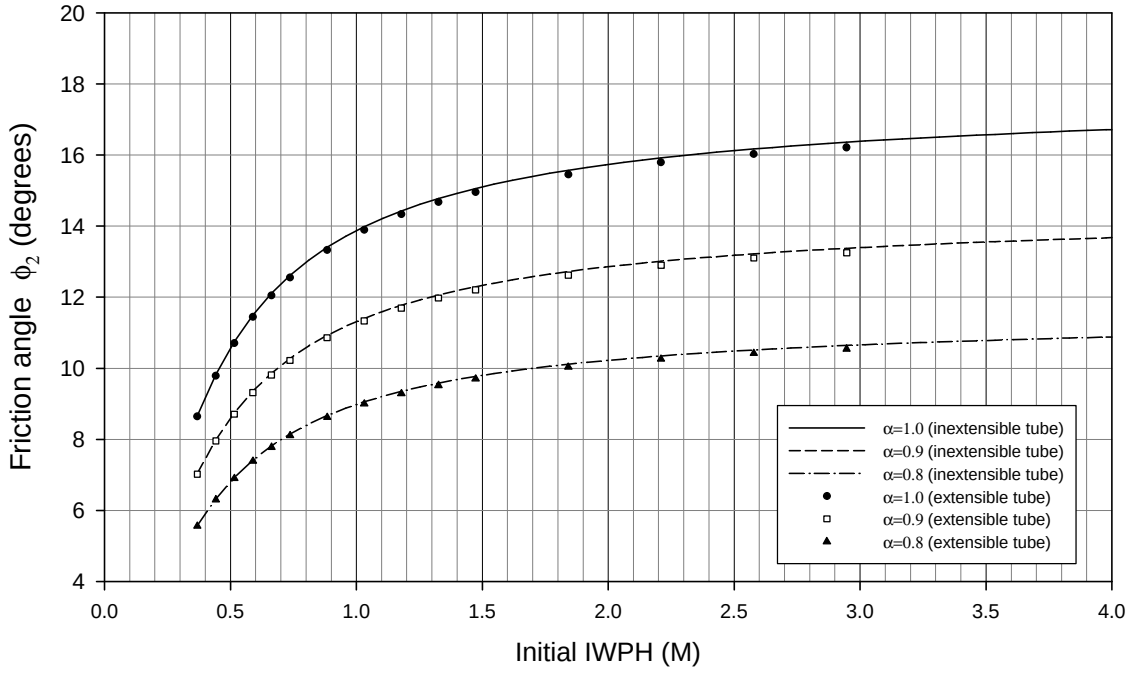

Figure 5.28. Relation between the friction angle ϕ_2 and IWPH of tube for tube slip failure case (circumference of tube=1.4732 m)

If the value of the friction angle f_2 is above the solid line for a given initial IWPH of the tube, the apron-tube dam cannot fail by slip between the tube and the drain. For example, if the initial IWPH of the tube is 0.5 m and the friction angle f_2 is 15 degrees, then the apron-tube dam does not fail by slip of the tube, if the apron length is long enough. If the apron-tube dam fails because of a short length of apron, the critical external water height will be the same for different IWPH cases, just as in the previous parametric study.

As another example, if the friction angle f_2 is 7 degrees, and the initial IWPH of the tube is 0.5 m, the apron-tube dam will fail at an external water level 80% of the height of the tube, even with an infinite length of apron.

Now consider an apron-tube dam that is installed on the drain material with a low friction angle, say 10 degrees, and the apron-tube dam has sufficient length of apron so the system cannot fail by slip between the apron and the ground. If the initial IWPH of the tube is 0.45 m, the critical external water height is almost equal to the height of the tube, which is approximately 0.33 m according to the formula for the tube height by Namias (1985). If the initial IWPH of the tube is 0.7 m, the critical external water height is 90% of the tube height and it is 0.34 m. Finally, if the IWPH of the tube is 1.0 m, the critical external water height is 0.35 m theoretically (see Figure 4.16).

With a frictional angle of 12 degrees between the tube and drain, the critical external water height of the tube increases as the initial IWPH of the tube rises up to 0.65 m of the initial IWPH, since the critical external water height is as high as the height of the tube and the height of the tube grows when the initial IWPH of the tube increases. But with higher initial IWPH of the tube, the critical external water height does increase, yet the increment is not noticeable, because the factor a gets smaller.

Therefore it is concluded that the initial IWPH of the tube does not influence the critical external water height much, whether the apron-tube dam system fails by slip between the apron and ground or slip between the tube and drain, if the tube lies on a drain that has a low frictional angle with the tube material, approximately below 10 degrees. If the tube lies on material with a higher frictional angle, such as 15 degrees, a higher IWPH produces a higher tube height and the critical external water height will increase up to the height of the tube if the apron is long enough. If the apron length is not sufficient to provide the required friction capacity against the external force, the apron-tube dam slips at the same level of external water regardless of the amount of IWPH of the tube.

It is noted that the above conclusions are suitable when the apron-tube dam is not set on very soft soil, since the formulas used to develop Figure 5.28 are based on a tube on a rigid foundation.

5.5.2. Slip Failure by Apron

It is expected theoretically that the critical external water level depends on the apron contact length and the friction angle between the apron and ground only when the frictional angle between tube and ground is larger than 15 degrees and the initial IWPHs of the tube are within a certain range (see the previous section).

The effect of the friction angle on the critical external water height is verified here by comparison with the numerical result and analytical calculations. The analytical results are based on guessed contact lengths of the apron. It is noted that the exact contact length of the apron cannot be determined without numerical modeling. It is discovered that the contact length of the apron shortens as the external water level rises in the numerical analysis (see Section 5.4.1). However, constant contact lengths of the apron are used in the analytical calculation of the critical external water height, since the change of the apron contact length on the external water level cannot be determined analytically yet.

For this study, the apron-tube numerical models are similar to the models in the other parametric study except for the friction angles. The apron-tube dam is assumed to have identical friction angles between the apron and ground and between the tube and ground. It is noted that the length CurB is 5.08 cm (2 in.) and CurB does not affect the contact length of the apron much. Further descriptions of the apron-tube dam model are:

- The length of the apron is 0.30 m (exactly 12 in.).
- The length of the apron on the sand, which is from the end of the apron to the beginning of the drain, is 0.15 m (6 in.).
- Friction angles applied in this study are 15, 20, and 25 degrees.
- The initial IWPH of the tube is 0.516 m (0.35 in normalized IWPH).

To find the critical external water height by calculation, we substitute $F_{\max\_a}$ in Equation 5.2 with half of the external water force from Equation 5.4, divide both sides by h_E and g_w, and solve for h_E:

$$h_E = 2L_{a1}\tan f_1 + 4(L_a - L_{a1})\tan f_2$$

The value h_E in the above equation is the critical external water height if the apron-tube dam fails by slip of the apron, so

$$h_c = 2L_{a1} \tan f_1 + 4(L_a - L_{a1}) \tan f_2$$

Equation 5.8

where h_c = Critical external water height

Since the total apron length is 0.30 m and CurB is 0.05 m, the length of apron contacting the ground, which has two parts, drain and sand, is presumed to be between 0.25 m and 0.30 m when the external water level is critical; therefore, guessed values for L_a in equation (7) are 0.25 m, 0.28 m, and 0.30 m. Table 5.5 presents the calculated critical external water heights (critical EWH) based on the guessed contact apron length.

Table 5.5. Critical external water height by Equation 5.8

Friction angle (degrees)	Contact apron length La (m)	Apron length on sand La1(m)	Apron length on drain (m)	Critical EWH (m)
15	0.305	0.152	0.152	0.245
	0.279	0.152	0.127	0.218
	0.254	0.152	0.102	0.191
20	0.305	0.152	0.152	0.333
	0.279	0.152	0.127	0.296
	0.254	0.152	0.102	0.259
25	0.305	0.152	0.152	0.426
	0.279	0.152	0.127	0.379
	0.254	0.152	0.102	0.332

Figure 5.29 shows the critical external water height when both friction angles, f_1 and f_2, are 15, 20, and 25 degrees numerically and analytically. The solid line designates the numerical result, and the dashed lines indicate the results from the manual calculation.

The horizontal axis presents the tangent values of friction angles, and the critical external water heights by Equation 5.8 on the vertical axis are perfectly proportional to the tangent values of friction angles. But the numerical results are not proportional even though the critical external water height increases as the friction angle becomes large, as predicted. The main reason for this is that the contact length of the apron in the numerical simulation changes; as the critical external water height increases, the contact length shortens as shown in Table 5.6 (also see 5.4.1).

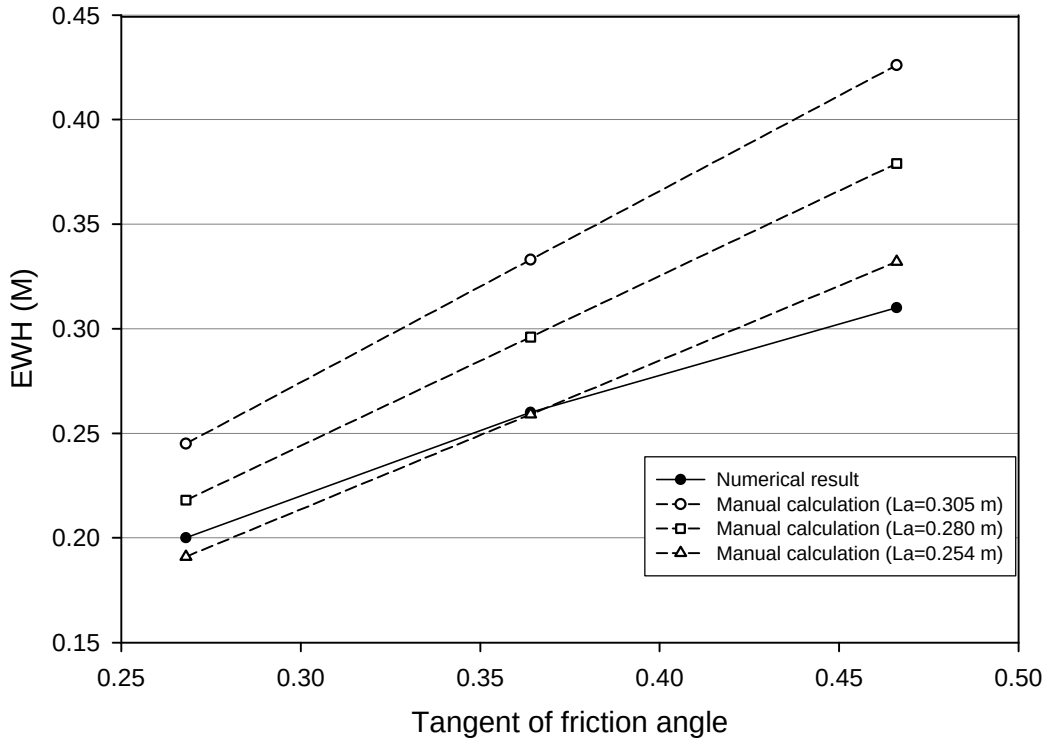

Figure 5.29. Critical external water heights for different friction angles

Table 5.6. Contact length of apron in numerical simulation

Friction angle (degrees)	Contact length numerical (m)	Critical EWH (m)
15	0.256	0.200
20	0.239	0.260
25	0.240	0.310

5.6. Summary and Conclusion

A tube dam with different lengths of an apron was numerically modeled and analyzed. The deformation and pore pressure effects of the soil were considered in the numerical analysis.

First, the numerical results were compared with the experimental results. The deformations of the cross-section of the tube show a good agreement with the experimental results, together with the critical external water heights for different lengths of apron. The internal water pressure head displays a fair agreement with the experiments. It is believed that some difference between the numerical and the experimental results are produced by observation error and leakage in the tests. In addition, the slightly different tube circumference may be another factor.

The pore pressures from the numerical and the experimental results were evaluated. Both competitive results displayed a pore pressure reduction near the drain. Also, it was found that the pore pressure decreased linearly beneath the apron-tube dam approaching the drain.

The internal water pressure head of the apron-tube dam increases as the flood level rises in the numerical simulation; as a result, the maximum tension of the tube increases. It is noted that the internal water pressure head of the tube which is exposed to external water usually decreased for other types of water-filled tube dams. The proper assessment of the tension in the tube provides guidelines regarding the design of the apron-tube dam, such as the material strength and the seam strength required of the geomembrane.

As a parametric study, the effects of the initial shape of the apron were investigated. It was found that there was little variation in the contact length of the apron during flooding, and the initial shape of the apron does not have much influence on the stability of the tube.

The relation between the critical external water height and the internal water pressure head was investigated. For a tube dam with an apron length of 0.30 m, the critical external water height was not affected by the internal water pressure head of the tube when the tube was set on a foundation which has 15 degrees of friction angle with the apron-tube dam. This is because the failure of this particular case was caused by slip between the apron and the foundation.

The apron-tube dam typically becomes unstable by slip and it is unlikely that the apron-tube dam will become unstable by rolling. Since the apron acts as a barrier between the external water and the lower portion of the tube and reduces the lifting force from the external water.

The slip failure of the apron-tube dam can occur at two interfaces, between the apron and the foundation or between the tube and the foundation. Since the failure mode of the apron-tube dam is slip and the friction under the apron and the tube are identical, the critical external water height can be evaluated with analytical formulations. The stability of the apron-tube dam is controlled mainly by the friction angle values f_1 and f_2 between the dam and ground, and by the length of the apron. Also, stability would surely be affected by the internal water pressure head of the tube theoretically if the apron-tube dam were installed on a material which has a lower friction angle (below 17.7 degrees).

Chapter 6. Baffle Tube Dam

6.1. Introduction

One of the water-filled tube dam manufacturers, Aqua Barriers, has developed and utilized baffle tube dams in several circumstances (http://www.aquabarrier.com, 2002). The tube dams have been used for dewatering in construction and work sites, mitigating flooding, and containing silt and sediments.

The baffle tube dams are constructed with one baffle or two baffles inside, running along the length of the tube dam. The manufacturer claims that the perforated inner restrained diaphragm prevents rolling of the tube when the tube dam is exposed to external loading.

According to the product specification of Aqua Barriers, the circumference of the single baffle tube varies from about 3 m to 7 m and the height of the baffle varies from 0.6 m to 1.2 m. The proportion of the baffle height to the circumference of the tube is about 0.17 to 0.20.

In this study, the single baffle tube case is investigated numerically. The circumference of the tube is fixed at 1.4732 m, which is used in other types of tube dam case studies here. The height of the baffle is determined as a proportion of the circumference of the tube. The thickness and the material of the baffle are assumed to be identical to those of the tube.

Even though the company does not use a drain system under the tube dam, it is assumed here that a geotextile layer is installed underneath the baffle tube dams in the numerical analysis to act as a drain. It is expected that the drain reduces the pore pressure and provides more stability regarding possible slip failure of the tube. The effect of internal water pressure head change is considered during the simulation of the flooding.

6.2. Numerical Modeling

The height of the baffle is specified to be a portion of the circumference. The circumference of the tube is 1.4732 m (58 in.). The baffle and the tube are modeled with beam elements in FLAC and the properties of the baffle and the tube are identical to those used in the apron-tube dam case (See Section 3.2.1).

The soil and drain also are modeled with grid meshes. The Mohr-Coulomb Soil model is employed to represent silty sand. The same soil and drain properties as in the apron-tube dam case are used.

Interface elements are assigned between the tube and the foundation. It is assumed that the cohesion properties of the interface are negligible, and the friction angles are determined from direct shear tests (Fitzpatrick et al., 2001; Moler et al., 2002). The interface properties are presented in Section 3.2.4

The external water and internal water are simulated by hydrostatic pressure, and then the pressures are converted to point loads on the nodes of the beam elements of the tube. Since water inside the tube can go through the baffle, the hydrostatic pressure is not applied on the beam elements of the baffle in the model.

6.2.1. Initial Shape of Baffle Tube Dam

The initial shape of the baffle tube is developed to simulate close to the real situation. As shown in Figure 6.1, the initial empty tube is a long capsule shape with an "s" shape of a baffle inside.

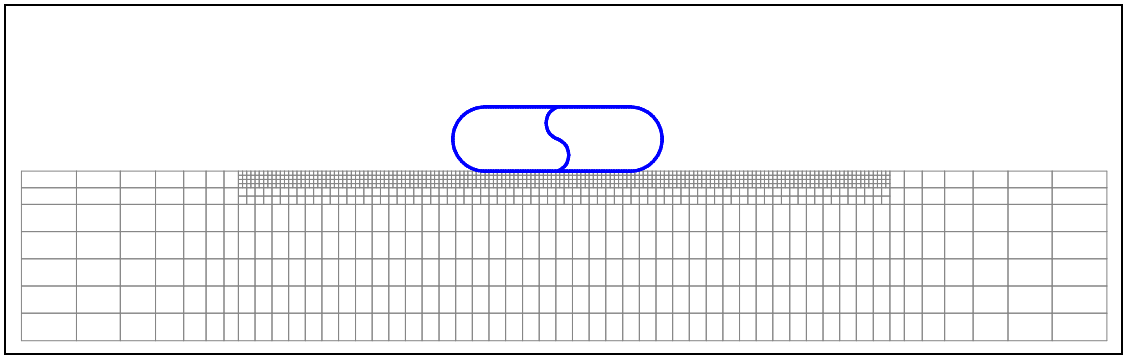

Figure 6.1. Initial shape of the baffle tube with soil grids

The beginning shape of the baffle is determined so that a certain length of baffle can fit within the height of the tube. With given length of baffle, L_b, and the initial height of the tube, h_{t0}, the interior angle, q, of an arc of the "s" shape can be found from equation 2.3, which was derived using equations 2.1 and 2.2 (see Figure 6.2). The radius, r, then can be determined from equation 2.2 with the interior angle, q. A beam element of the baffle is produced as a chord of an arc which has the radius r and the interior angle $q/2n$ where n is the number of beam elements in the baffle.

$$\frac{h_{t0}}{2\sin q} = \frac{r}{\cos(\frac{q}{2})} \qquad \text{Equation 2.1}$$

$$rq = \frac{L_b}{2} \qquad \text{Equation 2.2}$$

$$\frac{L_b}{h_{t0}} = \frac{q\cos\frac{q}{2}}{\sin q} \qquad \text{Equation 2.3}$$

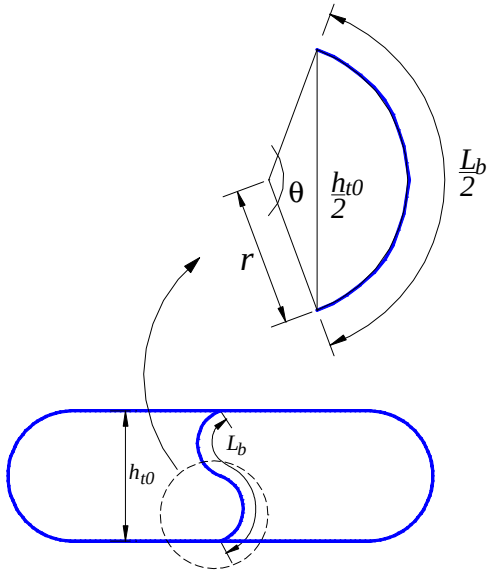

Figure 6.2. Initial shape of baffle

Since the two arcs are represented by the connections of linear beam elements, it is possible that a difference between the two arc lengths and the sum of beam element

lengths might not be negligible. However, the difference can be significantly reduced if there are a sufficient number of elements for the baffle. For example, when the number of beam elements for the baffle length, 0.25 m, is 40, the difference is within 0.1 %. Therefore, 40 beam elements are used for the baffle, and 200 beam elements are employed for the tube.

After the setup of the initial shape of the baffle tube on the grid, the inflation process begins by applying the water pressure normal to the tube. The internal water pressure is increased gradually up to the given initial water pressure to induce a stabilized calculation in FLAC, since the deformation of the tube is extremely nonlinear. In addition, the hydrostatic pressures are continuously altered because of the large deformations of elements of the tube. It is noted that the internal water pressure is not applied on the baffle in the numerical model since the baffle is assumed to be perforated and the internal water pressures of the headwater side and the tailwater side of the baffle are the same.

Figure 6.3 presents an example of deformations of the baffle tube during the inflation procedure. During the progression, from the initial curved shape, the baffle becomes vertical and straight.

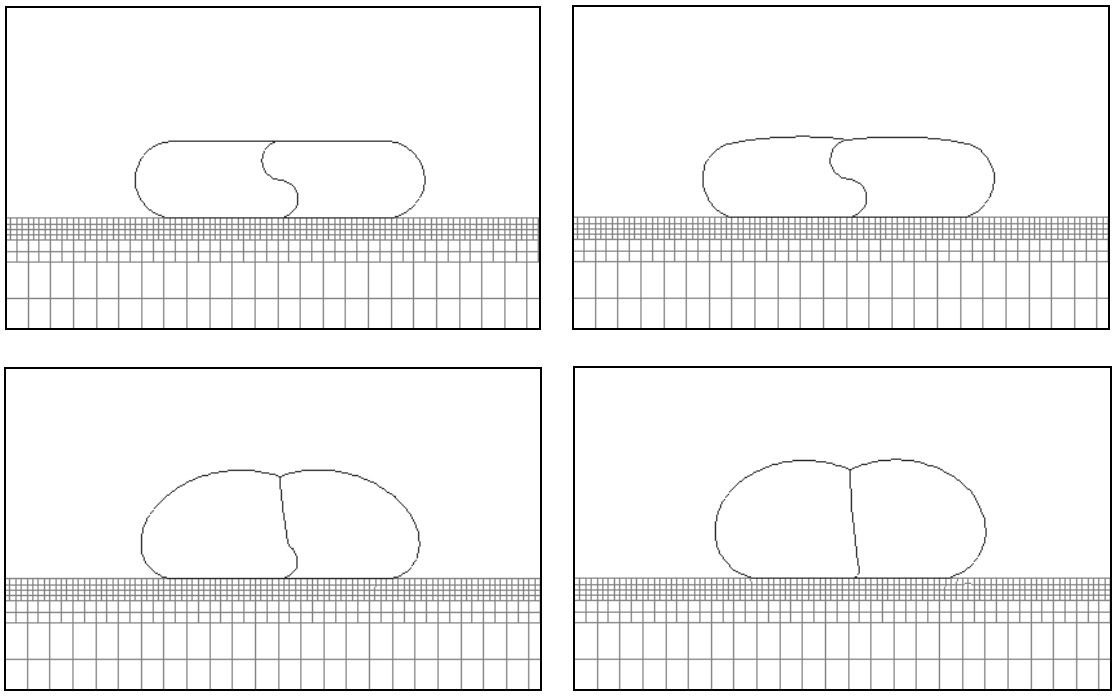

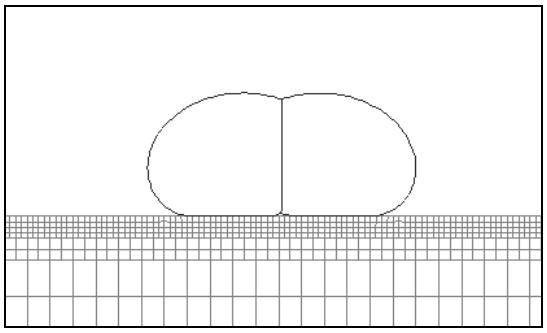

Figure 6.3. Detailed inflation (length of baffle = 0.17L, 0.2504 m)

6.3. Numerical Analysis

A single baffle tube dam is examined numerically. It is assumed that the area of the tube remains constant when the tube is deformed, since the tube is sealed after inflation in the real situation. To determine the internal water pressure head (IWPH) of the tube for constant area, the factored secant method (see Section 3.4) is employed.

First, the inflation of baffle tubes is investigated based on the length of the baffle and IWPH of the tube.

Next, the effect of the friction angle of the interface between the tube and the foundation is examined. In addition, two lengths of baffle are analyzed numerically to investigate the influence of the baffle length. In these two parametric studies, the internal water pressure heads are 0.3683 m, 0.5156 m, and 0.6629 m, which are 0.25, 0.35, and 0.45 as normalized pressure heads[1]. The frictional angles of the interface are 15, 25, and 35 degrees. The deformation of the foundation is not considered in these studies; however, the pore pressure effect beneath the tube is considered. The critical external water levels are determined for each case.

Lastly, baffle tube dams on sand foundations are analyzed numerically. The deformation and the groundwater flow of the soil are considered. It is expected that the stability of the tube dams is affected by the deformation and pore pressures of the soil in addition to the internal water pressure head of the tube.

---

[1] Normalized pressure head: the pressure head divided by the circumference of the tube.

6.3.1. Inflation of Baffle Tube Dam

Baffle tube dams with two different baffle lengths are inflated with different initial internal water pressure heads. The lengths of baffle used here are 0.2580 m and 0.2946 m, which are 0.175 and 0.20 as normalized lengths. The hydrostatic pressure heads of the inflation are 0.3683 m, 0.4420 m, and 0.5156 m, and these are 0.25, 0.30, and 0.35 as normalized heads.

Figure 6.4 shows the inflated shape of each baffle tube dam. Note the bottom center of the baffle tubes in Figure 6.4, which is in contact with the foundation at the beginning of the inflation procedure, but is separated from the soil when the baffle tube reaches its equilibrium shape under the internal water pressure. However, the separation of the bottom center of the tube does not happen always. It depends on the internal water pressure and the length of the baffle.

Table 6.1 presents the tension in the baffle tube dam. The tension in the tube mainly depends on the IWPH of the tube, as expected, but the tension in the baffle depends on the ratio of baffle length and the internal water pressure head. When the ratio increases, the tension in the baffle decreases, as shown in Figure 6.5. Theoretically, the upper limit of the tension in the baffle cannot be greater than the sum of the tensions in the two sides of the tube connected to the baffle, yet the upper limit will be governed by the strengths of the membrane material and the bonding between the baffle and the tube.

Figure 6.6 displays tube areas and the product of IWPH and contact length. The solid lines represent the tube areas for baffle lengths 0.2580 m and 0.2946 m, and the dashed lines denote the product of IWPH and contact length of the tube. For a simple tube, the weight of the internal water per unit length is equivalent to the product of the contact length under the tube and the normal pressure acting on it. In other words, the product of the IWPH and the contact length corresponds to the tube area when there is no external water pressure (See Section 3.4). Differences between the tube area and the product of the IWPH and contact length vary from 0.3 percent for 0.3683 m (0.25L) IWPH in the baffle length 0.2946 m case to 6.3 percent for 0.5156 m (0.35L) IWPH in the baffle length 0.2580 m case. The differences are not great.

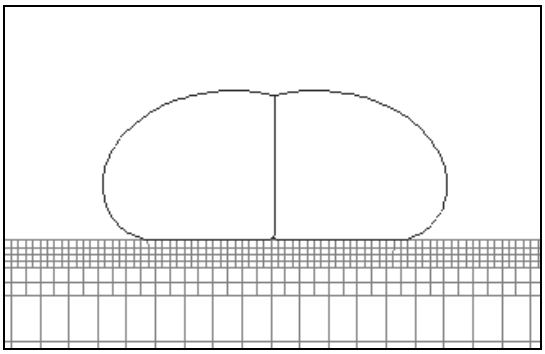

(a) Baffle length = 0.2504 m (0.17L)
IWPH = 0.3683 m (0.25L)

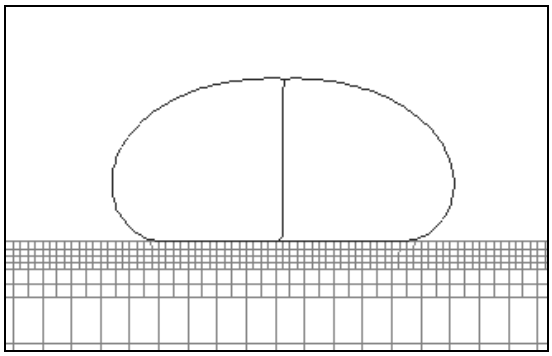

(b) Baffle length = 0.2946 m (0.20L)
IWPH = 0.3683 m (0.25L)

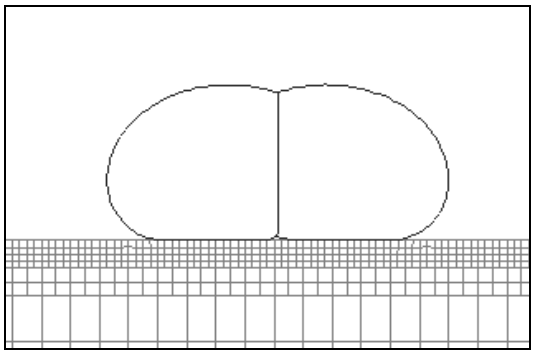

(c) Baffle length = 0.2504 m (0.17L)
IWPH = 0.4420 m (0.30L)

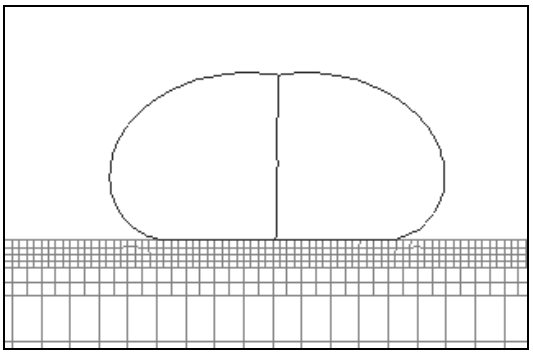

(d) Baffle length = 0.2946 m (0.20L)
IWPH = 0.4420 m (0.30L)

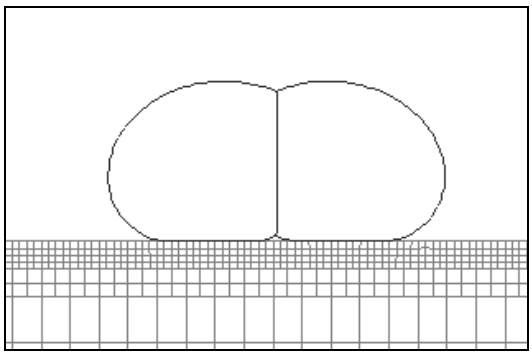

(e) Baffle length = 0.2504 m (0.17L)
IWPH = 0.5156 m (0.35L)

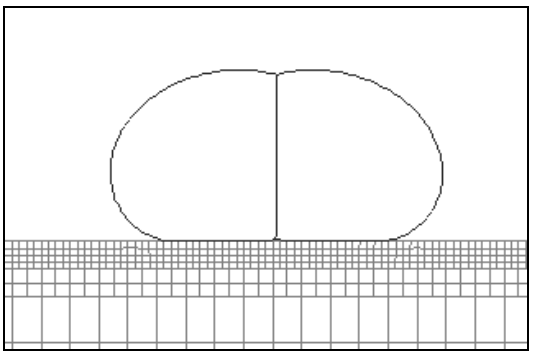

(f) Baffle length = 0.2946 m (0.20L)
IWPH = 0.5156 m (0.35L)

Figure 6.4. Different inflated shapes based on length of baffle and IWPH

Table 6.1. Tensions in tube and baffle

IWPH	Baffle length = 0.2580 m (0.175L)		Baffle length = 0.2946 m (0.20L)	
	Tension in tube (N)	Tension in baffle (N)	Tension in tube (N)	Tension in baffle (N)
0.3683 m (0.25L)	307.8	142.3	317.7	31.9
0.4420 m (0.30L)	413.4	277.7	429.5	142.6
0.5156 m (0.35L)	523.2	417.4	544.6	268.1

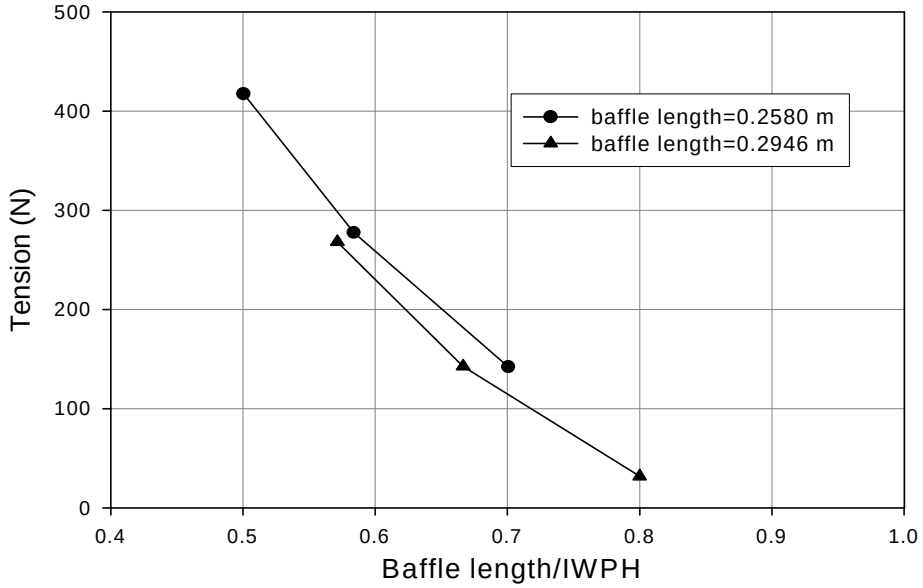

Figure 6.5. Tension in baffle

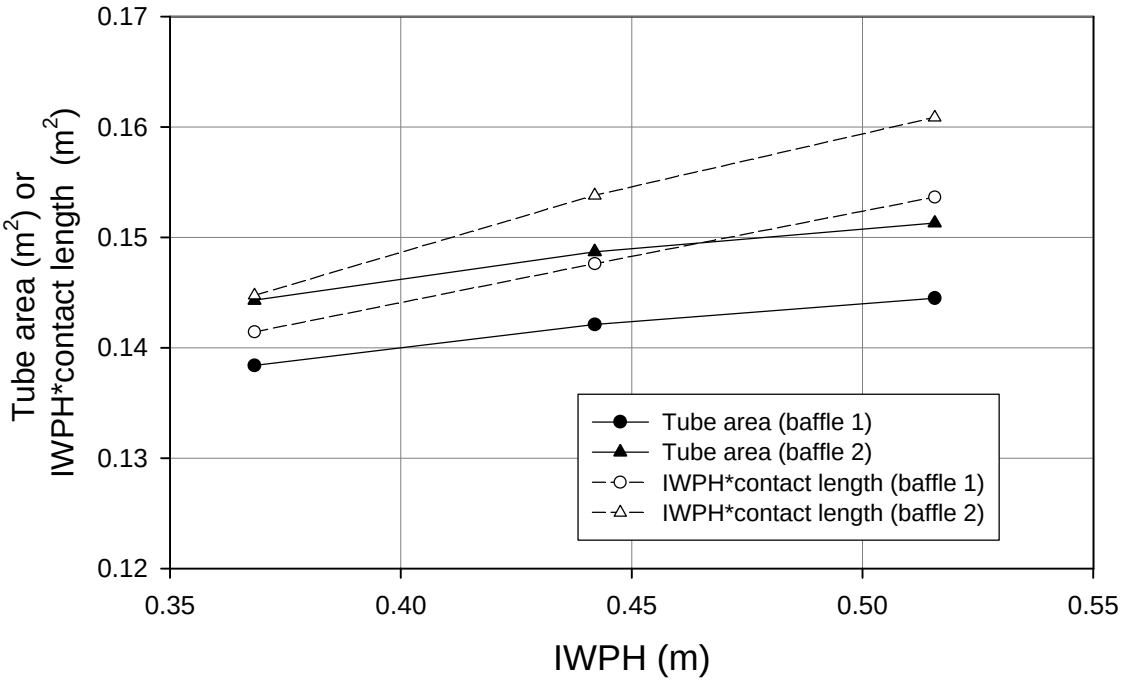

Figure 6.6. Tube area

(baffle 1 : baffle length 0.2580 m (0.175L); baffle 2 : baffle length 0.2946 m (0.20L))

6.3.2. Baffle Length

To investigate the effect of the baffle length regarding the critical external water level, two lengths of baffle, 0.2504 m (0.17L) and 0.2946 m (0.20L), are considered. Each baffle tube dam is inflated with three internal water pressure heads, 0.3683 m (0.25L), 0.5156 m (0.35L), and 0.6629 m (0.45L).

The drain is assumed to be located under the tailwater side of the tube with its left end 8.5 cm from the center line as shown in Figure 6.7, and the length of the drain is 88 cm. It is assumed that the friction angles between the tube and the soil and between the tube and the drain are the same. The friction angles are assumed to be 25 degrees. The foundation is assumed to be rigid, yet the underground water flow is considered in order to obtain an assessment of the pore pressure beneath the tube.

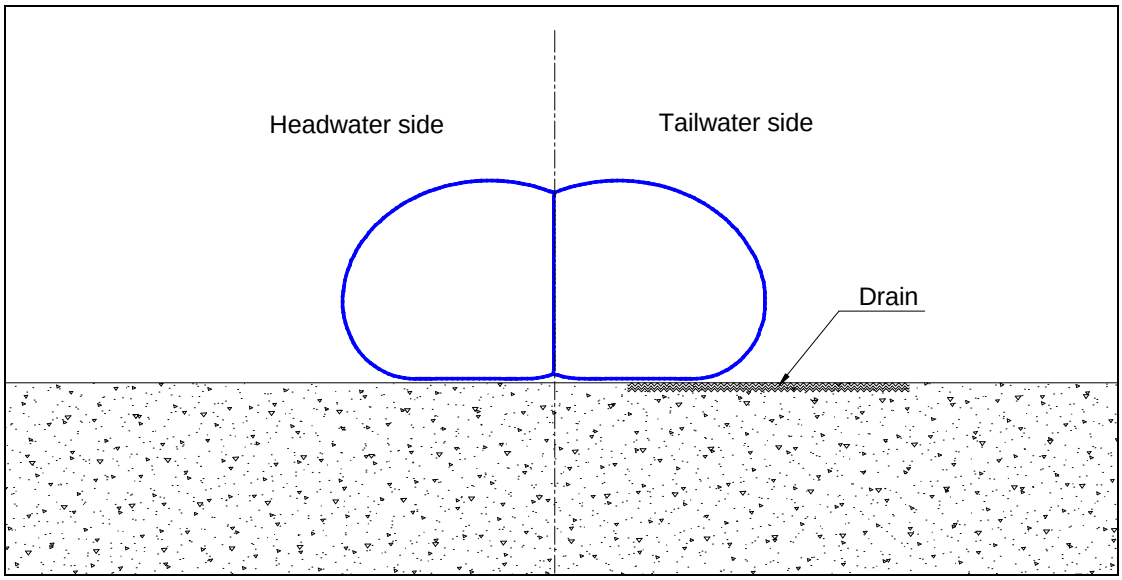

Figure 6.7. Baffle tube dam with drain

The external water pressure is applied at the headwater side of the tube to simulate the flooding. The external water level is increased to 0.0737 m (0.05L), 0.1473 m (0.10L), 0.1842 m (0.125L), and 0.2210 m (0.30L) from the bottom of the foundation in the beginning, and then the level rises by 0.737 cm (0.005L) increments after the 0.2210 m level until the tube fails.

The change of the internal water pressure head during the flooding is computed using the factored secant method (see Section 3.4.2). Figure 6.8 shows the internal water pressure head (IWPH) for each case as a function of the external water level. The solid lines and the dashed lines symbolize baffle 1 and baffle 2, respectively. Baffle 1 denotes the tube dam with baffle length 0.2504 m (0.17L), and baffle 2 represents the tube dam with baffle length 0.2946 m (0.20L). When the external water levels are low, the internal water pressure head does not change significantly. However, as the external water level approaches the critical level, the contact region becomes smaller and the internal water pressure head increases notably. For baffle 1 and baffle 2 with initial IWPH of 0.3683 m, the IWPH increases 11.3 % and 16.8 % in total. But the increments of IWPH for higher initial IWPH cases are smaller. For example, the IWPH increases 2.7 % for baffle 1 with

initial IWPH of 0.6629 m, and 3.9 % for baffle 2 with the same initial IWPH. In general, the baffle 2 cases have higher increases of IWPH than the baffle 1 cases.

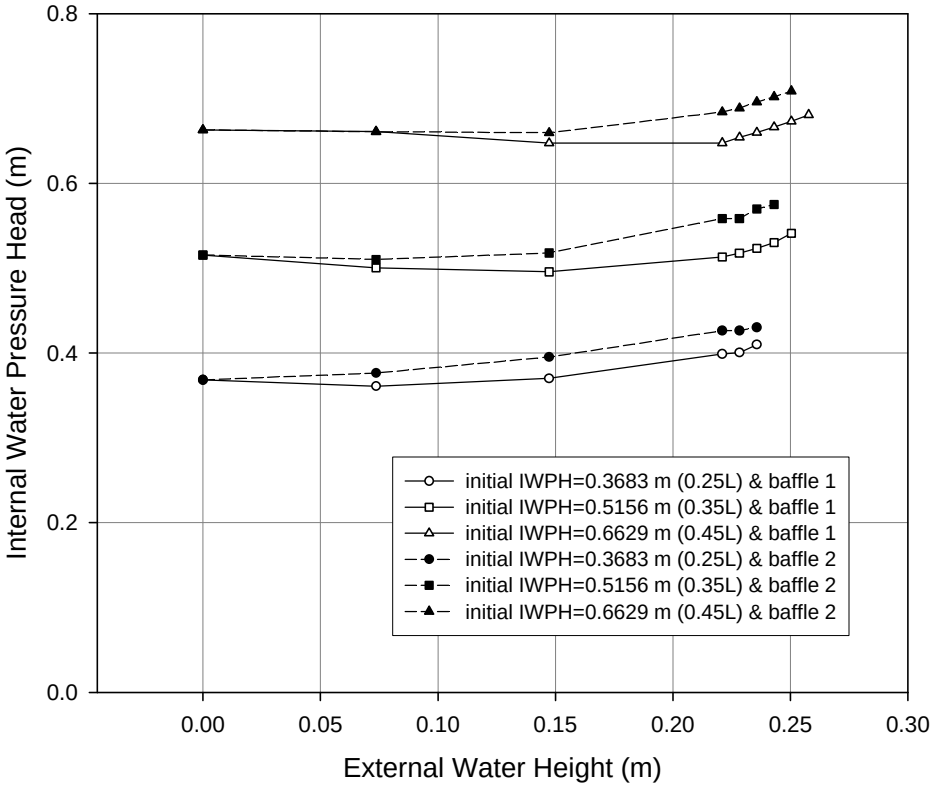

Figure 6.8. Change of internal water pressure head with external water height

Figure 6.9 and Figure 6.10 depict the deformations of the baffle 1 case with IWPH of 0.3683 m and the baffle 2 case with IWPH of 0.5156 m, respectively. As the external water level approaches the critical external water level, the headwater side of the tube slips toward the tailwater side, but the tailwater side of the tube does not slip until the critical external water level is reached. At the critical external water level, the tailwater side of the tube begins to slip and simultaneously the headwater side rolls over the tailwater side, as shown. However, when the external water level is low, the headwater side does not slip.

The critical external water height (EWH) for baffle 1 and baffle 2 cases are presented in Figure 6.11 for three initial internal water pressure heads. The critical external water levels of baffle 1 and baffle 2 are identical for the IWPH of 0.3683 m, and

the level is 0.2357 m (0.16L). For the IWPH of 0.5156 m, the critical external water level of baffle 1, 0.2504 m (0.17L), is slightly higher than the critical level of baffle 2, 0.2431 m (0.165L). The baffle 1 case with IWPH of 0.6629 m fails after an EWH of 0.2578 m (0.175L), while the baffle 2 case with the same IWPH fails after 0.2504 m (0.17L). The difference is 7.4 mm (0.005L).

Therefore, it can be concluded that the length of the baffle influences the critical external water level. In these examples, the shorter baffle length provides slightly more stability than the longer one when the friction angle of the interface between the tube and the foundation is 25 degrees. The reason for this is that the tube dam with the shorter baffle has a flatter shape compared to the other one and this generates a larger resistance to rolling.

For example, consider a rigid body subjected to external forces, that rotates about a point in plane motion. The resultants of the external forces acting on the body have two components, the resultant force through the center of the mass and the corresponding couple about the center of the mass. Also, the resultant force creates a rotation about the point, and the moment is the product of the resultant force and the perpendicular distance between the point and the line of the force. Hence, the resistance of the body about the rotation is provided by the mass moment of the inertia and the perpendicular distance to the line of the force between the center of the mass and the instantaneous center of rotation.

Since the tube dam deforms a great deal when it is subjected to the floodwater, the above theory cannot be fully applied to the understanding of the rotation of the baffle tube dam. However, the total area of the tube remains constant, and the mass moment of inertia and the distance between the center of the tube and the instantaneous center of the rotation, change during the deformation. Under the same circumference and IWPH, the baffle 2 case has a larger tube area than the baffle 1 case, but the baffle 1 case has a flatter shape and this results in more resistance to rotation.

If the conditions of the foundation produce slip failure of a baffle tube dam rather than rolling failure, there is a strong possibility that the longer baffle case has more stability than the shorter baffle tube case since its area is larger.

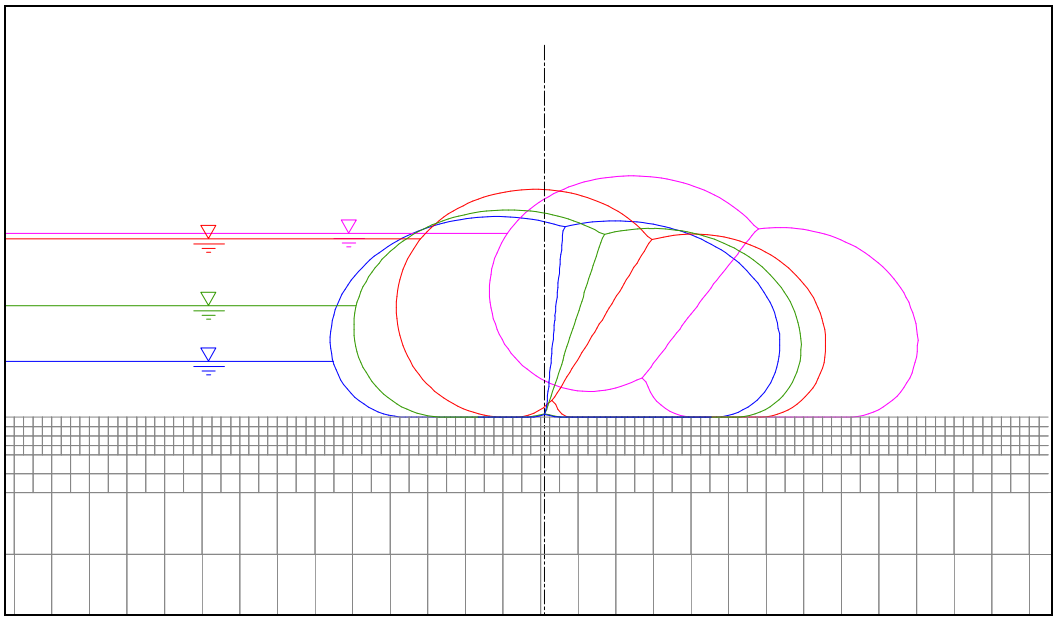

Figure 6.9. Deformations of tube with baffle 1 and IWPH 0.3683 m (0.25L)

(friction angle 25 degrees)

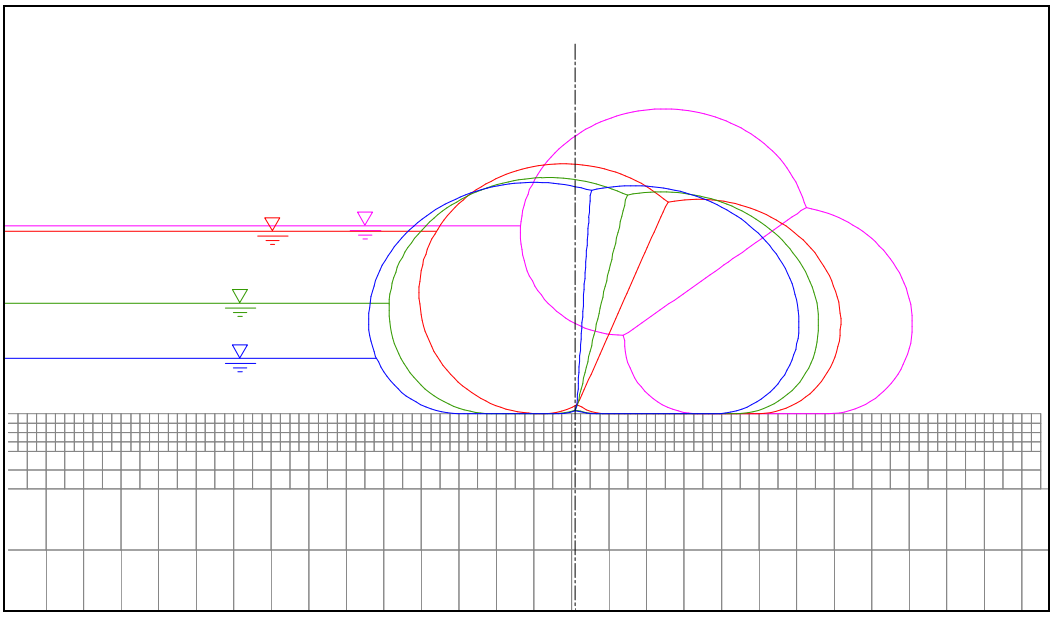

Figure 6.10. Deformations of tube with baffle 2 and initial IWPH 0.4420 m (0.35L)

(friction angle 25 degrees)

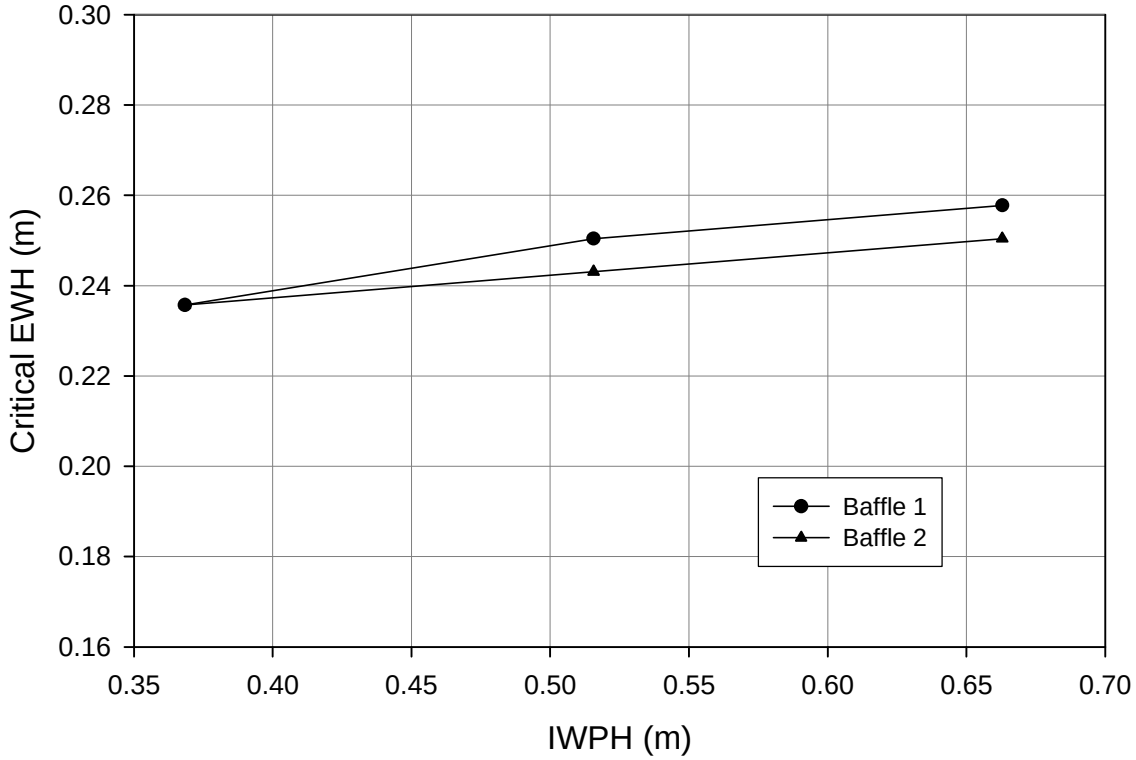

Figure 6.11 Critical external water heights

6.3.3. Friction Angle

When a baffle tube dam is placed in the field, the characteristics of the foundation affect its performance. The foundation can be a clay or sand type of soil. Also, a baffle tube dam can be installed on grass or pavement. If the deformation of the foundation under the baffle tube dam is not considered, the effect of the different types of foundation can be considered by variations of the friction angle for the interface between the tube and the foundation, since the cohesion factor is ignored. Therefore, the baffle tube dam is investigated here with three different interface friction angles, 15, 25, and 35 degrees.

As in the previous section 6.3.2, the location of the left end of the drain is 8.5 cm from the center line as shown in Figure 6.7 and the length of the drain is about 88 cm. It is assumed that the friction angles between the tube and the soil and between the tube and the drain are the same. Also, the foundation is assumed to be rigid, yet the underground water flow is considered to account for the pore pressure effects.

The length of the baffle here is 0.2504 m, which is 0.17 in normalized terms. The initial internal water pressure heads used for the inflation of the baffle tubes are 0.3683 m, 0.5156 m, and 0.6629 m and these are 0.25, 0.35, and 0.45 in normalized pressure heads, respectively. The tube area is kept constant during the deformation caused by the flooding.

Figure 6.9, Figure 6.10, and Figure 6.12 - Figure 6.15 depict the deformations of the baffle tube dam at various external water levels. The blue and green lines represent the deformations at the flood levels 0.0737 m (0.05L) and 0.1473 m (0.10L), respectively. The red line indicates the shape of the baffle tube at the critical external water level, just before failure. Last, the magenta line shows how the baffle tube dam fails. As shown in the figures, the contact region under the headwater side of the tube becomes smaller as the external water level rises.

When the baffle tube dam is installed on the foundation which produces 15 degrees of friction angle with the tube material (Figure 6.12 and Figure 6.13), the failure mode of the baffle tube after the critical external water level is slip.

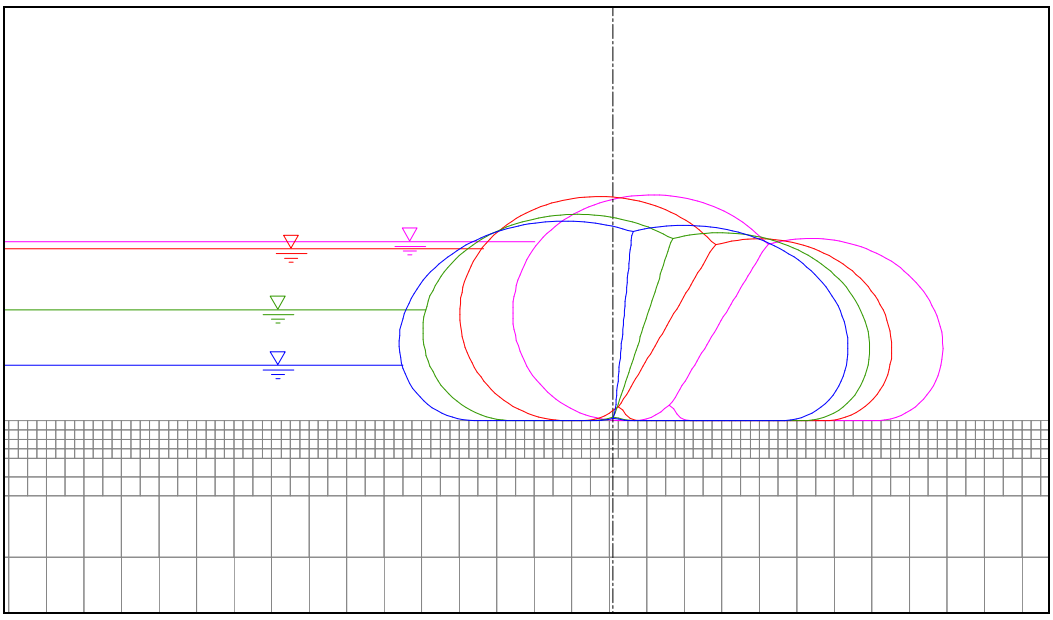

Figure 6.12. Deformations for baffle length 0.2504 m (0.17L) with IWPH 0.3683 m (0.25L) and friction angle 15 degrees

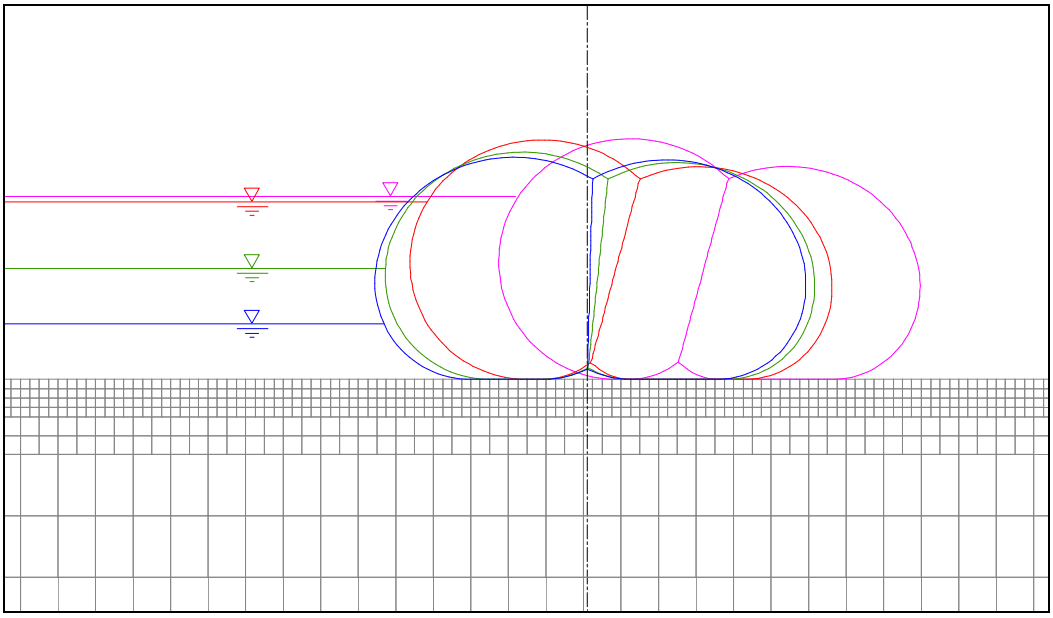

Figure 6.13. Deformations for baffle length 0.2504 m (0.17L) with IWPH 0.6629 m (0.45L) and friction angle 15 degrees

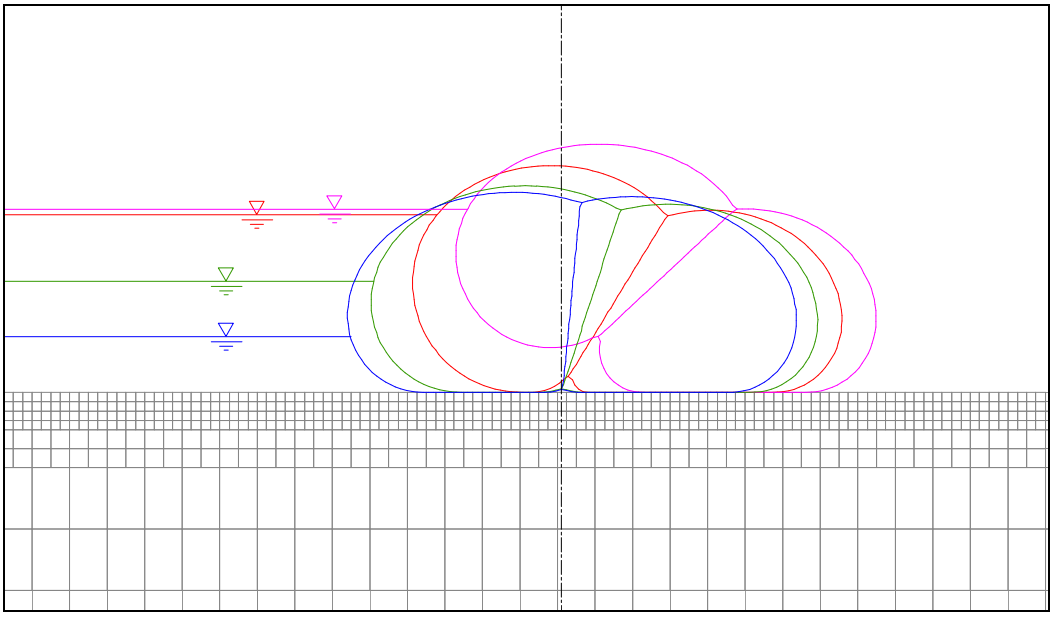

Figure 6.14. Deformations for baffle length 0.2504 m (0.17L) with IWPH 0.3683 m (0.25L) and friction angle 35 degrees

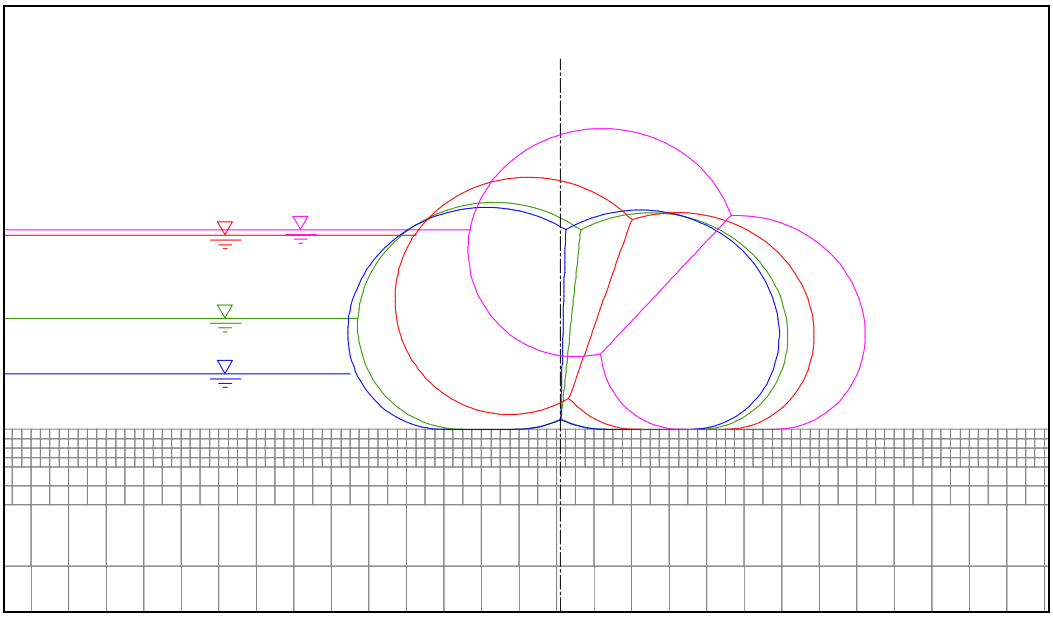

Figure 6.15. Deformations for baffle length 0.2504 m (0.17L) with IWPH 0.6629 m (0.45L) and friction angle 35 degrees

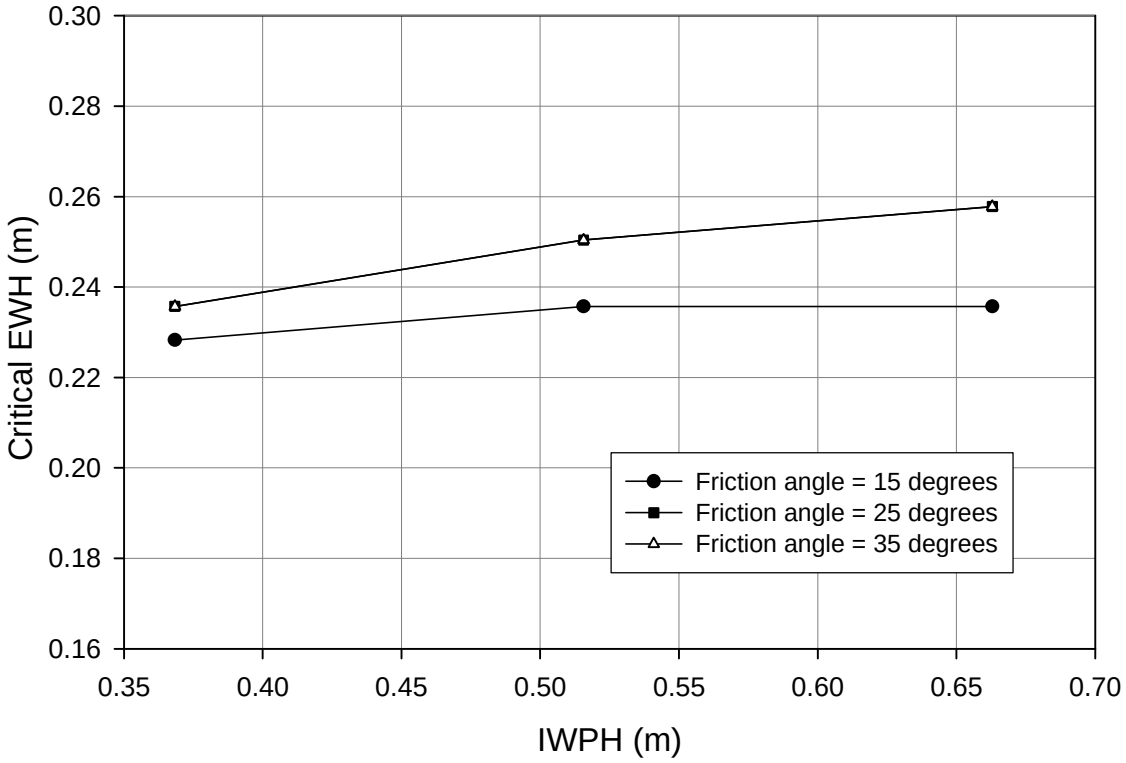

Figure 6.16. Critical external water heights

The external water loading at the headwater side of the tube increases up to the shear strength of the contact region, and then the tube begins to slip. For example, for the IWPH of 0.3683 m, the tube slips after the external water level is 0.2283 m (0.155L). At this critical external water level, the external water generates 256 N of horizontal force on the tube and the increased IWPH, 0.4021 m, together with the tube contact length, 0.273 m, produces a total shear strength of 259 N between the tube and the foundation. Therefore, after this external water level, the horizontal force becomes larger than the shear strength, causing slip failure. It is noted that the shear strength is estimated from the effective normal stresses at the contact region. Both baffle tube dam cases with initial IWPH 0.5156 m and 0.6629 m fail after an external water height of 0.2357 m (0.16L) in Figure 6.16.

For an interface frictional angle of 35 degrees, the baffle tube dam fails similar to the 25 degrees of frictional angle case. The tube dam develops instability as the headwater side of the tube rolls over the tailwater side, since the higher friction angle provides enough shear resistance against slip failure. Again, the rolling resistance depends on the shape of the baffle tube dam and the distance between the centroid of the tube and the instantaneous center of rolling. In addition, the centroid of the baffle tube shifts to the tailwater side as the tube deforms, as seen in Figure 6.14 and Figure 6.15. Because of this, the resistance becomes smaller and eventually the headwater side of the tube rolls over the tailwater side like a number “8” shape.

In this study, as soon as the baffle tube dam starts to roll, the tailwater side of the tube begins to separate from the foundation. When the separation propagates to the beginning of the drain underneath the tailwater side, the pore pressure begins to build up and the baffle tube dam fails by slipping together with rolling.

Figure 6.16 shows the critical external water levels for each case. For 15 degrees of frictional angle, the critical external water levels are 0.2283 m (0.155L), 0.2357 m (0.16L), and 0.2357 m (0.16L) for the IWPH values considered. For 25 degrees and 35 degrees, both baffle tube cases fail at the same external water level, because, first, the rolling failure of the baffle tube dam depends on the geometry and the weight, and second, the drain is exposed to the floodwater when the baffle tube dam starts to roll.

6.3.4. Numerical Simulation of Baffle Tube Dam on Sand Foundation

In this section, the baffle tube dam is assumed to be on a silty sand foundation. Deformation of the soil together with the groundwater flow, are considered and their effects on the baffle tube dam are investigated.

As shown in Figure 6.7, the left end of the drain is assumed to be located 8.5 cm from the center of the tube to the tailwater side and the length of the drain is about 88 cm. The friction angles between the tube and the sand and between the tube and the drain are 32 degrees and 17 degrees, respectively.

The baffle length used here is 0.2504 m. Three initial internal water pressure heads are used to inflate the baffle tube dam, 0.3683 m (0.25L), 0.4420 m (0.30L), and 0.5156m (0.35L). The factored secant method is employed to simulate the change of the internal water pressure head to maintain the constant tube area.

Figure 6.17 presents one example of the pore pressure development together with the deformation of the soil when there is external water. The black arrows indicate the groundwater flow from the headwater side to the tailwater side. It is evident that the pore pressure builds up to 2000 Pa to 2500 Pa under the headwater side of the tube and the pore pressure drops evidently close to the drain. As shown in the enlargement, the pore pressure causes the soil to elevate into the space between the headwater side of the tube and tailwater side of the tube. To reduce the pore pressure more, the drain may be installed underneath the headwater side of the tube instead of the tailwater side. However, this may produce failure of the tube dam system at a lower external water level because the drain will be exposed to floodwater.

Figure 6.18 and Figure 6.19 show the deformations of the baffle tube at various external water levels for IWPHs of 0.3683 m and 0.5156 m, respectively. In addition, the progressions of the soil deformation are depicted as the external water level increases.

For all three cases of IWPH, the baffle tube dams are lifted up by the external water pressure after the critical external water level is reached and the dams begin to slip. Since the frictional angle between the drain and the baffle tube dam is less than the frictional angle of the interface of the sand foundation and the tube, the separation of the

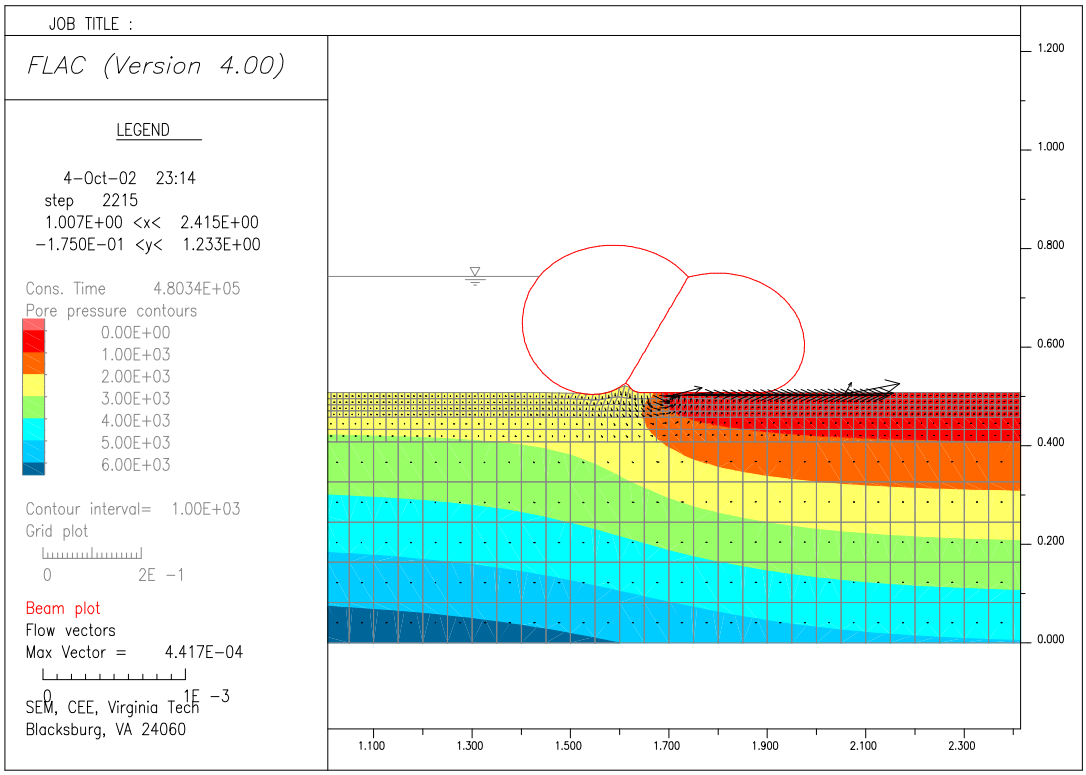

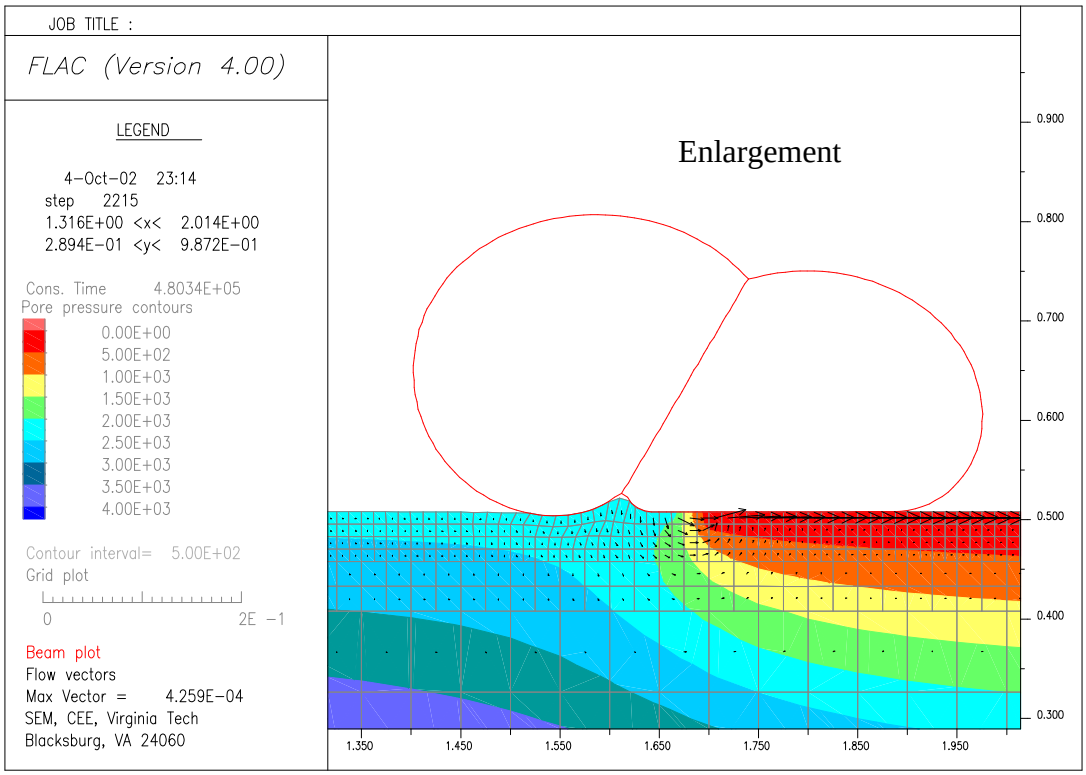

Figure 6.17. Pore pressure contours and deformation of the soil (EWH=0.2357 m)

headwater side of the tube from the foundation results in a reduction in shear strength between the tube and the foundation, and it causes slip failure.

The critical external water heights for this case are 0.2357 m for IWPHs of 0.3683 m and 0.4420 m, and 0.2283 m for an IWPH of 0.5156 m. These results are not collaborated with the results in the preceding sections. It was found previously that, when the deformation of the soil is not considered, a higher IWPH provides more stability. But when the deformation of the soil is considered here, the baffle tube inflated with higher IWPH does not withstand a higher external water height.

The numbering of elements is presented in Figure 6.20. The tube is constructed from beam elements 1 to 200 in a loop and then the baffle is composed of elements 201 to 240. Among the elements of tube, the elements from 71 to 170 are on the headwater side of the tube. Figure 6.21 - Figure 6.23 display the tensions in the baffle tube dam at each external water level. The sign of the tension is negative in FLAC and the tensions are plotted according to the number of the element.

For the IWPH of 0.3683 m (Figure 6.21), the tension in the tube is approximately 306 N and the tension of the baffle is 165 N when there is no external water. Once the external water increases, the tension in the headwater side of the tube decreases, because the net pressure acting on the tube below the external water level is reduced. At the critical external water level, the tension in the headwater side drops to 240 N and the tension in the tailwater side increases to 340 N. For the baffle, the tension rises from 165 N to 335 N. For other IWPH cases, 0.4420 m and 0.5156 m, the tension varies similarly to the case of 0.3683 m initial IWPH (Figure 6.21 and Figure 6.23).

It is of interest that the shear resistance of the tube dam against the horizontal force of the flood is provided mainly by the friction between the headwater side of the tube and the soil when the floodwater level is low, like 0.0737 m and 0.1473 m. At higher external water levels, the shear resistance is produced mostly by the friction of the tailwater side of the tube, as the contact region of the headwater side is reduced significantly.

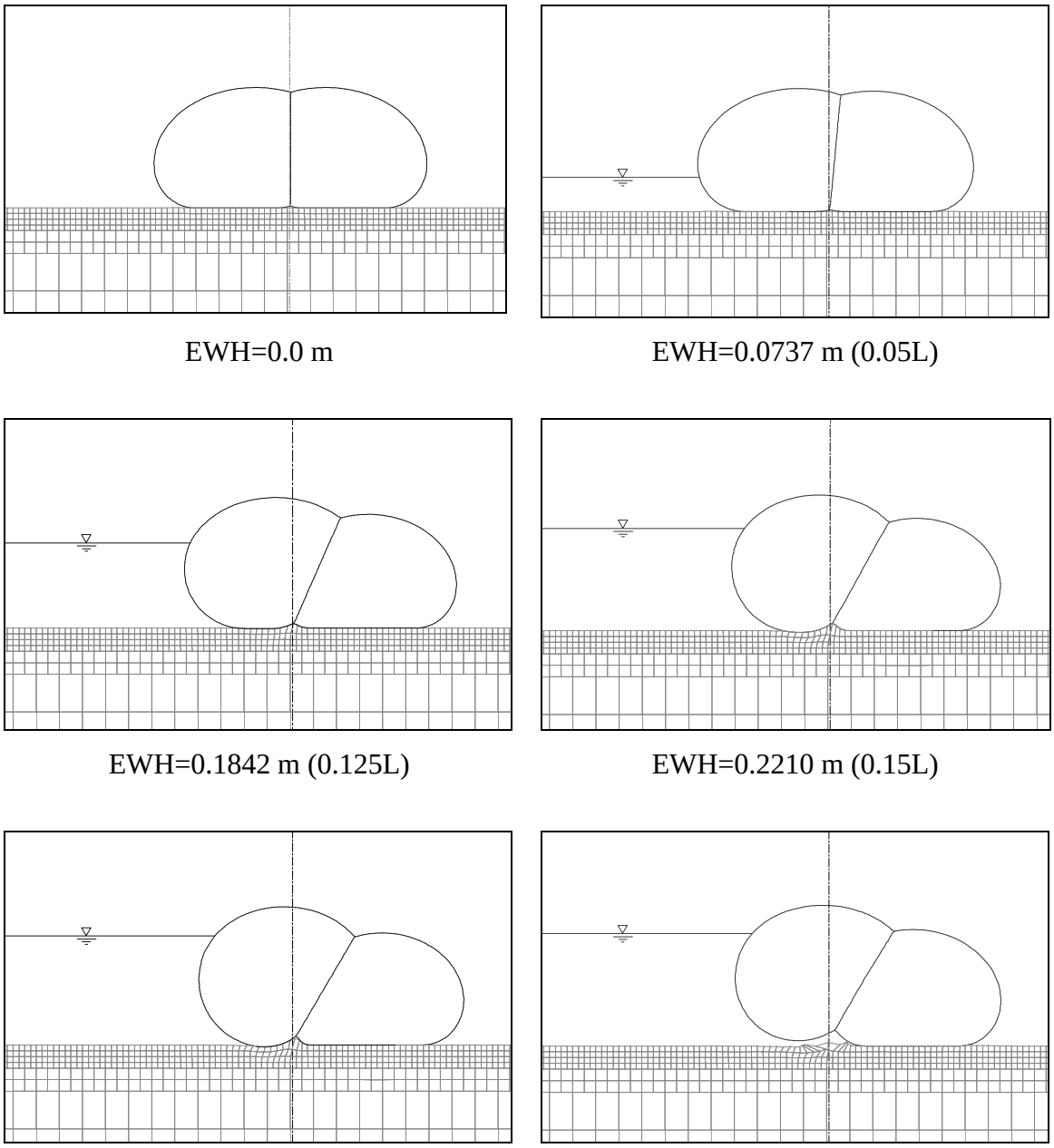

Figure 6.18. Deformations and failure of baffle tube dam (IWPH=0.3683 m)

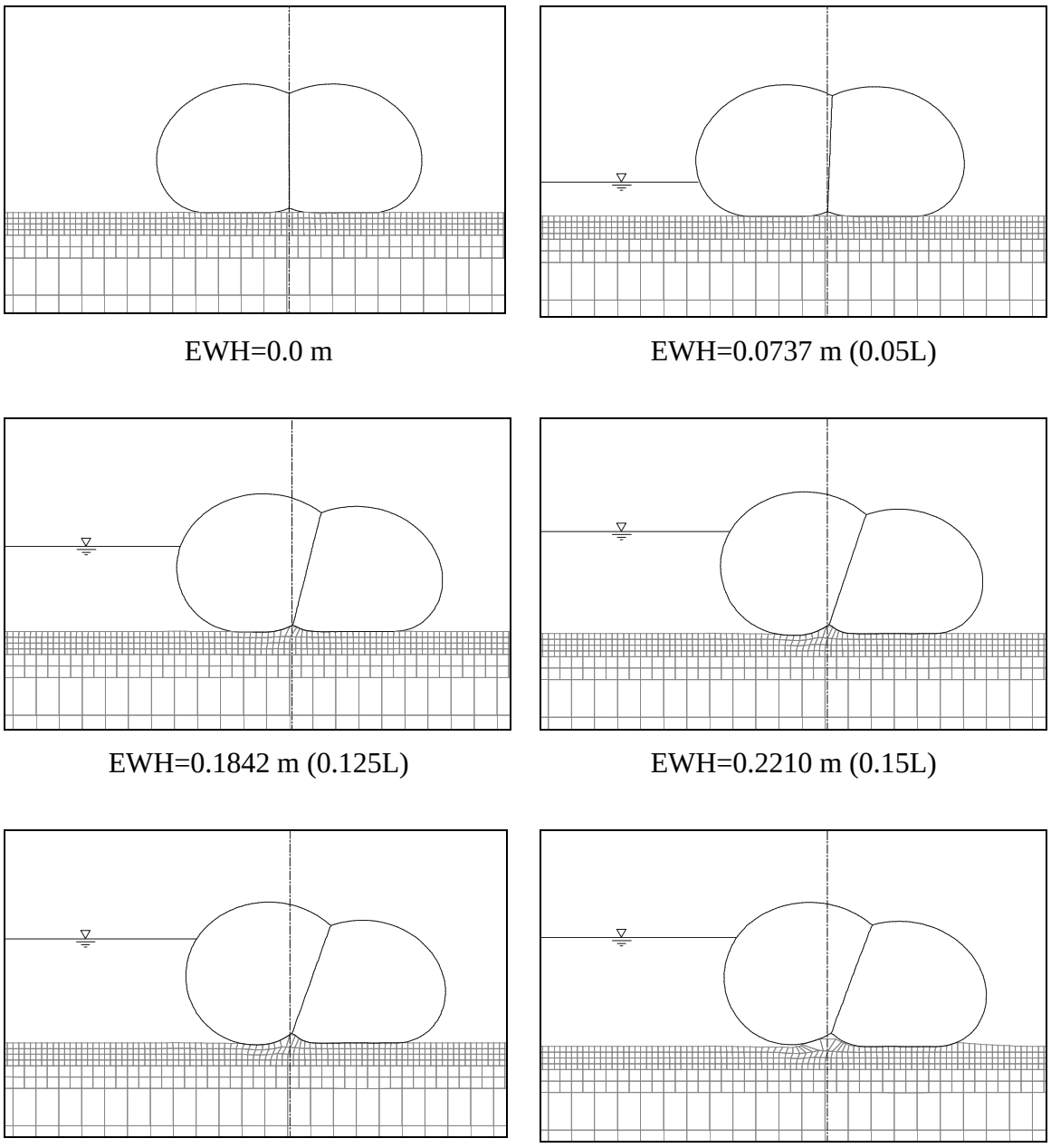

Figure 6.19. Deformations and failure of baffle tube dam (IWPH=0.5156 m)

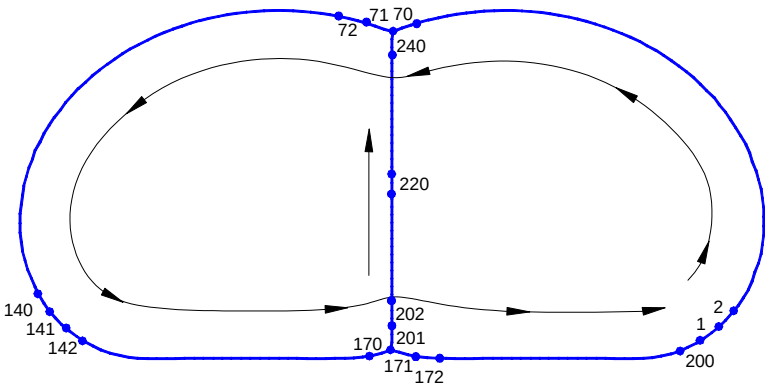

Figure 6.20. Numbering of elements

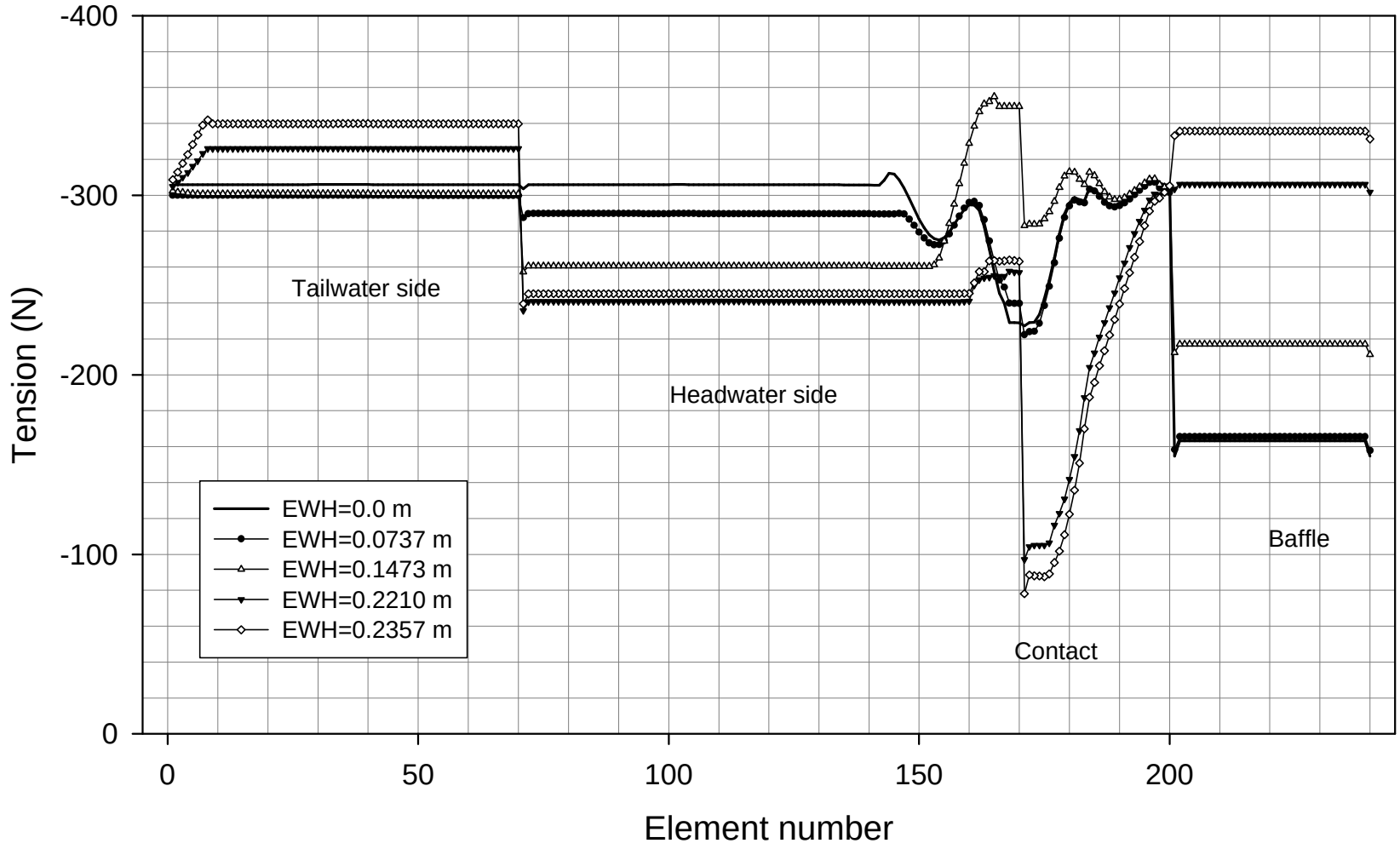

Figure 6.21. Tension in baffle tube dam (IWPH=0.3683 m, 0.25L)

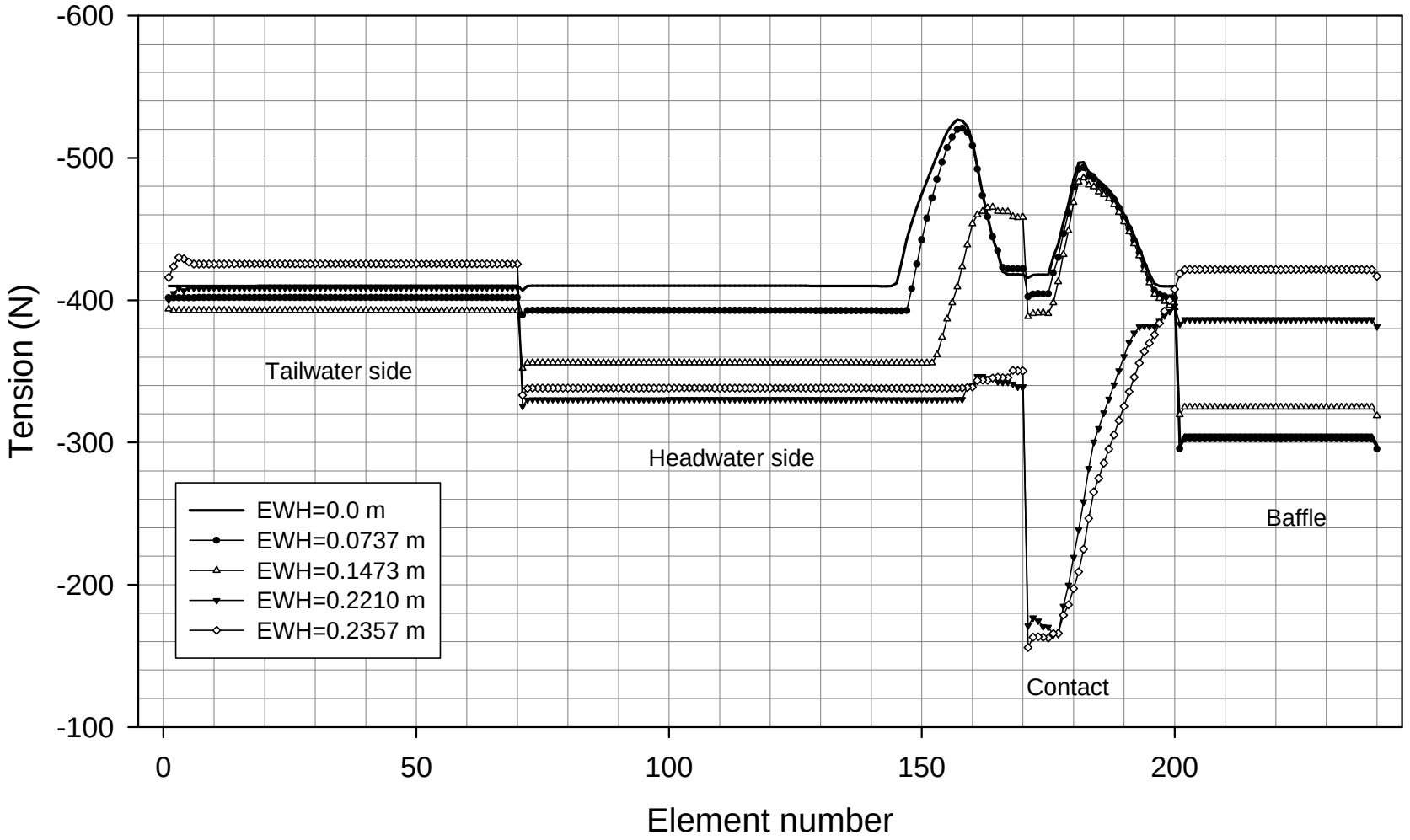

Figure 6.22. Tension in baffle tube dam (IWPH=0.4420 m, 0.30L)

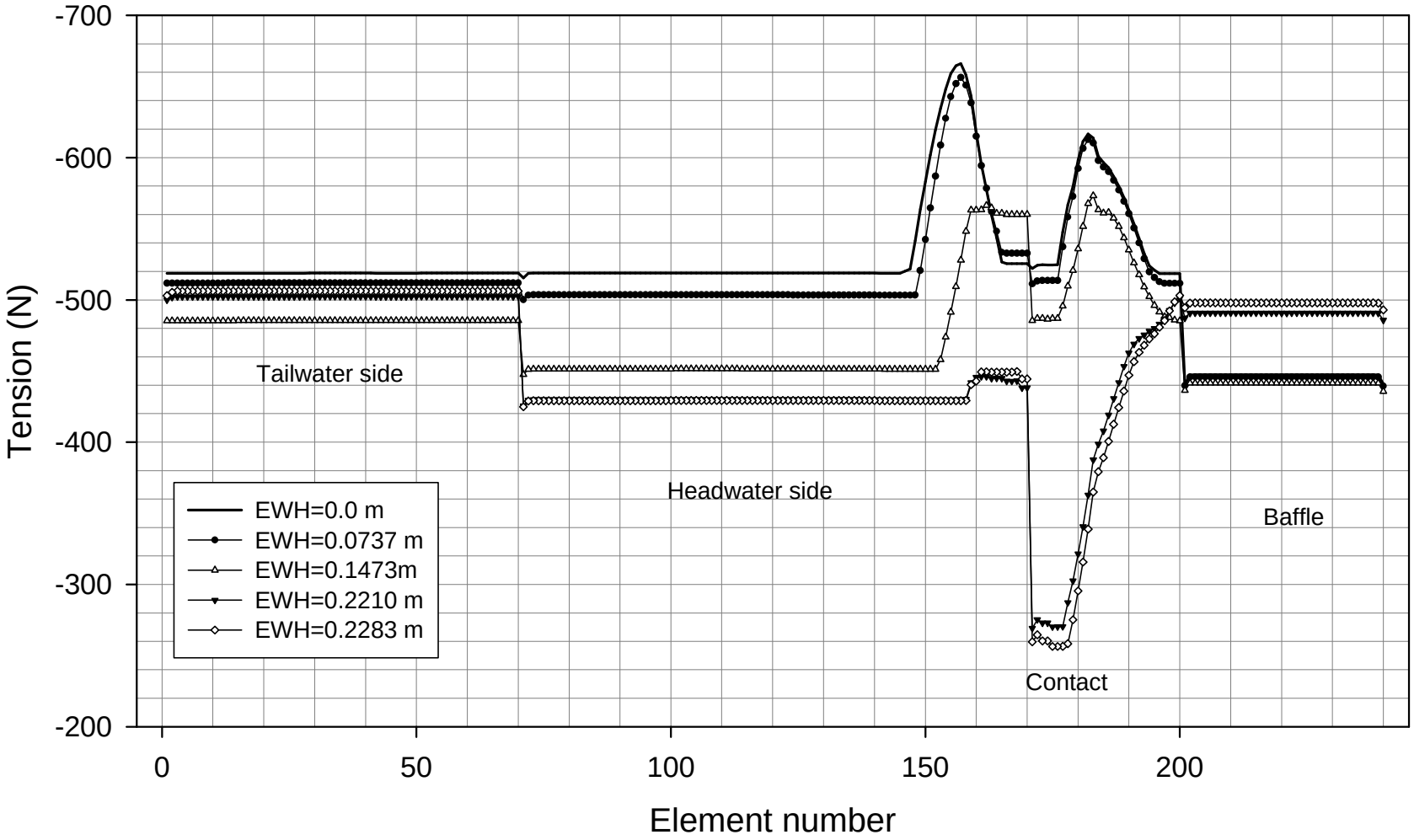

Figure 6.23. Tension in baffle tube dam (IWPH=0.5156 m, 0.35L)

6.4. Summary and Conclusions

The behavior of the single baffle tube dam was investigated when the tube dam was exposed to the floodwater. The critical external water heights were determined under various conditions. In all numerical analyses, the pore pressure effect underneath the baffle tube dam was considered. Also, it was assumed that a drain is installed to reduce the pore pressure.

First, two different lengths of baffle with the same tube circumference were analyzed numerically and their effect on the critical external water heights were examined. The numerical results show that when the baffle tube dam fails by rolling, the tube dam with a shorter baffle has more resistance to floodwater. However, if the tube dam fails by slip, it is predicted that the longer baffle case will have more resistance.

Second, the effects of the foundation condition on the baffle tube dam were investigated. Since the deformation of the foundation is neglected in this study, the foundation contact with the baffle tube dam is characterized by considering different friction coefficients, or friction angles. It was found that the failure mode of the baffle tube dam depends on the nature of the foundation. If the foundation provides a high friction coefficient with the tube material, the tube dam fails by rolling. If the baffle tube dam sits on a foundation with lower frictional angle, the tube dam fails by slip.

In these numerical studies, the baffle tube dam was inflated with different internal water pressure heads (IWPH), from 0.25 to 0.45 in normalized pressure head. The numerical result shows that a higher IWPH provides more stability regardless of the failure mode or the baffle length within the range of IWPH considered when the deformation of the foundation is not included. However, it is possible that a baffle tube dam with much higher IWPH relative to the external water pressure head is less stable than a baffle tube dam with lower IWPH, because a higher IWPH results in a rounder shape of the tube, which has less resistance to rolling than a flatter shape. This phenomenon can be visualized if we compare a baffle tube dam with low IWPH, such as 0.25 normalized, and a baffle tube dam with much higher IWPH, such as 2.5 normalized.

Last, numerical simulations of the baffle dam on silty sand were conducted. The characteristics of the foundation were based on the laboratory tests. Along with

groundwater flow and its pore pressure effect, the deformation of the soil was considered. The critical external water height for this case does not increase when the initial IWPH increases, unlike the results from the previous cases. Along with the alteration of the IWPH to keep the tube area constant during the flooding, the tension in the baffle tube changes. Overall, the tension in the tube increases near the critical external water heights. Also, the tension in the baffle increases as the tube deforms to the tailwater side.

The baffle tube dam during flooding shows very interesting characteristics. The failure mode of a single baffle tube can be slip, rolling, or slip and rolling. The resistance to slip is produced by the weight (or mass) and the frictional resistance between the tube and the foundation, while the resistance to rolling is provided by the geometry of the tube[2].

In this study, the location of the drain was not changed. However, it is important to install the drain in the proper location, depending on the failure mode. When a single baffle tube dam is expected to fail by slipping, the drain should be located under the headwater side of the tube, so the pore pressure beneath the tube can be minimized. On the other hand, if the drain is installed too close to the headwater, it will cause a piping failure near the end of the tailwater side. Also, it is possible that the drain will no longer be effective if the tube deforms to the tailwater side and the drain is exposed to the floodwater. If the single baffle tube dam is predicted to fail by rolling, the drain should be located underneath the tailwater side of the tube, close to the end of the tube, because, when the baffle tube dam starts to roll, if the drain is located near the center of the tube, the drain will be exposed to the floodwater.

---

[2] In this study, the cohesion of the interface between the tube material and the foundation is neglected, based on the nature of the foundation. If there is a circumstance for which the cohesion can not be neglected, the cohesion will be a factor in the rolling resistance.

Chapter 7. Sleeved Tube Dam

7.1. Introduction

Among the several types of commercialized tube dams, a sleeved tube dam has been developed by Water Structures Unlimited®. A sleeved tube dam consists of three tubes, two tubes inside of one bigger tube. The two inner tubes are constructed with polyethylene and the outer tube is made with a woven polypropylene geotextile. After inflation of the sleeved tube dam, the approximate height versus the width of the dam is 1:2 (Water Structures Unlimited®, 2002). The manufacturer claims that the friction between the two inner tubes makes the tube dam system more stable than a single tube.

Since the shape of the tube dam cannot be defined with a simple function and the responses against external forces are very complicated, the company estimates the stability of the sleeved tube dams based on rough assumptions. For example, the inner tubes are assumed to have a rectangular shape, and the pore pressure effects under the tube are neglected. In addition, they assume that the friction between the two inner tubes and between the inner tube and the outer tube resists rolling of the inner tubes, and the sleeved tube structure remains as it is. They establish the safety factor of the tube dam based on two failure modes: slide (or slip) failure between the soil and the sleeved tube dam, and lift up and rollover failure of the sleeved tube (similar to the rolling failure of a baffle tube dam, see Chapter 5). However, it is predicted in this study that the failure of a sleeved tube dam can happen in three ways. In addition to the slip and the rollover failures, the sleeved tube dam can become unstable due to rolling of the two inner tubes.

Experiments of a sleeved tube dam were conducted by FitzPatrick et al. (2001). Two inner tubes and one outer tube of the sleeved tube dam were fabricated with the same geomembrane material. The deformations and the internal water pressure heads of the tubes were measured. The external water height at the failure of the sleeved tube dam was observed as well.

The primary objective of this chapter is the investigation of the stability of the sleeved tube dam numerically. To achieve accurate and reliable results, the development of a realistic numerical model is needed. Then, the model is analyzed based on the reasonable assumptions. Next, the numerical analysis results are compared with previous experimental results to verify the model, and are examined to understand the behavior of the sleeved tube dam. The effects of different friction coefficients between the two tube materials are investigated.

7.2. Numerical Modeling

As for other types of water-filled tube dams, the tubes are modeled with beam elements, and the soil underneath the tube dam is modeled with groups of grid meshes. The predicted contact regions are modeled with interface elements.

The properties of the beam element, grid mesh, and interface elements are primarily based on laboratory tests which were conducted by FitzPatrick et al. (2001) and Moler (2002).

The modeling of the sleeved tube is very complicated because two inner tubes must be placed inside the outer tube, so the shape of the outer tube can only be determined after the inflation of the inner tubes. During the development of the model, two different approaches were attempted to model a sleeved tube dam. The fundamental difference between the two methods is the shape of the outer tube.

The first method has an open outer tube and two inner tubes inside, and the open outer tube was connected after the inflation of the two inner tubes. The second method had an outer tube encasing two inner tubes from the start, and this required a special initial shape for the inner tubes to fit in the outer tube. Though this method more likely represents the real situation in the physical world, it was not certain that the inflation of the inner tubes would be successful in the beginning of the development of the model. Therefore, a sleeved tube dam with an opened outer tube model was tried first (Figure 7.1).

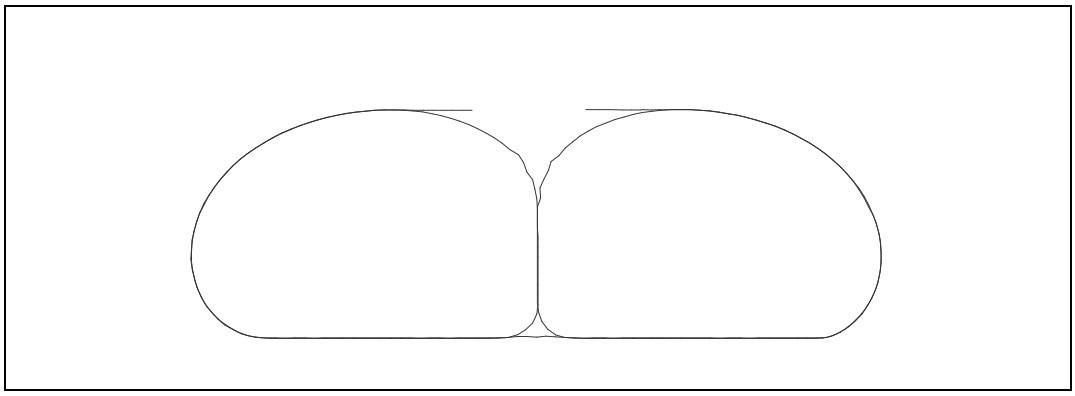

Figure 7.1. Example of sleeved tube dam model with an open outer tube

For the open outer tube model, the initial shape of the inner tube was a regular long capsule shape, which was used in the apron tube dam and other cases, and the inflation process of the inner tubes was easy to handle. During the inflation of the inner tubes, the tension was applied at each end of the outer tube in the direction of the beam elements at the end. The purpose of the tension was to hold the outer tube in place and to ensure contact between the inner tubes and the outer tube. After the inflation of the inner tubes, the tension was increased progressively to close the gap between the two ends. After closing the gap, the applied tension was reduced to zero gradually.

Despite the advantage of having the simple initial shape of the inner tubes, this method was not easy because of the control of the increment and the directions of the tensions at the ends of the outer tube.

Later, the other approach, a closed outer tube encasing the two inner tubes, was tried. The biggest advantage of this model was that it represents the sleeved tube dam in the experiment closely. Above all, it does not require additional processes like the open outer tube model during the inflation. The difficulty in the second method was caused by the fact that two long capsule shapes of inner tubes simply could not fit into the longer capsule shape of the outer tube.

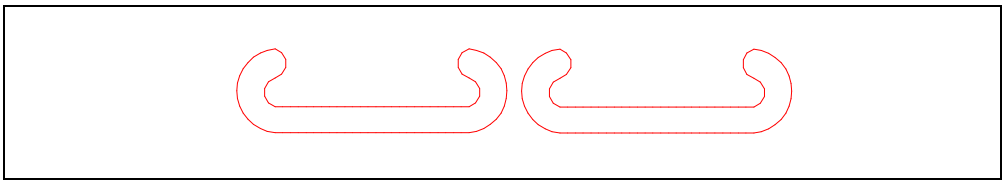

Initial shape (a)

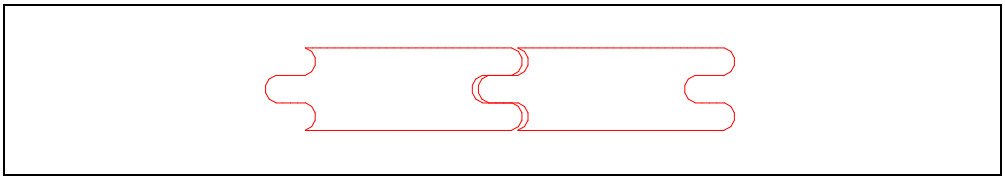

Initial shape (b)

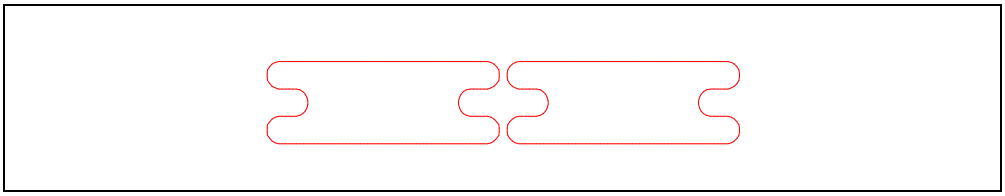

Initial shape (c)

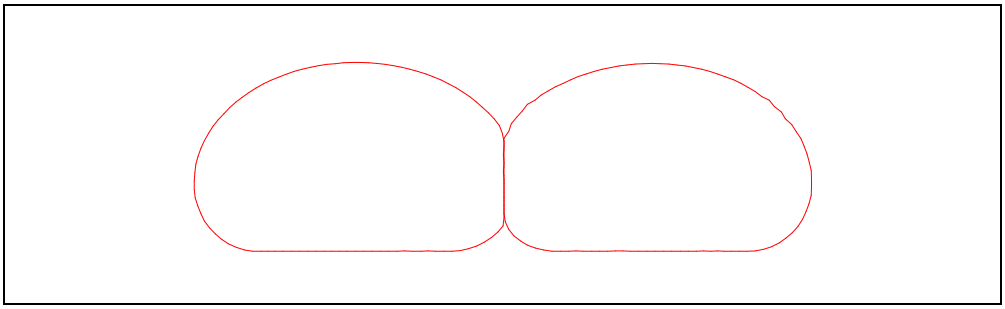

After inflation without outer tube

Figure 7.2. Initial shapes of inner tubes and their inflation

Therefore, special initial shapes for the inner tubes were developed as shown from Figure 7.2 (a) to Figure 7.2 (c). To explore the possibility of the successful inflation for the new shapes, first, the several initial shapes of the inner tubes were inflated without the outer tube. Surprisingly, all shapes inflated into the expected shape without much trouble in FLAC, as shown in Figure 7.2. After the verification of the successful inflation of these initial shapes, the inner tubes were placed in one long capsule shape of the outer tube. Next, the inner tubes were inflated with a given internal water pressure head (IWPH). At this stage, problems arose, because the deformations of the inner tubes were restrained by the outer tube. One type of inner tube, Figure 7.2 (a), could not be inflated at all. The other types of inner tubes failed to achieve a smooth inflated shape. Sometimes there were

wrinkles between the two inner tubes, or one of the inner tubes had a permanent folding between adjacent beam elements. The problems are more severe if the circumference of the outer tube is short.

However, these problems were resolved after some modifications in modeling. First, the numbers of beam elements for the inner tubes and outer tube were increased. Secondly the shear stiffness was slightly modified. Also, the updates for the configuration during the early stage of the inflation were adjusted. For the final sleeved tube dam model, the closed outer tube model was chosen with the initial shape (c) in Figure7.2. Figure 7.3 shows the final model of the sleeved tube before the inflation.

Each inner tube consists of 200 beam elements, and the outer tube has 300 beam elements. Since all three tubes were fabricated with the same material in the experiment, the properties of the inner tubes and the outer tubes are assumed to be identical in this study[1]. The properties are the same as in the other tube dam cases.

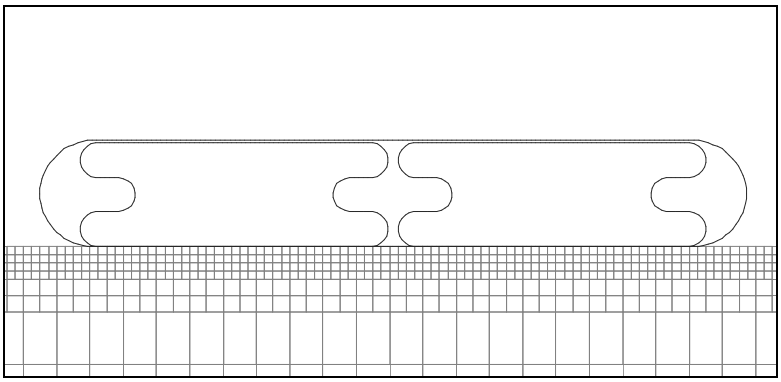

Figure 7.3. Final sleeved tube dam model

For the predicted contact region between the tubes and between the tube and the foundation, five interface groups are assigned. The first and the second interface element groups are assigned between the headwater side inner tube and the outer tube, and between the tailwater side tube and the outer tube. The third interface element group is allocated between the headwater side inner tube and the tailwater side inner tube. The fourth and fifth

[1] Water Structures Unlimited® manufactures the inner tubes and the outer tube with two different materials.

interfaces are designated between the silty sand and the outer tube, and between the drain and the outer tube.

The properties of the interface between the tubes are slightly altered with regard to the shear stiffness compared to the other tube dam models to help the inflation of the inner tubes. The friction angle is 14 degrees, which is the residual friction angle between the materials[2], for the comparison with experiments. It is expected that the use of the residual friction angle produces conservative results. For a parametric study, other friction angle values are employed. The properties of the interface between the tube and the soil or between the tube and the drain are identical with those used in other models.

The external water pressures are applied on the headwater side of the outer tube. Then, the force will be transmitted to the inner tubes by the interface elements in the contact regions between the outer tube and the inner tubes.

7.3. Numerical Analysis

Two different sleeved tube dams are modeled. The sleeved tube dam 1 has a circumference of the outer tube of 2.3114 m (91 in.) and the sleeved tube dam 2 has 2.4638 m (97 in.) as the circumference of the outer tube. Both cases have the same circumference for the inner tubes, which is 1.4732 m (58 in.). Again, the two cases have the same numbers of beam elements for the tubes.

The inflations of the sleeved tube dam 1 and 2 are investigated first, and the areas of the inner tubes and the contact lengths of the interfaces are examined. Then the external water forces are exerted on the headwater side of the sleeved tube dam. The numerical results are compared with the available experimental results. This comparison will give the verification of the model besides insight into the experiment. For this comparison, the pore pressures and the deformation of the foundation are considered.

Last, the effects of the friction coefficients (or friction angles) between the tube materials are explored, since the materials for the tube dams certainly vary among

---

2 The characteristics of the interfaces between the tube materials are introduced in section 3.2.4

manufacturers of geomembranes and geotextiles. Also, the frictional coefficient can be the main factor governing stability when the sleeved tube dam fails by slip between the two tube materials.

7.3.1. Inflation of Sleeved Tube Dam

Figure 7.4 shows the inflation process of the sleeved tube dam. Figure 7.4 (a) displays the initial shapes of the tubes. The initial internal water pressure head (IWPH) of the inner tubes is 0.475 m and the pressures are applied to the inner tubes gradually. Figure 7.4 (f) depicts the shape of the inflated sleeved tube after it reaches equilibrium. It is noted that the updates for the configuration of the deformed shape should be controlled carefully at the stages of Figures 7.4 (a) and (b) to induce a stable calculation by FLAC.

Figure 7.5 presents the notation used for the sleeved tube dam. The inner tubes on the headwater side and the tailwater side are designated “inner tube H” and “inner tube T” for convenience. The contact regions between the headwater side of the outer tube and the inner tube H, and the tailwater side of the outer tube and the inner tube T, are called CR1 and CR2, respectively. The contact region between the two inner tubes is denoted CR3.

In addition, the lengths of the contact regions under the headwater side and the tailwater side of the outer tube are examined. They have the same length if there is no floodwater, and the contact lengths of the sleeved tube dam 1 and the sleeved tube dam 2 are 0.325 m and 0.321 m, respectively. The product of these contact lengths and the IWPH, and the area of one inner tube are compared in Table 7.1. The differences between the product of the IWPH and the contact length, and the tube area, are 2.6 % and 0.9%, respectively. When there is no external water, the product should be equal to the area. The differences are insignificant. The sleeved tube dam 2 has a slightly larger inner tube area and shorter contact length than the sleeved tube dam 1. However, the difference of the areas or the products of the IWPH and the contact length between the sleeved tube dam cases are small. Therefore, the resistance to the sliding of the sleeved tube dam as a whole is predicted to be almost the same for both cases.

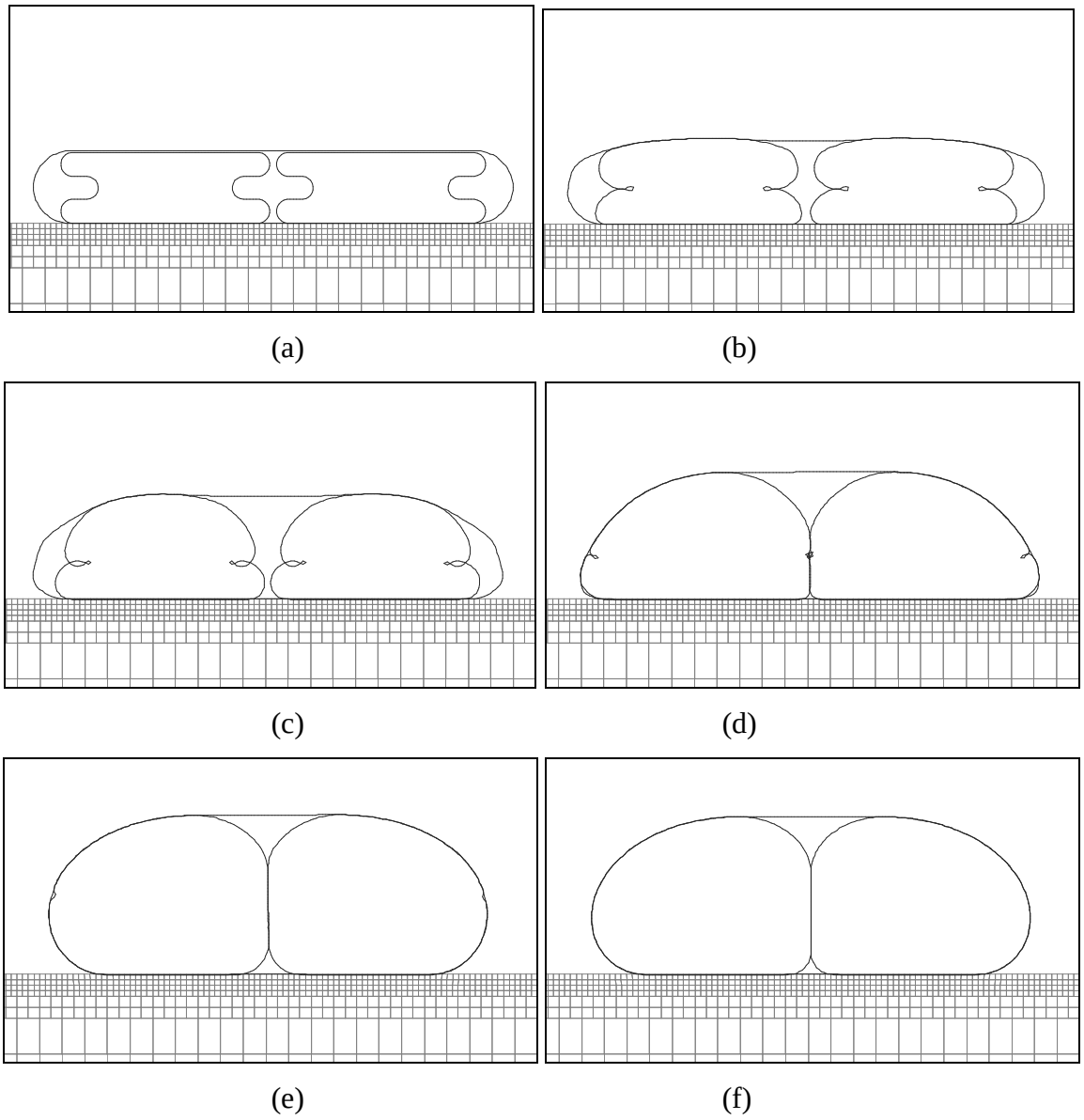

Figure 7.4. Inflation of sleeved tube dam

Table 7.2 shows the contact length between the two inner tubes, which is CR3, and the pressure heads at the top and the bottom of the CR3. The contact length of the sleeved tube dam is more than three times the contact length of the sleeved tube dam 2. Hence, the expected shear resistance of CR3 for the sleeved tube dam 1 is approximately 200 percent greater than for the sleeved tube dam 2 based on the undeformed shapes of the tube dams. However, the shear resistance will change when the tubes deform during flooding and cause IWPH changes.

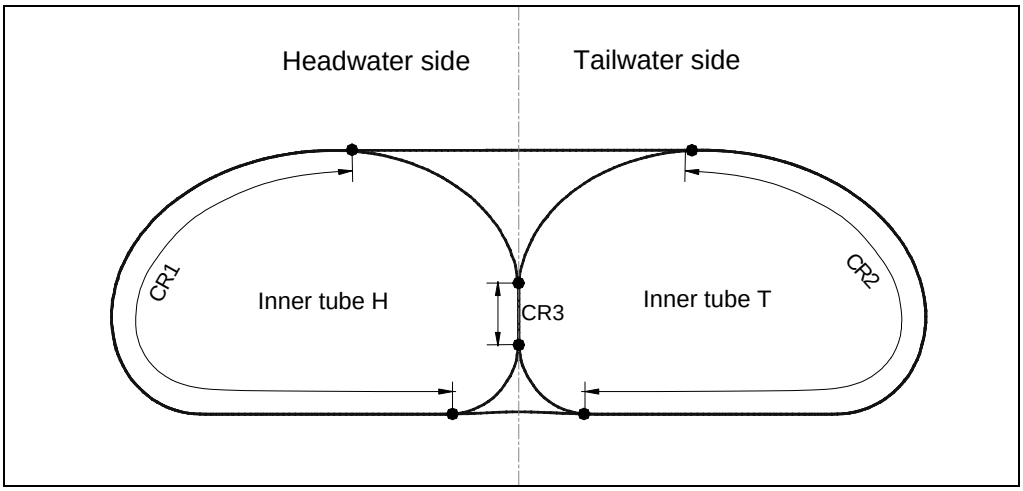

Figure 7.5. Notations used for sleeved tube dam

Table 7.1. Comparison of tube area with product of IWPH and contact length

	Sleeved tube dam 1 2.3114 m (91 in.)	Sleeved tube dam 2 2.4638 m (97 in.)
Area of inner tube (m^2)	0.1504	0.1512
IWPH × Contact length (m^2)	0.1544	0.1525
Difference (%)	2.6	0.9

Table 7.2. Contact length of interface between two tubes

		Sleeved tube dam 1 2.3114 m (91 in.)	Sleeved tube dam 2 2.4638 m (97 in.)
Contact length (m)		0.184	0.059
Pressure head (m)	Top	0.244	0.319
	Bottom	0.423	0.376

7.3.2. Numerical Simulation of Experiments

For a comparison with the experiments of the sleeved tube dam, two sleeved tube dam cases, sleeved tube dam 1 and sleeved tube dam 2, are analyzed numerically. The

initial IWPH for both cases is 0.475 m. In the experiment, two trials were conducted for the sleeved tube dam 1 and one trial for the sleeved tube dam 2.

The soil condition is the same as for other numerical simulations of the experiments. The groundwater flow is considered in addition to the deformation of the soil. The drain grid is also placed in the numerical model according to the experiments. The drain was installed approximately 30.1 cm and 6.3 cm from the centerline to the tailwater side for sleeved tube dams 1 and 2, respectively, in the experiment and the numerical model.

The friction angle between tube materials is assumed to be 14 degrees here.

The external water pressure is applied on the headwater side of the outer tube after inflation of the sleeved tube dam to simulate flooding. The stability of the tube dam system is investigated. Also, critical external water levels are determined. During the flooding simulation, the area of each inner tube is maintained constant. The IWPHs of the inner tubes are controlled separately using the factored secant method.

For the sleeved tube dam case 1, the external water pressure head is raised to 0.0762 m (3 in.), 0.1524m (6 in.), and 0.2032 m (8 in.). After that, the head is increased in increments of 0.0127 m (0.5 in.) until the sleeved tube dam fails. In the case of the sleeved tube dam 2, the external water pressure head is raised to 0.0762 m (3 in.) and 0.1270 m (5 in.). After that, the increment process is identical with that of case 1.

The sleeved tube dam 1 fails at the external water level of 0.2413 m (9.5 in.) in the numerical simulation and at the levels of 0.2667 m (10.5 in.) and 0.2604 m (10.25 in.) approximately in the experiments. For the sleeved tube dam 2, the tube dam becomes unstable at the external water level of 0.1524 m (6.0 in.) from the numerical analysis, while the level from the experiment is 0.2921 m (11.5 in.).

Figure 7.6 and Figure 7.7 depict the deformations obtained from the numerical analysis and the experiments for the sleeved tube dam case 1 and case 2, respectively. The solid line represents the deformed shape of the numerical simulation. The dots and crosses both represent the measurements of the tests. The dots are the measurements of the inner tubes, while the crosses are the measurements of the outer tube. For the sleeved tube case 2 there is no measurement for the outer tube. It is noted that most dots represent the targets which were attached on the surface of the inner tubes, except for the dot in the gap between the two inner tubes, the dots on the leftmost and left bottom of the headwater side tube, and

the rightmost and the right bottom of the tailwater side. Each trial has three series of measurements along the longitudinal direction. Generally the measurements from the middle of the length of the tube dam, which is series 2, are plotted for comparison with the numerical result. But, for the comparison of the sleeved tube dam case 1, the data of series 3 of trial 2 are chosen because the data looked most reasonable for this case[3]. The comparison of the deformation of experimental and numerical results shows a good agreement overall.

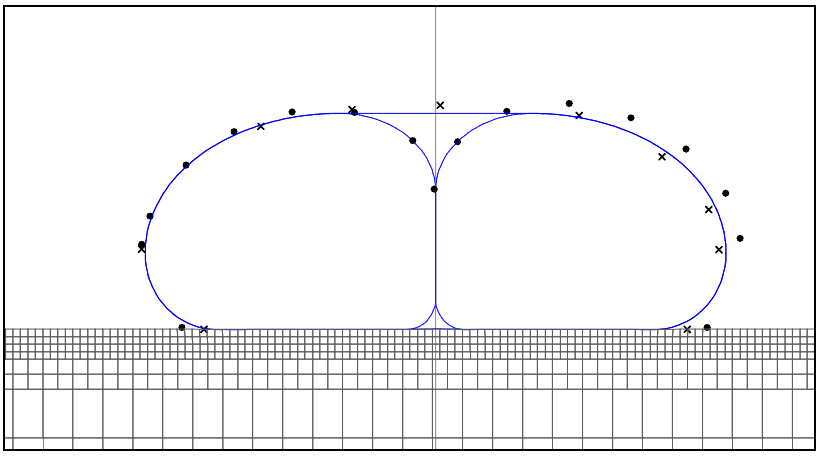

EWH=0.0

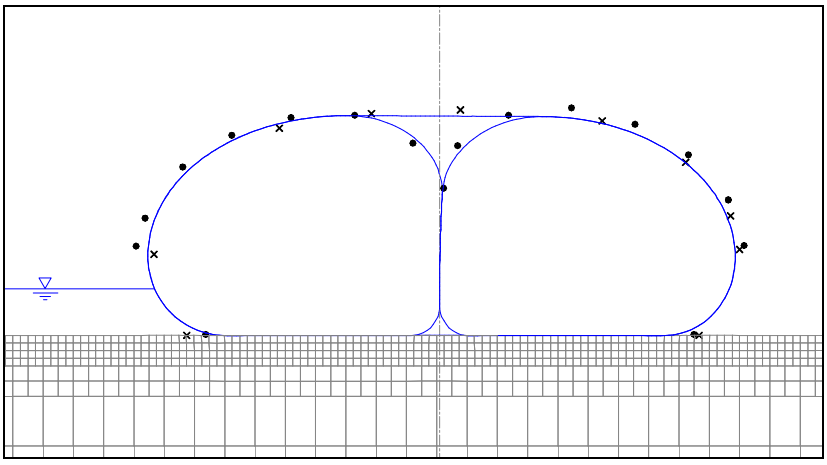

EWH=0.0762 m

[3] When there is no external water on the side, the series 3 data from trial 2 show the most symmetric cross sectional shape.

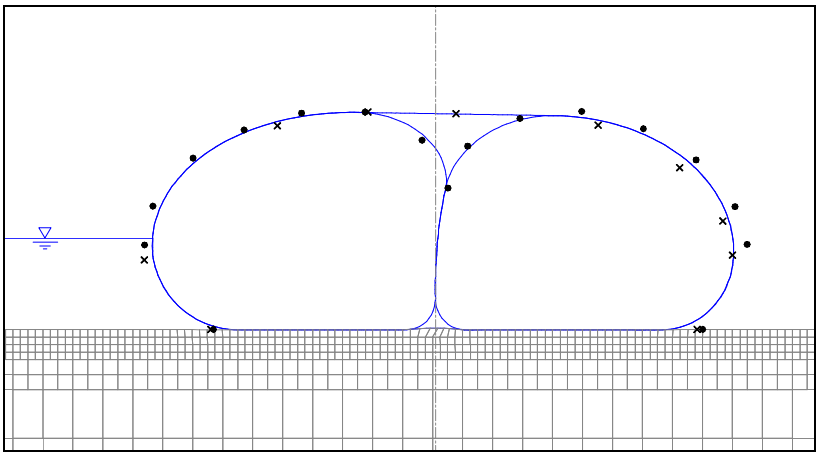

EWH=0.1524 m

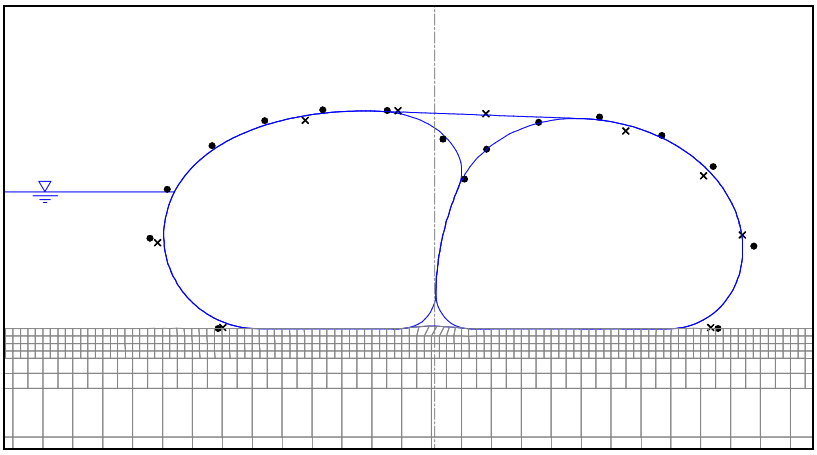

EWH=0.2286 m

Figure 7.6. Comparison of deformations with experiment (sleeved tube dam 1)

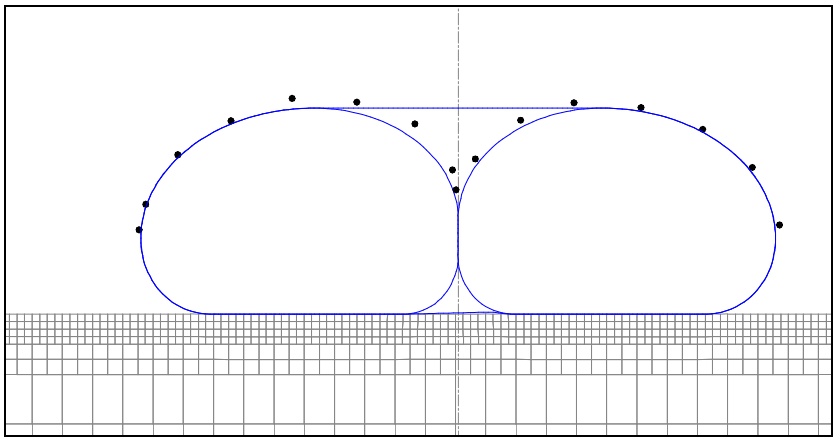

EWH=0.0 m

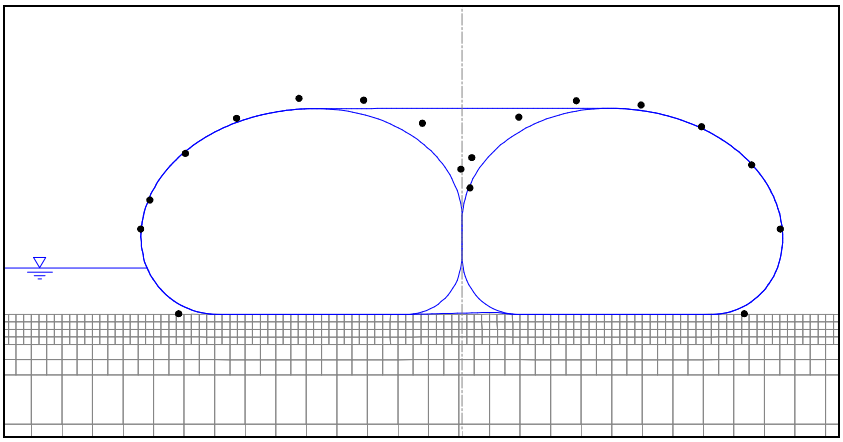

EWH=0.0762 m

Figure 7.7. Comparison of deformations with experiment (sleeved tube dam 2)

From Figure 7.6, it is clear that the upper portion of the headwater side of the tube deforms to the tailwater side, while the contact region under the tube does not slip, based on the numerical analysis. In the result, the inner tube H together with the headwater side of the tube leans on the inner tube T. Also, from the observation of the experiments, the location of the gap between the two inner tubes at each external water level supports this idea.

The deformation of the sleeved tube dam 2 is not as evident as that of the sleeved tube dam 1, but the comparison of the sleeved tube dam 2 also shows a similar deformation pattern (Figure 7.7). The gap between the two tubes is displaced to the tailwater side.

When the external water height increases, the foundation deforms little for both cases. There is no evident lift-up of the soil between the two tubes.

Since the sleeved tube dam can fail by rolling or slipping, or the system can fail by slip between the two inner tubes, the behavior of the tube dam system can be explained by monitoring the reference points shown in Figure 7.8. Five reference groups of points are assigned. Each group consists of two nodal points from the contacting objects. Because two points are initially contacting each other, they look like one point in Figure 7.8. Two groups are allocated at the bottom of each side between the inner tubes and the outer tubes (CR1 and CR2 in Figure 7.5). The other two groups are assigned at the top of each side. The last group is located at the middle of the sleeved tube dam, which is between the inner tube H and the inner tube T (CR3).

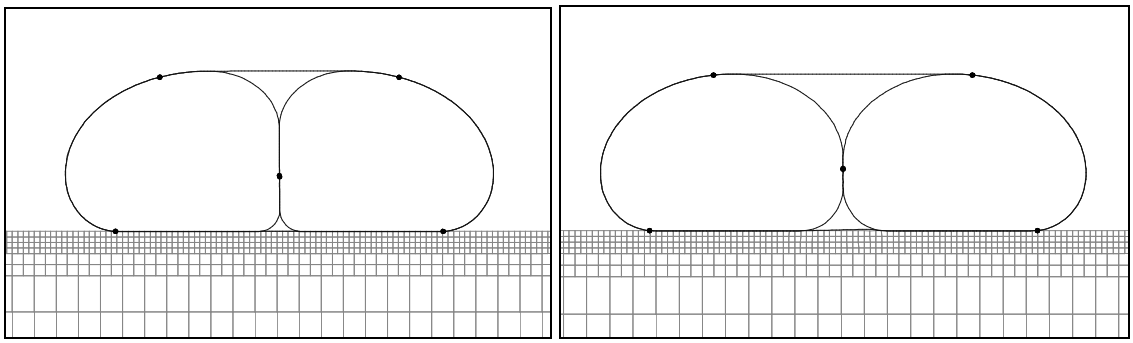

(a) sleeved tube dam 1 (b) sleeved tube dam 2

Figure 7.8. Location of reference points

Figures 7.9 and 7.10 present the deformation of the sleeved tube dams 1 and 2 from the numerical result in detail. For a better understanding, the deformed shapes at the external water levels are displayed together. The black color represents the shape of the inflated sleeved tube dam without external water on the side. The green and blue lines represent the deformed shape of the tube at the certain external water levels. The red line depicts the deformation at the external water height, just 0.0127 m (0.5 in.) before the sleeved tube dam fails.

As shown in Figures 7.9 and 7.10, the bottom point group on CR1 moves upward, while the bottom point group on CR3 does not move at all when the external water height is increased. Two top point groups move to the tailwater side. The point group on CR3 moves slightly to the tailwater side as the inner tube H leans on the inner tube T. This observation clearly proves that there is no slip failure between the tube and the foundation. However, after the critical external water level, the point group on the CR3 begins to separate into two points. The point on the inner tube H moves down, while the point on the inner tube T moves up along the CR3. Because the shear strength between the two inner tubes is less than the shear force induced by the external water, slip occurs at this interface. The other point groups on the CR1 and CR2 are still in contact at the critical external water height. Therefore, the sleeved tube dam fails by slip failure between the two inner tubes in this study. The slip failure between the two inner tubes causes rolling of the sleeved tube and makes the sleeved tube dam unstable.

Throughout the flooding, the internal water pressure head of the inner tubes changes since the tubes are sealed after the inflation. Figures 7.11 and 7.12 show the changes of IWPH from the numerical and experimental results. The IWPHs of the inner tube H and tube T are designated with solid and hollow symbols, respectively.

For the sleeved tube dam 1 (Figure 7.11), the numerical results show a decrease of the IWPH of the inner tube H and an increase of the IWPH of the inner tube T when the external water height increases. The experimental results display a decrease of the IWPH of the inner tube H also for the two trials; however, the IWPH of the inner tube T does not increase. For the sleeved tube dam case 2 (Figure 7.12), the numerical results show a decrease of the IWPH of the inner tube H and an increase of the IWPH of the inner tube T. The experiments display similar results.

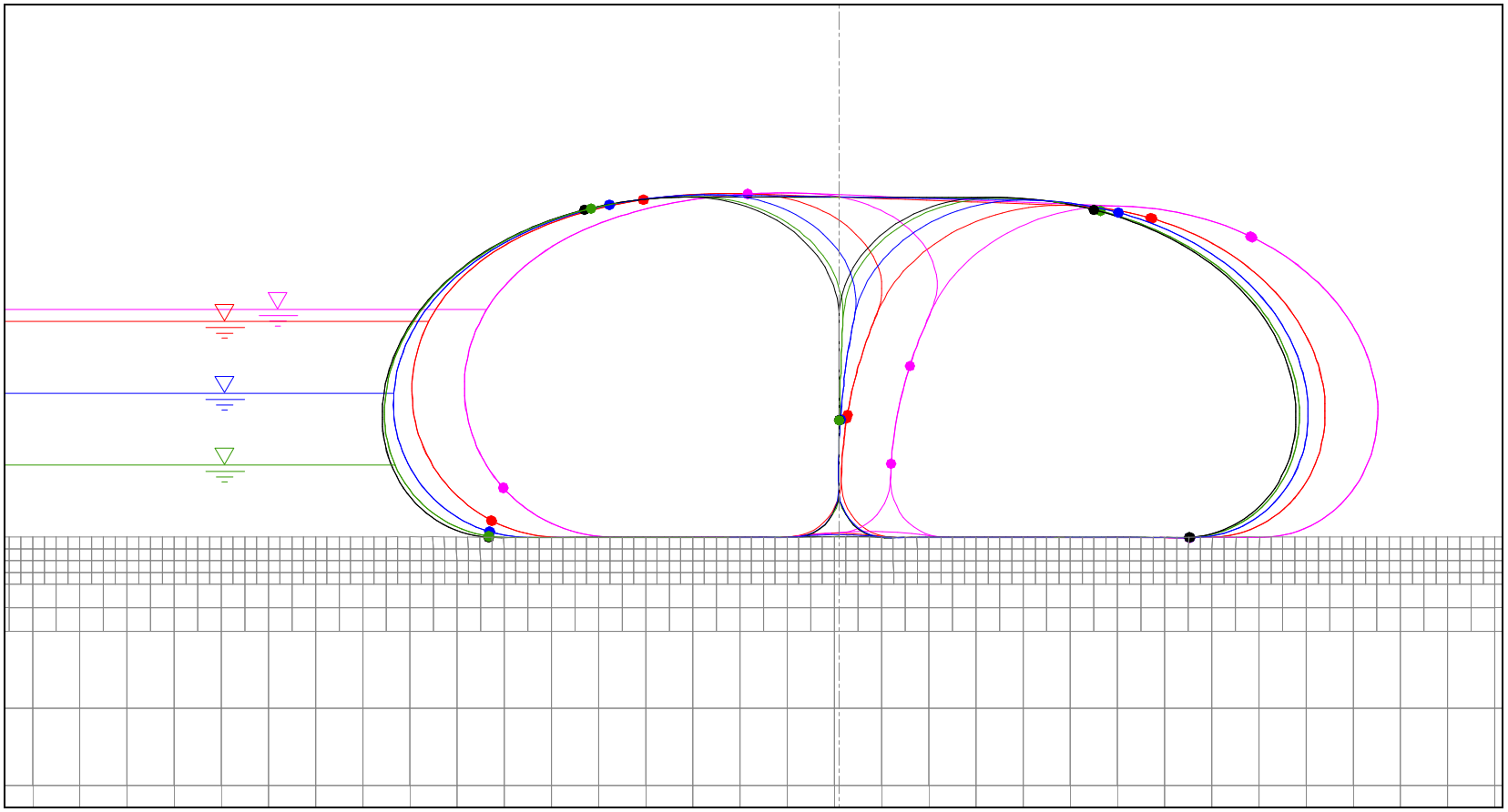

Figure 7.9. Deformation of sleeved tube dam 1 (numerical results)

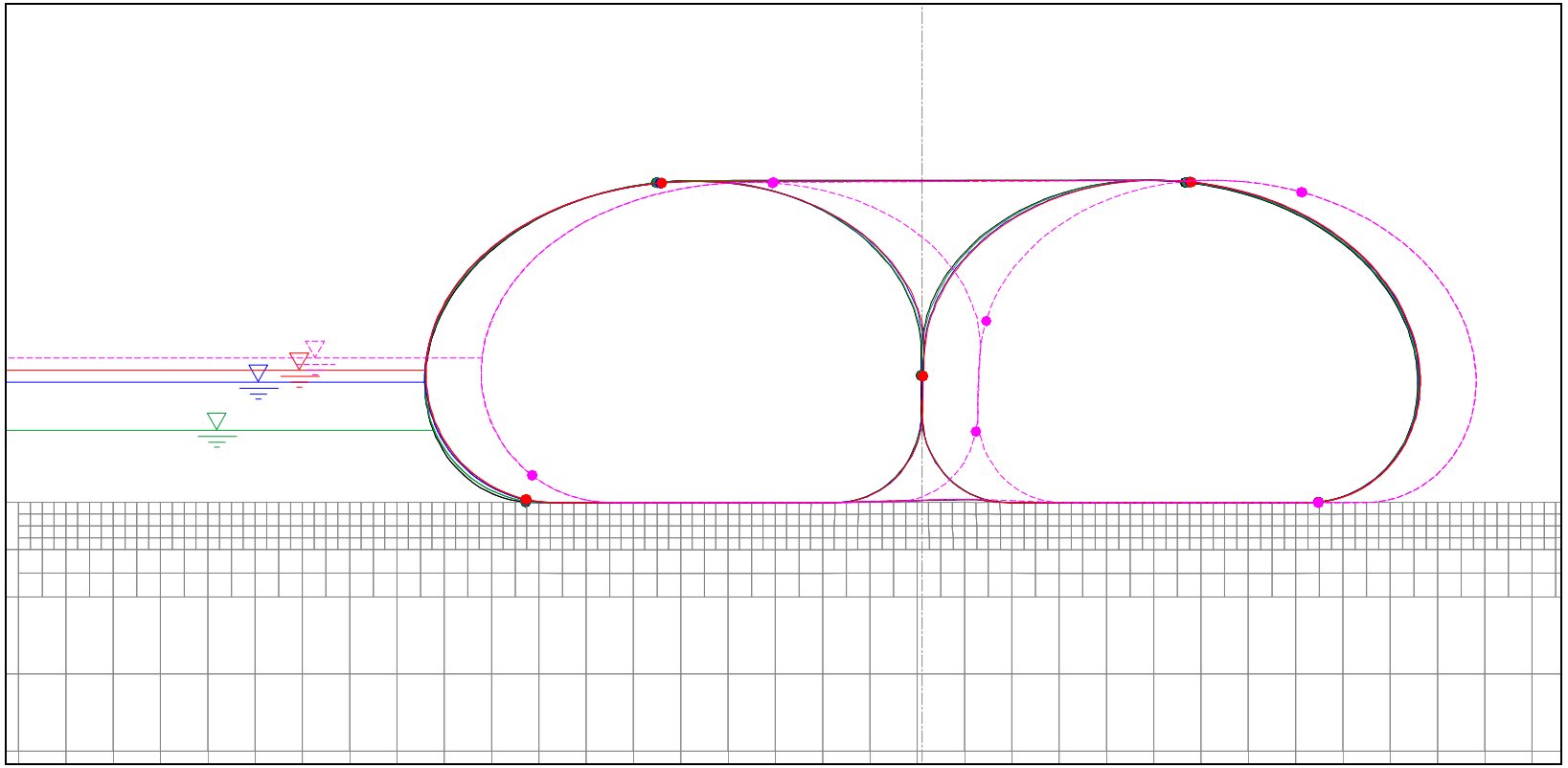

Figure 7.10.Deformation of sleeved tube dam 2 (numerical results)

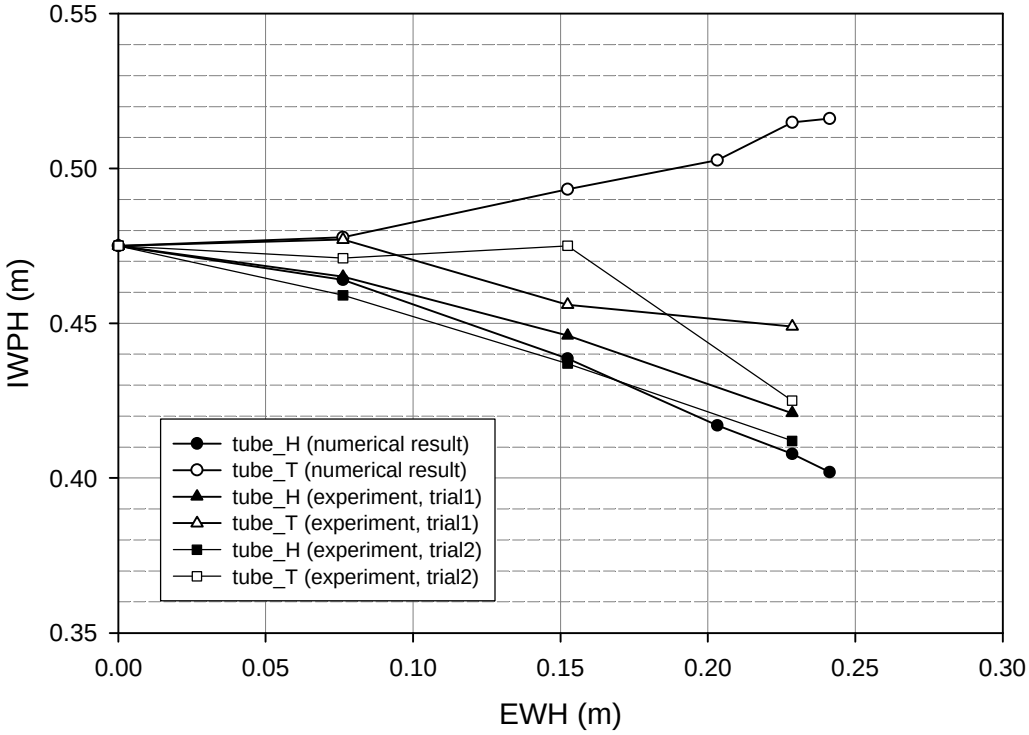

Figure 7.11. Comparison of IWPH (sleeved tube dam 1)

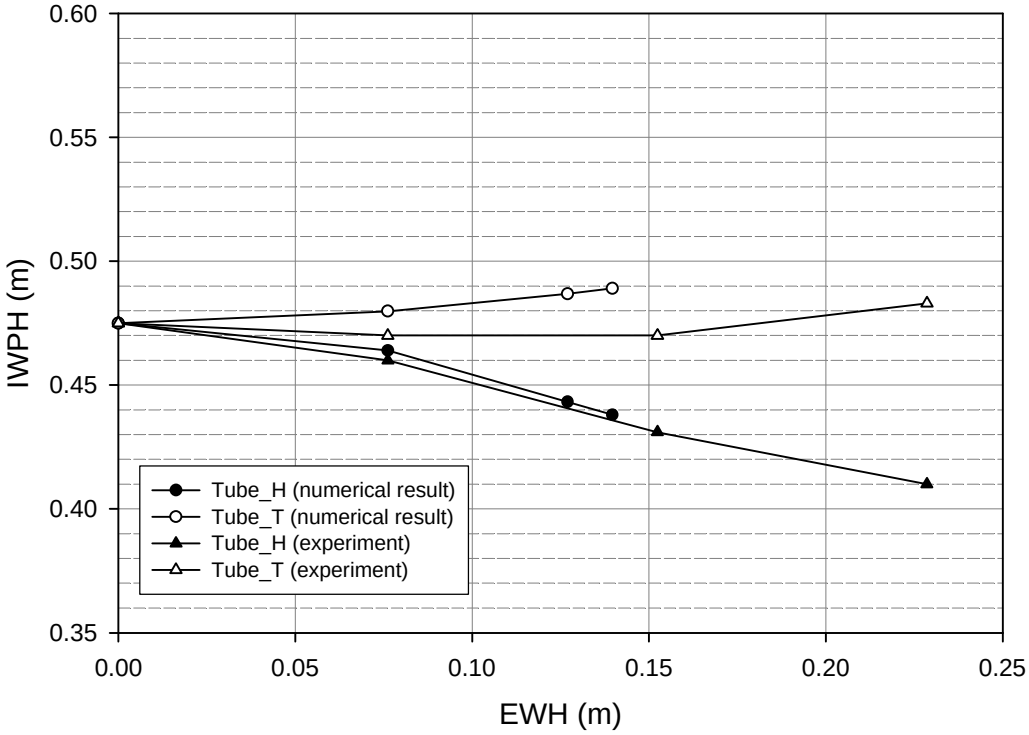

Figure 7.12. Comparison of IWPH (sleeved tube dam 2)

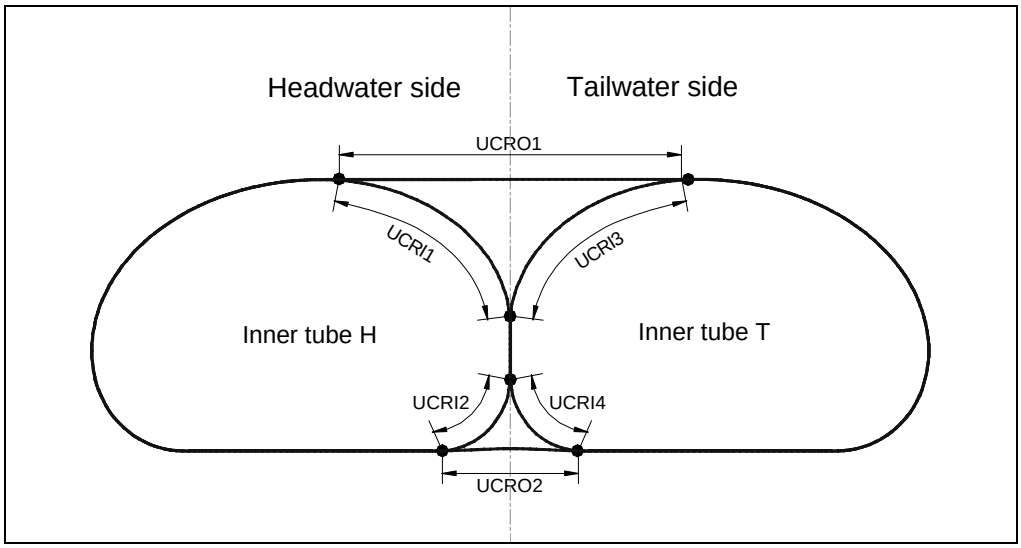

Figure 7.13. Notation for sleeved tube dam (tension)

The tensions in the sleeved tube dams are investigated. Figure 7.13 shows the notation for the non-contact regions of the sleeved tube dam. The regions at the top and the bottom between the two tubes are designated UCRO1 and UCRO2. It is noted that there is no contact between the outer tube and the foundation between the two inner tubes (UCRO2). UCRI1 and UCRI2, and UCRI3 and UCRI4, are non-contact regions between the outer tube and the inner tube H, and between the outer tube and the inner tube T, correspondingly.

Figure 7.14 and Figure 7.15 display the tension for the sleeved tube dams 1 and 2. The element numbers 1 to 200, 201 to 400, and 401 to 700 are for the inner tube H, inner tube T, and outer tube, respectively. When there is no external water, for the sleeved tube dam 1 the maximum tensions in the non-contact regions of the inner tube H and the inner tube T are about 225 N. The maximum tension in the non-contact region of the outer tube is 300 N. In the case of the sleeved tube dam 2, the maximum tensions in these regions are about 410 N for the two inner tubes and 100 N for the outer tube.

Generally, as the external water height (EWH) is increased, the tension in the inner tube H is decreased, the tension in the inner tube T is increased, and the tension in the outer tube is decreased. The tension in a tube is mainly a function of the net pressure applied on it. As shown in Figures 7.11 and 7.12, the IWPH of the inner tube H is decreased and that of the inner tube T is increased in the numerical results. Also, the net pressure head on the outer tube is decreased when the external water pressure is increased. As a result, the

tensions of the tubes are altered. Similar to the deformations of the sleeved tube dam, the tensions in the sleeved tube dam 1 change more rapidly than those in the sleeved tube dam 2 in response to an external water height increment.

Figure 7.16 and Figure 7.17 depict the pore pressure contours of the sleeved tube dams 1 and 2 at the critical external water height, 0.2286 m (9.0 in.) and 0.1397 m (5.5 in.), respectively. The pore pressure begins to drop underneath the headwater side of the tube, and becomes almost zero near the drain location (see the enlargements in Figure 7.16 and Figure 7.17). The sleeved tube dam has the longest flow distance and a gentle flow gradient because of its large width compared to the other types of tube dams considered here. Therefore, it is unlikely to have a piping failure at the tailwater side.

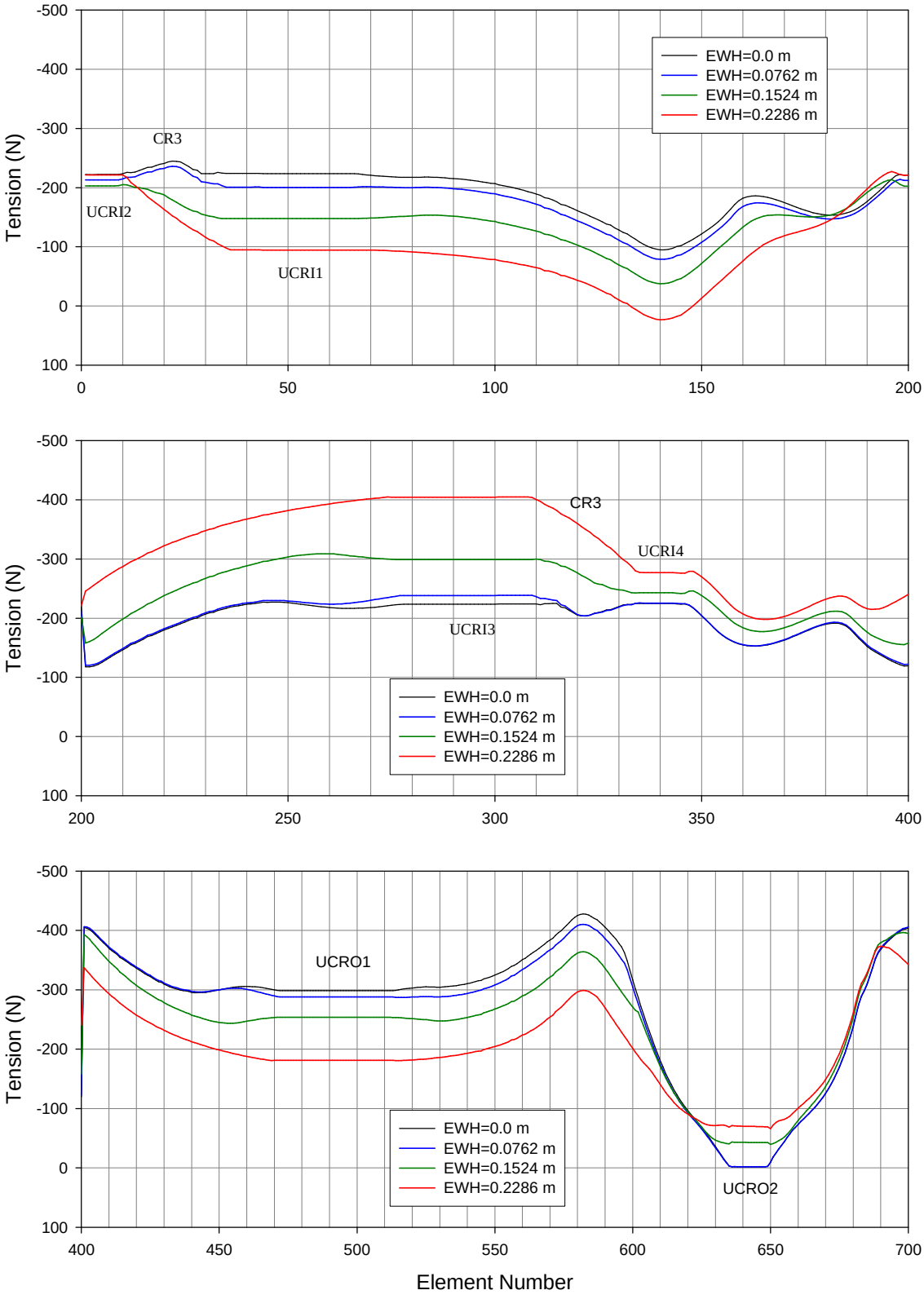

Figure 7.14. Tension in sleeved tube dam 1

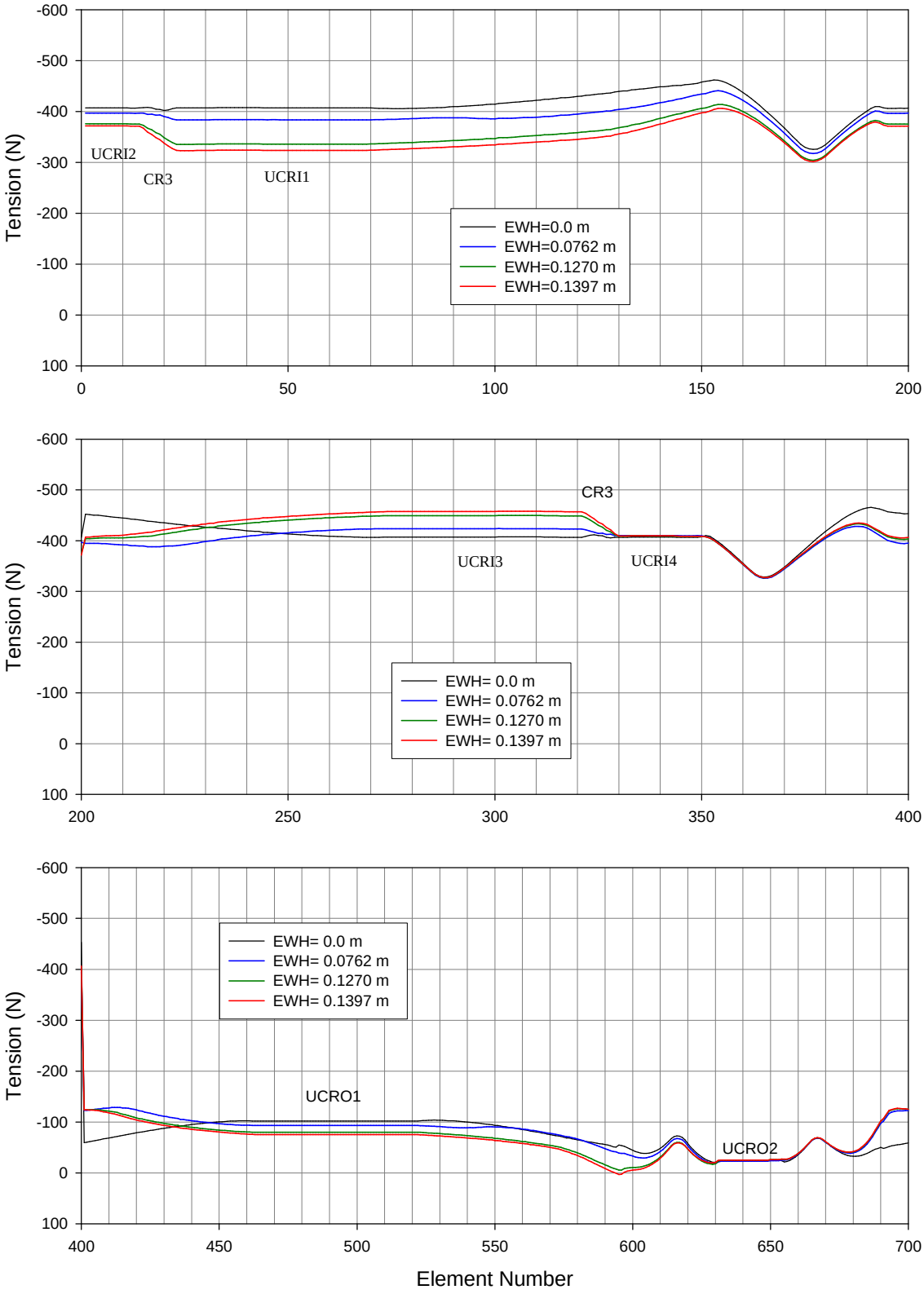

Figure 7.15. Tension in sleeved tube dam 2

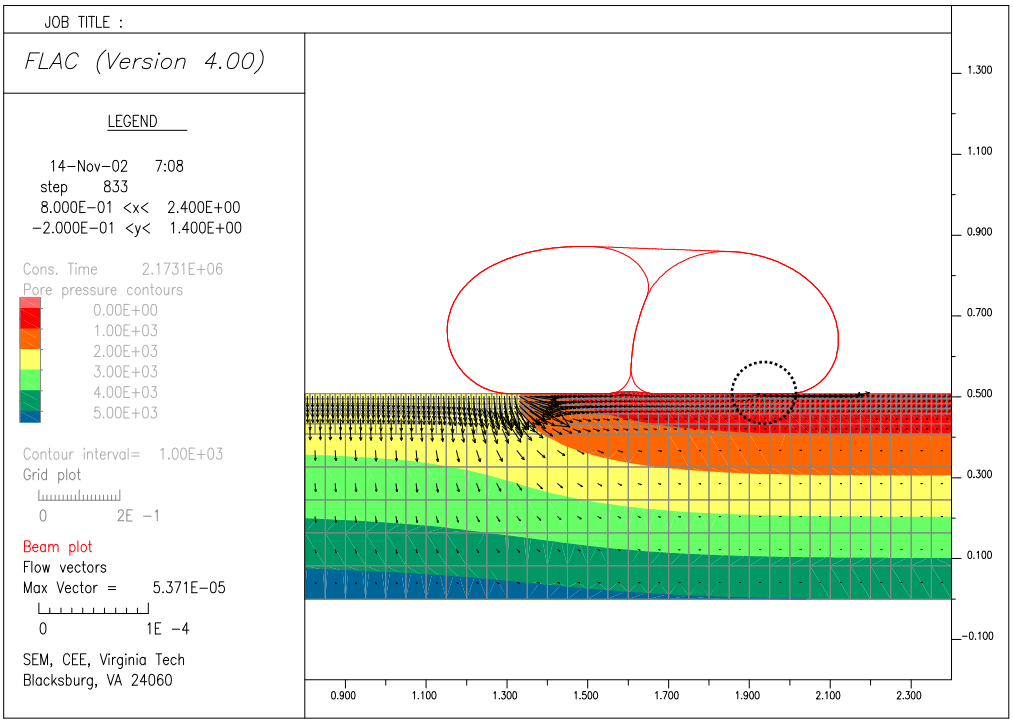

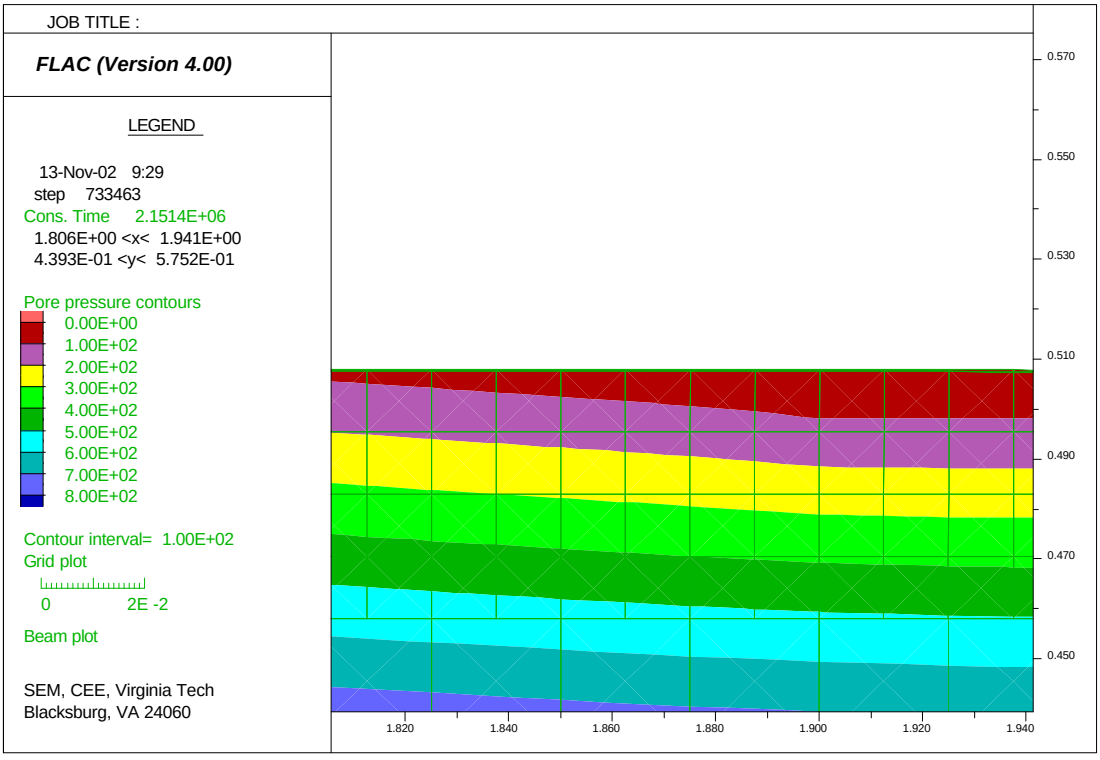

Figure 7.16. Pore pressure of the sleeved tube dam 1

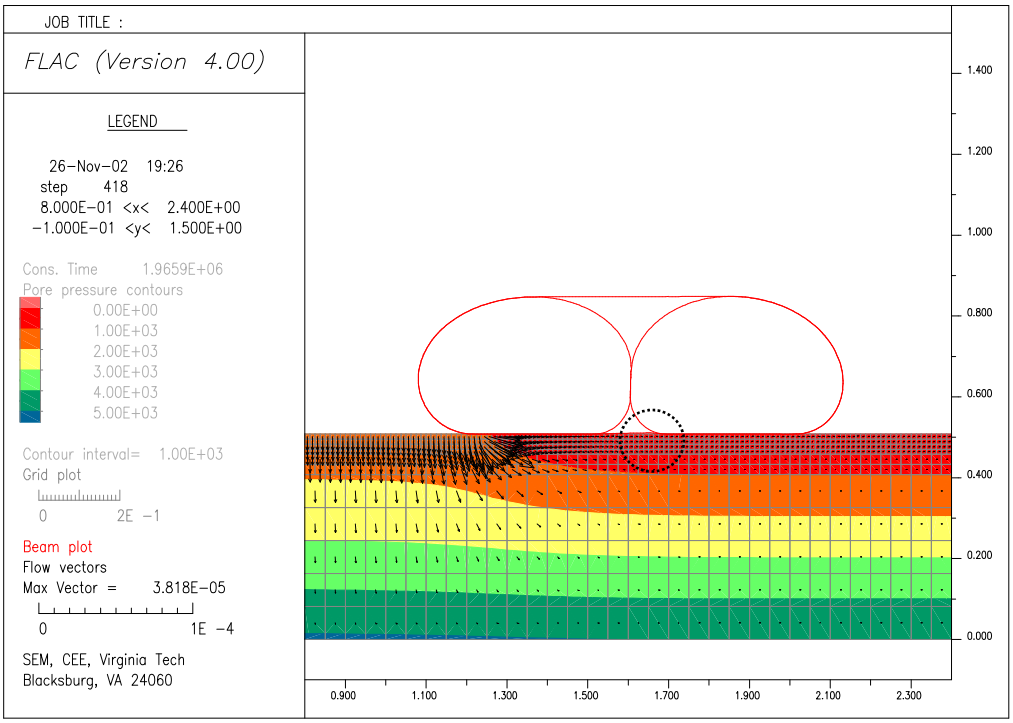

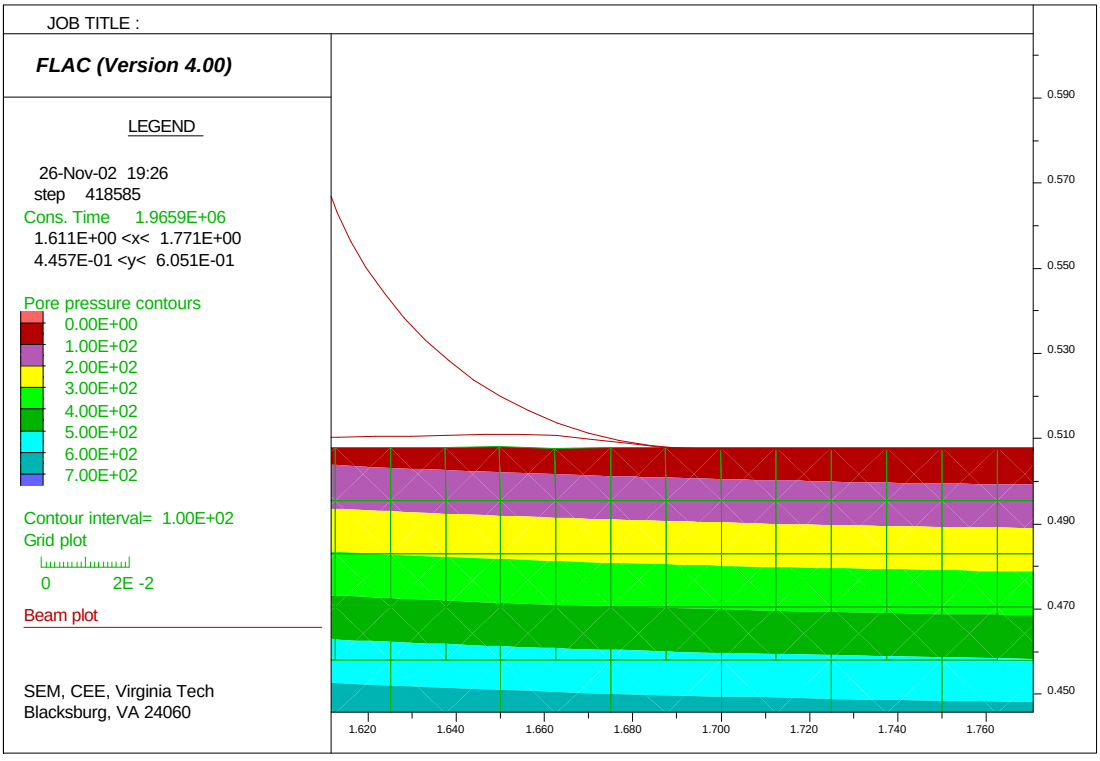

Figure 7.17. Pore pressure of the sleeved tube dam 2

7.3.3. Effect of Friction Angle between Tube Materials

The effects of the friction angle between the tube materials should be investigated since the sleeved tube dam becomes unstable in this study by slip failure between two inner tubes. In addition, the interface between tube materials, which are geomembranes, has a big difference between the peak and the residual friction angle (see section 3.2.4). Also, there is a wide variation of the peak and the residual friction angle values.

Besides 14 degrees for the friction angle, 20 degrees and 25 degrees are studied here. The new friction angle values are applied between the outer tube and the inner tubes (CR1 and CR 2) and between the two inner tubes (CR 3). Other interface properties are the same as in the previous case.

The foundation is considered to be rigid since the deformation of the soil hardly affects the failure of the sleeved tube in this study. The other reason is to have a faster run time for the numerical analysis. However, the groundwater flow is included, to assess the pore pressure effect beneath the sleeved tube dam.

The external water height is increased in a similar way as in the previous section. Also, the area of each inner tube is kept constant during the external water loading.

For the sleeved tube dam 1, three values, 14 degrees, 20 degrees, and 25 degrees of friction angle, are analyzed. Then the results from the case of 14 degrees are compared with those of the previous case and it is verified that the deformation of the foundation does not influence the important results. However, if a sleeved tube dam is set up on very soft soil, there are certain differences between the cases in the numerical analysis. The deformation of the sleeved tube dam will be affected, and the contact length between the two inner tubes will be changed.

For the sleeved tube dam 2, 20 degrees and 25 degrees of friction angle are analyzed numerically. Their results are examined together with the result from the previous section.

The critical external water heights for each case are presented in Figure 7.18. The critical external water heights are plotted against the frictional coefficient, which is the tangent of the friction angle. For the sleeved tube dam 1, the critical external water heights for different friction angles are 0.2286 m (9.0 in.), 0.2667 m (10.5 in.), and 0.2921 m (11.5 in.). For the sleeved tube dam 2, they are 0.1397 m (5.5 in.), 0.1651 m (6.5 in.), and 0.1905

m (7.5 in.). As the friction coefficient increases, the shear resistance of the interface increases almost linearly.

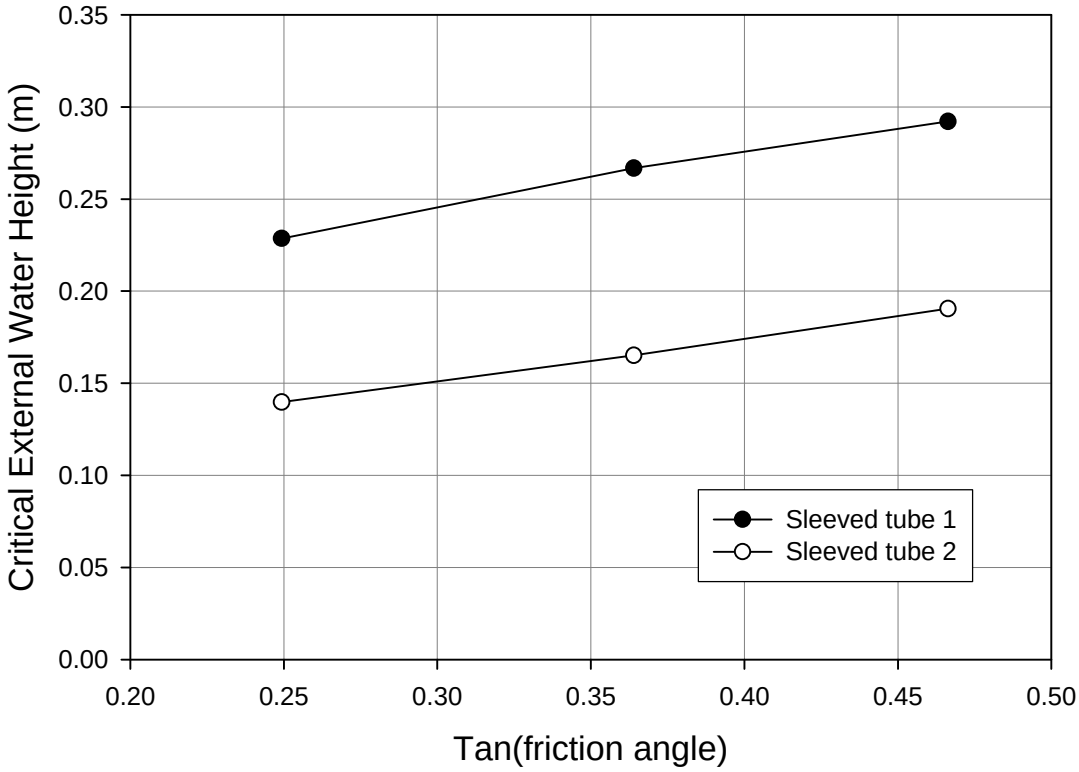

Figure 7.18. Critical external water height versus friction coefficient.

The deformations of these cases are depicted from Figure 7.19 through Figure 7.22 for friction angles 20 degrees and 25 degrees. In Figure 19 and Figure 20, sleeved tube dam case 1, the blue line represents the deformation at EWH = 0.1524 m (6.0 in.). The green line and the red line designate the deformation at 0.0127 m (0.5 in.) before the critical EWH and at the critical EWH. The pink dashed line shows an example of how the sleeved tube dam rolls at its failure. For the sleeved tube dam 2, Figure 21 and Figure 22, the blue line represents EWH = 0.127 m (5.0 in.).

The deformations clearly support the idea again that the sleeved tube dam becomes unstable as soon as the two inner tubes begin to slip. The deformations of the sleeved tube dam 1 are more distinctive than those of the sleeved tube dam 2. The lateral displacements of the top, and the vertical displacements of the bottom of the headwater side of the sleeved tube dam 1, are much greater, because the circumference of the outer tube of the sleeved

tube dam 1 is smaller than that of the sleeved tube dam 2. It is noted that the contact length of the two inner tubes is not influenced by the friction angle values.

The tensions in the sleeved tube dams 1 and 2 are shown from Figure 21 through Figure 24. Similar to the tension plots in the previous section, the tensions of the sleeved tube dam 1 are altered more than for the sleeved tube dam 2 in response to the rise of the external water height due to the changes of net pressure.

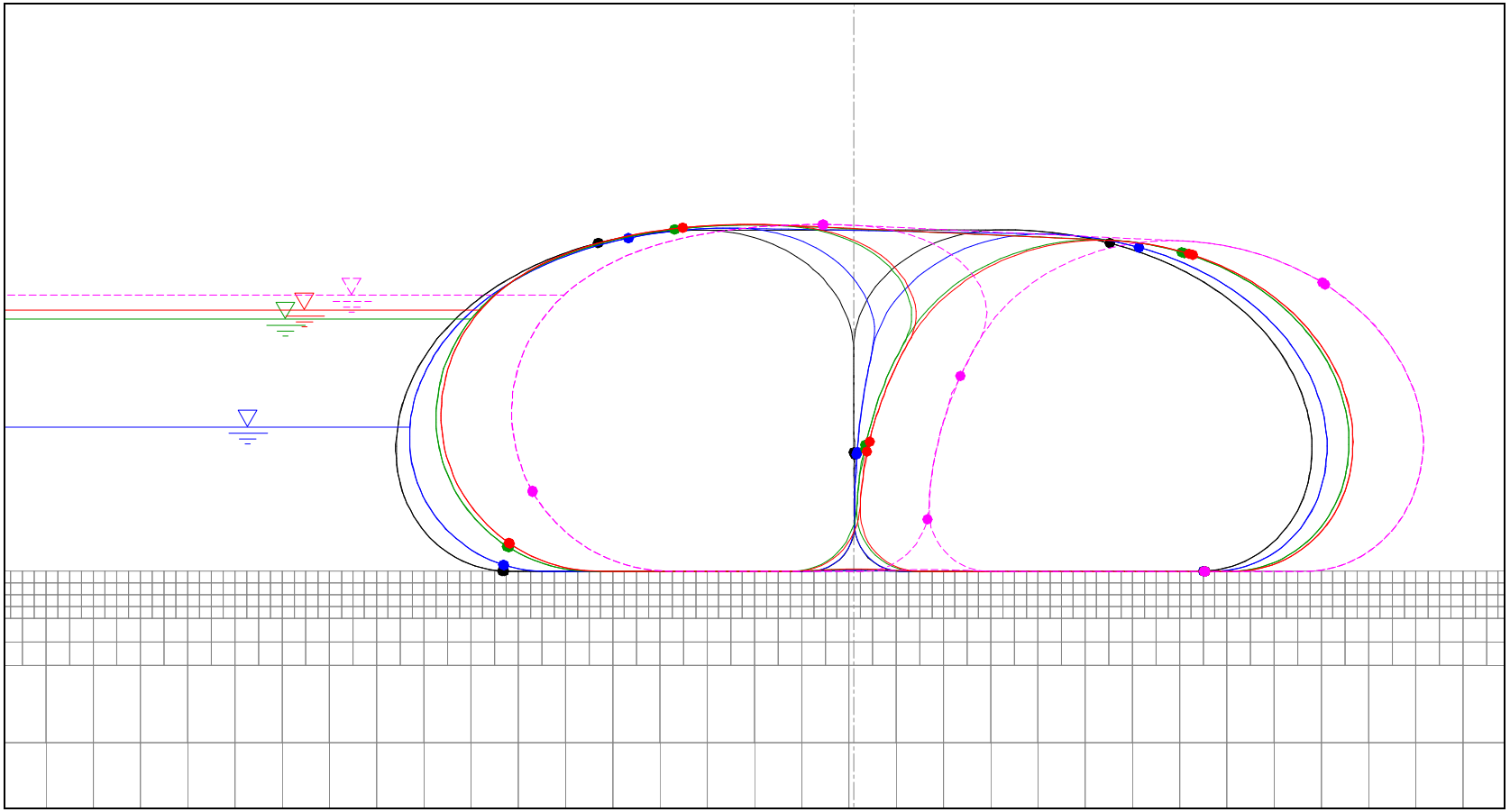

Figure 7.19. Deformation of sleeved tube dam 1 (friction angle = 20 degrees)

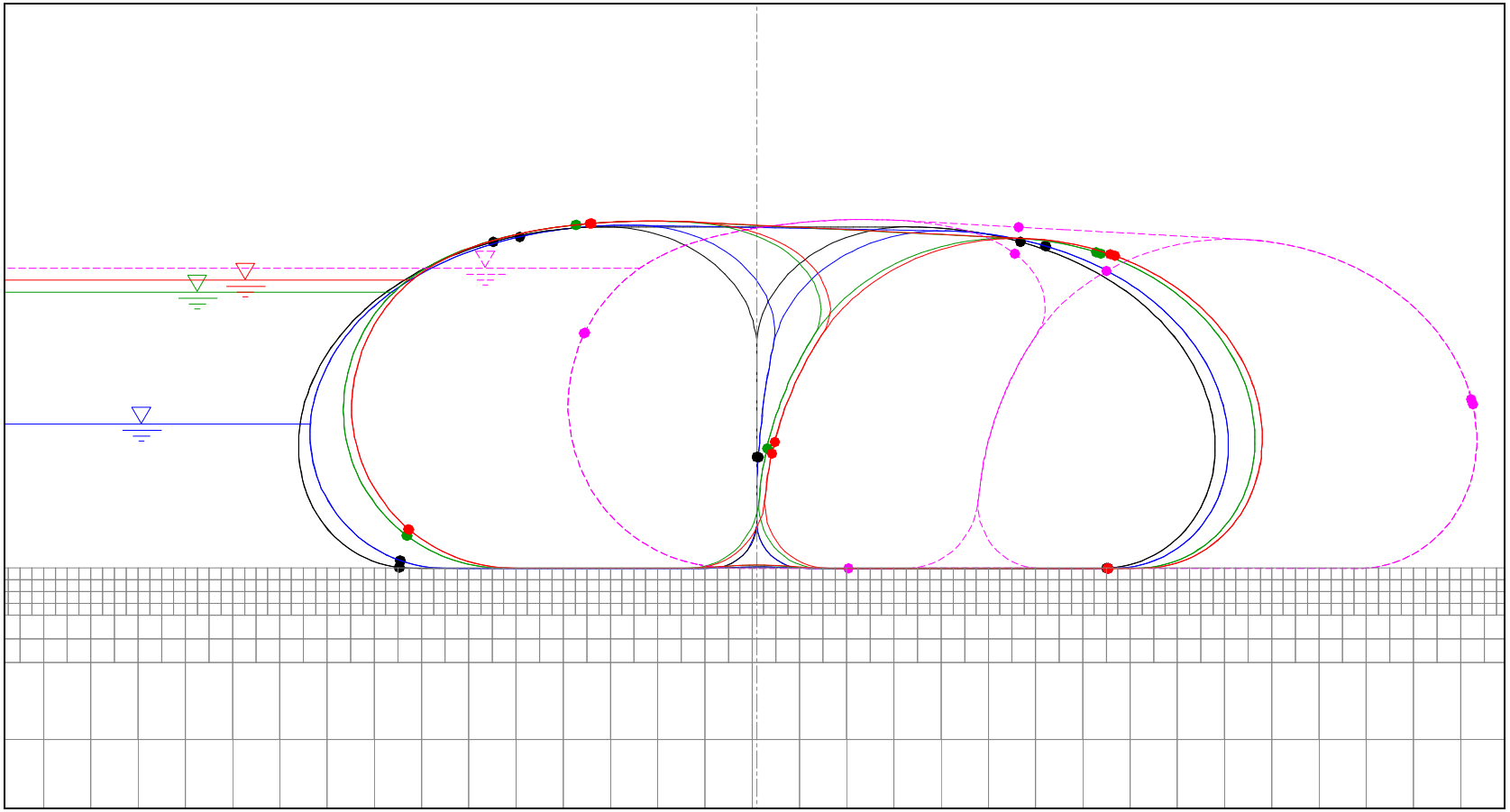

Figure 7.20. Deformation of sleeved tube dam 1 (friction angle = 25 degrees)

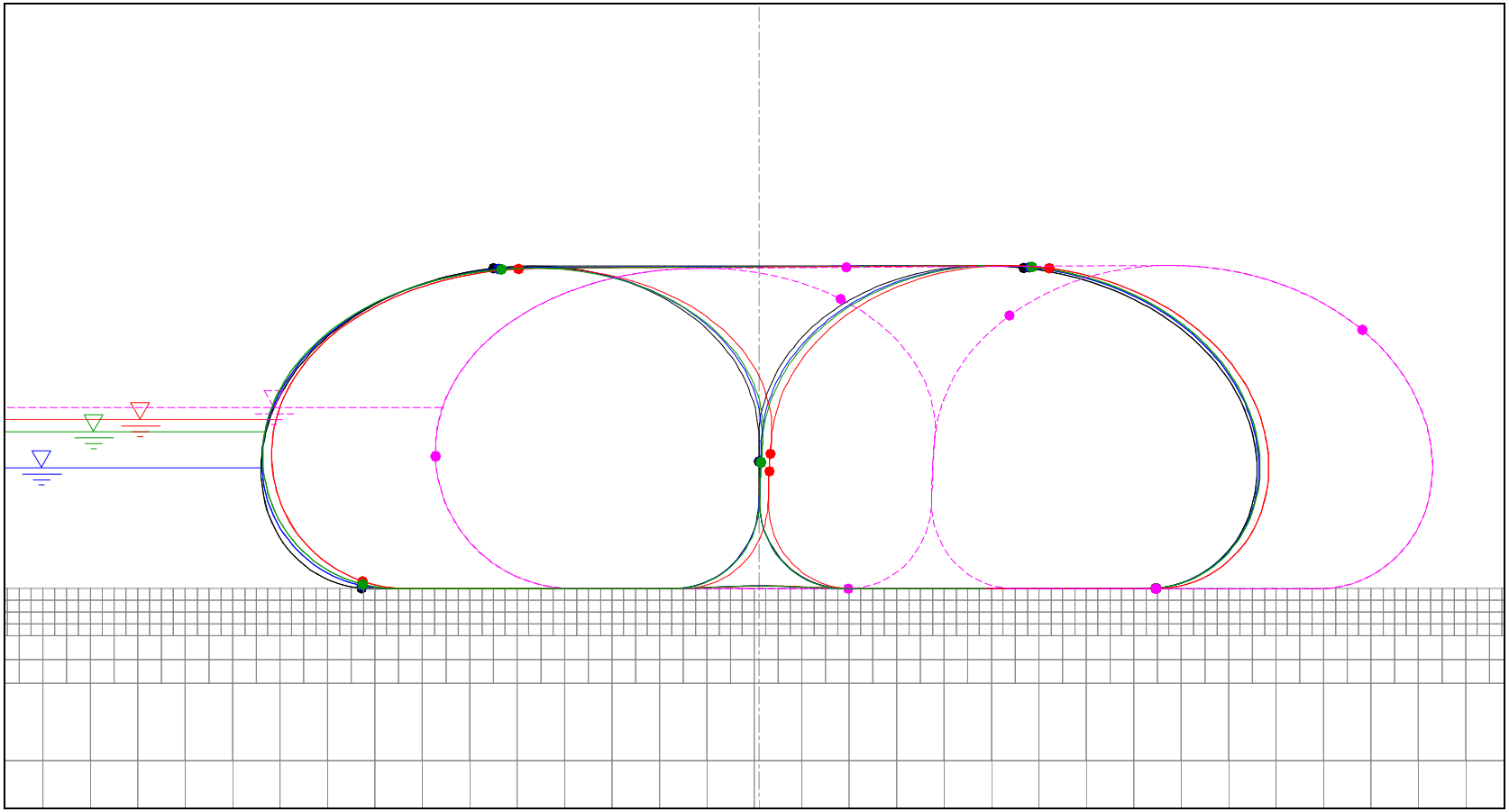

Figure 7.21. Deformation of sleeved tube dam 2 (friction angle = 20 degrees)

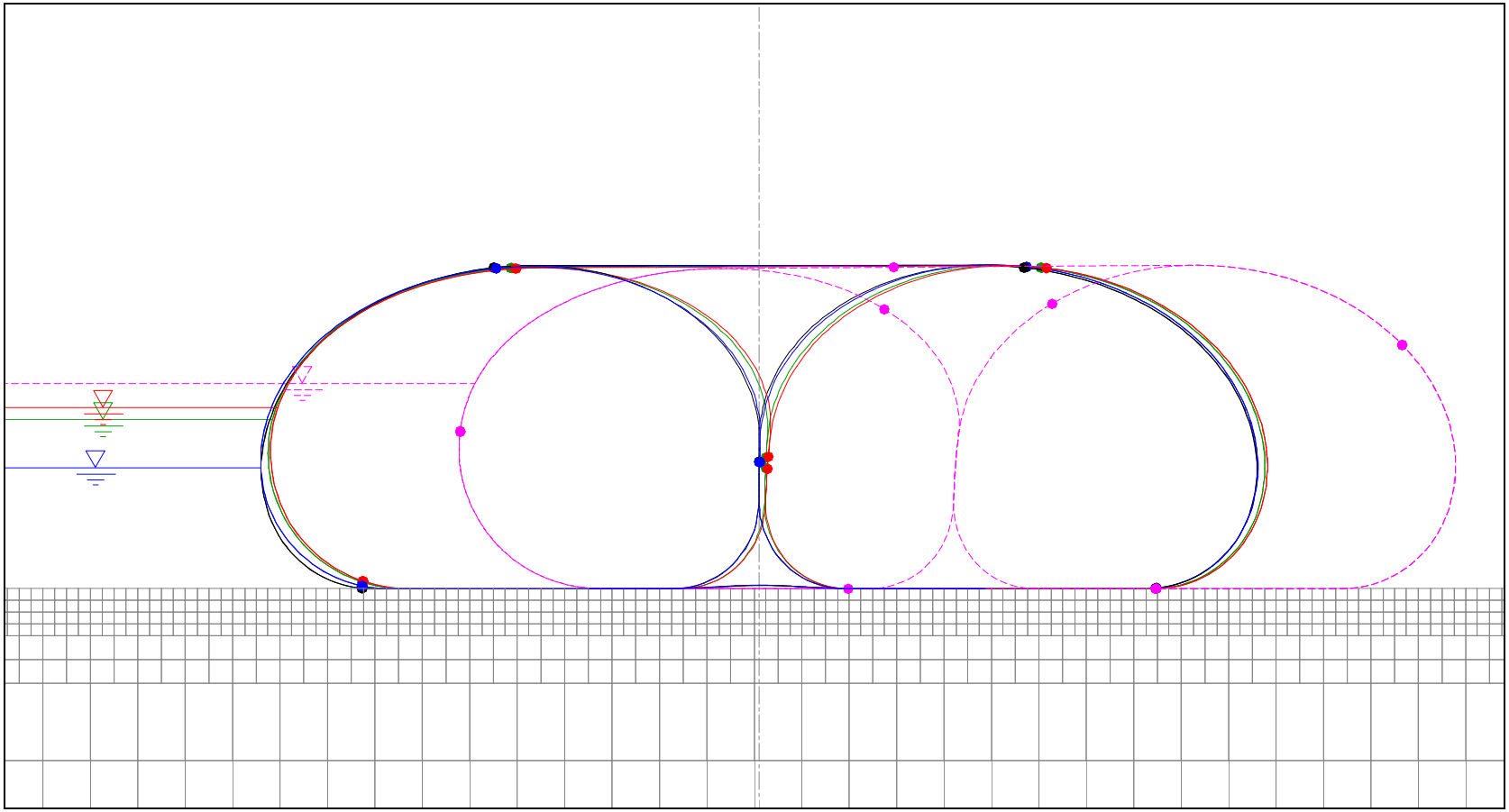

Figure 7.22. Deformation of sleeved tube dam 2 (friction angle = 25 degrees)

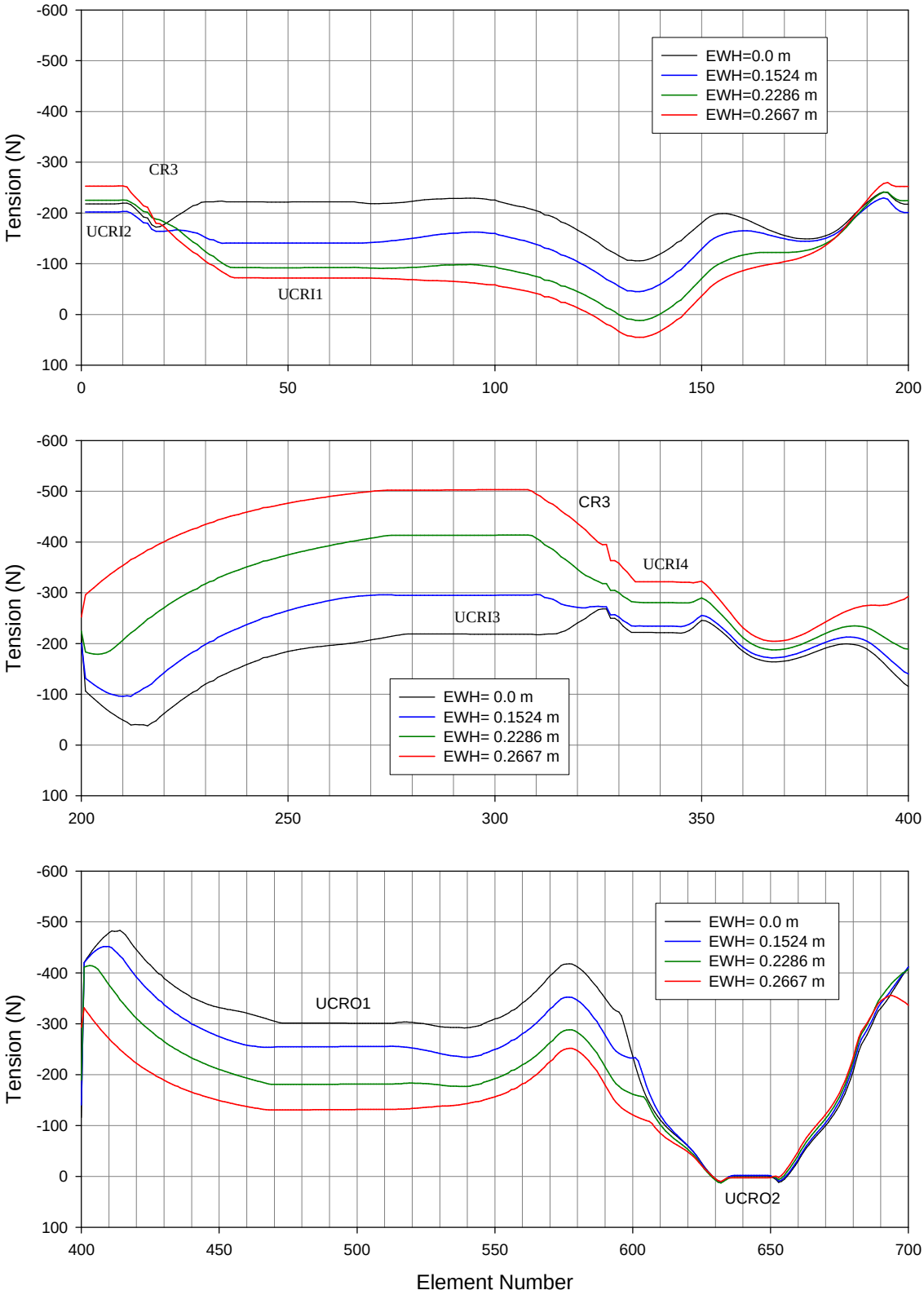

Figure 7.23. Tension in sleeved tube dam 1 (Friction angle = 20 degrees)

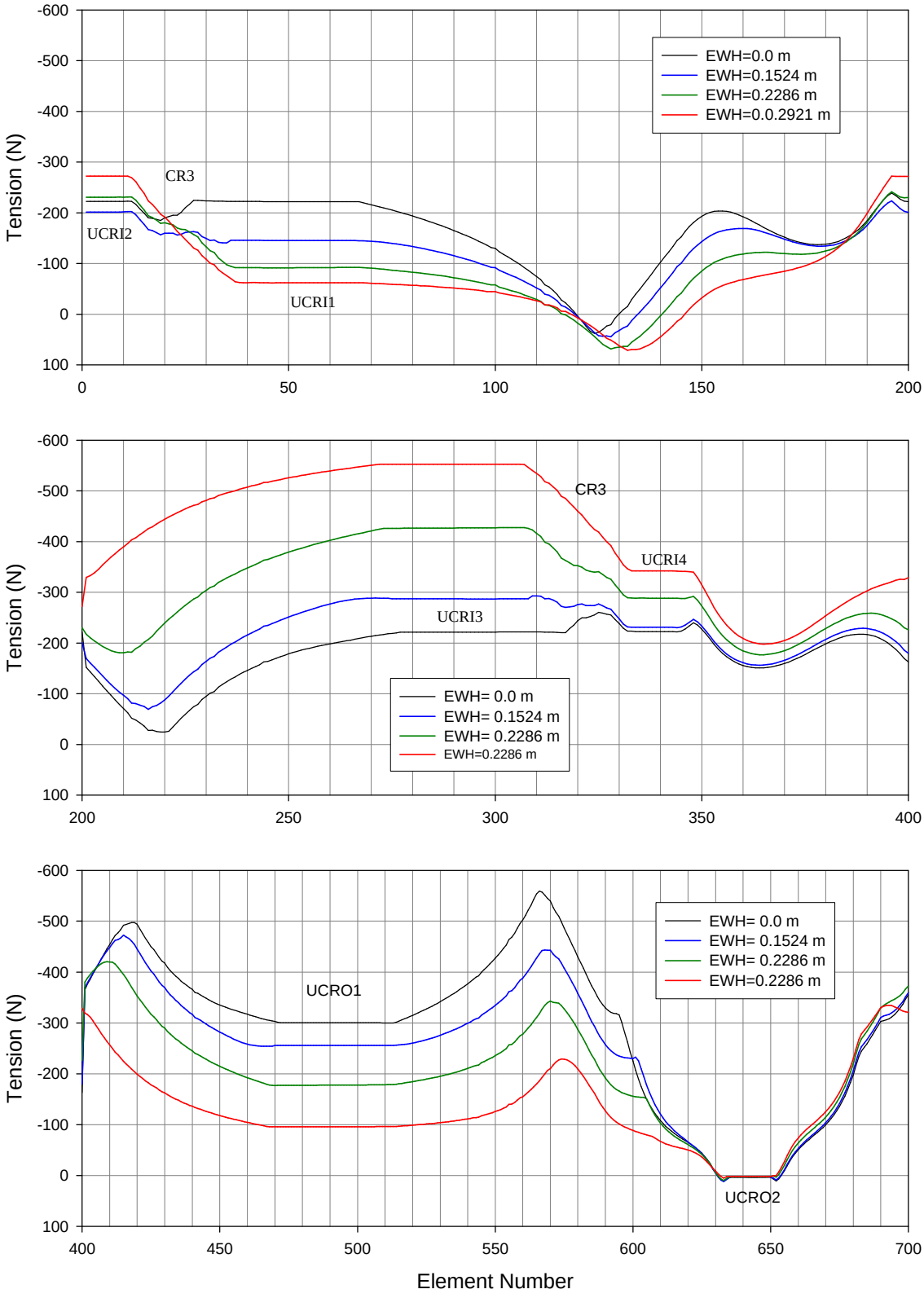

Figure 7.24. Tension in sleeved tube dam 1 (Friction angle = 25 degrees)

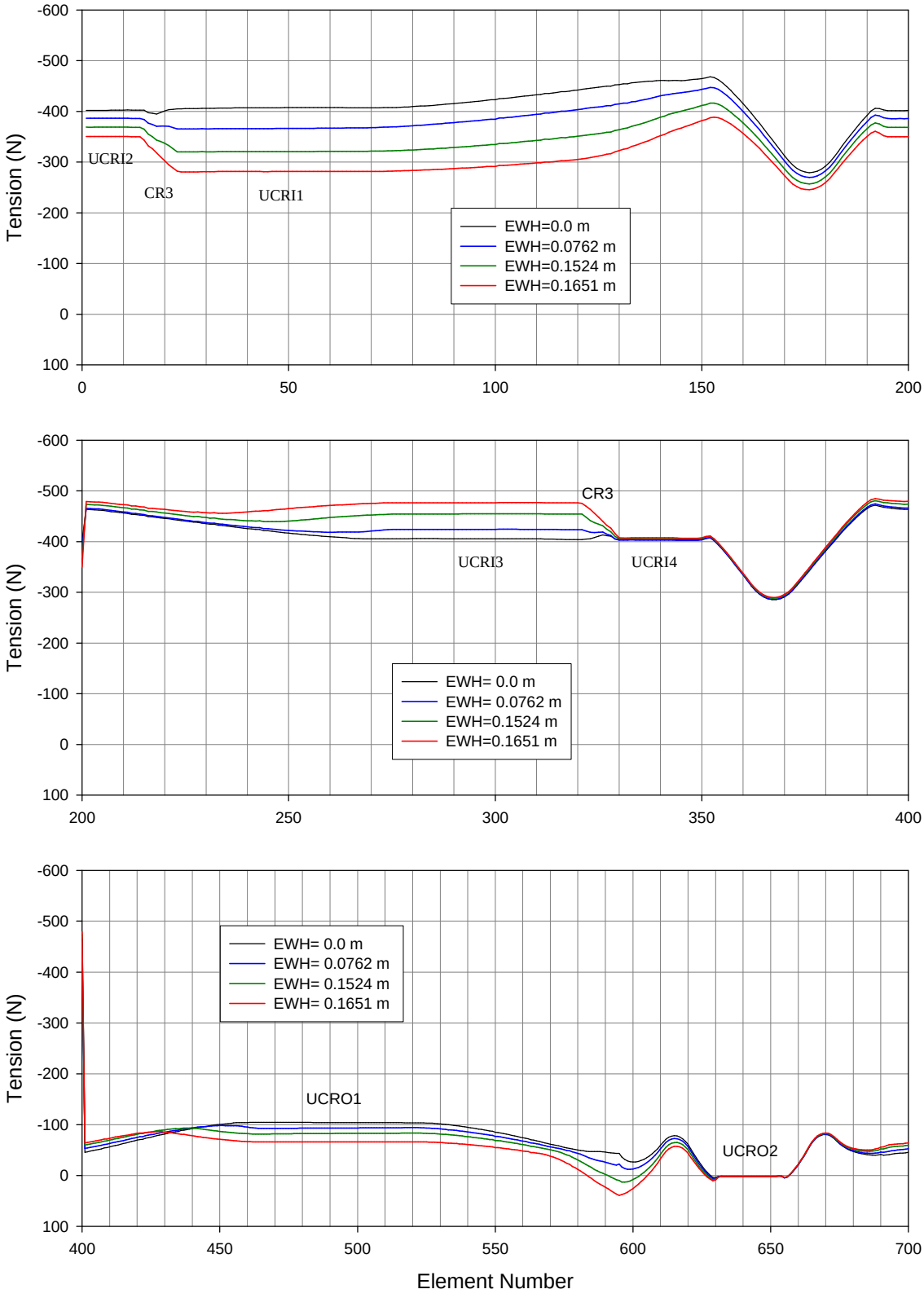

Figure 7.25. Tension in sleeved tube dam 2 (Friction angle = 20 degrees)

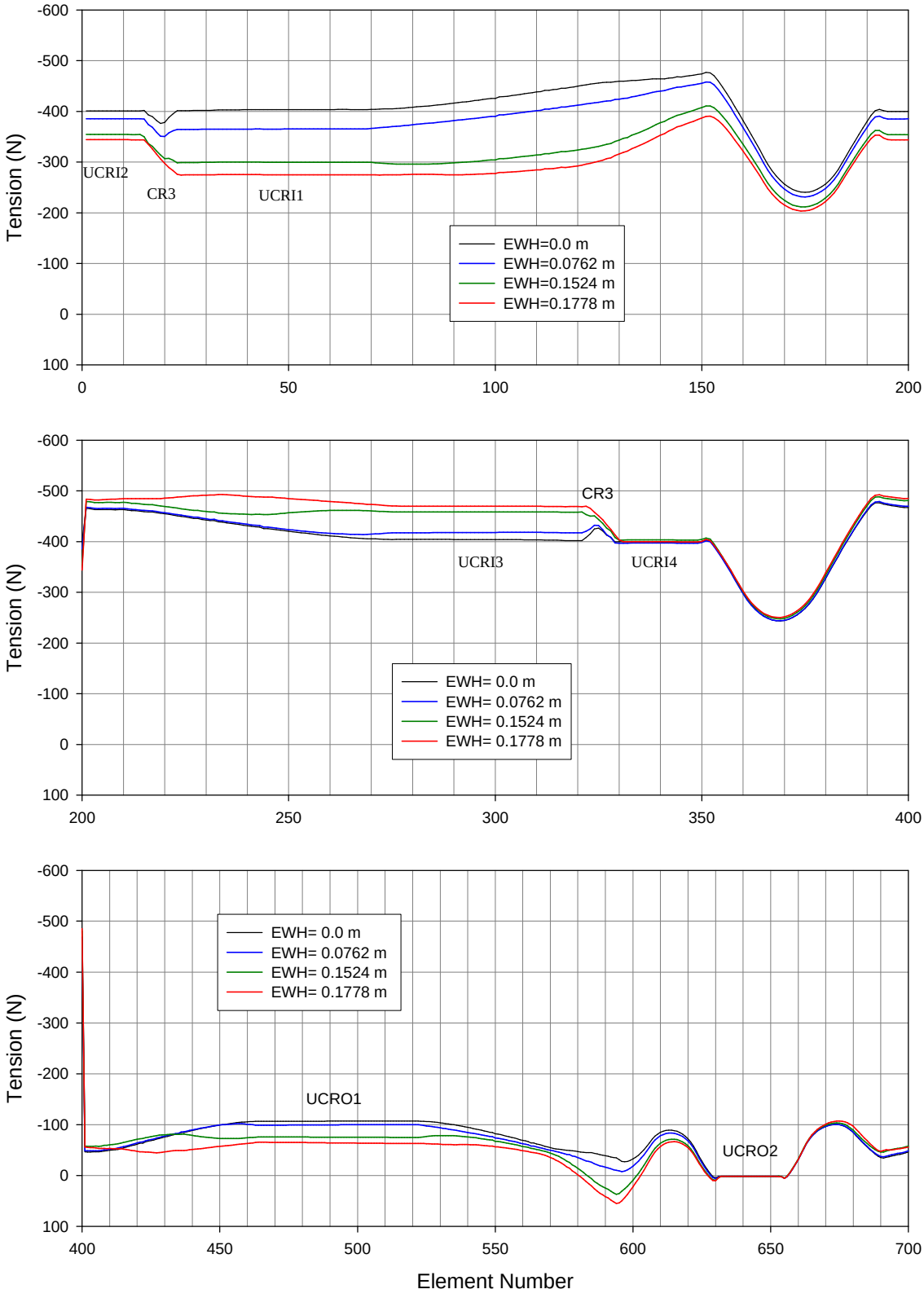

Figure 7.26. Tension in sleeved tube dam 2 (Friction angle = 25 degrees)

7.4. Summary and Conclusion

From the numerical analysis of the sleeved tube dam, the following summary and conclusions can be drawn.

The comparison of the deformation between the numerical result and the experimental result shows a good agreement for both sleeved tube dam 1 and 2. The critical external water height from the numerical analysis for the sleeved tube dam 1 is estimated at slightly less than from the experiment.

However, the critical external water height for the sleeved tube dam 2 does not agree well with the observation of the experiment. The numerical result is much less than the experiment, about 50 %.

The IWPHs of the two inner tubes are changed; the IWPH of the inner tube H decreases, while the IWPH of the inner tube T increases in the numerical analysis. The experimental result shows similar changes and a fair agreement for the sleeved tube dam case 2. For the sleeved tube case 1, the IWPHs of the inner tube H for trial 1 and trial 2 decrease, similar to the numerical result, but the IWPH of the inner tube T for both trials does not increase.

The numerical simulation demonstrates that the sleeved tube dam fails by rolling which is induced by slip failure of the two inner tubes in this study. Yet the failure mode of a sleeved tube dam can be changed depending on the inner tube materials, the soil conditions, and the cross-sectional shape of the dam.

Among these factors, the effect of the friction angle between the two tube materials is assessed in a parametric study. The shear resistance of the contact region of the two inner tubes increases almost linearly with the friction coefficient. Note that the length of the contact region is not influenced by the friction coefficient. However, the external water force is increased as the square of the external water height and so the shear force transmitted in the contact region increases similarly. As a result, the critical external water height increases exponentially as the friction coefficient increases in this study.

It is conjectured that the large difference between the critical external water height of the numerical and experimental results for the sleeved tube dam 2 is attributed to the characteristics of the interface between the two geomembrane materials. The interface test

showed that there was a large scatter of the friction angle values (Moler et al., 2001). The proper estimation of the friction angle values is not an easy task. In addition, there is much difference between the peak and the residual friction angle[4] value from the test, 54 degrees and 14 degrees. So, it is not certain that it is appropriate to use the residual friction angle value, 14 degrees, as the friction angle in the numerical model, since the current interface element cannot account for both in FLAC.

For the sleeved tube dam 1 case, the contact length of the two inner tubes is longer than for the sleeved tube dam 2 (see Table 7.2). Because of that, the normal pressures at the top of the contact length of sleeved tube dam 1 are much smaller than those at the bottom, and the shear strength at the top is also much smaller than at the bottom. As a result, the slip at the top starts at a lower EWH even with the high peak friction angle value, and it will induce progressive slip failure between the two inner tubes. In other words, as soon as the slip at the top occurs, the remaining contact region begins to slip without reaching its peak.

In contrast to sleeved tube dam 1, sleeved tube dam 2 has a shorter contact length between the two inner tubes. For that reason, the shear strengths at the top and at the bottom do not have a big difference, so slip at the top and at the bottom occurs at almost the same time after reaching their peaks.

Therefore the residual friction angle 14 degrees as the friction angle value in the interface element between the two inner tube materials provides the proper estimation of the critical EWH for sleeved tube dam 1, which has a long contact region. But, the peak friction angle 54 degrees is a more appropriate value for the friction angle of the interface for sleeved tube dam 2, which has a short contact region.

[4] It is not unusual to have a comparatively large difference between the peak friction angle and the residual friction angle of woven geosynthetic materials (Jones and Dixon, 1998).

Chapter 8. Stacked Tube Dam

8.1. Introduction

The most straightforward way to improve the stability of a simple tube dam is by stacking the tubes. Two tubes can be simply piled vertically (one tube at the bottom and the other tube at the top: 1-1 formation). Also, three tubes can be stacked (two tubes at the bottom, the other tube at the top: 2-1 formation) for more stability. If a situation requires a more stable dam, other tubes can be added to create a wider dam such as one with three tubes at the bottom and two tubes at the top (3-2 formation). Moreover, another tube can be installed at the top of 3-2 stacked tube dam to make a higher dam (3-2-1 formation). However, the tube dam requires strapping to tie the tubes together and restrain the tubes in position. These stacked tube dams are illustrated in Figure 8.1.

Experiments on the stacked tube dams were conducted by Moler et al. (2001). The 2-1 formation, two tubes at the bottom and one tube at the top, was tested. All three tubes were constructed with the same material and the same circumference, and they were held together by a strapping system. The strapping system consisted of four sets of strap along the longitudinal length of the dam. Several strapping techniques were attempted in an effort to find the best method. The best strapping system tried in the test was “a clamp model”. The strapping technique requires implementation of a clamp at the crossing of the bottom strap, which has a shape like on “8 ” with itself, so the displacement of the strap can be restrained. Then the top strap starts from one of the sides of the bottom strap, goes over the top tube, and reaches the other side of the bottom strap. The top strap was connected to the bottom strap ratcheting device and no-slip buckle. The bottom strap and the top strap were tightened to secure the tubes in place.

The IWPHs of all three tubes were measured carefully, together with the deformation of the tubes when the external water level increased. The critical external water heights were observed. Thirteen trials were conducted.

Two trials of the experiments are numerically simulated and analyzed here. It is assumed that the tube areas are constant throughout the tests. The pore pressure effects are considered jointly with the deformation of the foundation. The numerical results are compared with the experimental results and this will provide a better understanding of the behavior of the stacked tube dam.

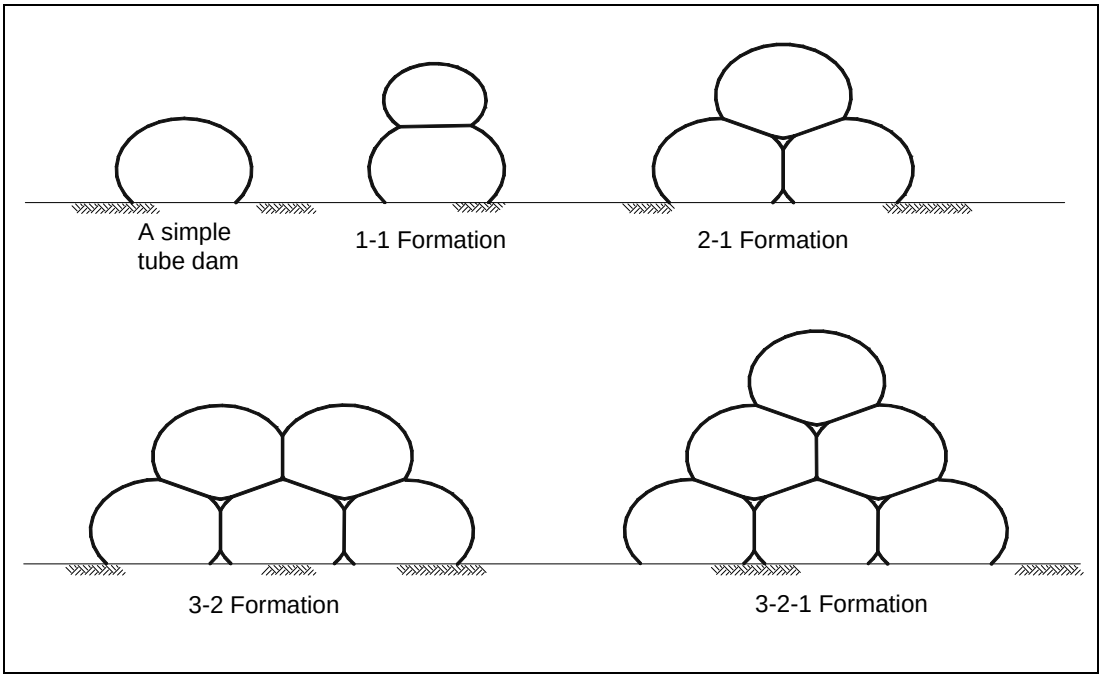

Figure 8.1. Types of stacked tube dam formations

8.2. Numerical Modeling

The big difference between the modeling of the other types of the tube dam and the stacked tube dam is the strapping system. Four sets of straps are located along the length of the tubes in equal spacing in the experiment. To model the stacked tube dam with the strapping system in two dimensions, the total width of the straps of the stacked tube dam is assumed to be the same as the length of the tube dam.

The cross-sectional area of the strap per unit length in the numerical model is adjusted based on the total cross-sectional area of the straps which was measured in the experiment. Generally, the value of Young's modulus should be adjusted for the strap. The

reason for the modification of the thickness instead of the Young's modulus is that a very low Young's modulus can induce fatal errors of calculation in FLAC. Since the main resultant force of the water-filled tube dam is tensile force (see Chapter 4), an adjustment of the cross-sectional area will produce a fair assessment in the numerical results.

Also, the modeling of the stacked tube dam itself involves numerical analysis of the deformation of the bottom tubes caused by the placement of the top tube. When the top tube is placed on the two bottom tubes, the weight of the top tube exerts forces on the bottom tubes. As a result, the bottom tubes are deformed and so the areas of the bottom tubes are altered. The secant method is employed to keep the bottom tube areas constant (see Section 3.4.1).

8.2.1. Properties of Model

The numerical model of the stacked tube dam consists of three tubes, two straps, and eleven interfaces, together with soil and drain grids. Each tube has 102 beam elements. The properties of the tubes are identical with those used in other models, but the circumference of the tube is 1.4859 m (58.5 in.)[1]. The soil grid and its properties are identical with those in the other models. The properties of the tube and the soil can be found in Section 3.2.

Two straps are modeled, a bottom strap and a top strap. The bottom strap has an "8 " shape and it wraps around the two bottom tubes. The bottom strap restrains the two bottom tubes when the top tube is placed on them. The beam elements of the headwater side and the tailwater side of the bottom strap are connected to a node in the middle (between the two bottom tubes). The top strap starts from the rightmost point of the tailwater side tube, over the top tube and to the leftmost point of the headwater side tube. Figure 8.2 shows the

---

[1] Note that the circumference of the tube is slightly greater than in the other models. It was inferred from the previous numerical simulations of the experiments that differences of the cross-sectional shape of the tube might be induced by the incorrect estimation of the circumference of the tube. Thus a slightly bigger circumference is used in this study.

straps with the three tubes. The gaps between the tubes and the straps in this figure are exaggerated for better illustration.

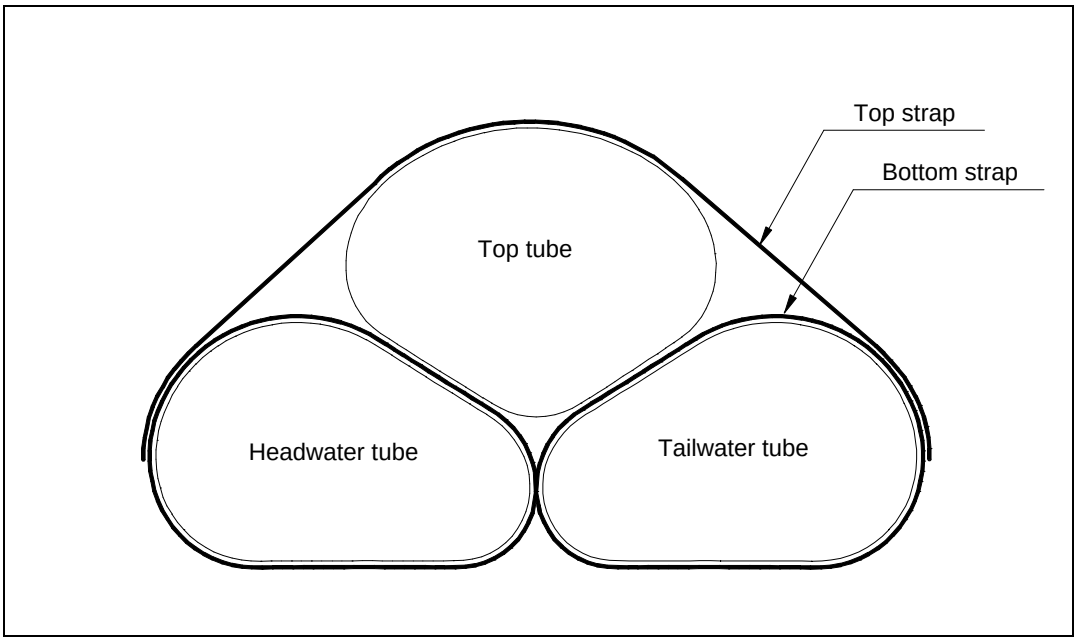

Figure 8.2 General notation of stacked tube dam

The straps are modeled with beam elements with very low value of moment of inertia (see Section 3.2). As mentioned earlier, the cross-sectional areas of the straps are adjusted, and the area is 3.64×10^{-5} m^2/m. The secant modulus 0.20 GPa from the material extensometer tests is used (Moler et al., 2001).

A total of 11 interfaces are assigned in the model. Three interfaces are located beneath the two bottom tubes, one interface is located between the two bottom tubes, and two interfaces are placed between the top tube and the two bottom tubes. Two interfaces are assigned between the bottom tubes and the bottom strap, and the other three interfaces are assigned between the top strap and the top tube.

The properties of the interfaces between the two tube materials, and between the tube and the foundation, can be found in Section 3.2. The interface properties of the strap and the tube material were tested (Moler et al., 2001). The residual friction angle 18 degrees and the shear stiffness 10 MPa/m are employed in the numerical model.

8.2.2. Procedures of Modeling

Unlike the other numerical models of the tube dam, the initial configuration of the stacked tube dam cannot be determined by a few simple routines, because the stacked tube dam is constructed with several components. In addition, the installation involves tightening of the straps and stacking of the tubes, which exert forces on the other tubes. Hence, the initial configuration of the stacked tube dam is determined by several procedures.

· **Installation of bottom tubes**

Two bottom tubes are placed on the ground and are inflated with the initial IWPHs. Then one of the two bottom tubes is moved so the rightmost point of the headwater tube is located as close as possible to the leftmost point of the tailwater side tube as shown in Figure 8.3. It is noted that the original locations of the tubes are determined in order to move the tubes least after the inflation, since the deformation of the ground is considered in the numerical analysis. In addition to the interfaces between the ground and the bottom tubes, another interface element is assigned between the two bottom tubes.

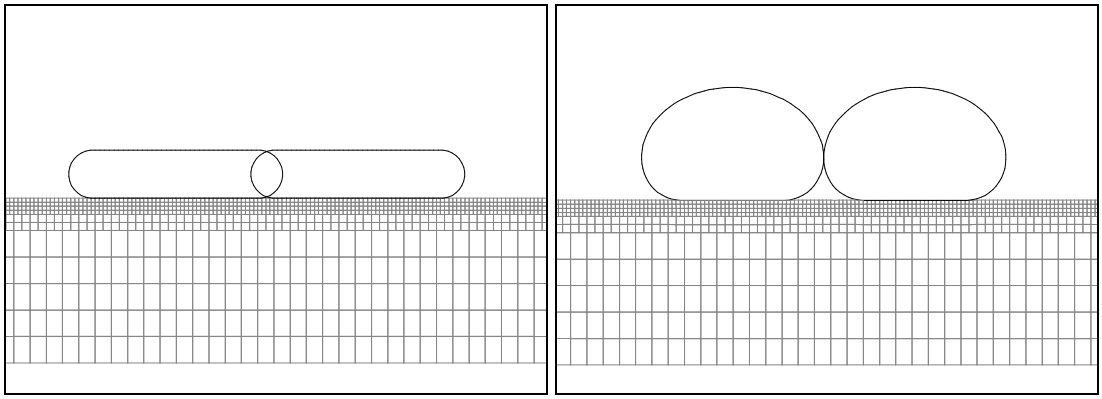

(a) Initial shape of two bottom tubes (b) After inflation

Figure 8.3 Setup of two bottom tubes

· **Strapping of bottom tubes and placement of top tube**

A bottom strap wraps around the two bottom tubes in an shape. The strap is constructed with a total of 204 beam elements. The bottom straps from the headwater side and tailwater side intersect at a node between the two tubes to simulate the clamp. Between

the headwater tube and the headwater side of the bottom strap, and the tailwater tube and the tailwater side of the bottom strap, two interfaces are allocated.

In the experiments, slight increases of the IWPH were observed in both tubes because of the fastening of the bottom strap. However, the fastening effect of the bottom strap is not reflected in this numerical model and it is assumed that the bottom strap is just wrapped around the two bottom tubes. This fastening effect can be imitated by a slight increment of IWPHs of the bottom tubes, or a tensile force can be applied to the beam elements of the bottom strap.

After the strapping of the bottom tubes, the top tube is installed at the top (see Figure 8.4.). The expected contact regions, between the top tube and the bottom tubes, are prepared with interface elements.

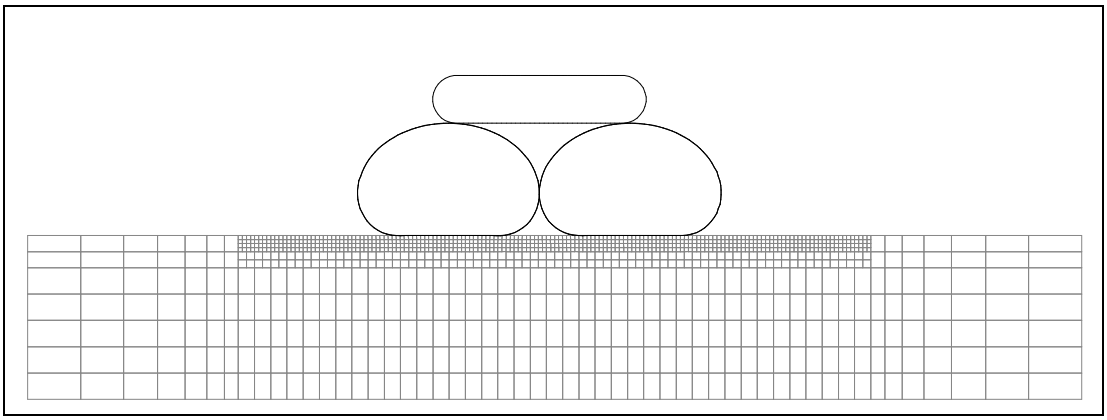

Figure 8.4 After bottom strapping and setup of top tube

· **Inflation of top tube**

The top tube is inflated gradually to the given IWPH. Updating of the deformed configuration is carefully controlled in FLAC at the beginning of the inflation. Figure 8.5 (a) through Figure 8.5 (c) show the progress of the inflation, and Figure 8.5 (d) depicts the top tube with the bottom tubes after the inflation.

It is clear from Figure 8.5 that the areas of the bottom tubes are altered by the weight of the top tube, which does not represent the stacked tube dam in the physical world. Since the bottom tubes are sealed after inflation, the areas of the bottom tubes should remain constant during the installation of the top tube.

For that reason, the IWPHs of the bottom tubes are adjusted using the Secant iteration method (see Section 3.4.1) to keep the same areas of the bottom tubes after the inflation. Figure 8.6 displays the top tube on the bottom tubes after the iterations. Without the iterations, or assuming constant IWPH, the resulting deformed shapes of the bottom tubes are very different as can be confirmed by a comparison between Figure .85 (d) and Figure 8.6. The IWPHs of the bottom tubes are increased more than 60 percent to keep the areas constant.

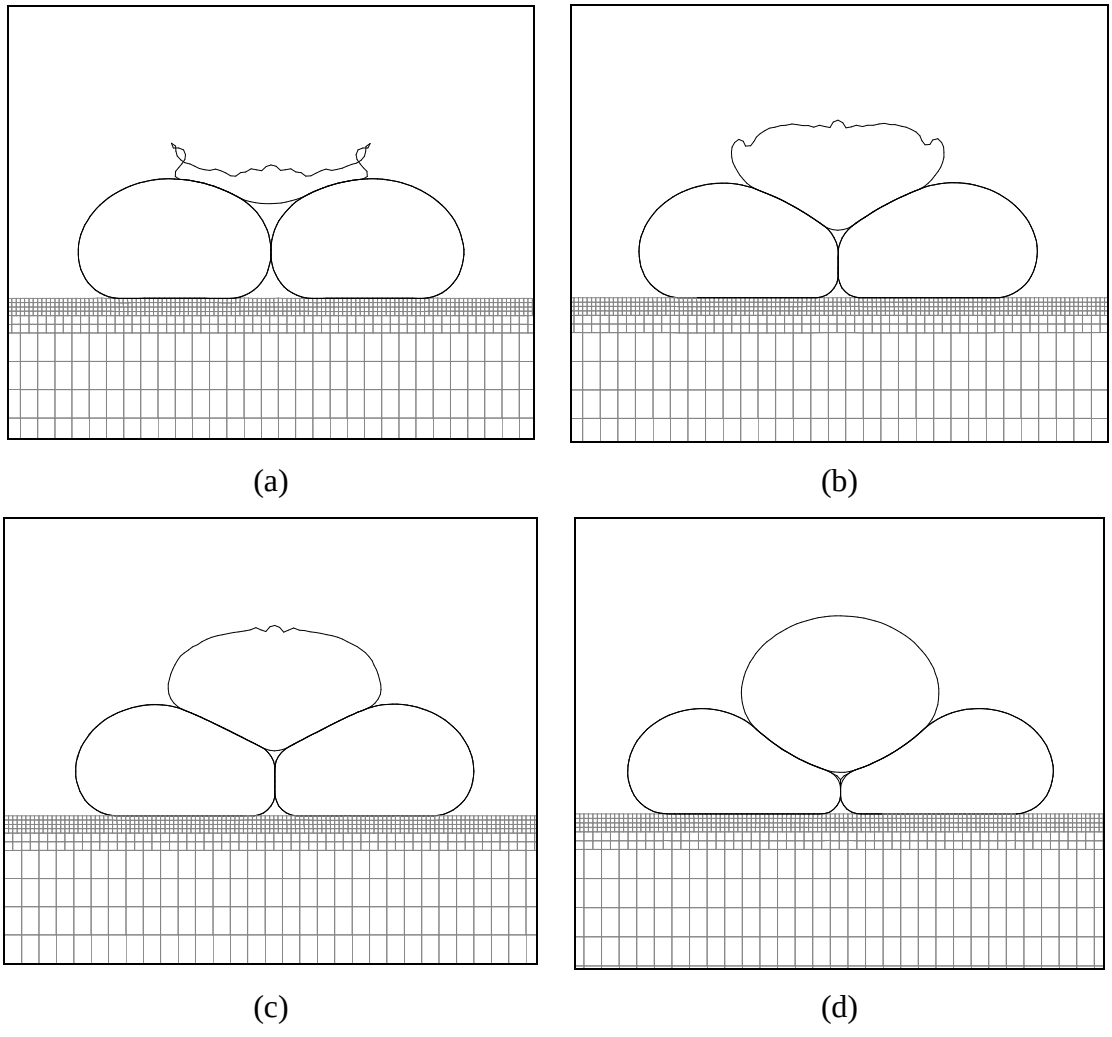

Figure 8.5 Process of inflation of top tube (assuming constant IWPH)

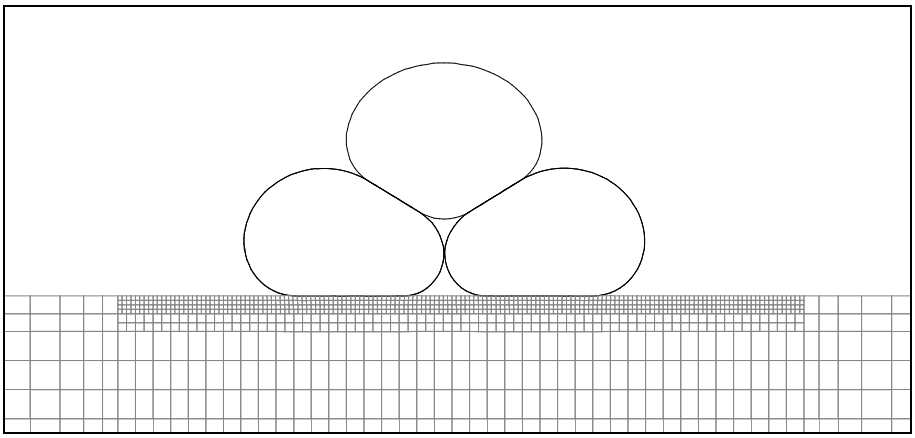

Figure 8.6 Inflation of top tube (assume constant bottom tube areas)

· **Strapping of top tube**

A top strap is constructed from the rightmost point of the bottom strap (tailwater side) and the first beam element of the top strap is connected with the node at the rightmost side of the bottom strap. Then the strap goes around the top tube and near the leftmost point of the bottom strap. At the end of the last beam element of the top strap, 150 N of tension is applied (see Figure 8.7 (a)). The tensile force 150 N is just an estimation for the numerical modeling. The dots in these figures represent the beginning and the end of the top strap. This will simulate the tightening of the stacked tubes in the tests. Figure 8.7 (b) presents a stage during the tensioning and Figure 8.7 (c) shows when the end of the top strap is pulled to the leftmost point of the bottom strap.

After that, the end of the top strap is directed adjacent to the bottom strap by changing the direction of the tension, and then the end node is connected with the node at the leftmost node of the bottom strap. After connecting the end of the top strap to the bottom strap, the tension is released. Also, the IWPHs of the two bottom tubes are adjusted manually to maintain the original tube areas since the areas of the tube are changed slightly by the top strapping. Figure 8.7 (d) depicts this final stage of the top strapping.

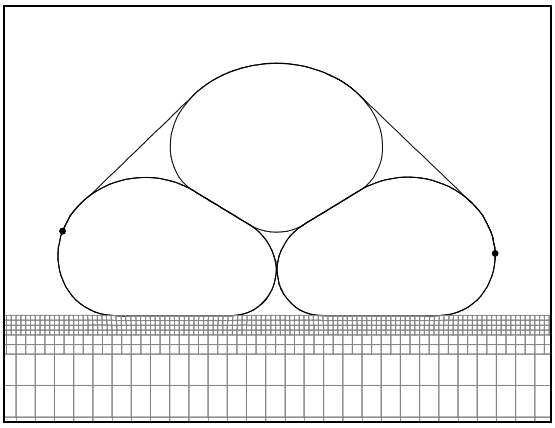

(a) Before tension process

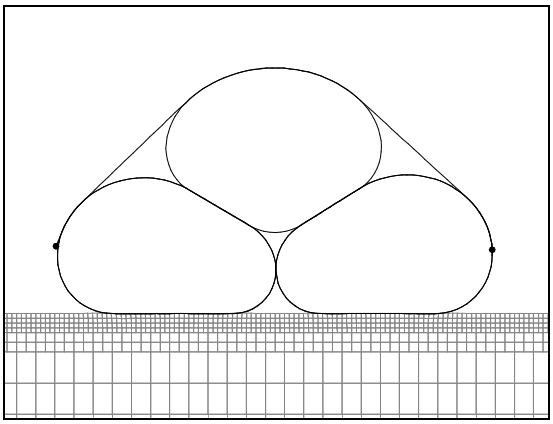

(b) During tension process

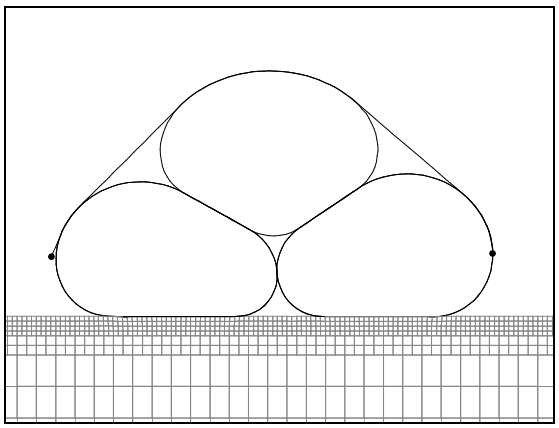

(c) After tension process

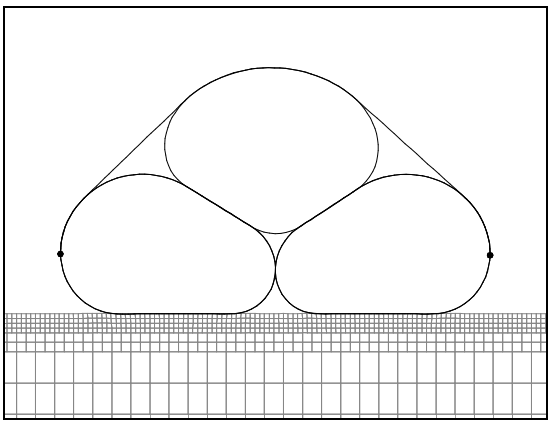

(e) Final shape of stacked tube dam with top strap

Figure 8.7 Top strapping process

8.3. Numerical Simulation

Among five trials of the stacked tube dam with the clamped bottom strap from the experiments, two trials, (trial 9 and trial 13) are numerically modeled.

For trial 9, the drain is located under the bottom tubes starting 0.406 m from the leftmost point of the headwater tube and is extended 1.118 m to the tailwater side. In the case of trial 13, the drain starts 0.457 m from the leftmost point of the headwater side of the tube and has a length of 1.118 m. Again, the drains are modeled here as a layer of the grid.

With the given external water height (EWH), the external water force applies on the headwater side of the stacked tube dam in parts. Depending on the parts, the forces are exerted in different structures of the stacked tube dam. For example, if the EWH is lower than the height of the headwater tube and higher than the top of the contact between the top strap and the headwater tube, the external water force application is divided into three parts. The first part is from the foundation to the connection of the top strap and the bottom strap. The second part is from the connection to the top of the contact region between the top strap and the headwater tube. The last part is from the top of the contact region to the given external water height. The external water force exerts on the bottom strap for the first part, on the top strap for the second part and on the headwater tube for the last part. As the stacked tube dam deforms, the contact region between the top strap and the headwater tube is continuously updated.

Because the stacked tube dam model involves a large number of elements of beams and interfaces, in addition to the fine grid meshes, a solution requires much computer running time and resources. The solution time is lengthened more when the deformation of soil and the flow of the groundwater are considered. Besides, the total solution time is stretched out by the iterations needed to find the changed IWPHs of the three tubes needed to have constant tube areas.

For these reasons, only a limited number of external water heights are analyzed numerically, using mainly the same heights as in the experiments to compare the results. In the numerical simulation of trial 9, the external water height is raised from 0.0 m to 0.3175 m (12.5 in.), 0.4064 m (16.0 in.), and 0.4318 m (17 in.). For trial 13, the external water height is increased to 0.3175 m (12.5 in.) and 0.3810 m (15.0 in.). The deformations and the IWPH changes of the tubes are investigated and the numerical results are compared with the experimental results. The critical external water heights are evaluated approximately here, and the behavior of the stacked tubes at the critical external water height is discussed.

8.3.1. Deformation of Stacked Tubes

Figures 8.8 and 8.9 display the deformations of the stacked tube dam for trial 9 and trial 13, respectively. The solid lines represent the numerical results and the dots denote the measurements from the experiment.

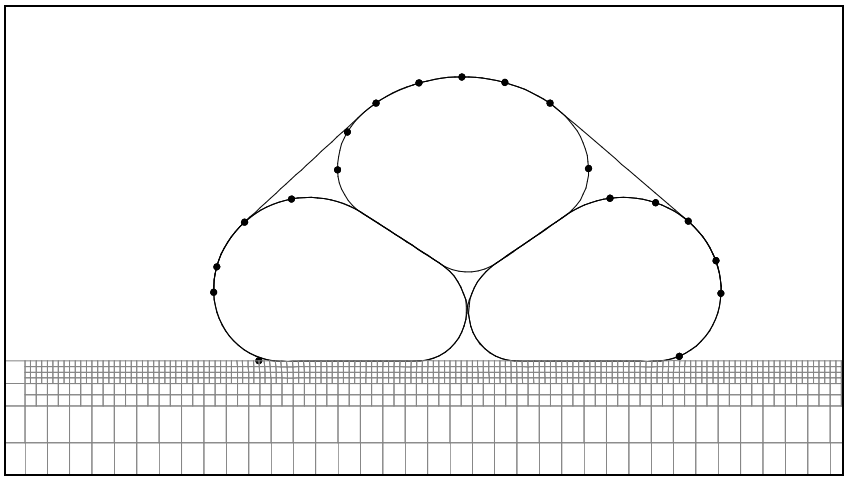

(a) EWH=0.0 m

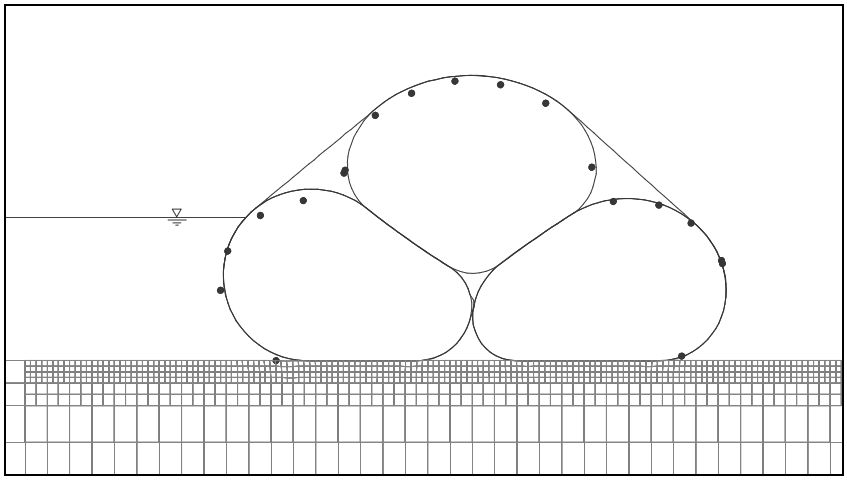

(b) EWH=0.3178 m (12.5 in.)

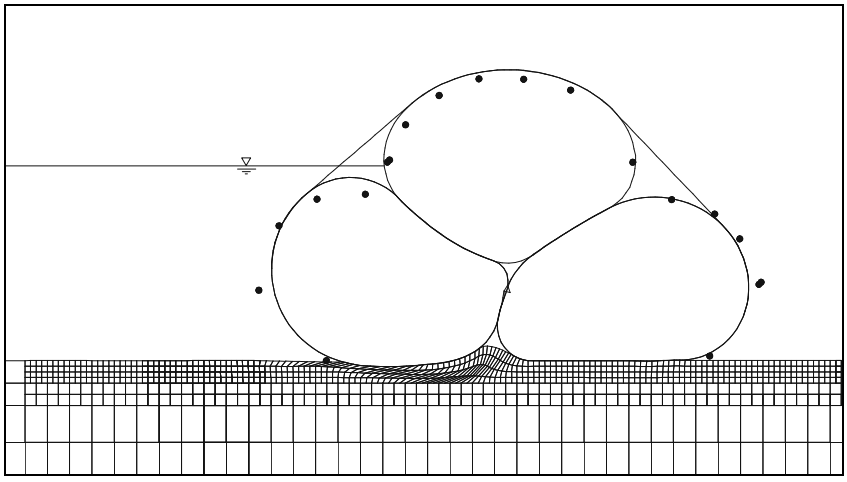

(c) EWH=0.4318 m (17.0 in.)

Figure 8.8 Comparison of deformation; Trial 9

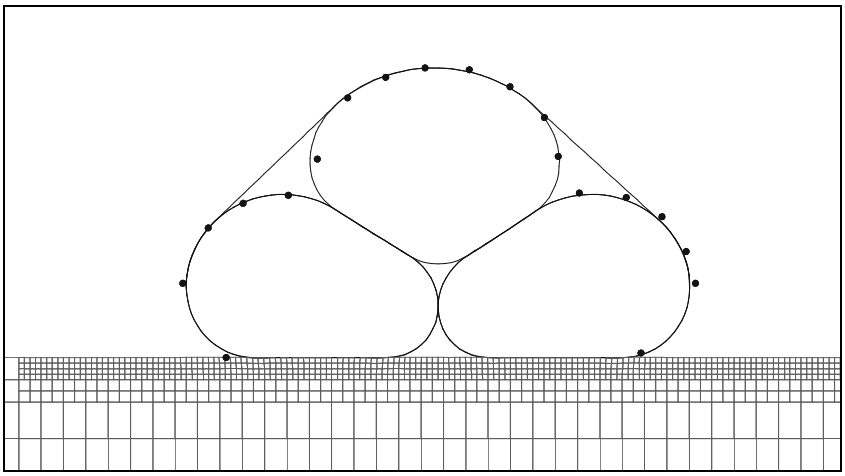

(a) EWH=0.0 m

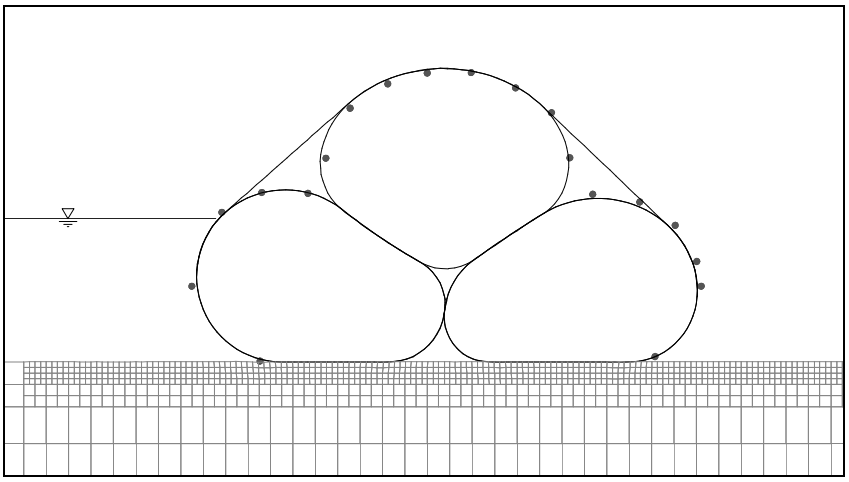

(b) EWH=0.3178 m (12.5 in.)

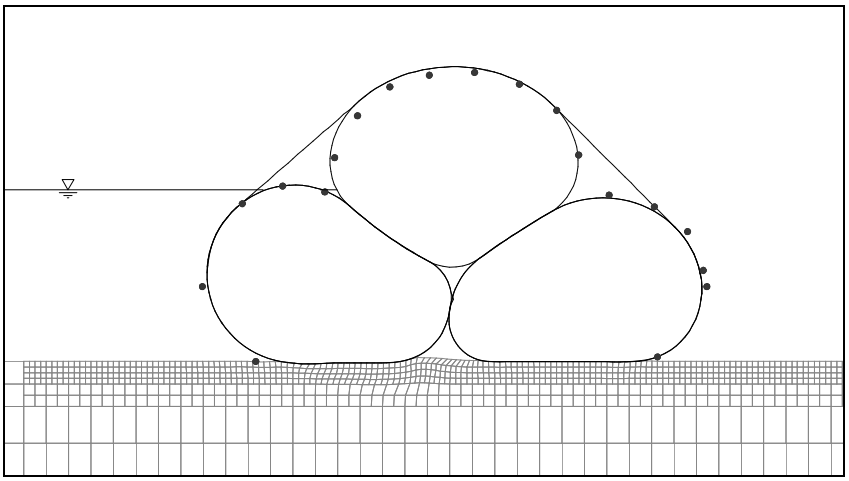

(c) EWH=0.3810 m (15 in.)

Figure 8.9 Comparison of deformation; Trial 13

For trial 9, the initial configuration of the stacked tube dam from the numerical analysis, which is obtained after several procedures of inflations of the bottom tubes and the top tube, and strapping, agrees very well with the experimental result (Figure 8.8 (a)). However, there are some difference between the numerical results and the test measurements at the external water heights of 0.3178 m and 0.4318 m, particularly in the configuration of the headwater tube. The deformed shape of the headwater tube from the numerical analysis displays a greater height and is rounder than in the experiment. This difference can be explained by the fact that there was a considerable leak from the headwater tube in the experiment, which results in a lower height and the flatter shape of the tube. This idea is supported by Figure 8.9, which shows very close agreement between the numerical result and the experiment for trial 13 at the external water heights of 0.3178 m and 0.3810 m. There was no leakage report in trial 13 in the experiment.

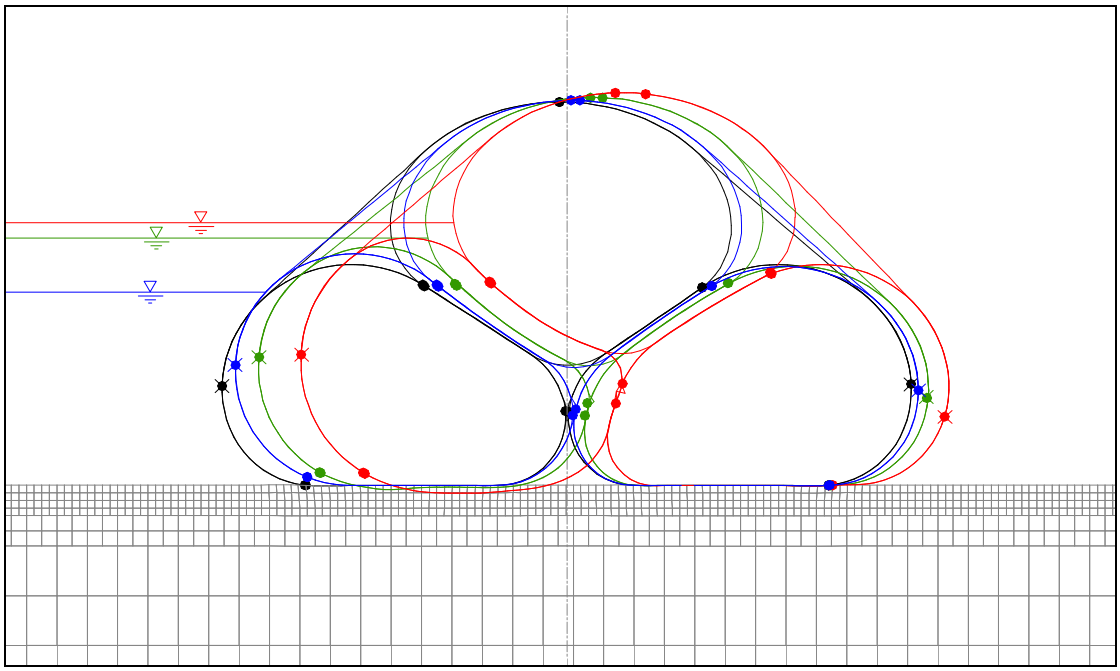

Figure 8.10 Overall deformation of trial 9

The behavior of the stacked tube dam during the flooding can be estimated by monitoring the displacements of the nodes on the tubes and the straps for trial 9 as shown in Figure 8.10. The black color represents the stacked tube dam after installation. The blue, green, and red depict the deformed shape at the external water heights of 0.3175 m, 0.4064

m, and 0.4318 m, respectively. The nodes with the crosses denote the locations of the connection of the top strap and the bottom strap. The other dots consist of two nodes from the interfacing beam elements; for example, the dots on the bottom of the headwater side are composed of nodes from the bottom strap and the tube.

At the external water height of 0.3175 m, the displacements of the dots on the bottom of the headwater tube and the tailwater tube indicate no sliding (or slip) between the bottom tubes and the ground. Then, the dot on the bottom of the headwater tube begins to show a slight slide at the external water height of 0.4064 m. With the interpretation of the displacement of the dots, it is clear that the headwater tube slides toward the tailwater tube at the external water height of 0.4318 m, yet the tailwater tube does not slide. Since the slide of the headwater tube is resisted by the weights of the tailwater tube together with the top tube, the headwater tube begins to lift up in response to the forces exerted from the headwater side tube and top tube. The lifting of the headwater tube lowers the tension on the top strap and induces rolling failure of the stacked tube dam system.

8.3.2. IWPH Changes

In the experiments, the internal water pressure heads (IWPHs) of the three tubes are measured at each external water height. However, the measurements of the IWPH from the installation of the stacked tube dam are only available for trial 10 and trial 13. Therefore, the IWPHs from the numerical simulation of trial 13 are compared with those from the experiment. It is noted that the IWPHs of the three tubes are controlled separately using the secant method in the numerical analysis.

At the beginning of establishment of the stacked tube dam, the two bottom tubes are inflated with 0.510 m of water pressure head in the numerical analysis. In the experiment, the headwater tube and the tailwater tube were filled with water pressure heads of 0.518 m and 0.502 m in that order. After the inflation of the top tube, the IWPHs of the bottom tubes are increased more than 60 percent for both the numerical analysis and the experiment, as shown in Figure 8.11. When the inflated top tube was secured by the strapping, the IWPH of the tailwater tube in the experiment was changed very little, while the IWPH of the tailwater tube in the numerical analysis goes up about 0.05 m.

When there is external water, the IWPH of the headwater tube is decreased, while the IWPH of the tailwater tube is increased both numerically and experimentally. The IWPH of the top tube in the experiment is reduced more than in the numerical analysis.

Generally, the numerically simulated IWPH changes of the stacked tube dam are in very good agreement with the observations from the experiment.

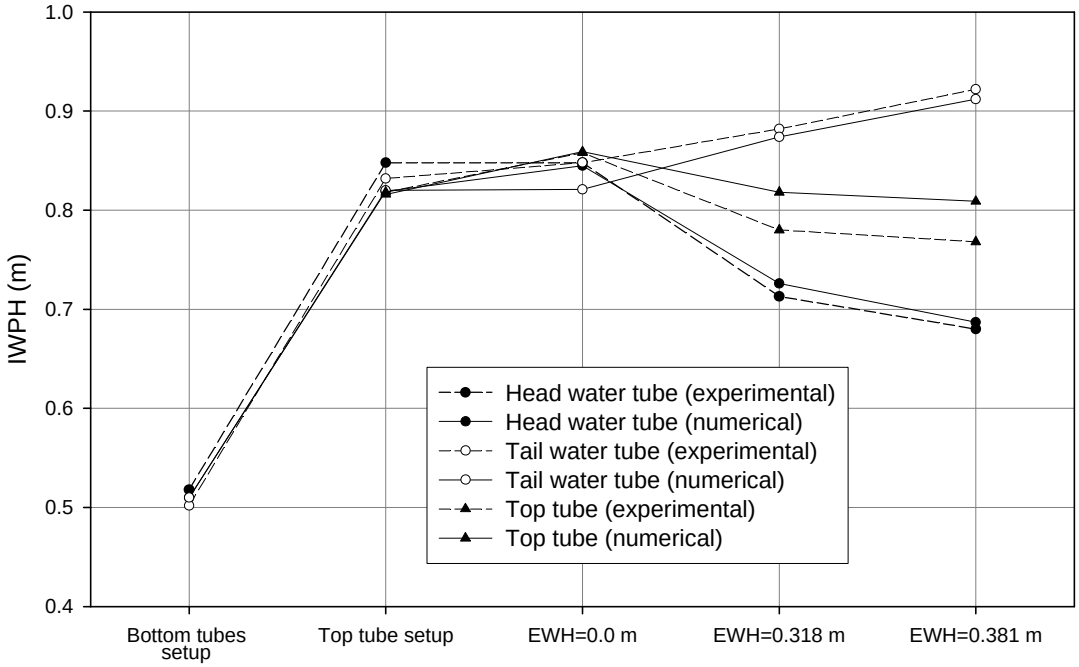

Figure 8.11 IWPH changes of stacked tube dam; trial 13

8.3.3. Tension

Figure 8.12 describes the numbering of the beam elements of the tubes and their approximate locations. The beam elements of the headwater tube and the tailwater tube start from elements 1 and 103, respectively, and each tube is constructed with 102 elements. The numbering of beam elements for the bottom strap begins from 205 and the bottom strap consists of 204 elements, 102 elements from the headwater side and another 102 elements from the tailwater side. The numbering of the top tube elements starts from 409 and ends at 510. Then the top strap is composed of the beam elements 511 through 605.

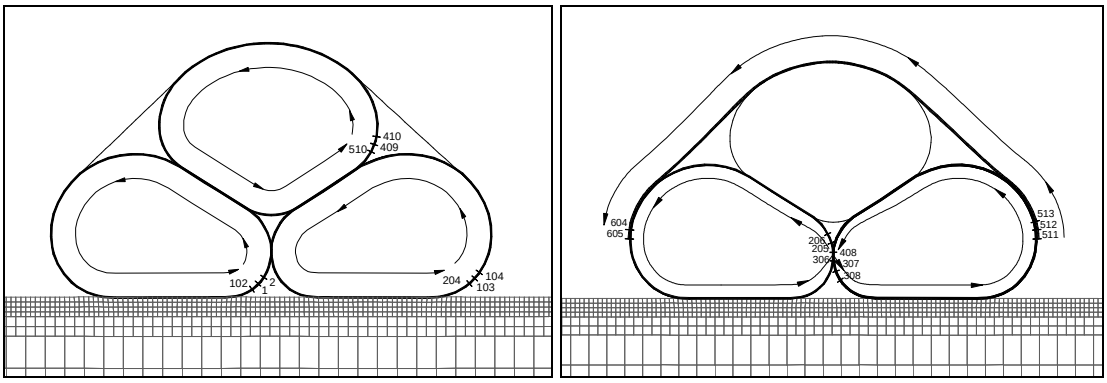

Figure 8.12 Element numbering of three tubes

Tensions in the stacked tube dam are plotted for trial 9 in accordance with the beam element numbers in Figure 8.13. As shown in Figure 8.13 (a), the tension in the stacked tube dam varies depending on the components. Again, the tension is listed as negative values here. The tension of the bottom strap is initially 50 to 70 N. As the external water height increases, the tensile force on the strap begins to changes to compression at the top of the headwater side strap and at the bottom of the tailwater side strap. In contrast, the bottom of the headwater side and the top of the tailwater side of the bottom strap shows an increase of tension.

Note that the strap cannot sustain compression in reality. This situation is caused by the modeling of the strap with beam elements in the numerical model. In addition, the tightening process of the bottom strap is omitted during the modeling procedure. However, it is believed that the effect of the compression of the bottom strap is minimal.

The tension of the top strap shows an overall decrease from about 140 N to 30 N. This is caused by the lifting of the headwater tube during the flooding and it results in relaxation of the top strap.

The decrease of pressure inside the headwater tube, together with the increase of the external water pressure at the side of the tube, yields much reduction in the net pressures acting on the tube. This reduces the maximum tension in the headwater tube from 1100 N to 400 N as shown in Figure 8.13 (b).

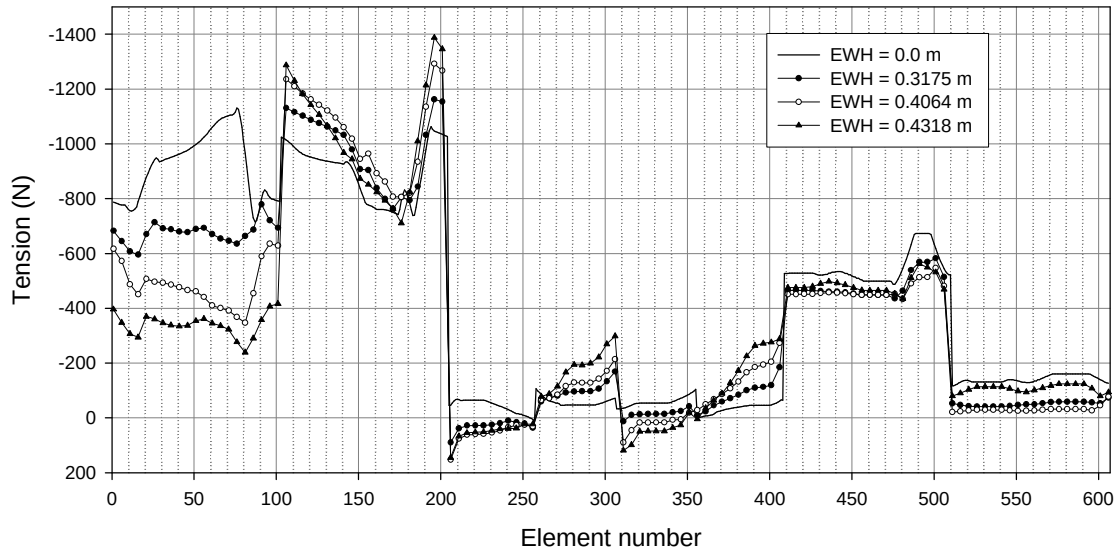

(a)

Tension in the stacked tube dam (whole)

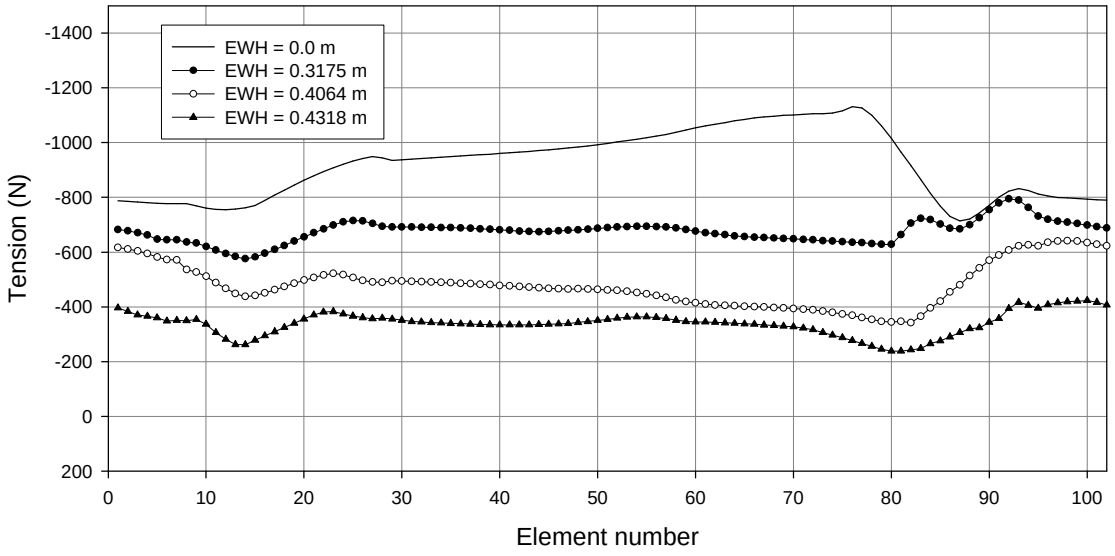

(b)

Tension in the headwater tube (detail)

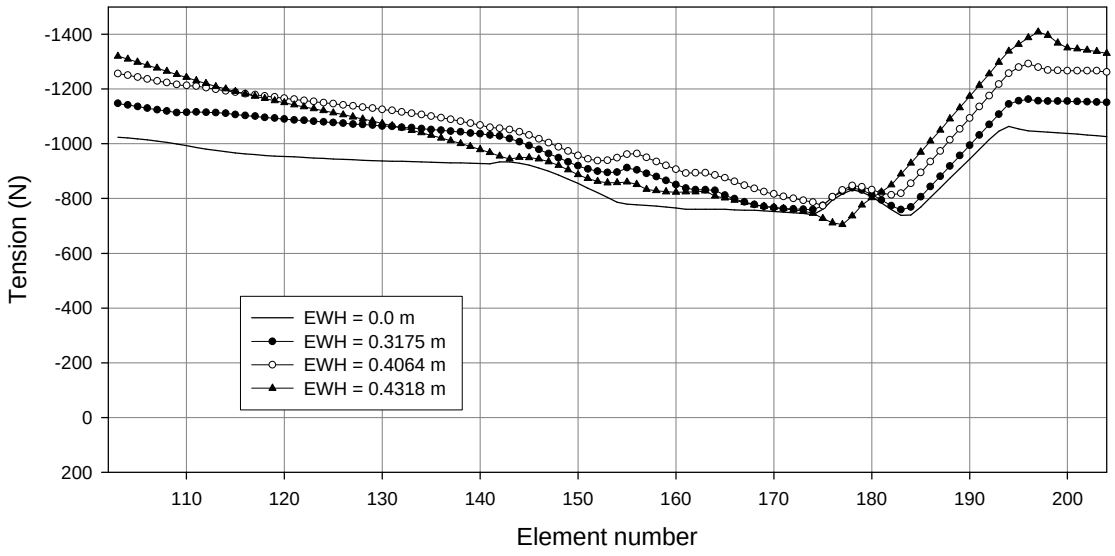

(c)

Tension in the tailwater tube (detail)

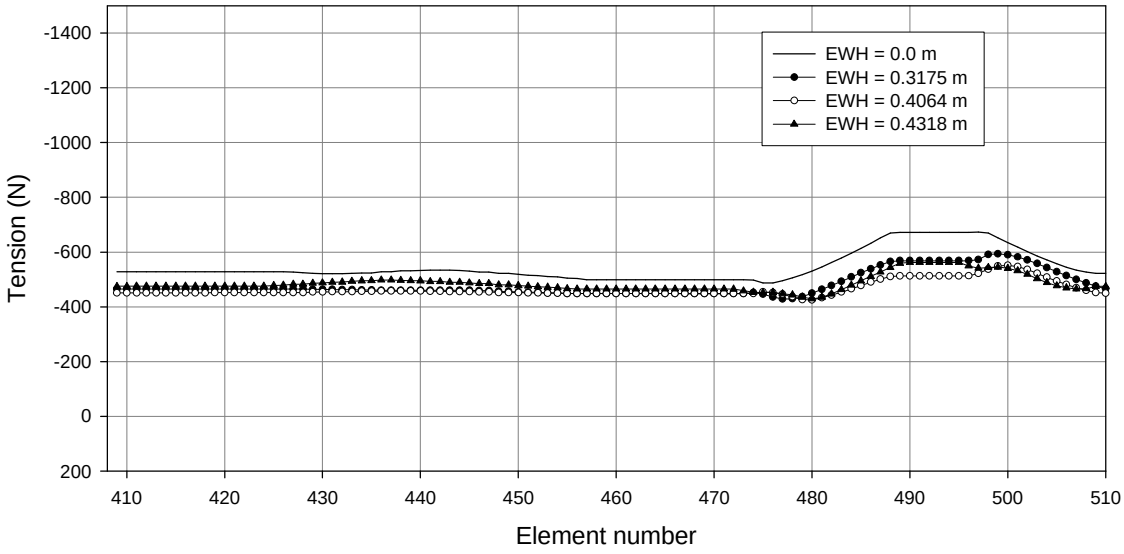

(d)

Tension in the top tube (detail)

Figure 8.13 Tension of stacked tube dam in whole and detail; trial 9

The maximum tension in the tailwater side increases approximately from 1000 N to 1400 N in accordance with the increase of the IWPH of the tailwater tube, as shown in Figure 8.13 (c).

The tension in the top tube is slightly decreased. The maximum tension of the top tube occurs at the bottom of the top tube, which is located between the two bottom tubes.

8.3.4. Pore Pressure Comparison

The pore pressure of the soil is plotted in Figure 8.14 for trial 9 when the external water height is 0.3175 m (12.5 in.). The colored contours represent the pore pressures in soil; the pore pressure of red color ranges from 0 Pa to 1000 Pa, and the light green color is from 3000 Pa to 4000 Pa.

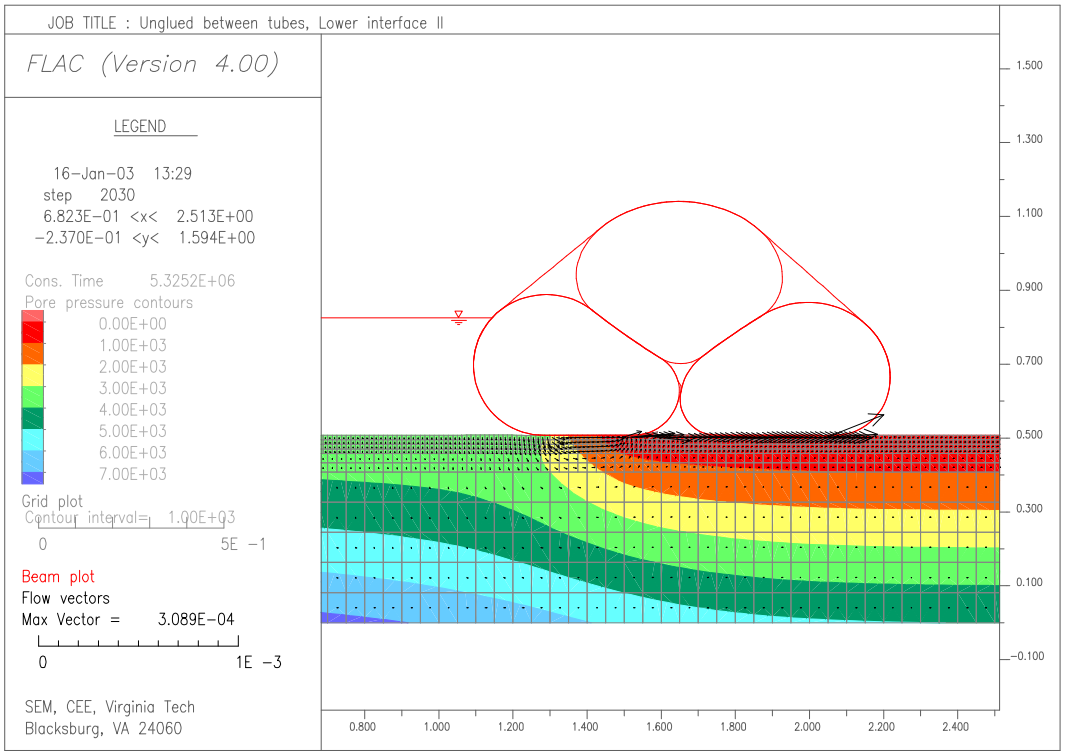

Figure 8.14 Pore pressure contour (at EWH=0.3175 m)

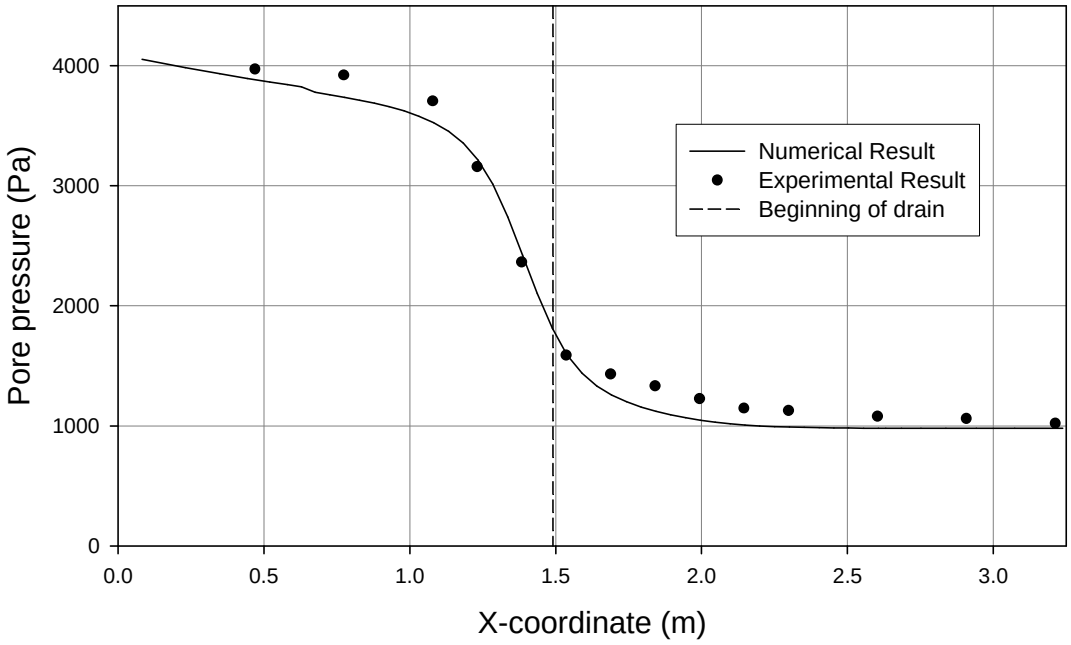

Figure 8.15 Comparison of pore pressure at 10 cm below ground

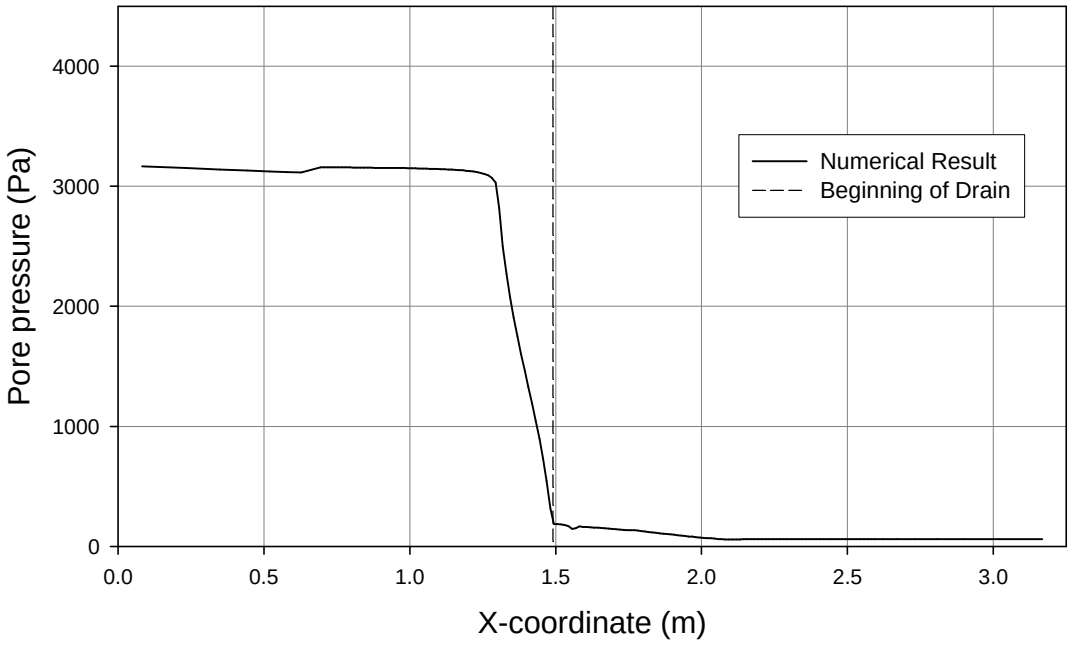

Figure 8.16 Comparison of pore pressure just below ground

The pressure heads at the various external water heights were measured in the experiments 10 cm below the ground. Figure 8.16 depicts the comparison of pore pressures

between the experiment and the numerical results. Dots represent the experimental results and a curved solid line indicates the result from the numerical analysis. The vertical dashed line shows the location of the beginning of the drain. The experimental measurements and the numerical results agree very well. The pore pressure begins to drop as it approaches the drain location. This tendency of pore pressure is more evident at just below the ground as shown in Figure 8.16. Therefore the drain helps effectively reduce the pore pressure beneath the stacked tube dam.

8.4. Summary and Conclusions

Two trials of the stacked tube dam were numerically modeled and analyzed. The bottom and the top straps were modeled with beam elements and they were assumed to be wrapped the whole length of the tube. The area of the straps was adjusted instead of Young's modulus. Also, the internal water pressure heads of the three tubes were altered separately using the secant method to keep the tube areas constant not only during flooding but also throughout the process of inflation. The circumference of the tube was slightly lengthened compared with the other water-filled tube dams in expectation of a better agreement of the cross-sectional shape of the tube. In addition, the top strap was connected with pretension to the bottom strap.

The results of the numerical analysis were compared with the experimental results. The comparison of the cross-sectional shape shows a better agreement than the other water-filled tube dam case. It implies that the circumference of the tube used in the experiment is close to 1.4859 m, not 1.4732 m. Also, the internal water pressure head from the numerical analysis corresponds well to the experiment. The numerically simulated pore pressure depicts well the observation in the experiments.

It was found that the stacked tube dam fails by rolling in this study. The rolling of the stacked tube dam is induced by slip and lifting up of the headwater tube. In addition, the release of the tension of the top strap makes the top tube easy to roll. However, it is possible that the stacked tube dam can become unstable by sliding, even on the same conditions of the soil in this study, if the internal water pressure is lower than in the current cases. When a stacked tube dam is inflated with lower pressure head, the cross-sectional shape of the stacked tube dam is flatter and has a better resistance to rolling. But this condition creates less resistance toward sliding. It would be interesting to establish which stacked tube dam has an equal amount of resistance to rolling and to sliding.

The evaluation of the tensile force in each component of the stacked tube dam provides guidelines for design; the maximum tensile force can be a reference for selecting the proper material strength and bonding or seaming strength.

Chapter 9. Summary, Conclusions, and Recommendations for Future Research

9.1. Summary and Conclusions

Two-dimensional analysis of water-filled tube dams has been conducted using the commercial finite difference program FLAC. Four different types of water-filled tube dams were numerically modeled, an apron-tube dam, a single baffle tube dam, a sleeved tube dam, and a stacked tube dam.

The tubes were assumed to be extensible and weightless and were modeled with beam elements having low bending stiffness. The internal water of the tube and the flood water were modeled with hydrostatic pressure. The foundation was represented by a Mohr-Coulomb model to consider the permanent, path-dependent deformations of soil. The groundwater flow was also considered and the pore pressures underneath the tube dams were simulated. The contact regions between the tube dams and the foundation and between the tubes were modeled with interface elements. The interface elements in FLAC were characterized by Coulomb sliding and /or tensile separation.

Because of the large deformation due to the characteristics of flexible tube structures, several user-defined subroutines were implemented in FLAC. The subroutines which control the load increment and update the loads depending on the deformed shape are two examples.

In addition, two iterative procedures have been utilized to simulate the internal water pressure head (IWPH) changes needed to maintain the constant tube area. One procedure simulates the IWPH changes using the secant method. The second procedure, the factored secant method, was developed for this research to evaluate the IWPH within the range between the initial IWPH and the unknown final IWPH.

The numerical simulations of the water-filled tube dams were performed in two phases, the inflation or the installation of a tube dam and the external water loading (flooding).

The inflation or the installation of each type of tube dam started from the very initial shape of a tube, without water inside. Then the tube was deformed with the internal water pressure to achieve the inflated shape. Because of that, a certain initial configuration of the tube was developed. For a single baffle tube dam, a tube with an “s” shape of the initial baffle was created. For the initial shape of an inner tube in a sleeved tube dam, a folding shape was employed. A stacked tube dam required many processes to imitate the installation of the tube in the field, the inflation and the shifting of the two bottom tubes, the strapping of the two bottom tubes, the inflation of the top tube, and the strapping of the top tube.

The flooding was simulated by applying water pressure at the headwater side of the tube dam. The external water height was raised incrementally and the external water pressures were continuously updated depending on the deformed configuration of the tube dam. As the external water height increased, the pore pressure boundary conditions at the surface and the edge of the headwater side of the soil were revised.

The numerical results for the apron-tube dam, sleeved tube dam, and stacked tube dam were examined and compared with the experimental results. The deformation of the cross section, the change of the IWPH, the pore pressure, and the critical external water height were compared.

The cross section of the apron-tube dam and the sleeved tube dam from the numerical analysis displayed fair agreement with the measurements of the tests. The numerical models showed a slightly smaller cross section overall, along with other minor differences. In the case of the stacked tube dam, the cross sections of the tubes corresponded almost perfectly with the experiments. The comparison of the internal water pressure heads of the tubes and the pore pressures during the flooding also showed general agreement with the experiments. The critical external water heights from the numerical analysis were slightly lower than the experimental results overall.

The difference of the numerical analysis and the experiments were caused by the following reasons:

- The end conditions in the longitudinal direction of the tube dams: it was assumed in the numerical analysis that the tube dam is infinitely long by modeling it as two-dimensional. The ends of the tubes were treated with bentonite material in the tests,

so the friction between the tube end and the box wall did not affect the overall stability significantly.

- The circumference of the tube: the circumference of the tube in the numerical model was 1.4732 m (58 in.) for the apron-tube dam model and the sleeved tube dam model. The circumference of the stacked tube dam was increased to 1.4859 m (58.5 in.). The results for the 1.4859 m stacked tube dam showed a closer resemblance to the experimental results than those for the 1.4732 m tube dams.
- Leakage and measurement errors in the experiments: there were leakages and they resulted in decreases in internal water pressures during the tests. Also, some of the test measurements were not highly accurate.

From the numerical simulations of the experiments for the various types of water-filled tube dams, together with the parametric study, the following conclusions were made regarding the stability of the tube dams:

- Apron-tube dam: the tube dam becomes unstable by slip failure between the dam and the foundation. The slip failure can be produced by insufficient shear strength between the apron and the foundation or between the tube and the foundation. However, the apron-tube dam cannot fail by slip of the tube when the tube dam is installed on the ground, which has friction angle greater than about 9~17 degrees, and these friction angles depend on the IWPH of the tube. Since the failure mode of the apron-tube dam is only slip (or slide), the critical external water height can be evaluated comparatively easily.
- Single baffle tube dam: the tube dam has two failure modes, sliding and rolling, and it is determined by the foundation and IWPH. If the shear resistance between the tube dam and the foundation is large enough to resist slip failure, the tube dam fails by rolling. The resistance to rolling cannot be calculated easily because of the configuration of the baffle tube dam; it is related to the shape of the tube dam, and a rounder tube is more vulnerable. If the shear resistance of the tube dam is not sufficient, the tube dam becomes unstable by sliding before rolling failure can occur.

- Sleeved tube dam: the sleeved tube dam begins to roll when slip failure between the two inner tubes occurs, in this study. The critical external water height of the tube dam is related directly to the shear resistance of the two inner tubes. However, it is not possible to have slip failure between the outer tube and the inner tube considering the contact length. Also, it is unlikely to have slip failure between the sleeved tube dam and the foundation as long as the drain is installed in the proper location. It is noted that the sleeved tube dam with a shorter outer tube has larger displacements.
- Stacked tube dam: the tube dam becomes unstable as the headwater tube slides and is lifted up by the external water. The strapping technique around the bottom and top tube also contributes to the stability of the stacked tube dam.

It is noted that when the IWPH increases, the resistance to sliding increases because the weight of a tube dam increases, but the resistance to rolling decreases as the shape of the tube dam becomes rounder, so if one of these resistances is not sufficient, the tube dam becomes unstable. Therefore it may not be possible to say that a certain type of tube dam fails in a certain way since the numerical result of this study shows that.

Table 9.1. Efficiency of various water-filled tube dams[1]

Water-filled tube dam	Critical external water height (m)	Total circumference (m)	Efficiency Ratio
Apron-tube dam (apron length=0.40 m)	0.343	2.368	0.145
Single baffle tube dam[2] (baffle length=0.25 m)	0.250	1.723	0.145
Sleeved tube dam (outer tube=2.31 m)	0.241	5.257	0.046
Stacked tube dam (Trial 9)	0.407	4.458	0.091

[1] The location of the drain is not considered in this evaluation.

[2] The friction angle between the tube and the foundation was 25 degrees.

The efficiency of the various tube dams may be determined by the critical external water height related to the height of the dam. Since tube dams have different configurations, the efficiency of a tube dam cannot be evaluated merely by the ratio of the critical external water height and the tube height. Thus, the total usage of the tube materials is considered and it is represented here by the sum of the circumferences of the tubes involved in the specified tube dam. Note that the sum of the circumferences is replaced by the sum of the total apron length (including overlapping portion of the apron on the tube) and the circumference of the tube in the case of an apron-tube dam. In addition, the length of baffle is added in the sum of circumference in the case of a baffle tube dam.

The stacked tube dam shows the highest critical external water height; the ratio of the critical external water height to the dam height is about 70 percent. But the apron-tube dam withstands the highest critical external water height compared to the dam height, 100 percent. The apron-tube dam and the single baffle tube dam are shown to be the most effective water-filled tube dams among the four types in this study.

Comparison of the two-dimensional numerical analysis of various water-filled tube dams in this study with previous experimental results shows that the principal assumptions made in the numerical modeling are valid and effective. The present study also indicates that considering IWPH changes during the deformation (by keeping a constant tube area) is important since it represents an interaction between internal fluid, tube structures, and external fluid and this fact was strongly supported in the stacked tube dam case. In addition, the study supports the idea that the pore pressure effect is an important factor for the proper assessment of the stability.

9.2. Recommendations for Future Study

The following are recommended for the future analysis of flexible tube structures and the development and design of a water-filled tube dam:

- When the instability of a tube dam is induced by slip (or slide) failure in one of the contact regions, such as an apron-tube dam or a baffle tube dam, the behavior of the

tube dam can be explained with the present study clearly. However, the behavior becomes more complex when the failure mode is rolling and cannot be easily explained since the rolling stability is related to the configuration of the flexible structure. Thus, more study should be conducted on the rolling failure mode of the tube dam.

- The interface element in FLAC is represented simply by Coulomb's Law. This law is suitable for the description of the interface between the tube material (geomembrane) and the soil since there is not much difference between the peak and the residual friction angles. However, the interfacial characteristics between the two tube materials could not be represented by the current model. To simulate this interface properly, a new interface element should be developed and it can be accomplished with user-defined functions in FLAC.
- It was assumed that the flood water exerts a static force on the tube dam. The assumption can be justified by the limited conditions. Dynamic disturbances, such as a surge of water, waves, or winds, can surely affect the stability of the tube dam and the effects of these dynamic forces should be investigated.
- To utilize a water-filled tube dam as a flood protection device, the tube dam should provide sufficient stability. Moreover, the stability of the tube dam should be easily evaluated to insure its safety. From the conclusion of the current work, it was found that the stability can be measured straightforwardly in case of slip failure. Therefore it might be a good idea to develop a new water-filled tube dam which has a slip failure mode only, such as an apron-tube dam.
- It is recommended that a combination of different types of tube dams can be used to provide more stability against the flooding water. For example, a stacked tube dam with an apron, and a baffle tube dam with an apron, should be studied.

References

Anonymous, “Geotextile tubes are installed in Maryland to fight erosion”, Civil Engineering News, May, 1997, p. 14.

Anonymous, “Rubber dam holds water”, Civil Engineering, Vol. 62, No. 2, February, 1992, p. 88.

Anonymous, “Tube dunes protect New Jersey beach”, Civil Engineering, Vol. 68, No. 2, February, 1998, p. 2.

Aqua-Barriers, “Flood Fighting Tools and Flood Protection”, http://www.aquabarrier.com/flood.html , 2000.

Aqua dam, “Aqua dam; Temporary water control, User’s Guide”, Aqua Dam and Diversion Ltd., 2002.

Associated Press, “The Flood of ’93; America’s greatest natural disaster photographed and reported by The Associated Press”, A Thomas Dunne Book, New York,1993.

Biggar, K. and Masala, S., “Alternatives to Sandbags for Temporary Flood Protection,” Alberta Transportation and Utilities Disaster Services Branch, Canada, October, 1998.

Chapra, S.C. and Canale, R.P., “Numerical Methods for Engineers”, 2nd edition, Applied Mathematics Series, McGraw-Hill, New York, 1990.

Erchinger, H.F., “Geotextile tubes filled with sand for beach erosion control, North sea coast, Germany”, Geosythetics Case Histories, G.P. Raymond and J.P. Giroud, eds., International Society for Soil Mechanics and Foundation Engineering, March, 1993, pp. 102-103.

FitzPatrick, B.T., Nevius, D.V., Filz, G. M., and Plaut, R.H., “Pilot-scale tests of water-filled tubes resisting floodwaters”, Technical Report, Virginia Tech, January, 2001.

Gruntfest, E., “Nonstructural mitigation of flood hazards”, Inland Flood Hazards, Cambridge University Press, Cambridge, UK, 2000, pp. 394-410.

Huong, T. C., “ Two-Dimensional Analysis of Water-filled Geomembrane Tubes as Temporary Flood-fighting Devices”, M.S. Thesis, Virginia Tech, 2001.

Huong, T.C., Plaut, R.H., and Filz, G.M. "Wedged geomembrane tubes as temporary flood-fighting devices", Thin-walled Structures, 2002, Vol. 40, pp. 913-923.

Itasca Consulting Group, "Fast Lagrangian Analysis of Continua, Command Reference", Itasca Consulting Group Inc., 1999a.

Itasca Consulting Group, "Fast Lagrangian Analysis of Continua, FISH in FLAC", Itasca Consulting Group Inc., 1999b.

Itasca Consulting Group, "Fast Lagrangian Analysis of Continua, Theory and Background", Itasca Consulting Group Inc., 1999c.

Itasca Consulting Group, "Fast Lagrangian Analysis of Continua, User's Guide", Itasca Consulting Group Inc., 2000.

Jones, D.R.V. and Dixon, N., "Shear strength properties of geomembrane/ geotextile interfaces", Geotextiles and Geomembranes, Vol. 16, 1998, pp. 45-71.

Kazimierowicz, K., "Simple analysis of deformation of sand sausages", 5th International Conference on Geotextiles, Geomembranes and Related Products, Singapore, 1994, pp. 775-778.

Koerner, R.M. and Welsh, J.P., "Fabric forms conform to any shape", Concrete Construction, Vol. 25, No. 5, May, 1980, pp. 401-409.

Landis, K., "Control floods with geotextile cofferdams", Geotechnical Fabrics Report, Vol. 18, No. 3, March, 2000, pp. 24-29.

Leshchinsky, D., Leshchinsky, O., Ling, H.I. and Gibert, P.A., "Geosynthetic tubes for confining pressurized slurry: some design aspects", Journal of Geotechnical Engineering, Vol. 122, August, 1996, pp. 682-90

Moler, M., Freeman M., Filz, G. M., and Plaut, R.H., "Pilot-scale tests of stacked three-tube configuration of water-filled tubes for resisting floodwaters", Technical Report, Virginia Tech, December, 2001.

Namias, V., "Load-supporting fluid-filled cylindrical membranes", Journal of Applied Mechanics, Vol. 52, December. 1985, pp. 913-918

NOAQ, "NOAQ Flood Protection AB", http://www.siaq.se, 2002.

Ogihara, K., "Auto-rubber dam under flood conditions", International Conference on the Hydraulic Aspects of Floods and Flood Control, London, England, September, 1983, pp. 99-109

Parker, D.J. "Floods, Volume I, II", Routledge Hazards and Disasters Series, Routledge, 2000

Plaut, R. H, and Klusman, C.R., "Two-dimensional analysis of stacked geosynthetic tubes on deformable foundations," Thin-walled Structures, 1999, Vol. 34, pp. 179-194.

Plaut, R. H. and Suherman, S., "Two-dimensional analysis of geosynthetic tubes," Acta Mechanica, Vol. 129, 1998, pp 207-218.

Plaut, R. H., Liapis, S.L. and Telionis, D.P., "When the levee inflates," Civil Engineering, ASCE,Vol. 68, No. 1, 1998, pp. 62-64.

Seay, P.A., "Finite element analysis of geotextile tubes", M.S. Thesis, Virginia Tech, 1998.

Superior Dam LLC, http://www.superiordam.com, 2002.

Tam, P.W.M. and Zhang, X.-Q., "Management of rubber dams in Hong Kong", Canadian Journal of Civil Engineering, Vol. 26, No. 2, April, 1999, pp. 123-134.

UNDHA, "Floods; people at risk, strategies for prevention", United Nations Department of Humanitarian Affairs, United Nations Publication, 1997.

Van Santvoort, G., "Geotextiles and Geomemebranes in Civil Engineering." Revised Edition, A. A. Balkema, Rotterdam, 1994.

Water Structures Unlimited®, "Water Structures/Aqua dam complete User's Guide", Water Structures Unlimited®, 2002.

Water Structures Unlimited®, http://www.aquadam.com, 2002.

Vita

Meeok Kim was born in Pusan, Republic of Korea. As a daughter of a small local estate developer, she was exposed to construction sites and blueprints at an early age. She attended Pusan National University in Pusan, where she received a Bachelor's degree in Civil Engineering in 1993.

She began her graduate work directly and continued at the same school until 1996 and received her Master's degree in Civil Engineering in 1995. During graduate school, she was actively involved as a research assistant in various structural projects. The projects included the on-site investigations of major structures on Pusan Urban Highway and the numerical analysis of several bridges and subway stations in Pusan using finite element programs. She also worked as a part-time instructor at the Pusan National University and at the Dongeui Institute of Technology from 1995 to 1996.

She enrolled for her Ph.D. in the Department of Civil and Environmental Engineering at Virginia Polytechnic Institute and State University in 2000. She focused her doctoral study in structural engineering under the guidance of Professors R. Plaut and G. Filz.